

**Vibration Assisted Machining:
Modelling, Simulation, Optimization,
Control and Applications**

A thesis submitted for the degree of
Doctor of Philosophy

by

Rasidi Ibrahim

School of Engineering and Design
Brunel University

September 2010

Abstract

Increasing demand for precision components made of hard and brittle materials such as glasses, steel alloys and advanced ceramics, is such that conventional grinding and polishing techniques can no longer meet the requirements of today's precision manufacturing engineering. Particularly, in order to undertake micro-milling of optical glasses or other hard-machining materials, vibration assisted machining techniques have been adopted. However, it is essential and much needed to undertake such processes based on a scientific approach, i.e. the process to be quantitatively controlled and optimized rather than carried out with a trial-and-error manner.

In this research, theoretical modelling and instrumental implementation issues for vibration assisted micro-milling are presented and explored in depth. The modelling is focused on establishing the scientific relationship between the process variables such as vibration frequency, vibration amplitude, feedrate and spindle speed while taking into account machine dynamics effect and the outcomes such as surface roughness generated, tool wear and material removal rate in the process.

The machine dynamics has been investigated including a static analysis, machine tool-loop stiffness, modal analysis, frequency response function, etc, carried out for both the machine structure and the piezo-actuator device. The instrumentation implementation mainly includes the design of the desktop vibration assisted machining system and its control system. The machining system consists of a piezo-driven XY stage, air bearing spindle, jig, workpiece holder, PI slideway, manual slideway and solid metal table to improve the system stability. The control system is developed using LabVIEW 7.1 programming. The control algorithms are developed based on theoretical models developed by the author.

The process optimisation of vibration assisted micro-milling has been studied by using design and analysis of experiment (DOE) approach. Regression analysis, analysis of variance (ANOVA), Taguchi method and Response Surface Methodology (RSM) have been

chosen to perform this study. The effects of cutting parameters are evaluated and the optimal cutting conditions are determined. The interaction of cutting parameters is established to illustrate the intrinsic relationship between cutting parameters and surface roughness, tool wear and material removal rate. The predicted results are confirmed by validation experimental cutting trials.

This research project has led to the following contribution to knowledge:

- (1) Development of a prototype desktop vibration assisted micro-milling machine.
- (2) Development of theoretical models that can predict the surface finish, tool wear and material removal rate quantitatively.
- (3) Establishing in depth knowledge on the use of vibration assisted machining principles.
- (4) Optimisation of cutting process parameters and conditions through simulations and machining trials for through investigation of vibration assisted machining.

Acknowledgements

I would like to express my gratitude especially to my Director of Studies, Professor Kai Cheng, and the research supervisors who have given me hope and accepted me under their supervision. My special thanks go to Professor Kai Cheng for his valuable advice, guidance, support, motivation and encouragement in developing this research successfully.

Recognitions are highlighted to Brunel University for their financial support, which made this research achievable. Thanks also go to the People's Trust Council, commonly abbreviated as JPA and the University of Tun Hussein Onn Malaysia (UTHM) for putting their faith in me to pursue my studies to doctoral level.

Special thanks are to my colleagues Dr. Dehong Huo, Dr. Sarah Sun, Mr. Robin Wang, Mr. Hui Ding, Mr. Khir Harun, Mr. Saiful Ghani, Mr. Konstantinos Angelopoulos and Mr. Ilias Barlias for supporting me with my research work, also to Dr. Frank Wardle, Mr. Paul Yates, and all the technicians for their assistance. I am also grateful to all of the individuals who have directly or indirectly helped me in completing my research.

I would like also to acknowledge my parents, Hj. Ibrahim, Hjh. Khadijah, for their love, encouragement and support throughout my research studies.

Finally, thanks should go to my beloved wife, Suhaila Alias, for her warm comfort and great assistance and for her patience and understanding which has inspired my research work from the beginning to the end.

Table of Contents

Abstract.....	i
Acknowledgements.....	iii
Abbreviations.....	ix
Nomenclature.....	xi
List of Figures.....	xiv
List of Tables.....	xviii
Chapter 1 Introduction.....	1
1.1 Background of the research.....	1
1.1.1 Overview of vibration assisted machining.....	1
1.1.2 The current needs in industry.....	3
1.1.3 History of vibration assisted machining.....	4
1.2 Aim and objectives of the research.....	5
1.3 Scope of the thesis.....	7
Chapter 2 Literature Survey.....	10
2.1 Introduction.....	10
2.2 Vibration assisted machining.....	11
2.3 Vibration assisted machining systems.....	15
2.3.1 Cutting mechanism in vibration assisted machining (VAM).....	16
2.3.2 Comparison between 1D and 2D VAM.....	19
2.3.3 System specifications.....	24
2.4 Dynamic machining system identification.....	25
2.5 3D surface profiler.....	27
2.6 Simulations.....	28
2.7 Optimisation and control.....	28
2.7.1 Minitab.....	28
2.7.2 ANOVA.....	29

2.8	Summary	29
Chapter 3	Machine system design and implementation	31
3.1	Introduction	31
3.2	Design approach and machine setup	34
3.3	The input to the machine design	36
3.4	Electrical hardware and machine design.....	36
3.4.1	XY25XS piezo-actuator	36
3.4.2	Air bearing spindle	39
3.4.3	X slideway.....	41
3.4.4	Data acquisition card.....	42
3.4.5	RS 232 box integrated interface.....	43
3.5	Software analysis and machine control.....	45
3.5.1	Ansys 11 and Ansys workbench	45
3.5.2	AutoCAD Mechanical desktop 2007	46
3.6	Data acquisition and machine system control.....	46
3.6.1	Matlab	46
3.6.2	LabVIEW	47
3.6.3	Mercury controller and coder C-842 for Windows.....	48
3.6.4	3D Zygo surface profiler.....	50
3.7	Summary	51
Chapter 4	Dynamic analysis of the machine system	52
4.1	Introduction	52
4.2	Design analysis	54
4.3	Finite Element (FE) analysis of the machine	55
4.3.1	Machine loop.....	57
4.3.2	Static analysis.....	60
4.3.3	Modal analysis	62
4.3.4	Hammer testing.....	69
4.3.5	Frequency response function	74

4.4	Mechanism of the piezo-electric actuator and controller	76
4.4.1	Permittivity.....	79
4.5	Finite element analysis of the piezo actuator	80
4.5.1	Static behaviour of the piezoactive actuator	80
4.5.2	Static structural analysis.....	80
4.5.3	Modal analysis	84
4.6	Dynamic capacitance and electrical driver response	86
4.6.1	Electrical limits	87
4.6.2	Thermal limits	87
4.6.3	Driving and electrical response.....	88
4.7	Summary	90
Chapter 5	Process modelling and simulation.....	91
5.1	Introduction	91
5.2	Process modelling approach.....	92
5.2.1	The proposed model for 2D VAM	96
5.2.2	Motion shape in 2D VAM	98
5.2.3	Tool path trajectory	100
5.2.4	Vibration cutting ratio	103
5.3	Cutting mechanics in 2 dimensional VAM.....	105
5.3.1	Cutting force and chip thickness	106
5.3.2	Cutting temperature and tool life	110
5.3.3	Surface roughness (R_a) and chip formation.....	113
5.3.4	Ductile regime cutting in chip formation	114
5.4	Machining dynamics model of 2D VAM.....	115
5.5	Summary	117
Chapter 6	Validation of the modelling and simulation through machining trials	118
6.1	Introduction	118
6.2	Facilities and workpiece materials for cutting experiments.....	118

6.2.1	Facilities for vibration assisted machining experiments	118
6.2.2	Workpiece materials for desktop vibration assisted machining.....	121
6.2.3	Cutting tools	122
6.3	The experimental plans	123
6.3.1	Machine setup accuracy	123
6.3.2	Machining trials plan.....	124
6.4	Result and discussions	125
6.4.1	Cutting force validation.....	125
6.4.2	Surface roughness validation	127
6.4.3	Tool wear validation	130
6.4.4	Material removal rate validation	132
6.5	Summary	133
Chapter 7	Process optimisation and control	135
7.1	Introduction	135
7.2	Optimization control	136
7.3	Optimization parameters	136
7.4	Optimization modelling	137
7.4.1	Surface roughness, tool wear and material removal rate	137
7.5	Design of experiment	138
7.5.1	Minitab 15	142
7.5.2	ANOVA	142
7.5.3	Response surface method (RSM).....	142
7.5.4	Taguchi method.....	143
7.6	Optimisation analysis of surface roughness, tool wear and material removal rate..	143
7.6.1	Regression analysis and ANOVA.....	143
7.6.2	Taguchi analysis.....	147
7.6.3	Contour plot in response to surface methodology.....	150
7.6.4	Interaction between factors	152
7.7	Summary	154

Chapter 8	Conclusions and recommendations for future work	156
8.1	Conclusions	156
8.2	Recommendations for future work.....	157
Rereferences		158
Appendices		175
Appendix I.....		176
	List of publications arising from this research	177
Appendix II.....		178
	Desktop Vibration Assisted Micro-milling Drawing Details	179
Appendix III.....		196
	Machining Trial Plan.....	197
Appendix IV		201
	Part of MatLab Programming.....	202
Appendix V		206
	Part of Minitab Programming.....	207
Appendix VI.....		215
	Part of LabView Programming.....	216

Abbreviations

1D	One dimensional
2D	Two dimensional
ANOVA	Analysis of variance
CAD	Computer aided design
CPU	Computer processing unit
CTE	Coefficient of thermal expansion
DAQ	Data acquisition card
dB	Decibel
DOE	Design of experiment
DVAM	Desktop vibration assisted machining
EDM	Electrical discharge machine
FEA	Finite element analysis
FRF	Frequency response function
Hz	Hertz
ISO	International Standards Organization
LBS	Pound
LEMO	Leon Mouttet
LTD	Limited
MDOF	Multi-degree-of-freedom
NI	National Instrumente
ODS	Operating deflection shape
OEM	Original equipment manufacturer
PC	Personal computer
PI	Physik Instrumente
PZT	Piezoelectric Transducer
RA	Regression analysis
RMS	Root mean square
RPM	Revolutions per minute

RS	Recommended standard
RSM	Response surface methodology
SDM	Structural data modification
SEM	Scanning Electron Microscopy
VAM	Vibration assisted machining
VI	Virtual Instrument

Nomenclature

Symbol

A	Amplitude in X direction (μm)
B	Amplitude in Y direction (μm)
A_1	Amplitude distance one
B_1	Amplitude distance two
b	Width of cut (mm)
C	Experimental material constant
C_e	Damping coefficient ($\text{N}/\mu\text{m}/\text{s}$)
\cos	Cosine
D	Induction
d_z	Piezoelectric strain per unit field
E	Field (piezo-electric)
E_m	Elastic modulus (Pa)
$e^{i\omega t}$	Exponential harmonic frequency function
F	Cutting force (N)
f	Feedrate (mm/min)
F^a	Total applied load vector
F_c	Principal cutting force
F_n	Amplitude of cutting force with occurrence number (N)
F^r	Reaction load vector
F_r	Radial cutting force
F_s	Shear plane force
F_x	Force in x direction (N)
F_y	Force in y direction (N)
f_x	Frequency in X direction (Hz)
f_y	Frequency in Y direction (Hz)

F_t	Thrust cutting force
f_t	Feed per tooth
F^{ac}	Acceleration load vector
f_{fc}	Flank face contact force
f_{ft}	Flank face normal force
F^{nd}	Applied nodal load vector
F_e^{pr}	Element pressure load vector
F_e^{th}	Element thermal load vector
F_z	Force in z direction (N)
G	Gravitational constant
g	Gravitational acceleration
h	Chip thickness
K	Total stiffness matrix
k	Stiffness
k_e	Element stiffness matrix
K_{hinge}	Stiffness of flexure hinge
ΔK_{piezo}	Nominal stiffness of piezo
K_m	Material coefficient
l	Distance of object (mm)
l^2	Length vector form centre object (mm)
ΔL_{eff}	Effective stroke length
L_f	Flank face length (mm)
ΔL_{piezo}	Nominal stroke
M or m	mass (kg)
Ms^2	Mass relative to Laplace transforms (N)
N	Number of element
N_s	Shear plane normal force (N)

N_f	Normal rake face
r	Tool radius (μm)
R_a	Average roughness (μm)
S	Strain
sin	Sine
S^E	Compliance at constant field
T	Stress (N/m^2)
t	Time (second)
T_C	Pulse duration
u	Nodal displacement vector
U	Piezo displacement
V	Velocity (mm/min)
x_d	Displacement in X axis
Y	Yield strength
Z	Number of tool teeth
Z_i	The ordinal number of tool teeth
$Z(s)$	Dynamic stiffness
ε^T	Permittivity
μ_f	Coefficient of friction
ω	Palstance (rad)
π	pi (3.147)
ϕ	Shear angle (rad)
ϕ_y	Phase angle in Y direction (rad)
ϕ_x	Phase angle in X direction (rad)
σ	Flow stress ($\text{N}/\mu\text{m}$)
θ	Tool rotation angle (rad)

List of Figures

Chapter 1

Figure 1.1: Structure of the thesis	7
---	---

Chapter 2

Figure 2.1: The aspect of literature survey	11
Figure 2.2: Block diagram of a VAM system	12
Figure 2.3: Basic system in 2D VAM.....	15
Figure 2.4: 1D vibration assisted cutting (Shamoto, 2004)	16
Figure 2.5: 1D and 2D elliptical vibration cutting (Cerniway, 2001).....	17
Figure 2.6: 1D vibration assisted machining (Dow, 2007)	18
Figure 2.7: Shamoto and Moriwaki model for circular motion lifting phenomena	18
Figure 2.8: Comparison of thrust forces in 3 machining methods (Ma, 2004).....	20
Figure 2.9: Fraunhofer servo design (Klocke, 2004)	21
Figure 2.10: Servo design from Bremen University, Germany (Brinksmeir, 1999).....	22
Figure 2.11: Servo design from Pusan National University, Korea.....	23
Figure 2.12: Resonant servo design by Kobe University, Japan (Moriwaki, 1999)	24

Chapter 3

Figure 3.1: The modelling of desktop 2D vibration assisted micro-milling machine	31
Figure 3.2: Schematic diagram of the VAM.....	35
Figure 3.3: Piezo-electric actuator model XY25XS from Cedrat SA.....	37
Figure 3.4: Piezo-electric power amplifier from Cedrat SA	38
Figure 3.5: Air bearing spindle from Loadpoint LTD	40
Figure 3.6: Spindle amplifier modelled Mk 5A from Loadpoint LTD	41
Figure 3.7: X slideway driven by leadscrew	42
Figure 3.8: DAQ card from the National Instrument.....	43
Figure 3.9: DB9/F (Female pin) connector	44
Figure 3.10: The connecting of RS232 cable.....	45
Figure 3.11: User interface for machining operation	47

Figure 3.12: Binary control box	49
Figure 3.13: User interface for PI slideway	49
Figure 3.14: Zygo surface profiler	50

Chapter 4

Figure 4.1: Schematic of the Structural Dynamic Modification (SDM).....	52
Figure 4.2: Finite element analysis solver.....	53
Figure 4.3: Machine FEA model.....	55
Figure 4.4: Desktop machine for vibration assisted machining.....	56
Figure 4.5: Machine tool-workpiece loop in desktop micro-milling machine, machining process and dynamic effects.....	58
Figure 4.6: Loop stiffness physical model	59
Figure 4.7: Stiffness experiment	59
Figure 4.8: Spring modelled for air bearing stiffness	62
Figure 4.9: MDOF system	64
Figure 4.10: Frequency Domain ODS from a set of FRF (Schwarz & Richardson, 1999) ...	67
Figure 4.11: Graph in LabView 7.1 with 4 natural frequencies.....	67
Figure 4.12: The first four natural frequencies and mode shapes.....	68
Figure 4.13: Hammer testing equipment setup	70
Figure 4.14: Typical impact force pulse and spectrum.....	71
Figure 4.15: Instrument for hammer testing	72
Figure 4.16: Comparison of natural frequency by Ansys and hammer testing.....	73
Figure 4.17: Frequency response functions defined	75
Figure 4.18: Frequency response	76
Figure 4.19: A sample of FRF plot taken from 2D VAM test bed	76
Figure 4.20: Piezo ceramic basic principal	77
Figure 4.21: Piezoelectric effects on body shape.....	78
Figure 4.22: The XY25XS model piezo-actuator	81
Figure 4.23: 3D drawing and piezo-actuator in detail.....	82
Figure 4.24: Static displacement on piezo and structure	83
Figure 4.25: 4 Modal shapes of piezo-actuator.....	86

Figure 4.26: Electrical field-strain relation in a piezoelectric material.....	87
Figure 4.27: Limitation of the standard of piezo due to self heating	88
Figure 4.28: Synoptic of a driving system	89
Figure 4.29: Synoptic of a closed loop system	89

Chapter 5

Figure 5.1: Process modelling and simulation	91
Figure 5.2: Micro and macro cutting mechanics.....	92
Figure 5.3: Conventional end milling	94
Figure 5.4: Contribution of element cutting edge	96
Figure 5.5: 2D VAM setup	96
Figure 5.6: Oblique cutting force	97
Figure 5.7: (a) physical model (b) real setup model	98
Figure 5.8: Effect value a and b in VAM	99
Figure 5.9: Difference of chip thickness affecting cutting force reduction	107
Figure 5.10: Comparison between VAM and conventional machining in cutting force	109
Figure 5.11: Variation of hardness with temperature for tool materials and coatings.....	111
Figure 5.12: Cutting mechanism in VAM 2D VAM during the cooling period.....	111
Figure 5.13: Gap in 2D VAM and its influence on tool temperature and tool life	112
Figure 5.14: Illustration of R_a and peak to valley as determined	113
Figure 5.15: Effect of VAM in surface tool produced (a) Without VAM, (b) with VAM..	114
Figure 5.16: Spring damper vibratory model.....	115

Chapter 6

Figure 6.1: Experimental configuration of the cutting trials.....	119
Figure 6.2: Cutting setup.....	120
Figure 6.3: Zygo New View 5000 optical microscope	121
Figure 6.4: A sample in cutting trials.....	122
Figure 6.5: Measuring the run-out of spindle.....	123
Figure 6.6: Piezo-actuator and the signal response.....	124

Figure 6.7: Experimental plan and flow chart.....	124
Figure 6.8: Simulated cutting forces in X, Y and Z axis directions.....	125
Figure 6.9: Average cutting force without and with 2D VAM.....	126
Figure 6.10: Machined surface.....	127
Figure 6.11: Simulated surface	128
Figure 6.12: Cutting trials result	128
Figure 6.13: Peak and valley surface maps with 2D VAM and without 2 DVAM	129
Figure 6.14: Peak height histogram	130
Figure 6.15: (a) Endmill without vibration (b) Endmill cutter with vibration assisted.....	131
Figure 6.16: The specified volume calculated	132
Figure 6.17: Material removal rate with and without 2D VAM	133

Chapter 7

Figure 7.1: Design of experiment flow chart	139
Figure 7.2: Average Ra versus fr (mm/min), Amp. (micron),	145
Figure 7.3: Tool wear versus fr (mm/min), Amp. (micron),	145
Figure 7.4: Material removal rate versus fr (mm/min), Amp. (micron),	145
Figure 7.5: Optimum setup SN ratio in surface roughness	148
Figure 7.6: Optimum setup SN ratio in tool wear.....	149
Figure 7.7: Optimum setup SN ratio in material removal rate.....	149
Figure 7.8: Contour plot in Ra	150
Figure 7.9: Contour plot in tool wear.....	151
Figure 7.10: Contour plot in MRR.....	151
Figure 7.11: Interaction between factors for surface finish	152
Figure 7.12: Interaction between factors for tool wear.....	153
Figure 7.13: Interaction between factors for MRR	154

List of Tables

Chapter 3

Table 3.1: Machine specifications.....	32
Table 3.2: Properties and standard technical data of piezo-actuator (Cedrat, 2009)	38
Table 3.3: Standard technical specifications for the piezo amplifier	39
Table 3.4: RS232 Pin assignment for DB9 signal set	44
Table 3.5: Binary coding for RS232 program.....	48

Chapter 4

Table 4.1: Comparison of finite element predictions with modal test results.....	74
Table 4.2: First ten natural frequencies of the piezo-actuator.....	85

Chapter 5

Table 5.1: Comparison between 2D VAM and conventional machining	105
---	-----

Chapter 6

Table 6.1: Material properties of the workpiece in VAM.....	122
Table 6.2: Dimension and geometry of the cutting tools in VAM	123

Chapter 7

Table 7.1: Machining parameters and their coded labels.....	140
Table 7.2: Optimum of each factor at the response	150

Chapter 1 Introduction

1.1 Background of the research

1.1.1 Overview of vibration assisted machining

Vibration provides a lot of benefits in our life, such as in manufacturing, medical, communications, transport, industries, etc. In the machining process, vibration can lead to improvements when applied in the correct manner. The same occurs in manufacturing technology. Vibration assisted machining is a cutting technique in which a certain frequency of vibration is applied to the cutting tool or the workpiece (besides the original relative motion between these two) to achieve better cutting performance (Shamoto et al, 1990). There are a number of different experiments setup to simplify the process, but the tendency is to give a wide range of machining processes to machine hard and brittle materials. Matsumura (2005) developed a vibration machine using micro a end mill to machine glass in the ductile mode. However, this method of machining is not suitable for mass production. The design of the cutting tool, holder and machine resulted in the cutting process effect of tool wear, cutting angle and limited profile. If they are not concerned about this problem, the productivity in the area will be seriously affected.

Many researchers try to machine hard and brittle materials such as glass, ceramic, stainless steel, and steel alloys to a mirror surface finish in different types of machining applications. There are number of machines equipped with vibration devices for cutting purposes. However, the existing vibration machining process does not efficiently cut on hard and brittle materials because of excessive wear of the diamond cutting tool due to high chemical activity with iron (Bonifacio et al. 1994). Due to this phenomenon, researchers have explored a number of ways using ultrasonic and vibration to improve the design, frequency, cutting tools and equipment devices. It also to improve the efficiency with some basic experimental concepts carried over from conventional machines.

This project and research intends to review the various research experiments carried out in the past decade involving the ultrasonic and vibration assisted machining process. Even though this fundamental technique is still an ongoing investigation, the widely accepted principle based on vibration frequency and vibration amplitude is presented together with applications. The research review identifies the capability of vibration assisted machining technology in ultrasonic technology. Furthermore, this research discusses the future directions for 2 dimensional vibration assisted micro-milling research and applications.

Chern and Lee (2005) designed and developed a vibrating worktable in their drilling machine to create a vibration during the drilling process. The design was named the ultra-precision micro-drilling worktable. It was attached to a conventional drilling machine. They machined aluminium alloy (A1 6061-T6) and structure steel (SS41) investigated the effect of vibration assisted drilling. They found that the uniform distance between drilled holes center was greatly reduced with an increase of frequency. High frequency of vibration helped to align to the desired position. Hole roundness and oversize were also improved when high vibrating frequency was imposed. However, displacement of the hole centre and surface roughness of the drilled wall could be improved by increasing frequency of vibrating and amplitude. On the other hand, from their experimental setup, vibrating frequency has a negative effect on the drill life and there is a decrease in the number of holes produced because of the increased cutting speed, causing more collision with and rubbing of the edge of the workpiece. Therefore, this could be improved by applying additional axis of vibration.

The efficiency of the drilling process in reducing hole oversize was enhanced when frequency was increasing from 2 kHz to 10 kHz and hole oversize improved from 0.027 μm to 0.004 μm . The differences at the entrance of the hole produced without vibration are obvious when entering the workpiece surface. During the drilling cutting process, the drill bit rubbing the workpiece makes the uncut material at the edge at the hole, however when the vibration is applied, a nearly perfect circular shape can be obtained.

Chern and Chang (2005) presented another design for a vibrating worktable using a piezo-actuator affixed to a milling machine centre (model: MC- 1050P). The vibrating worktable used a piezo-actuator, two dimensional XY axis, a maximum operating frequency of 16 kHz and maximum travelling distance was 10 μm . It operated with a 2 channel high power amplifier to create the desired vibration to cut a slot of aluminium alloy A1 6061-T6. Through this experiment, they found that slot oversize about 20 μm , displacement of slot centre and slot surface roughness could be improved: employment of vibration cutting increases the number of slots produced within tolerance when high amplitude and proper frequency were imposed. However, higher frequencies have a negative effect on tool life according to a previous study (Chern et al, 2005). Even though higher frequencies affected tool life, the amplitude in vibration cutting had the highest influence on the interaction between the cutting tool and workpiece.

In vibration assisted machining, vibration amplitude (normally sine wave) lead to an intermittent gap during cutting and was identified as an important mechanism in vibration cutting. Increasing the vibration amplitude means an enlargement in the gap that allows more cutting fluid to extract the heat during the cutting process, thus enhancing the tool's life and reducing production cost.

In order to maintain its stability and precision, the vibrations within the machining system need to be monitored and controlled so as to achieve the optimum vibration displacement between the tool and a workpiece.

1.1.2 The current needs in industry

The development of precision metal cutting in recent years has not only been focused on better surface finishes, but also on expanding the sphere of applications. The machining of micro-scale parts is one such application. With the miniaturisation and increasing complexity of audio/visual products, the demand for high-precision micro machining is going to increase (Liu and Cheng, 2005).

Vibration assisted machining was introduced at early 1950s and has now become widely accepted in precision metal cutting industries. It has become a well known method, and many researchers have developed various kinds of design that suit their applications. For example, cutting hard and brittle material has now become popular with the help of vibratory cutting. Some factories have multi-function components such as Fresnel lenses or other varying profile optics requiring higher forms of accuracy and lower cutting forces that can be achieved with the help of vibration cutting. Workpiece deformation, chatter, built-up-edge (BUE) and burrs become major challenges at this micro scale (Isaev et al, 1961).

Many companies associated with aerospace or optical components production are considering diamond turning so as to achieve greater performance. Vibration assisted diamond turning is a process that uses a precision ground diamond cutter capable of nanometer positioning to produce nearly error free shapes (within micrometers of those desired) with high quality surface finishes (roughness at the nanometer scale). With the help of vibration assisted turning, the high modulus and fracture toughness of diamond make for a tool that retains a uniform, sharp edge over the extended cutting distance up to kilometers (Ikawa et al, 1991).

The new achievement in the material removal process is vibration micro-milling of steel using diamond tools, which has been under intensive investigation since the early 1990s (Brinksmeier et al, 1999). Carbon containing materials such as steel do not lend themselves to being machined with diamond tools. It is theorized that the carbon in the material either diffuse or mechanically weakens the carbon bonds in the diamond to produce rapid wear. If a surface finish of the same magnitude common on materials such as copper and aluminum (< 50 nm) could be realized in the machining one step on steel parts, such as valve seats, higher performance as well as tremendous time and money savings could be realized.

1.1.3 History of vibration assisted machining

Precision metal cutting is defined as a cutting technique, which enables the production of optical, mechanical and electronic components with micrometer or sub-micrometer form accuracy and surface roughness within a few tens of nanometers (Brehl, 2008). Starting with

the United States in the mid 1960s, research into precision metal cutting was driven by the technological demands mainly from the defense and aerospace industries. While still very important to the military complex, precision metal cutting has expanded its field of application to touch almost every aspect of manufacturing, including moulds for contact lens production and non-spherical mirror arrays used in the most advanced scientific research satellites.

Vibration assisted machining was founded in the early 1960s when this technology achieved great things in drilling wood. The hydrostatic bearing with its sub-micrometer rotational accuracy was the first component of precision metal cutting to benefit from the research push. Along with the refinement of conventional machine components (spindles, metrology frames, etc.), the development of linear motors in the late 1970s and piezoelectric driven stages in the 1980s allowed for tool positioning and control on the nanometer scale. Not to be left out, materials research and the development of the monocrystalline diamond tool with its nanometric edge sharpness enable the levels of form error and surface roughness lowered even further (Brehl, 2008).

The technology discovered and/or refined over the past 40 years has found its way into one of three primary machining techniques: turning, planing or milling. Of these, turning has established itself as the relevant method due to its combination of relatively short machining time and high quality surface finish. Regardless of which manufacturing process is used, an additional polishing step is sometimes required to meet the ever increasing demand of industry for better surface finish and higher form accuracy.

1.2 Aim and objectives of the research

Aim of the research

The research aims to get a scientific understanding of the vibration assisted machining process against the material removal rate, surface roughness generation and tool wear. The research includes the machining system development, process modelling, simulation and optimization, and application of case studies.

The research uses a systematic approach based on the desktop vibration assisted micro-milling machine designed and built by the author.

Objectives of the research

The distinct objectives of the research are as follows:

- To develop a micro-milling test rig using a piezo-actuator as the vibration actuator.
- To model the vibration assisted machining process to predict the surface finish, tool wear and material removal rate.
- To design a program for user interface on LabView to control the piezo-driven device vibration mode options including vibration frequency, vibration amplitude, spindle speed and feed rate online during the cutting process.
- To develop algorithm on Ansys, Workbench, MatLab to investigate the 2D VAM cutting.
- To investigate the optimization and control of the vibration assisted machining process for selected application case studies.

1.3 Scope of the thesis

The thesis contents are planned and structured based on the research findings as grouped consecutively. This dissertation is divided into eight chapters as shown in Figure 1.1.

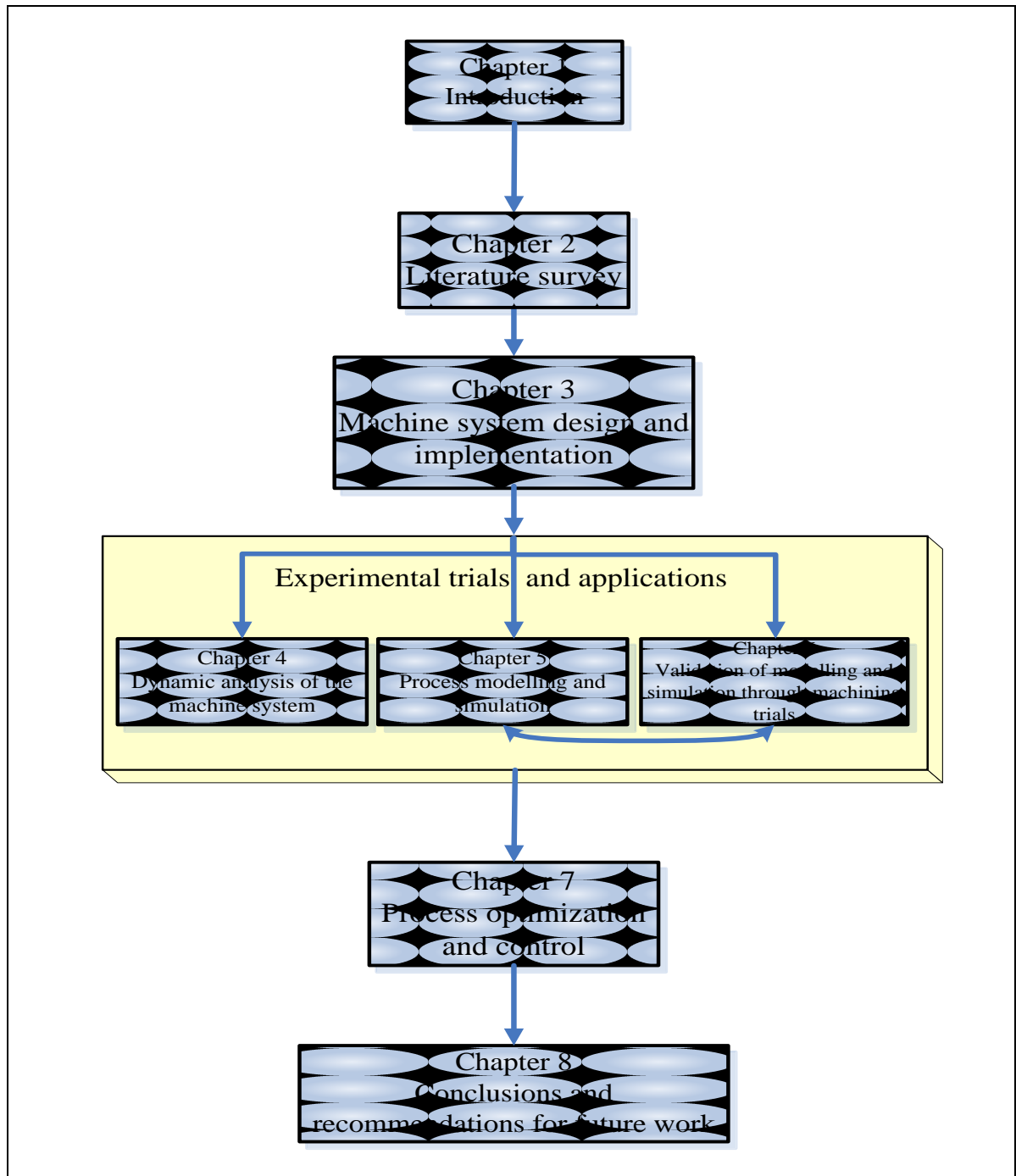


Figure 1.1: Structure of the thesis

Chapter 1 explains the historical background of the state of the art vibration assisted machining. It also consists of the current need of industries and a brief history of vibration assisted machining. The aim and objectives of the research have also been explained. Based on the objectives, the structure of this thesis is built and presented here.

Chapter 2 critically reviews the related ideas for the preparation of the research findings. The literature survey is responsible for the investigations of relevant and effective research to identify the related works that have been implemented on the vibration assisted machining based technology. Initially vibration assisted machining systems based on cutting process method were studied. A survey of recent developments in vibration assisted machining with their achievements is explained in this chapter. The discussion of machine design factors for test bed and piezo-actuator toward a response parameter system is carried out to highlight the errors of this system in this research area. With implementation of measurement on surface roughness, the tool wear and material removal rate are analysed.

Chapter 3 describes the system development design and implementation. This presents descriptions of software and hardware, focusing on the development and component assembly. The software and controller have been used, such as LabView 7.1 and MATLAB simulink, Ansys 11.0, Workbench and Mechanical Dekstop V2007 application software packages. Hardware devices took a part for these researches are piezo- electric XY stage, air bearing spindle with brushless motor, Physik Instrumente DC motor controlled X linear stage, data acquisition (DAQ) card, piezo-actuator amplifier and are also presented. Surface roughness measurement with equipment, such as the 3D Zygo Surface profiler explained in this chapter.

Chapter 4 focuses on investigating the machine dynamics of test bed. It includes the piezo-actuator analysis and machine dynamic behaviour by using Ansys and Ansys Workbench. These include all the dynamic simulation models, which are static structural, modal analysis, harmonic analysis, frequency response, etc. These investigations will be validated using hammer testing and modelling simulation. The limitation of the piezo-actuator in electrical and thermal failure will be described with different types of parameter condition. For piezo

side, the driving response and electric capacitive response towards the synoptic of a driving system has been discussed by presenting the modelling and controller using the, LabView and Physik Intrumente software.

Chapter 5 presents a process modelling approach which will elaborate the simulation of the cutting process, modelling and surface generation and the motivation to use MatLab programming in the research. The discussion of modelling is focused on the cutting force, cutting tool trajectory, cutting mechanics and machine dynamics which is adopted from conventional machining. The related factors in 2D VAM are discussed and in depth investigation of tool temperature, chip thickness and chip formation presented. The comparative investigation between conventional and 2D VAM for its potential is discussed in great detail.

Chapter 6 reports the validations of the modelling through machining trials. These include the experimental plan, facilities and workpiece material and the condition monitoring of machine. The cutting forces, surface roughness, tool wear and material removal rate have been evaluated and validated between the simulation with 2D VAM and without 2D VAM. In addition, the effect of significant variables and machining parameters on the responses is further analyzed with the results from both the machining trials and the simulation.

Chapter 7 presents a discussion of the machining results, evaluation and optimum condition of the 2D VAM cutting process. The interactions between the each key parameter have been outlined for further future analysis.

Chapter 8 highlights the conclusions drawn from the research work and recommendations for future work.

Chapter 2 Literature survey

2.1 Introduction

Vibration assisted cutting is a cutting method in which periodic or oscillating cycles are imposed on the cutting tool or the workpiece, besides the original relative motion between these two, so as to get improvements in cutting performance. The fundamental feature of vibration assisted cutting is that the tool face is separated from the workpiece repeatedly. Historically, this technique was first employed in the precision drilling of wood and low carbon steel (Cerniway, 2005).

Vibration cutting started in the mid 1970s. It was reported in the beginning when this technique was used that the cutting tool underwent a circular distance of displacement towards the individual axis (X or Y or Z). Early experiments were primarily carried out at frequencies greater than 20 kHz. These “ultrasonic” frequencies were greater than 20 kHz. However, it showed vibration machining to have little practical value. It took nearly two decades of slow growth before this technology started to show promise.

Finally, in the early 1990s, research into vibration cutting at both low and high frequency produced results sufficient for industrial applications (Shamoto, 1991). This mature class of machining is called Vibration Assisted Machining (VAM).

It has been reported by Adachi and Arai (1997) that, unlike ultrasonic vibration cutting, low frequency vibration cutting has been found to prolong tool life and help reduce burr sizes in drilling. They developed an electro-hydraulic servo system to generate vibrations of 1,000 Hz in the spindle of an NC machine. Through their experimental studies on drilling aluminium, they found that burr size could be reduced considerably with the assistance of vibration in low frequency, especially 1,000 Hz.

The literature survey in this research covers all relevant as shown in Figure 2.1. The main element is the building up of the vibration assisted machining test rig where the applications

and various investigations can be carried out to analyse improvement, which is critical and essential in this research.

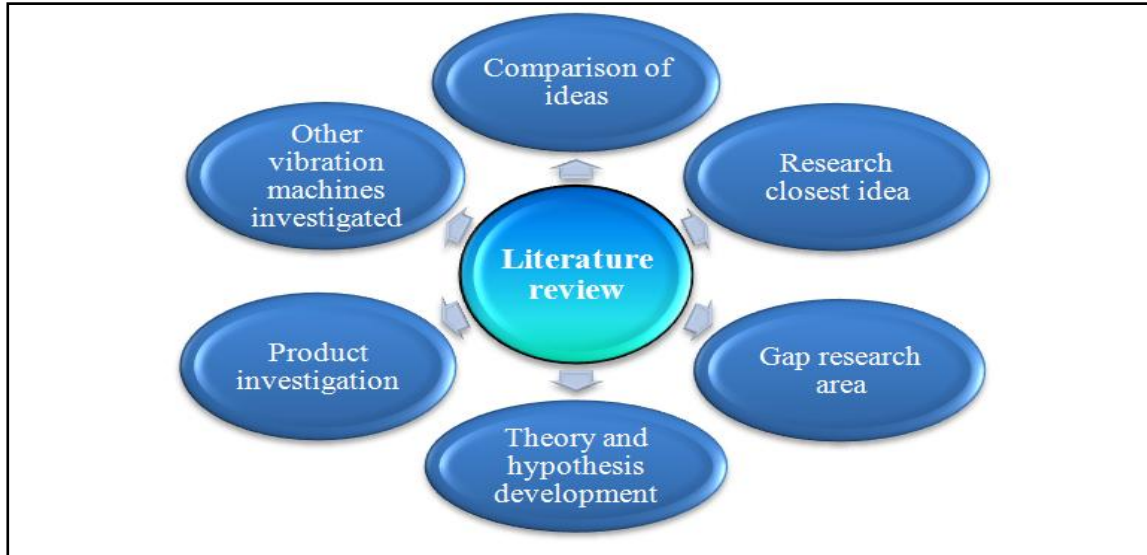


Figure 2.1: The aspect of literature survey

2.2 Vibration assisted machining

Vibration assisted machining techniques are becoming very demanding in many recent engineering developments, especially in relation to material removal rate, surface finish and tool wear. Generally, all vibration cutting has a common and different background. All the principal research has focused on the vibration itself. The main component used in the vibration cutting was the vibration generator. Figure 2.2 shows the fundamentals of vibration assisted machining in a wide range of applications.

The very basic component of vibration assisted machining is a piezo-actuator. Taking this stage as a starting point, many designs of the piezo-actuator have been developed into various application requirements, such as vibration assisted turning, milling, drilling, grinding, electric discharge machining (EDM) and, recently, the combination of electric discharge micro-milling with vibration assisted machining has been reported (Endo et al. 2008).

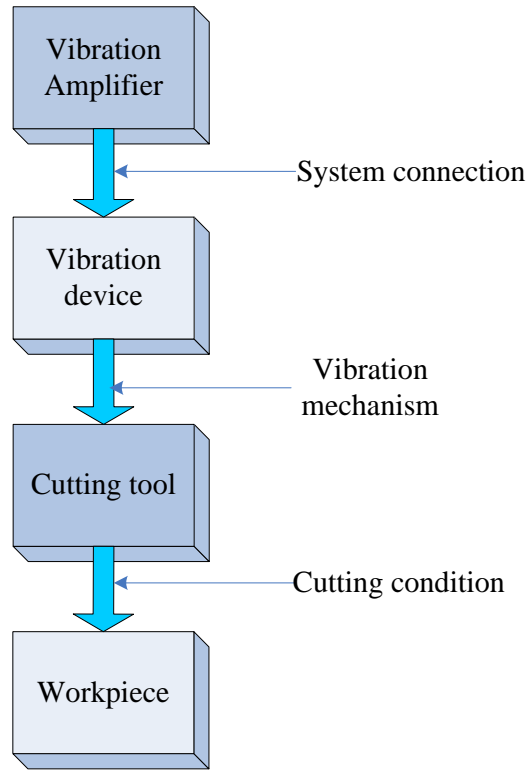


Figure 2.2: Block diagram of a VAM system

Vibration assisted machining technology has been studied by many cited references. All of these studies analyze in different ways the concept, design dynamics, characteristics and behaviours of vibrations by looking at surface generation, tool life and material removal rate.

Chern and Lee (2005) developed a milling machine with a vibration table, which vibrates the table holding a workpiece. They found that hole oversize, displacement of the hole centre and surface roughness of the drilled wall could be improved with the increase of vibrating frequency and amplitude. The results have demonstrated the potential of the vibration technique to be developed into a useful tool for enhancing the drilling technology.

Adachi and Arai (1997) found how to prolong tool life and help reduce burr sizes in drilling. They developed an electronic servo that vibrates in low frequency up to 1,000 Hz. Through their experimental studies on drilling of aluminum, they found that burr size could be reduced considerably with the assistance of VC. They built their servo machine on the

spindle of the NC milling machine. An advantage of this design is the ease with which it can be modified for different applications. The purpose of their work was to develop a technique applicable to the drilling process for surface-roughness measurement in the wall paths.

Wang and Zhou (2002) proved by their experiments they could cut hard and brittle materials in high critical depth of cut. By applying an ultrasonic diamond tool tip a surface roughness of 100 nm was achieved. The material cut was a fused silica with cutting conditions: vibration amplitude 3 μm , vibration frequency 40 kHz, spindle speed 90 rpm and feedrate 5 $\mu\text{m}/\text{rev}$. They also proposed the fundamental principles and material removal mechanism of ultrasonic machining, which is developed to measure both dimensions and surface roughness simultaneously. The principle of the developed vibration is based on the displacement curve of the tool tip through a cycle of the vibrations on the tool tip.

Wu and Fan (2003) developed a centreless grinding technique called the ultrasonic elliptic-vibration shoe centreless grinding. This new method employs an ultrasonic elliptic-vibration shoe to support the workpiece and control the workpiece rotational motion instead of using a regulating wheel such as that employed in conventional centreless grinding. The vibration ellipse is applied into the shoe or bed of the workpiece with frequency of 20 kHz. The shoe is given an intermittent force in micron scale to push the cylindrical workpiece towards a spot between the bed and the grinding wheel. They discovered the rotation of the workpiece was controlled by the friction force between the workpiece and the shoe so that the peripheral speed of the workpiece is the same as the bending vibration speed on the shoe end-face. On the other hand, the geometry or roundness of the workpiece can be controlled by tilting the two angles γ for shoe and ϕ for bed piezo.

Vibration assisted machining technology based on the piezo-electric actuator method is improving year by year. In the article by Brehl (2008), the objective was to assess the potential of applying vibration in machining understanding of zero burrs. From his finding, the process does not allow a complex shape to be made without grinding and polishing. Surface roughness and tool life are very important in the metal removal processes focused on diamond cutting of ferrous materials. It was found that tool life is extended by 1D and 2D

vibration assisted machining. From another point of view, vibration assisted machining experiments in steel, glass, and brittle ceramics confirmed that diamond tool life could be extended to allow economic machining of such materials and also demonstrated improvements in surface finish and ductile cutting when compared to conventional machining. The use of 1D vibration assisted machining led to significantly greater interest in 2D vibration assisted machining, starting in the mid-1980s (Brehl, 2008).

In their investigation of cutting aerospace materials, Babitsky and Kalanishikov (2003) made an experiment with a turning machine. The ultrasonic vibration process has a common problem when the load applied to the cutting tip and in results the loss of cutting efficiency. Through their experiment, the reduction of tip velocity also occurs during the cutting process due to the cutting tip's interaction with the workpiece, so the upper limit on surface speed is further reduced.

However, it can be eliminated with an auto-resonant control system. Efficient vibration cutting comes from the vibration design structure itself. They used bolted Langevin type transducers with maximum displacement of 20 μm and with maximum frequency of 20 kHz can improving the displacement efficiency. The reason for all of the improvements was a change in the nature of the cutting process, which was transformed into a multi-impact high frequency interaction between the tool and workpiece, giving a decrease in cutting force up to several times. The result has improved surface roughness by some 50% and noise reduction by 50%.

A simulation study to investigate vibration assisted machining was carried out by Cerniway (2005). This was achieved by using a computer technique which simulates the effect of Horizontal Speed Ratio (HSR) produced from kinematic tool tip surfaces, where a percentage of tool cycling between touched and untouched areas on the workpiece surface was calculated. The author proposed an initial attempt to evolve an application of the cycling or oscillating assessment technique by investigating how the frequency and amplitude of the machining tool tip location compared simulation.

2.3 Vibration assisted machining systems

The typical vibration assisted machining system consists of three main parts which are the data output (from desktop computer), data acquisition card (DAQ) and the vibration device (piezo actuator). The process involves the analogue and continuous time signals controlled by the LabView 7.1 software that transfers through signal conditioning circuitry in the data acquisition card and is amplified by an amplifier into the desired voltage and thus to the piezo actuator device.

Travis (1998) claims that DAQ is simply the process of measuring a real-world signal, such as the voltage or frequency, and bringing information into the computer for processing, analysis, storage, or other data manipulation. An overall system framework can be seen in Figure 2.3.

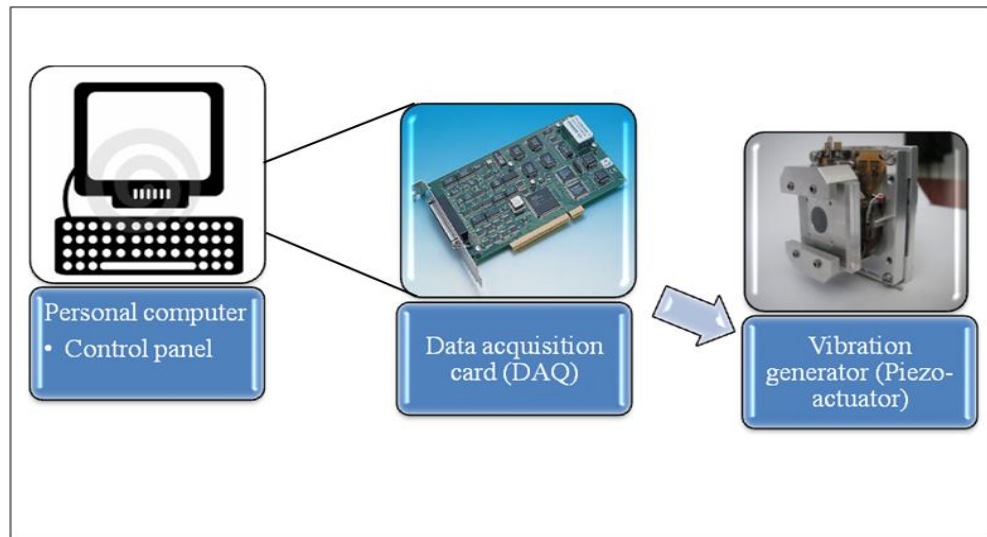


Figure 2.3: Basic system in 2D VAM

Suzuki and Nakamura (2003) constructed control systems by using data acquisition as a medium between the controller and actuator device. The acquisition is to keep and monitor the elliptical vibration to have a desired locus, where the amplitudes of the two directional vibrations and their phase shift are kept to the desired values, and the vibration frequency is locked to an average value of their resonant frequencies. Their idea was to locate the vibration control system which is mounted on the ultra-precision planing machine consisting

of three feed tables with double hydrostatic oil guideways in XYZ axes, two rotary index tables in B, C axes and a five axis control system.

The development of the elliptical vibration cutting system is applied to ultra-precision diamond planing of hardened die steel, and a high quality mirror surface finish is obtained over a large area of the whole finished surface. The maximum roughness was $0.04 \mu\text{m Ra}$, although the cutting distance reached 1,110 m. On the other hand, the surface finished by ordinary cutting without vibration was cloudy with maximum roughness of more than $0.52 \mu\text{m Ra}$, within a cutting distance of 1 km. Based on this advantage, the elliptical vibration cutting system was successfully applied to ultra-precision micromachining of dies for manufacturing the front light panel of the LCD.

An optical quality surface with fine microgrooves over a large area of $122 \times 91 \text{ mm}^2$ and with surface roughness of less than $0.04 \mu\text{m Ra}$ was obtained by the developed system. This is difficult for any conventional machining methods, including grinding, polishing and other ordinary cutting process.

2.3.1 Cutting mechanism in vibration assisted machining (VAM)

1D VAM

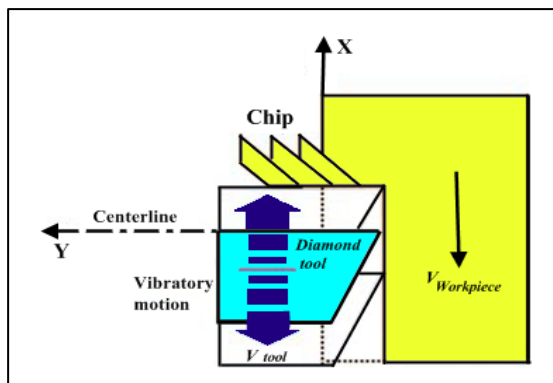


Figure 2.4: 1D vibration assisted cutting (Shamoto, 2004)

The 1D VAM moves in one plane parallel to the workpiece surfaces so as inline to the principal cutting force, as shown in Figure 2.4. By adding one more vibration motion a 2D

VAM system will be formed, moving the tool in elliptical tool motion (Figure 2.5). This can be observed when the major axis of the ellipse is inline with the cutting force and the minor axis is inline with the thrust force.

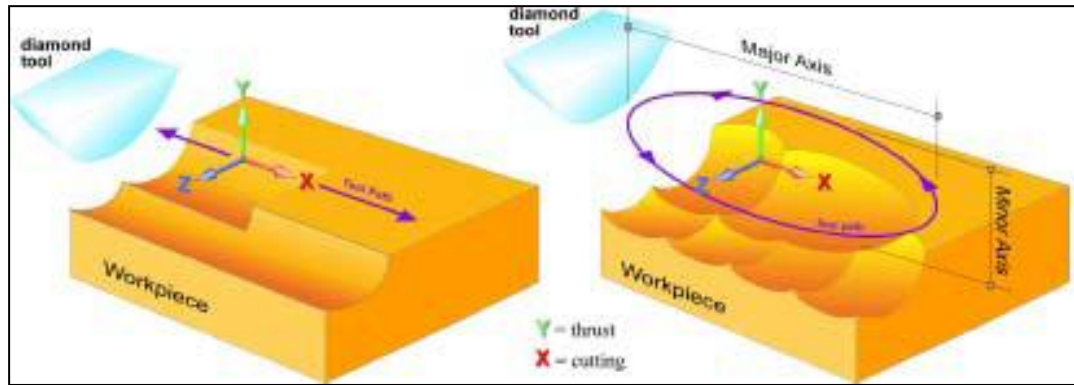


Figure 2.5: 1D and 2D elliptical vibration cutting (Cerniway, 2001)

Figure 2.6 shows the kinematic of 1D VAM where the tool is driven in a linear path subjected to the vibration frequency and vibration amplitude. It has been used by Shamoto, Moriwaki, Isaev, Kumbabe and Skelton, et. al. in their early investigations of vibration assisted machining. The intermittent contact of tool rake face relative to the workpiece is expressed as:

$$x(t) = A \sin(\omega) + Vt \quad (2.1)$$

$$\dot{x}(t) = \omega A \cos(\omega) + V \quad (2.2)$$

and are the intermittent position and velocity at , A is a amplitude, is vibration frequency equal to and is a velocity. is positive in 1 and 2, but negative in 3 and 4, this phenomenon is results because is the relative velocity between tool and workpiece.

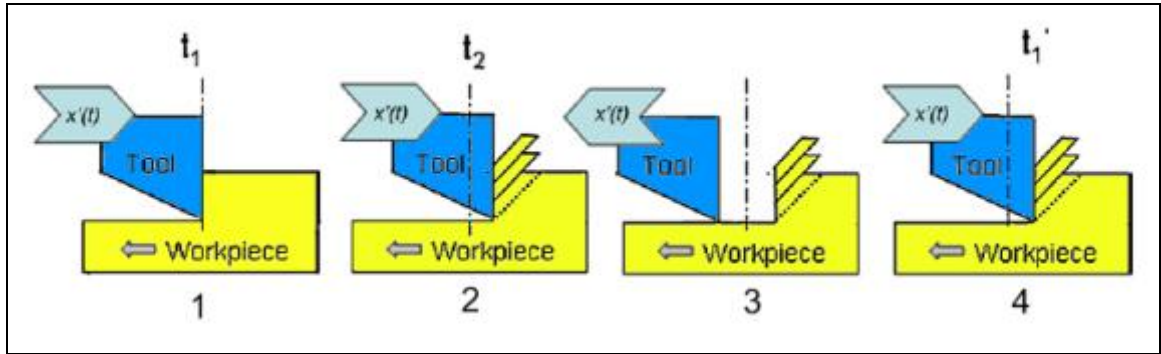


Figure 2.6: 1D vibration assisted machining (Dow, 2007)

2D VAM

Figure 2.7 shows the theory of reducing the cutting force in VAM which has been demonstrated experimentally by Shamoto and Moriwaki. Through their experimental study with low frequency systems operating at frequencies of 0 to 6 Hz they found that the instantaneous force (peak) cutting and thrust force are the same value as conventional cutting. But there is a zero time period when the tool has no cutting force at all. It is believed the zero cutting force condition came from the kinematic disengagement (tool separation) when there was a non-contact between the tool edge and the workpiece. Shamoto and Moriwaki have claimed that the reduction of cutting force was approximately 30% to 40% lower compared to conventional machining.

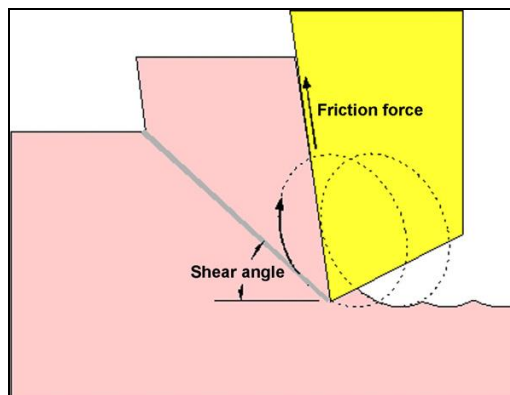


Figure 2.7: Shamoto and Moriwaki model for circular motion lifting phenomena

Ahmed (2007) claimed that the increase in the vibration amplitude leads to a 52% decrease in the average cutting force in vibration assisted machining. Again, it is because of an increase in part of a cycle of ultrasonic vibration without a contact between the tool and chip. An increase in the vibration frequency from 10 to 30 kHz results in a 47% drop in the level of average cutting forces, which could be attributed to an increased velocity of the tool vibration. Hence, an increase in either vibration frequency or amplitude leads to a decrease in cutting forces, which is beneficial to increasing accuracy and improving material removal rates.

2.3.2 Comparison between 1D and 2D VAM

Previous studies have shown that using one dimensional vibration assistance can extend tool life, lead to economies in machining, and also improvements in surface roughness compared to conventional machining (Wu and Fan, 2003). However, two dimensional vibrations assistance is much more effective, reliable and beneficial to the cutting process. The addition of vertical harmonic motion will bring the tool edge motion into a circle or ellipse that will impose an upfeed motion related to the workpiece. Experimental studies in previous research found the tool forces in two dimensional vibrations assistance are consistently smaller than one dimensional, even with the same tool geometry and machining conditions (Skelton and Wang, 2002). Average tool forces were reduced to 20% by one dimensional machining and by addition 2% more for two dimensional machining when compared with conventional machining.

Shamoto and Weber (1999, 1984) machined both ferrous and non-ferrous material using diamond and carbide tools. As shown by their experimental studies, longer tool life can be achieved by using two dimensional vibrations instead of one dimensional machining with the same condition of tool geometry, depth of cut and tool-workpiece material combination.

Figure 2.8 shows average thrust force versus cutting distance in meters in 1 D VAM (▲), conventional machining (◆) and 2D VAM (●). It is a major improvement when the thrust force drops to 20% of the conventional machining for 1D VAM and 2% more in 2D VAM.

The typical data were measured during cutting aluminium using carbide tools, but with no details about VAM conditions (Zhou, et al 2002).

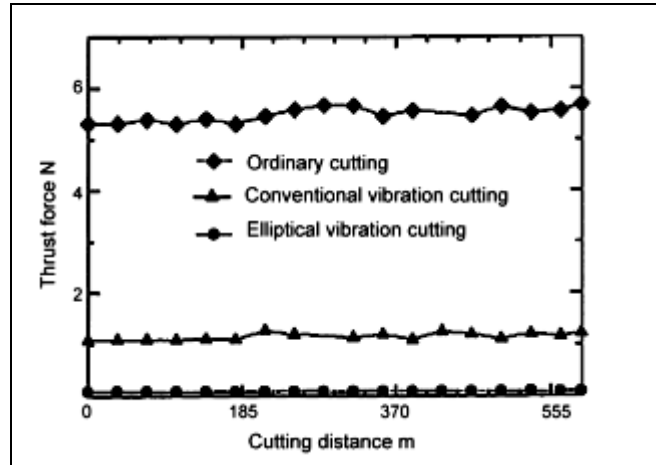


Figure 2.8: Comparison of thrust forces in 3 machining methods (Ma, 2004)

Significant improvements in accuracy have been achieved by two dimensional vibration assistance as measured by surface roughness and form, with reductions of up to 95% using two dimensional vibrations and 40% using one dimensional vibration (Brehl, 2007). Two dimensional vibrations also showed almost no burr formation, in comparison with the 60% to 80% reduction of burrs using one dimensional vibration, compared with conventional machining.

VAM actuator design

The evolution and market trending for vibration cutting changed rapidly when more researchers enhanced the piezo-actuator in their machine design on the shop floor. Circa, 1980-1990, developed a 1D actuation servo in his early research on a turning machine at the Fraunhofer institute, as shown in Figure 2.9. His investigations focused on the vibration assisted turning using a diamond cutting tool on hard and brittle steel and glass (Klocke, 2004).

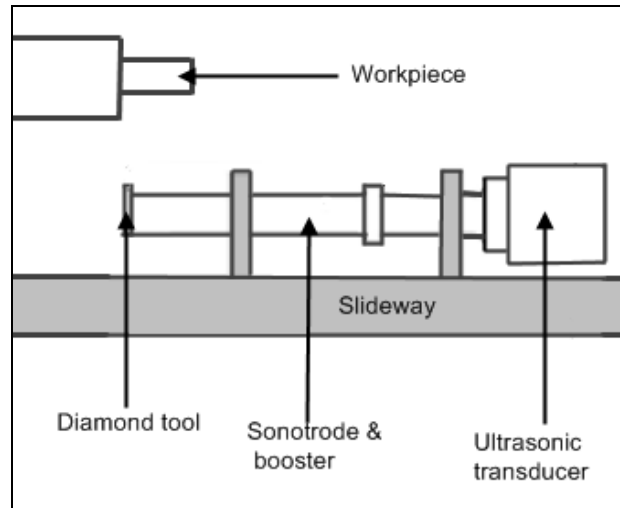


Figure 2.9: Fraunhofer servo design (Klocke, 2004)

Toh et al, 2004, developed a simple servo design. The operation of their servo design is similar to that of the Circa design, where the piezo-actuator transducer creates motion at longitudinal vibration and connected through a sonotrode to an amplification horn. Implementation of the non-amplifying resonator in his design brings the ultrasonic energy input and sets up a longitudinal resonance in the booster. The amplitude of the vibration is increased and this arrangement resulted in a $\pm 5 \mu\text{m}$ sinusoidal displacement of the diamond tool.

Following the principle of mass weight designed in the diamond cutting tool where the longitudinal is off in the centreline, some of the investigators noticed that the elliptical motion was possibly produced automatically. A researcher at the University of Bremen, Germany designed and constructed the elliptical motion from the imbalance of mass position, similar to the Fraunhofer design. It has been successfully proved that the Bremen design generates at 40 kHz, 700W ultrasonic generator coupled to a piezoelectric converter to produce a tool ellipse motion. By optimizing the sonotrode/booster arrangement, vertical amplitude of $6 \mu\text{m}$ was produced. The elliptical tool path is slightly tilted due to the phase of bending motion. Within certain limits, the elliptical motion of this servo could be controlled with the addition of a counterweight. Figure 2.10 illustrates this elliptical motion due to system imbalance and the orientation of the tool servo to the workpiece.

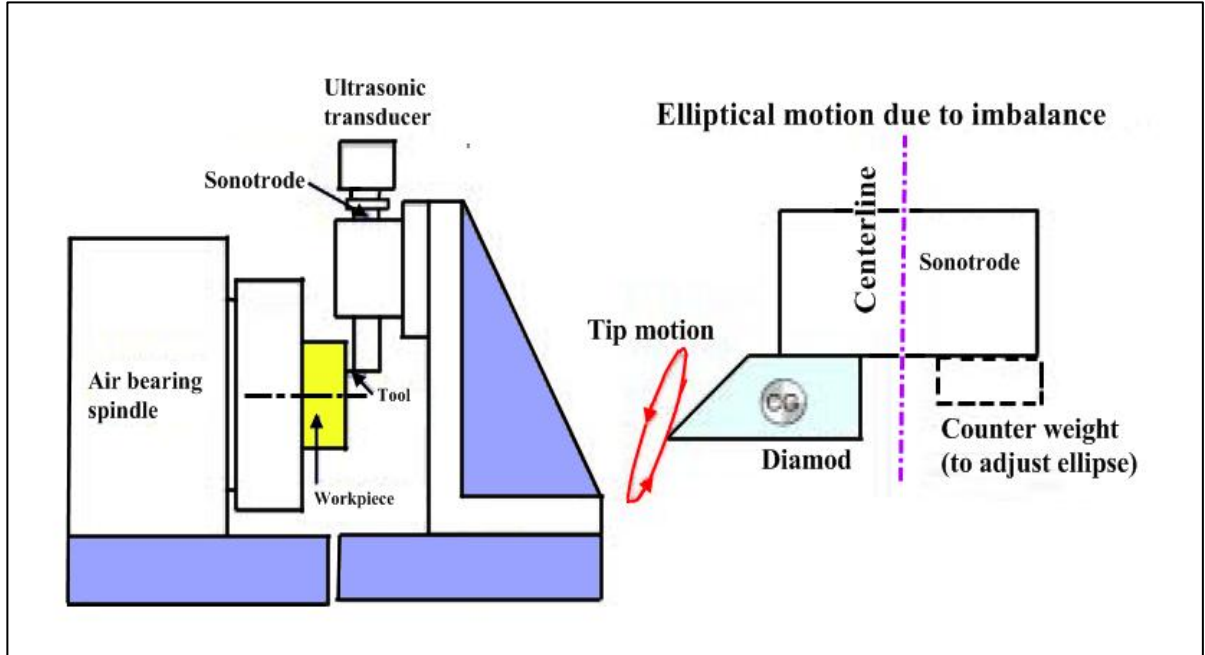


Figure 2.10: Servo design from Bremen University, Germany (Brinksmeir, 1999)

The success of the Bremen studies in servo design involving the diamond turning of steel shifted the focus away from 1D system to 2D system. As previously mentioned, aside from the dimension of cutting motion, servos operate either at or below resonance. The servos illustrated in Figures 2.9 and Figures 2.10 represent resonance and non-resonance designs respectively.

The research effort in vibration assisted machining allowed the researcher from Pusan University to design a two stacked piezo-actuator integrated into the tool holder, as shown in Figure 2.11. It is a non-resonant design utilizing two piezoelectric actuators oriented 90° parallel to each other. The flexures design is to eliminate the shear stress on the tool holder. The design of the flexure eliminates shear stress in one stack by the motion of the other (Hwan, et al, 1999). The tool path is a summation of two arcs, which produces a quasi-ellipse. This research effort was aimed at improving the machining accuracy of micro-scale parts by using elliptical vibration cutting.

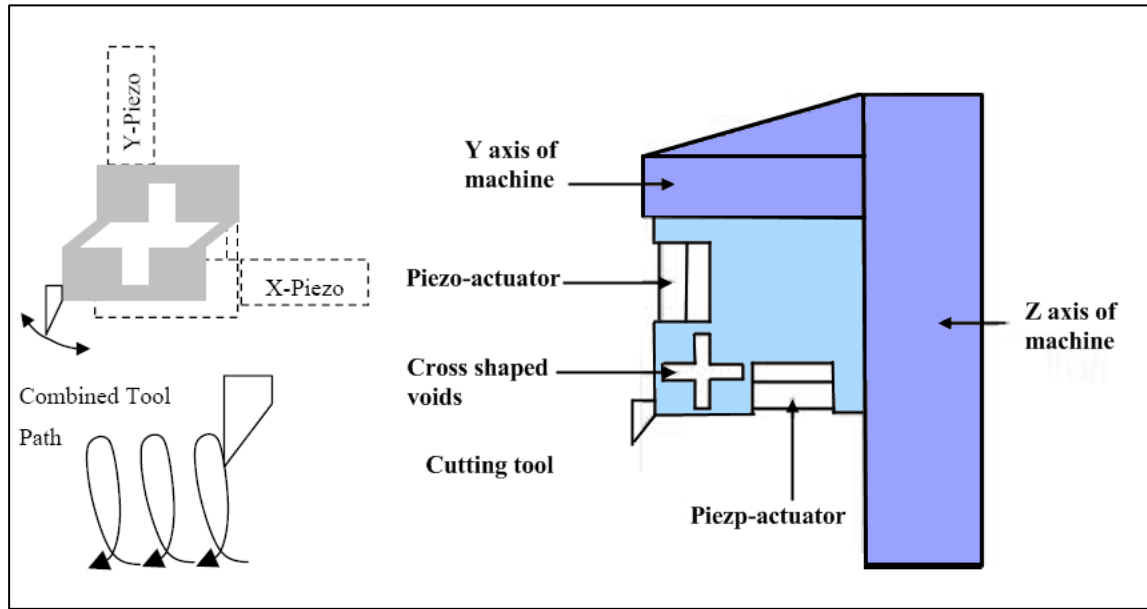


Figure 2.11: Servo design from Pusan National University, Korea

In 1999, Shamoto and Moriwaki developed a 2D servo using piezo stack in 2 directions to give ellipse tool motion, as shown in Figure 2.12. It efficiently operates at a resonance frequency of 20 kHz and produces an amplitude of 3.5 μm . The natural frequency of their machine was less than 5,000 Hz. Their investigation focused on the benefits of vibration diamond cutting of hardened steel towards the surface roughness and tool wear. This tool servo operated at the third resonant bending mode to produce a circular path.

Unlike previous designs where the actuators were in the same plane as the generated tool path, the actuators are perpendicular to the tool path. They found through their experiment using a single-crystal diamond tool-tip that cutting fused silica can be achieved even for 2 μm depth of cut. The increase in the critical depth of cut is significant and is a function of the ratio of vibration speed to cutting speed. A surface roughness R_a of 100 nm was obtained for up to 2 μm depth of cut.

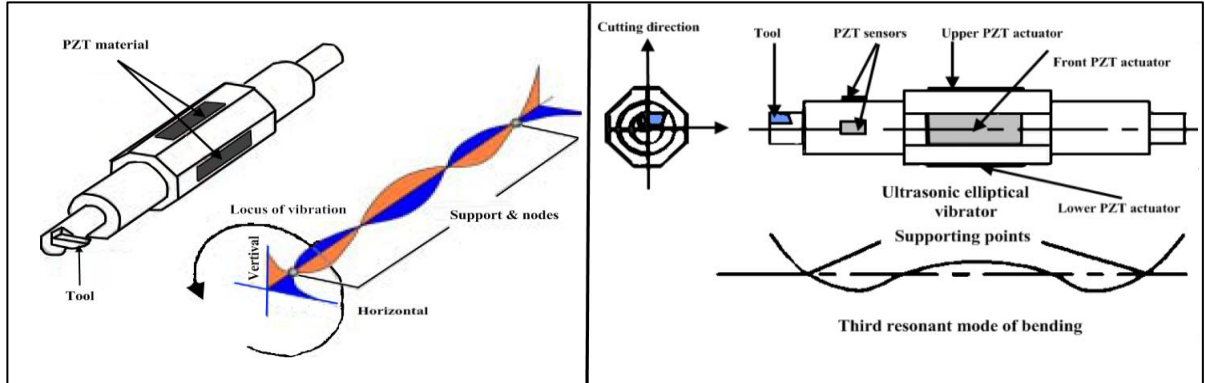


Figure 2.12: Resonant servo design by Kobe University, Japan (Moriwaki, 1999)

2.3.3 System specifications

In dealing with piezo-electric components, the tool servos on the VAM can be divided into two main categories:

i) Resonance

The vibration in an elliptical tool path at a resonant frequency in two directional tool motions is called the resonant system. Where the piezoelectric actuators are attached to the opposite side in 90° of the beam structure. The combination of the two bending vibrations makes the tool move in an elliptical path. Normally, it has advantages for tool vibration working at the greater frequency than 20 kHz. However, it is a limited service that can only operate at discrete frequencies and displacement amplitudes less than $6 \mu\text{m}$ (Figure 2.12).

ii) Non-resonance

Unlike resonant systems, non-resonance uses a mechanical linkage to convert the expansion and contraction of piezoelectric actuators into an elliptical tool path. The design of tool holder acts as the linkage. For a non-resonance system, the piezo-actuator component operates under the first natural frequency. This system can operate in a wide range of tool path. The huge working range in operating frequencies has been offered as well as amplitudes greater than ten times from the resonance servos. The disadvantage of this servo is that it required a large amount of electric energy to increase the performance in terms of displacement and frequency (Figure 2.11).

2.4 Dynamic machining system identification

Modern experimental modal analysis techniques have been reviewed by Schwarz and Richardson (1997). The three main topics pertaining to modal testing were covered: Frequency Response Function (FRF) measurement techniques, excitation techniques, and modal parameter estimation (curve fitting) methods. They also included in their work the knowledge that modes are used as a simple and efficient means of characterizing resonant vibration. The majority of structures can be made to resonate, that is, under the proper conditions, a structure can be made to vibrate with excessive, sustained, oscillatory motion. Modes (or resonances) are inherent properties of a structure where resonances are determined by the material properties (mass, stiffness, and damping properties), and boundary conditions of the structure. Each mode is defined by a natural (modal or resonant) frequency, modal damping and a mode shape.

The disturbance of force in a machine system is caused by a number of machining problems including bearing wear and failure, poor surface roughness, low product quality and higher energy consumption. Huo and Cheng (2009) investigate loop stiffness in the machine tool workpiece system. Through their experimental studies, the static loop stiffness and dynamic loop stiffness are very important things to consider in machine design. The deformation of machine or modal shape leads to high impact on the machine instability. From their point of view, the desired product quality is strongly dependent on the machining instability.

In addition, if either the material properties or the boundary conditions of a structure change, its modes will change. For instance, if mass is added to a machine structure, it will vibrate differently because its modes have changed. At or near the natural frequency of a mode, the overall vibration shape (operating deflection shape) of a machine or structure will tend to be dominated by the mode shape of the resonance.

All vibration is a combination of both forced and resonant vibration. Forced vibration can be due to internally generated forces, imbalances, external loads or ambient excitation. A further elaboration is that resonant vibration occurs when one or more of the resonances or

natural modes of vibration of a machine or structure are excited. Resonant vibration typically amplifies the vibration response far beyond the level of deflection, stress, and strain caused by static loading.

A statistical investigation of modal parameters of cutting tools in dry turning was carried out and published by Thomas and Beauchamp (1994). This distinguishes the significance of machining system modal identification factors and their effects. It is very important that optimized cutting parameters be selected in controlling the required product quality.

Thomas and Beauchamp also mentioned that surface roughness does not depend solely on the feed rate, the tool nose radius and cutting speed; the surface can also be deteriorated by excessive tool vibrations, built-up edge, friction of the cut surface against the tool point, and the embedding of the particles of the materials being machined.

In addition, forces - which can be considered as the sum of steady, harmonic and random forces - act on the cutting tool and contribute to the modification of the dynamic response of the tool by affecting its stiffness and damping. Their study focuses on the collection and analysis of cutting-force, tool-vibration and tool-modal-parameter data generated by lathe dry turning of mild carbon steel samples at different speeds, feeds, depths of cut, tool nose radii, tool lengths and workpiece lengths. Furthermore, this analysis investigated the effect of each cutting parameter on tool stiffness and damping and yielded an empirical model for predicting the behaviour of the tool stiffness variation.

Kim (2007) described how tool vibrations affect surface profiles at the microscopic level in the form of flutes whose number, orientation and spacing are determined by the integer and fraction of the frequency ratio of the tool vibration to the spindle speed. Kim has also proposed a metrological scheme to identify any existence of tool vibration with the minimum effort of surface measurement and analysis. As a systematic approach to identifying tool frequency from measured surface profiles, two methods have been proposed of spiral and radial-circumferential analysis using microscopic surface profile data obtained by phase measuring interferometry. Concluding from the computer simulation and experimental results it has been proven that Kim's approach is well capable of identifying

any existence of tool vibration with a minimum effort of surface measurement, tool wear and material removal rate and analysis.

Cho and Eman (1990) proposed a work study in solving the main problems associated with the in-process identification of the instantaneous dynamics of a machining system. The main problems are related to the time variant nature of the process and the three dimensionality of the system, which lead to complex analytical procedures and are both closely associated with the experimental difficulties. During the cutting experiments, the parameters of the machining process change due to factors such as temperature rise, tool wear, changing dynamic receptance along the feed direction, etc. Hence, a cutting experiment imposes the requirement that, for the identification of the instantaneous dynamics, relatively short data records must be used during which the system may be considered time invariant. They have concluded that the three dimensional closed loop milling dynamics were formulated in the form of a multi-variate time series model whose parameters can be estimated from relative displacements and force components measured under actual cutting conditions.

2.5 3D surface profiler

Zygo Corporation is a special equipment manufacturer that specializes in optical systems and equipment for areas such as optical metrology. Zygo's metrology systems are based on optical interferometry measuring displacement, surface figure, and optical wave front. Metrology and optical markets for end-user and OEM applications include semiconductor capital equipment, aerospace, automotive and research. Now in its fourth decade, Zygo Corporation leverages its core competencies in metrology and optics to serve a worldwide customer base. Recognized as a valued partner by its customers for its innovation, technology and responsiveness, the company assists these customers in becoming leaders in their respective markets.

In this research, a Zygo 3D surface profiler is substantially used for evaluation and validation of the models, simulations and the cutting trials.

2.6 Simulations

Traditionally, the formal modelling of the systems has been via a mathematical model, which attempts to find analytical solutions to problem which enable the prediction of the behaviour of the system from a set of parameters and initial conditions. While computer simulation might use some algorithms from purely mathematical models, computers can combine simulations with the reality of actual events, such as generating input responses, to simulate test subjects that are no longer present. Whereas the missing test subjects are being modelled, the system they use could be the actual equipment, revealing performance limits or defects in long-term use by the simulated users.

2.7 Optimisation and control

2.7.1 Minitab

The optimisation and control for this work has been carried out using Minitab R16. This powerful software package is easy to use, user friendly, flexible and can be installed on a personal computer in Windows and Mac operating systems. Minitab can perform a wide range of statistical analysis including Taguchi, response surface methodology and ANOVA. It is specially designed for students, researchers, planners, marketing, and those who are not familiar with using a computer or using complicated software. The number of worksheets that can be opened at one time is only limited by the computer's memory. By default setup, it can handle up to 100,000 cells or data items in one operation to process without missing values.

Data may either be entered via the PC's keyboard or retrieved from a file on disk. For convenience format it can be opened also in Microsoft excel and Matlab may then be modified, transformed and saved on file from within Minitab. Printed copies of results appearing on the screen may be produced for examination at leisure. Minitab is largely self-documenting through its help facility, so that only a minimum of preparation is needed in order to use the package.

2.7.2 ANOVA

Coroner and Iman (1981) suggested that in many cases, when the data does not meet the assumptions of ANOVA (analysis of variance), one can replace each original item of data valued by its rank from 1 for the smallest to N for the largest, and then run a standard ANOVA calculation on the rank – transformed data. Where no equivalent nonparametric methods have yet been developed such as for the two-way design, rank transformation results in tests are more robust to non-normality, and resistant to outliers and non-constant variance, than ANOVA without the transformation applied to the ranks, such that the resulting values have some defined distribution (often a normal distribution with a specified mean and variance). Further analysis of quantile-normalized may then assume the distribution to compute significant values.

2.8 Summary

This chapter has presented a literature survey with a critical review on the previous studies. The subtopics represent the structure of the research undertaken into 2D vibration assisted desktop micro-milling and its perspectives. Different types of vibration setup system based on various designs are presented.

The techniques of electrical controlled and data acquisition are the two used in any interfacing piezo-electric system. The effect of machine design including the piezo-attached on the machine has been discussed, focusing on the mounting of the piezo-actuator stage also presented in this chapter. Investigation into the machine dynamic, such as natural frequency, harmonic response and resonance during machining, has also been explained.

These parameter dynamic effects of the machine towards the workpiece will be taken into account in order to verify the vibration assisted efficiency of the machine system. The investigation continues with the capabilities of the vibration in 1D and 2D mode systems in these research areas.

The previous works presented are adapted and improved to produce a novel idea in desktop milling machine development and its applications by using piezo-actuator as a vibration generator. The implementation of research work is carried out from mechanical design and construction, modelling programming and industrial applications, algorithms manipulations and results analysis and discussions and documented in the following chapters of this research report.

Chapter 3 Machine system design and implementation

3.1 Introduction

The machine was initially constructed to be a low cost industrial system. However, it is aimed at accuracy, reliability and compactness desktop micro-milling machines for vibration assisted machining on the shop floor. As presented in the research objectives, the machine aims to machine a hard and brittle material such as glass, ceramic, heat treated steel. Therefore, in this exploration stage, the aluminium T6061 has been chosen as a workpiece, which is a common material in the industry.

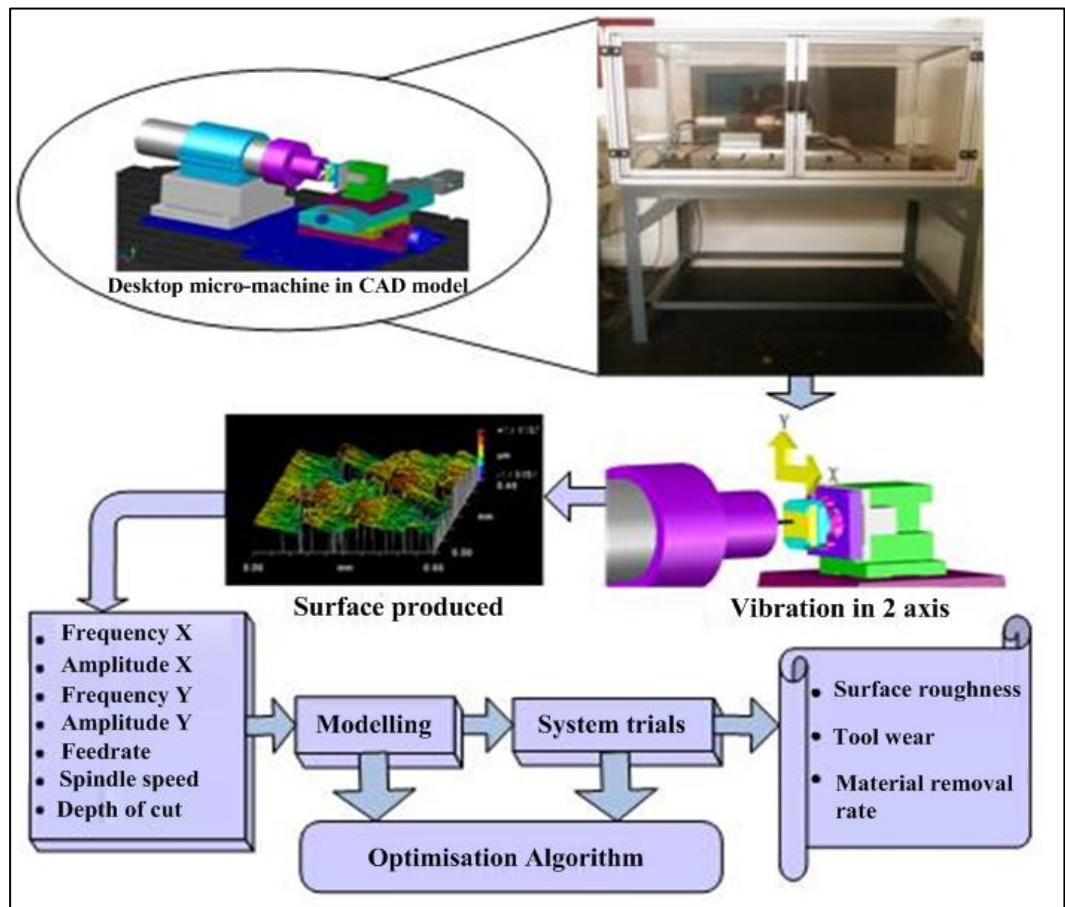


Figure 3.1: The modelling of desktop 2D vibration assisted micro-milling machine

Figure 3.1 shows the schematic illustration of the 2D vibration assisted micro-milling machine system. This machine is capable of cutting a workpiece in horizontal micro-milling operation and turning operation. The size of the workpiece depends on the jig and clamping design which is currently 30 mm × 30 mm × 6 mm in micro-milling and 50 mm diameter in turning.

Slocum (1992) has proposed that horizontal milling machines are generally more accurate than vertical spindle machines since the spindle is not cantilevered in a large C-shape support structure which is subject to greater deformation. It is because the load from the spindle acts as a point force on the column that horizontal machines are more rigid than vertical machines. Chip removal is also easier with respect to the gravitational direction. This advantage led to the mounting of the spindle in horizontal plane utilised in this desktop machine.

This chapter presents the conceptual design process of a desktop micro-milling machine developed by the author in collaboration with an industrial partner. The preliminary objective of this machine was to cut hard and brittle components made from glass, ceramics, etc., by using the XY25XS stage for vibration assistance. The research objectives include optimising the cutting parameters towards surface finish, and predicting tool wear and material removal rate during the cutting process. The final design specifications of the desktop micro machine are listed in Table 3.1.

Table 3.1: Machine specifications

Configuration	Desktop micro-machine for vibration assisted machining		
Base	100 x 40 x 10 cm metal table		
Axes	XY stage	X axis	Spindle
Type	Piezo actuator XY25XS	Linear motor	Air bearing
Stroke	X:20 μm Y:20 μm	100 mm	N/A

Stiffness	2.5 N/ μm	10 N/ μm	Radial 0.74 kg/ μm , Axial 6.8 kg/ μm
Motion accuracy	0.1 μm	1 μm	$\leq 0.05 \mu\text{m}$
Resolution	0.2 nm	0.0085 μm	N/A
Drive system	Servo amplifier	Servo motor	DC brushless motor
Maximum speed	3,000 Hz	1,000 mm/min	15,000 rpm

At this stage, the selection of key components for precision has to be considered. These key components include the structure and material, spindle, slides, feed-drive, control unit, tools and fixtures. In building this desktop machine, the advantages and disadvantages of these components were analyzed and evaluated with respect to dynamic behaviour, accuracy and fundamentals. The FEA analysis and simulation method have been used to determine the ‘hidden’ characteristics of the machine structures presented in the next chapter.

The analysis results were used to check the conformance to the desktop specifications and then provide data for structural modification to speed up the decision-making process. To provide robust data in the decision making process, a number of experiments were done, followed by analysis using Ansys 11.0 and Ansys Workbench. The selection of testing methods included static analysis, dynamic analysis, frequency response function analysis and validation with simulation.

In addition, chip removal is also easier with respect to the gravitational direction. On selecting this concept as a decision process, the mounting of the spindle in horizontal has been incorporated in this desktop machine. The advantages of micro-milling with a horizontal spindle were proven by the spindle axis allowing chips to fall off much easier than a vertical spindle axis machine.

Brainstorming is a method often used to generate conceptual design. In this stage, the selection of key components in precision was considered. These key components include the structure and material, spindle, slides, feed-drive, control unit tool and fixtures etc. The

analysis result identifies, compensates, and will be used to check the conformance to the desktop specification.

3.2 Design approach and machine setup

The fundamental design was followed by the mounting of the XY stages to drive the excitation and allow the desktop horizontal micro-milling to perform horizontal face milling using vibration for the cutting process. The XY25XS stage piezo-electric component has the ability to excite with maximum amplitude 20 μm , and 3,000 Hz maximum frequency, in unloaded condition. In addition, a jig was designed to hold the workpiece in one parallel line to perform a slot cutting operation, giving the optimum cutting conditions during the cutting process.

The cutting force acted into the tool tips in the XYZ axis but will be maximum in the X direction as the feedrate direction is in this axis. According to the theory of vibration assisted machining (Cerniway, 2007), by applying vibration in the axis this will compensate and reduce the cutting force significantly. An air bearing spindle is mounted in horizontal axis to reduce the force acting in Z or depth of cut direction, which will cause problems in most machine designs.

The development of a desktop vibration assisted micro-milling machine system was designed to present a practical approach to using a piezo-actuator as a vibration generator to generate a vibration during the cutting process. The aim was to cut hard and brittle material and evaluate the performance of machined surfaces in terms of material removal rate, surface roughness and tool wear.

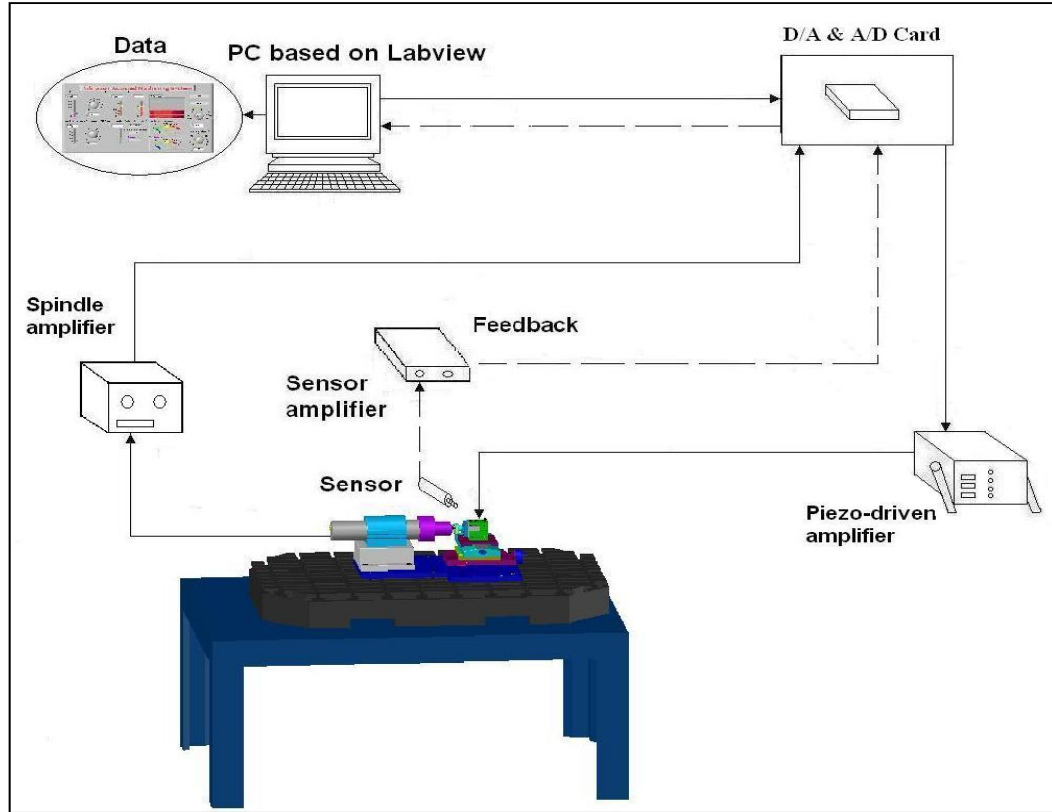


Figure 3.2: Schematic diagram of the VAM

An air bearing spindle with rotational speed of 15,000 rpm and spindle run-out of $0.1 \mu\text{m}$ was chosen to machine a slot with endmill diameter 1.0 mm. The air bearing spindle was mounted on the horizontal axis to reduce the force acting in the Z direction (depth of cut direction) which normally causes most problems in machine design. To facilitate relative motion between tool and workpiece, an electric linear stage 100.0 mm maximum displacement was selected with maximum feedrate (50 mm/min). Four piezo-electric stacks were assembled together to give a mechanical structure of 2 pairs of opposing X and Y axis vibration.

The overall size of the desktop machine was 550 x 500 x 300 mm excluding electronics and air supply system. In addition, to increase the rigidity of the desktop vibration assisted machine structure, a 25.0 mm thickness of aluminium T6061 was built as a platform for

component assembly on the top. This desktop machine was mounted on the 1,000 mm x 300 mm x 100 mm steel solid metal table to get improved stability, rigidity and accuracy.

The horizontal desktop micro-milling system is classified in the low range working frequency specifications in shop floor machine level. Basically, this machine design is carried from the other researchers' principle which uses piezo-actuator to vibrate a tool or workpiece. The machine plan to ensure the efficiency and reliability of the system is as illustrated before in Figure 3.2.

3.3 The input to the machine design

The actual setup of the desktop vibration assisted machining experiment is shown separately in Figures 3.2. It comprises a desktop machine setup, power supply unit, sensing devices, data acquisition interface for data acquisition and controller. The dynamic analysis investigation is initially started from static analyses and improved to dynamics where the arrangement of the experiment is carried out in a workshop environment. The condition of the workpiece trial is measured by using 3D Zygo surface profiler to verify the results obtained.

The equipment and component was provided by Cedrat Technology, Loadpoint Limited, Physik Instrumente (PI), National Instrument (NI) for piezo-actuator, air bearing spindle, linear slideway and data acquisition card respectively. Then the design and constructions of the experimental set-up were tested to make sure that the equipment is assembled in order to meet machining system requirements. The lists of equipment used in the experiment are introduced in the following sections.

3.4 Electrical hardware and machine design

3.4.1 XY25XS piezo-actuator

The XY25XS model of piezo-electric actuator provided by Cedrat Technologies SA is used as a vibration device and mounted into this desktop machine. In a wide range of machine

designs, the piezo-electric has been used for fine tool positioning in order to get a high accurate movement of the cutting tool.

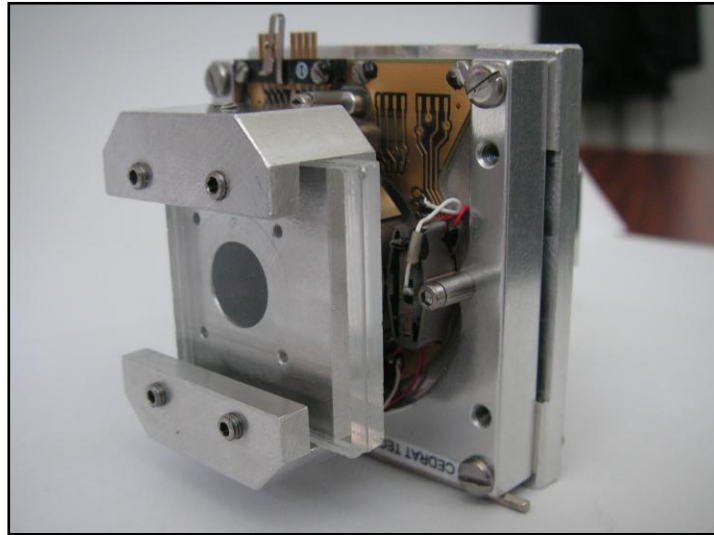


Figure 3.3: Piezo-electric actuator model XY25XS from Cedrat SA

This piezo-electric actuator was equipped with 4 mechanical hinges used to amplify the stroke length (displacement) in X and Y direction. It was designed and assembled with mechanical structure to give maximum and accurate displacement for each stroke, therefore minimizing hysteresis. The maximum stroke length was 20 μm with maximum no load displacement.

The stiffness, including the mechanical structure and piezo in X and Y direction, is 2.5 $\text{N}/\mu\text{m}$ under quasistatic excitation and blocked free. The actuation resolution is 0.2 nm. The full figure for XY25XS, including interfaces and jig for clamping a workpiece, is as shown in Figure 3.3, and the standard properties are listed shown in Table 3.2.

Table 3.2: Properties and standard technical data of piezo-actuator (Cedrat, 2009)

Properties	Standard technical condition	Unit	Nominal values	Min. Values	Max. Values
Sensor option	Strain gauges	-	-	-	-
Mastered motion	TX, TY	-	--	-	-
Max. no load displacement	Quasitatic excitation, blocked free	μm	20	18	23
Out of plane Z displacement	-	μm	0.5	0.3	0.7
Max. parasitic Z rotation	-	μrad	50.00	42.50	57.50
Max. parasitic XY rotation	-	μrad	40	32	48
Blocked force	Quasitatic excitation, blocked free	N	2.50	2.00	2.75
Stiffness	Quasitatic excitation, blocked free	$\text{N}/\mu\text{m}$	3,000	2,700	3,600
Unloaded resonance frequency (in the actuation direction)	Harmonic excitation, blocked-free, on the admittance curve	Hz	0.17	0.15	0.19
Capacitance	-	μF	0.5	0.45	0.65
Resolution	-	nm	0.20	-	-
Height	-	mm	18.0	17.9	18.10
Diameter	-	mm	45.00	44.90	45.10
Mass	-	g	80.0	-	-
Standard mechanical interface (Payload)	1 Dia. 17mm hole + 4 1.8 mm on 20 mm	-	-	-	-
Standard mechanical interface(frame)	4 dia. 2.8 mm holes on 45	-	-	-	-
Standard electrical interface	2 rgb17B/U coaxial cables	-	-	-	-



Figure 3.4: Piezo-electric power amplifier from Cedrat SA

The interface has been designed to assemble between interface holder and the fast tool servo. A round shape connection at the fast tool servo is tightened with H7 holes and screwed into a jig to transfer direct vibration signal for increasing the efficiency and reducing lag. XY25XS piezo-actuator is fixed between the jig and interface using $4 \times M3$ screw into mechanical structure.

Table 3.3: Standard technical specifications for the piezo amplifier

Reference	Unit	LA75A-2
Function	-	Linear amplifier
Main voltage	VDC	-20/180
Output voltage	V	-20 - 180
Maximum current (peak)	A	0.06
Maximal current (continuous)	A	1
Maximal output power (peak)	VA	50
Maximal output power	VA	16
Output load capacitance	μF	<30
Noise/signal ratio	%	0.01
Output bandwidth	Hz	100 Hz on 0.7 μF
DC offset setting	-	10 turn potentiometer
PZT connector		LEMO ERN.0.00250.CTL
External control input	-	BNC / 50 Ohms
Rear interface	-	DIN 41612 FormeC 64/94
Weight	Kg	0.2
Dimension	mm	10F wide, 3H high

The electric cable connected between piezo and amplifier uses LEMO 2 mini coaxial cable. The other end of the amplifier cable is connected to the CPU computer via data acquisition card (DAQ) which is approximately one half meter long coupled with 2 outputs for X and Y axes. This piezo-actuator used an amplifier provided by Cedrat Technologies as shown in Figure 3.4 and the standard technical specifications as shown in Table 3.3.

3.4.2 Air bearing spindle

The demand for air bearing spindles is on the rise because of the modern technological developments leading to increasing demand for rotation systems with lower

vibration, higher maximum rotational speed and low friction. Some notable features of air bearing spindles are as follows:

- extremely higher rotational speed
- higher accuracy
- good load capacity
- very low run-out
- maintenance free
- zero wear
- low friction

The air bearing spindles are suitable for high speed micro machining applications in a restricted space. They are ideal for high speed precision engineering applications. Figure 3.5 shows the air bearing spindle that used for this research.



Figure 3.5: Air bearing spindle from Loadpoint LTD

Considered in the decision making process, an air bearing spindle modelled GA02511 provided by Loadpoint LTD was chosen. The maximum rotation speed is 15,000 rpm, radial stiffness and axial stiffness are $7.4 \text{ N}/\mu\text{m}$ and $68 \text{ N}/\mu\text{m}$ respectively. It required 5.5 bar pressure inject to the casing through the orifice to float the spindle shaft. The air bearing spindle with run out was $0.5 \mu\text{m}$ during maximum speed 15,000 rpm.

This spindle is powered by Mk.5A amplifier at voltage range from 100 to 200 volts as shown in Figure 3.6. The characteristics of this air bearing spindle are below:

- Air supply pressure - 5.5 bar or 80 p.s.g
- Air consumption - 2.0 c.f.m free air 0.06 m³
- Radial load - 25 lbf or 12.3 kg
- Axial load - 70 lbf or 31.8 kg
- Maximum speed - 15,000 RPM
- Power output - 350 watts useable power at 15,000 RPM
- Motor - 3 phase, 0 – 46 volts, 0 – 300Hz



Figure 3.6: Spindle amplifier modelled Mk 5A from Loadpoint LTD

3.4.3 X slideway

Mercury II, C-860.10, as shown in Figure 3.7, is a Single-Axis DC-Motor Controller which is produced by Physik Instrumente. It is used to move the workpiece mounted on the jig and interface. The Mercury, claimed by PI, is a miniaturized servo-controller intended for motion control in research and industrial applications. It provides, in a single package, a complete stand-alone control system for the smaller motors typically used in high-precision positioning systems. It is a closed loop system with minimum incremental motion 0.1 μm for linear movement travel along X axis.



Figure 3.7: X slideway driven by leadscrew

The tool is clamped at a horizontal angle of 180° perpendicular to the workpiece surface to perform slot milling operation. The design of interface and jig as a workpiece holder is fixed at the post holder on top of the PI slideway. The starter package comes with all connecting cables, power supply and software necessary for immediate operation.

Mercury is designed to operate motorized PI stages. The function of the mercury in the experiment is to control the XY slideway which is controlling the feedrate or cutting speed in the X axis directions. The controller can be programmed by using the Mercury software version 3.20 or LabVIEW programming software from a personal computer connected with RS232 cable. The 5 MHz oscilloscope was used for monitoring the output from DAQ Card-1200 from the National Instrument. LabVIEW graphic software is used for data acquisition interfacing.

3.4.4 Data acquisition card

DAQ card is simply the process of measuring a real-world signal, such as a voltage and bringing that information into the computer for processing, analysis, storage, or other data manipulation. DAQ card-1200 from National Instruments was used in the experiment and shown in Figure 3.8. It is a legacy low-cost, multifunction I/O card for PCMCIA and its features are as follows:



Figure 3.8: DAQ card from the National Instrument

- 100 kS/s, 12-Bit, 8 eight single-ended or four differential analogue inputs.
- 2 12-bit analogue outputs, 24 digital I/O lines.
- Three 16-bit, 8 MHz counter/timers.
- NI-DAQ driver software, version 6.9.1 or earlier.
- Sampling rates - up to 500 kS/s.

The DAQ card in the experiment is used to interface the voltage and frequency controller from the output of the amplifier to a personal computer. The interfacing is done by using LabVIEW graphical data logging software.

3.4.5 RS 232 box integrated interface

The RS 232 Data Interface is used in the experiment as a serial communication between a Single-Axis DC-Motor Controller system and a personal computer. The following features of the connector are set by the factory and are 9,600 baud, 8 data, 1 stop and no parity. Since internal buffers are used, there is no handshake required.

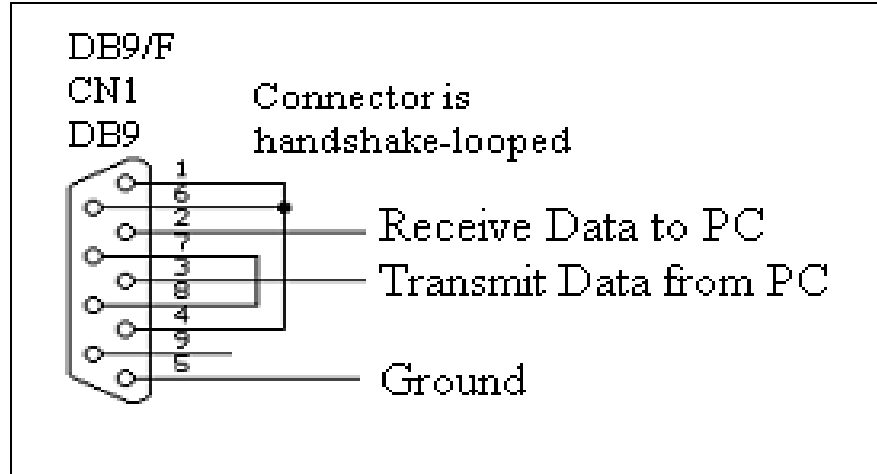


Figure 3.9: DB9/F (Female pin) connector

Table 3.4: RS232 Pin assignment for DB9 signal set

RS232 Pin Assignments (DB9 PC signal set)	
Pin 1	Received Line Signal Detector (Data Carrier Detect)
Pin 2	Received Data
Pin 3	Transmit Data
Pin 4	Data Terminal Ready
Pin 5	Signal Ground
Pin 6	Data Set Ready
Pin 7	Request To Send
Pin 8	Clear To Send
Pin 9	Ring Indicator

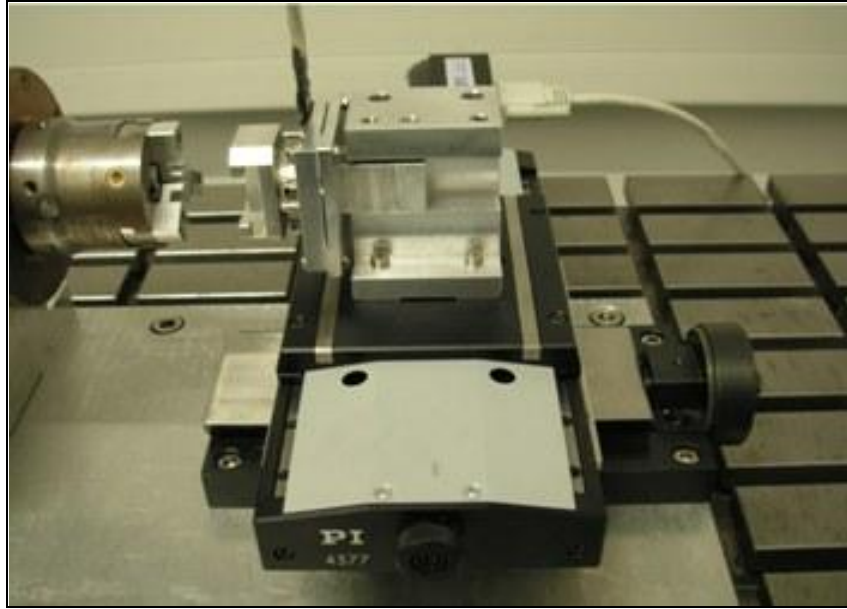


Figure 3.10: The connecting of RS232 cable

The RS 232 signals are represented by voltage levels with respect to a system common (power/logic ground) and the communication is done through a line length. The length of a data cable depends on the speed of the data and the quality of the cable. The connector wiring of the RS 232 or the female pin uses a ‘DB9 PC signal’ and is shown in Figures 3.9 and 3.10. This is important to know to make sure that the right RS 232 pin assignments are used. Figure 3.10 shows the RS232 cable connecting into the slideway.

3.5 Software analysis and machine control

3.5.1 Ansys 11 and Ansys workbench

ANSYS is a general-purpose finite element analysis (FEA) software package. Finite Element Analysis is a numerical method of deconstructing a complex system into very small pieces (of user-designated size) called elements. The software implements equations that govern the behaviour of these elements and solves them all, creating a comprehensive explanation of how the system acts as a whole. These results can then be presented in tabulated or graphical forms. This type of analysis is typically used for the design and optimization of a system far

too complex to analyze by hand. Systems that may fit into this category are too complex due to their geometry, scale, or governing equations.

With virtual prototyping techniques, users can iterate various scenarios to optimize the product long before the manufacturing is started. This enables a reduction in the level of risk and in the cost of ineffective designs. The multifaceted nature of ANSYS also provides a means to ensure that users are able to see the effect of a design on the whole behavior of the product, be it electromagnetic, thermal and mechanical.

3.5.2 AutoCAD Mechanical desktop 2007

In this research work, AutoCAD is used for designing and modelling the system into finite element analysis. From an early stage, this system design uses a 2D drawing and finally converted to 3D for more accurate data analysis. The drawing model for investigating the finite element of the machine structure also used the AutoCAD by converting the file format into the .IGES and .STL.

3.6 Data acquisition and machine system control

3.6.1 Matlab

In this research MATLAB is used to model and analyze the surface simulation. Some of the MATLAB programming is used to integrate into LabView software to calculate the output of cutting process in order to get the result. For example, the modelling from the user interface is calculated by MATLAB to give the output result which consists of several variables as input. The output from the modelling is surface roughness, tool wear and material removal rate. The programming coding is prepared to accommodate the developed algorithms designed for the experiments.

3.6.2 LabVIEW

LabVIEW Graphical Software is used to interface data of the optical measurement and to control the XYZ table with a PC through a DAQ card and RS232 cable respectively. A snapshot of the front panel user interface is shown in Figure 3.11.

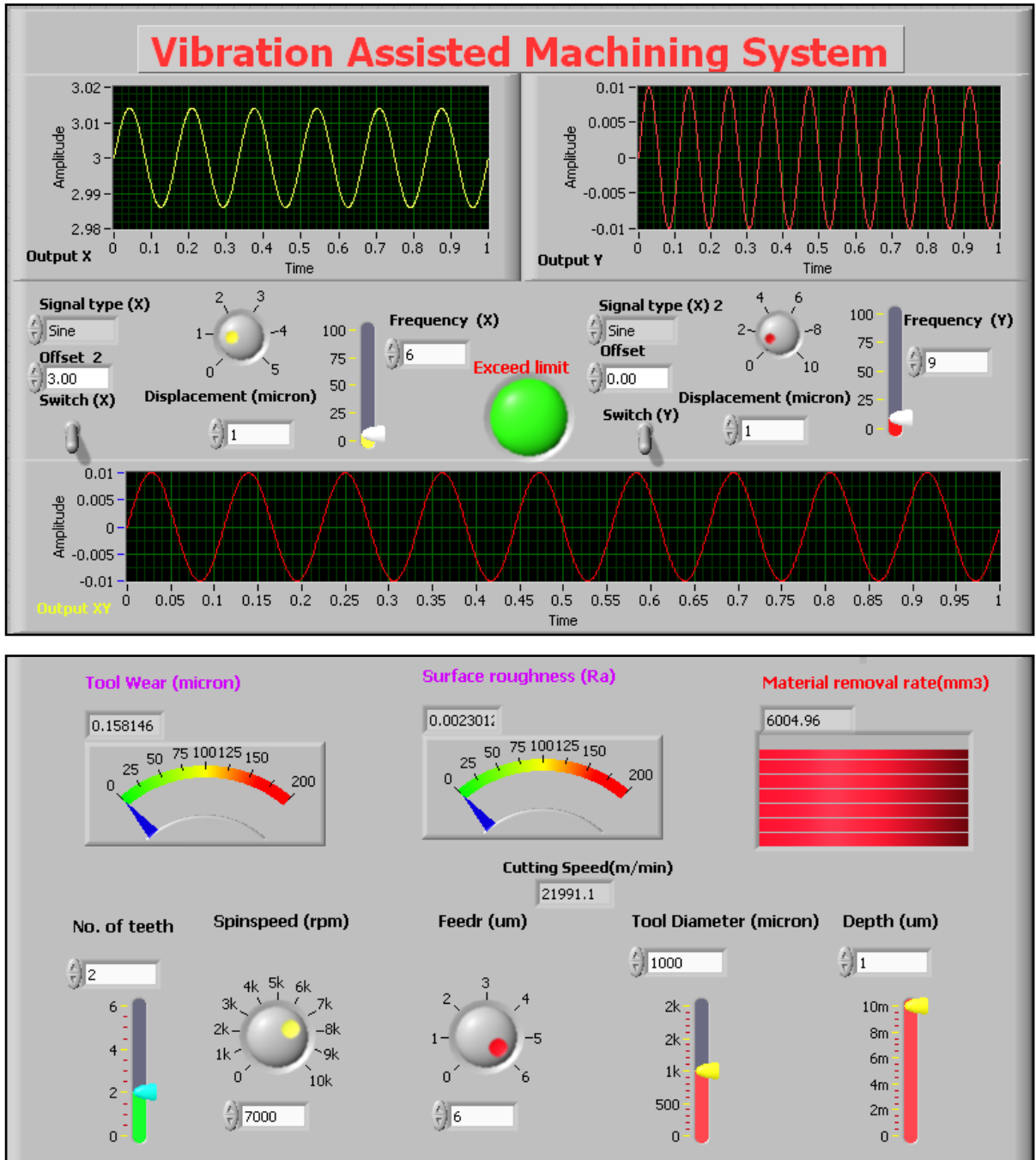


Figure 3.11: User interface for machining operation

This is used to control, monitor and deliver desired output from the CPU reflected to the voltage and frequency region. The arrangement is made so as to obtain the optimum setting range presented in voltage measurement which is referred to as limitation condition of piezo-actuator between -20 to 150 volt. From the virtual control panel, the output and input can be monitored directly and the machining condition process observed during cutting, such as material removal rate, tools wear and surface roughness.

3.6.3 Mercury controller and coder C-842 for Windows

The controller coder for this research work uses C-842 designed to be compatible with Windows 95 / 98 / 2000 / NT. It is a miniaturized servo-controller intended for motion control in research and industrial applications. It provides a complete stand-alone control system for the smaller motors typically used in high-precision positioning systems in a very compact, single package by using 32 bit Windows Library which allows it to communicate with the Mercury Controller via RS-232 Com ports 1 through 6. The program function uses a binary status code for example:

Table 3.5: Binary coding for RS232 program

Code	Status
0	Not moving
1	Moving
-1	Error : content
-2	Error: query
TP	Current motor position
TT	Target position
TF	Profile following error
TE	Distance to target
TY	Programmed velocity
TL	Programmed acceleration
GP	Programmed p-term
GI	Programmed i-term

The Mercury utilizes quadrature encoder signals for position feedback. Depending on the resolution of the encoder scale, incremental resolutions of 0.1 micrometer can be achieved.

Figure 3.12 shows the user interface for C-842 Mercury coder using binary and library language code compatible with Windows. Figure 3.13 below shows the control panel coding by Mercury C-842. It uses a count in MR (relative motion) and MA (absolute motion) to move the slideway in X axis.



Figure 3.12: Binary control box

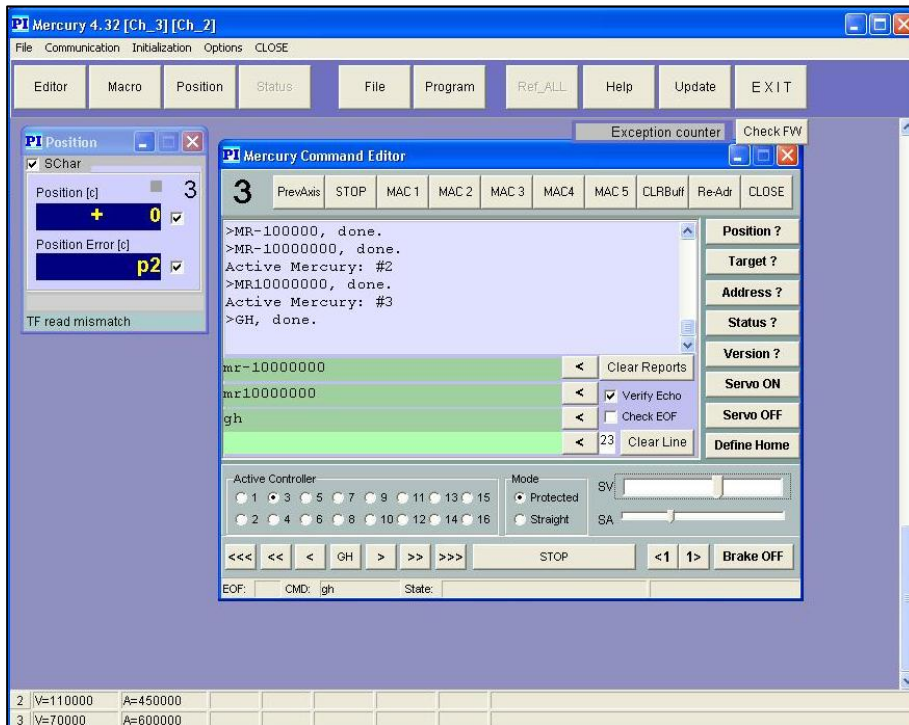


Figure 3.13: User interface for PI slideway

3.6.4 3D Zygo surface profiler

The machined surfaces from the vibration assisted machining are measured by using a 3D Zygo surface profiler, which is shown in Figure 3.14. The data obtained from 3D Zygo surface profiler are defined by Ra and as the reference data to calculate the percentage error of the data achieved from the optical based system.

The 3D Zygo surface profiler used for the measurements is Zygo NewView 5000 and it is a high performance 3D surface metrology system. It utilizes white light interferometry to produce a 3D topographical map and to characterize and quantify the roughness of the surface specimen. All measurements are non-destructive, fast, and require no sample preparation. Profile heights ranging from < 1 nm up to 15 mm are possible, with < 1 nm resolution.



Figure 3.14: Zygo surface profiler

The features of Zygo NewView 5000 are as follows:

- High speed measurement and analysis module.
- High speed, high resolution 640 x 480 CCD camera.
- MetroPro software for data acquisition and analysis.

- Motorized X, Y, Z, tip, tilt stage.
- Image stitching capability.
- 10x microscope objective with adjustable zoom from 0.4x - 2.0x.

The optical profiler is placed on a granite table which is a pneumatic vibration free table provided by Integrated Dynamics Engineering with a stable gantry column.

3.7 Summary

System design and implementation of the research is divided into two sections. The first section is about the approach and architecture of the experimental system development and setup. The whole experiment is assembled stage by stage and their compatibility from one stage to another is an important factor to be acknowledged.

As for the second section, it contains the descriptions of software and hardware tools used in the research experiment. This includes the LabVIEW Graphic software, Mechanical desktop, Ansys 11 and Ansys Workbench used to investigate the machine design. For the measurement purposes, the Zygo NewView 5000 surface profile has been described.

Chapter 4 Dynamic analysis of the machine system

4.1 Introduction

All machine designs and processes are subjected to dynamic effect due to the transient force of vibration, and the dynamic mechanism inherent to the process, such as regeneration. The machine, including cutting tool, part and fixture, etc, forms a complex system consisting of several coupled structural elements. During cutting, a substantial amount of energy is dissipated through plastic deformation and friction. Some of this energy is transmitted to the structural elements of the system, inducing vibrations relative motion between the tool and workpiece in particular (Stephenson et al, 2005).

The most important thing is to determine the dynamic behaviour, such as natural frequency, modal shape, frequency response, etc. Thus, any estimation of machine capability can be predicted to make some structural modifications (SDM) as shown in Figure 4.1. Finite element methods are the most practically useful approaches for analyzing machining system because they permit use of the most realistic assumptions. They can be used for dynamic analysis, including for static and thermal analysis using the same model.

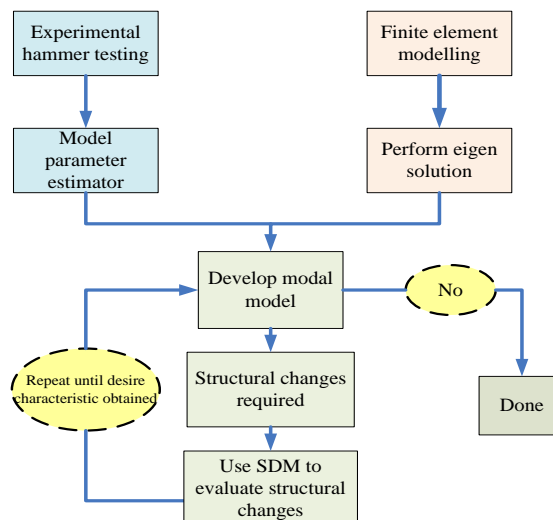


Figure 4.1: Schematic of the Structural Dynamic Modification (SDM)

In this chapter, an experiment using impact hammer, Ansys 11 and Workbench has been used in order to investigate the machine dynamics and bring about some structural modification. In Ansys 11 software, the advance in computational modelling in nodes, element generation, loads, constraint, force, etc, will make the finite element analysis promised result using equation solver, matrices and plot the result into the images as shown in Figure 4.2.

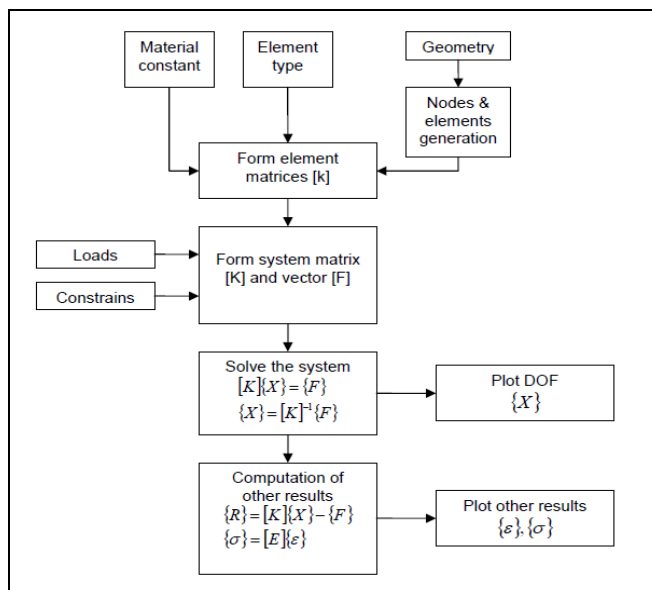


Figure 4.2: Finite element analysis solver

In this research work, a number of analytical and theoretical methods have been executed to study the dynamic behaviour of a machining system. Two common approaches can be used to apply finite element method to predicting the dynamic behaviour of the machining system. In the first approach, a single large model of the whole system is employed. In the second approach the overall system is subdivided into smaller subsystems (machine components) which are analyzed separately: the results of all the subsystem are linked together in an overall system structural response program using a generalized building block approach to predict the structural characteristics of the whole system.

The dynamic rigidity of the structures involved in machining is very important in determining the dynamic behaviour. Also if structural rigidity is not controlled, it may result

in high amplitude oscillation, instability and poor quality results. The elements that must be taken into account in a machining system are in the machine tool loop, such as the spindle, slideway, tool holder and base plate.

The stationary components in this desktop include base plate, spindle clamper, spindle block, spindle housing as part of the mechanical structure that normally accommodates the moving mechanical bodies, such as worktable, slide and carriages. The material selection for the basic structure was chosen for good stiffness, damping and thermal stability and also ease of fabrication and assembly. For example, the base plate and spindle block were made from aluminium T-6061 which has adequate stiffness and damping.

4.2 Design analysis

The dynamic characteristics of this desktop machine are dependant on several factors such as:

- a) Stiffness of the structures
- b) Damping coefficient
- c) Joining (parallel or serial)

Generally, the dynamic stability of the machine tool in the desktop milling machine essentially depends on the compliance of the design structure as well as on properties of the cutting process involved (Zhou and Cheng, 2009). The dynamic load generated due to phenomena during machining process such as milling, turning, drilling, etc. directly affects the machine tool and workpiece relations and consequently influences the machining quality.

In depth investigation was carried out on a dynamic model of vibration assisted micro-milling operation to present a novel approach to modelling the machining dynamics. For the integrity of the dynamic model, the vibration from the piezo-actuator applied was taken into account. The reliability of the proposed machining dynamic model included the vibration excitation from the piezo-actuator, in terms of frequency, amplitude, feed rate, cutting speed, depth of cut and frequency response.

Figure 4.3 shows the FEA mesh model of the horizontal milling machine structure. The finite element analysis method was used to investigate the dynamic behaviour of this test rig which was assumed attached to the rigid steel table. The modulus elasticity and density of stainless steel and aluminium were 2.1 GPa and 7,800 kg/m³ and 7,300 Pa and 2,700 kg/m³ respectively.

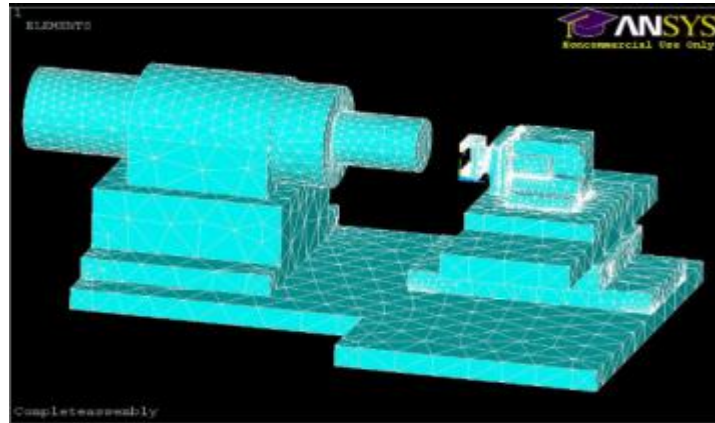


Figure 4.3: Machine FEA model

The selected analysis modelled the desktop vibration assisted micro-machine, for example static analysis, hammer testing, frequency response function analysis and finally modal updating and comparison with experimental results.

4.3 Finite Element (FE) analysis of the machine

A machine is an assembly of mechanisms and components which transforms, transmits or utilizes energy, force or motion for a specific purpose. A detailed knowledge of component properties/behaviours is desirable for the successful functioning, durability, efficiency and reliability of a designed machine. Therefore, the analyses of these components can lead to important improvements for the machine dynamic design. Recent progress in computer hardware and software enable us to numerical study of all types of machine elements. The most frequently used numerical method is the finite element method, as can be seen from many papers published.

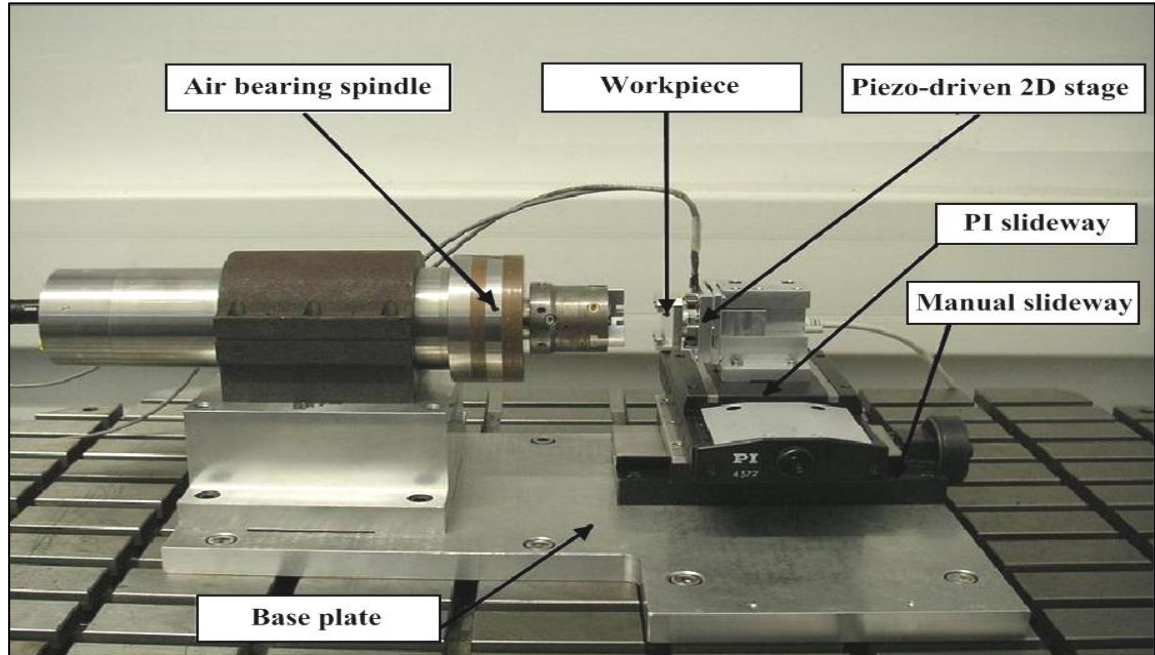


Figure 4.4: Desktop machine for vibration assisted machining

The reliability of finite element calculations depends on the validity of the assumptions used in the underlying theory and on the accuracy of predicted loads and service conditions, boundary conditions, material models, etc (Mackerle, 1999). This chapter is intended to investigate the needs of industry as a comprehensive design and analysis of various machine elements. Figure 4.4 shows a design for the desktop machine for vibration assisted micro-milling purpose, including a mechanical structure, spindle, driving system, a piezo-electric actuator, a linear slideway and base plate. These parts critically determine the overall machine tool system performance.

The mechanical structure provides a framework and mechanical support for all the machine components. It encompasses important components such as base plate, spindle block, spindle cases and base metal table. The major factors for machine design and selection include (Huo and Cheng, 2005):

- ✚ Structural configuration
- ✚ Stiffness and damping

- ✚ Structural connectivity and interface
- ✚ Structural dynamic and performance

A robust design of mechanical structure should aim to achieve high structural dynamic and static performance, such as high structural loop stiffness, good damping properties, a symmetrical and closed loop structure, minimize disturbance forces, and long term stability effects.

In order to determine machine performance in a finite element, material selection is also a significant factor that has to be considered. Aluminium and aluminium alloy has widely been used for mounting attachment, with cast iron for the metal table and granite for fabrication machine bases and slideway. Structural materials with low thermal expansion coefficient and high dimensional stability also have a great potential to increase the machine performance.

4.3.1 Machine loop

According to the machine specifications, some structural configuration must be considered, such as machining workspace, workpiece to be machined, possibility of machining accuracy etc. In this desktop machine analysis, the deformations occurring at the point load between the tool and workpiece (which are focused on the spindle shaft and XY stage) due to machining forces are results of all the forces transmitted from all relevant machine components, including fastenings.

In principle, the relationship between the contact of the cutting tool and uncut material is defined as a tool workpiece loop. Figure 4.5 shows a vibration assisted micro machine-tool-workpiece-loop. If the machine tool is taken as a dynamic loop, the internal and external vibrations and machining process should be integrated into this loop, as shown in Figure 4.6.

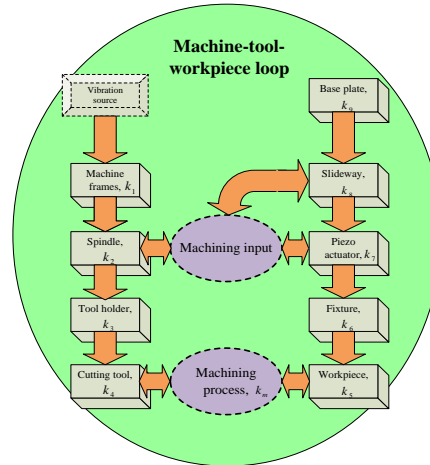


Figure 4.5: Machine tool-workpiece loop in desktop micro-milling machine, machining process and dynamic effects

Each of these components has their stiffness activities and each directly contributes to the precision of the machine tool but may also lead to machining errors. By using force flux and deformation analysis, a simplified approach with regards to the machine components which assumes a spring connected to each other in serial or parallel at a single point, which is,

$$Def_{total} = \frac{1}{k_{total}} = \frac{1}{k_1} + \frac{1}{k_2} + \frac{1}{k_3} \dots series \quad (4.1)$$

And,

$$Def_{total} = \frac{1}{k_1 + k_2 + k_3} \dots parallel \quad (4.2)$$

Where k is for stiffness of each component. From a joining viewpoint, the connection of 2D VAM prototype machine is joined by series and parallel methods. The series joining consists of spindle, spindle block, base plate, manual slideway, linear slideway and workpiece holder. The parallel joinings were between the interface XY stages and jig.

During machining, the cutting force will act upon the machining point (tool of end mill) and will be transmitted to the machine via the components connected by parallel and series

connections. The force will return to the original point, thus closing the loop (Huo and Cheng, 2009).

Using this principle, it can be assumed that the floor and table are rigid with no variation in stiffness and damping at all. Figure 4.6 shows the tool loop stiffness physical model between the tool and workpiece.

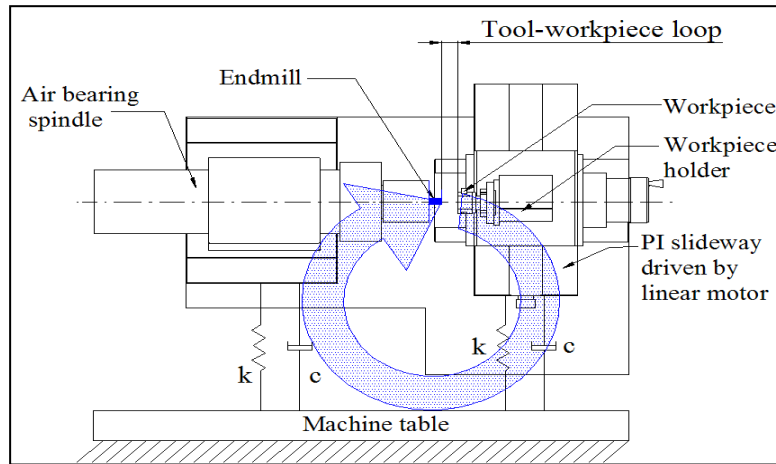
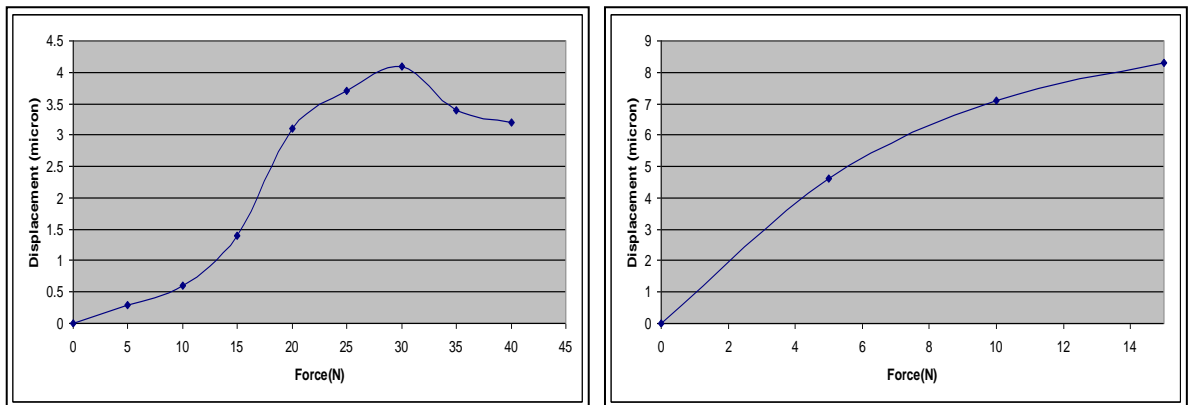


Figure 4.6: Loop stiffness physical model

For longitudinal direction, force hammer testing has been conducted for measuring the displacement using a capacitive sensor pointing towards the Z axis, in accordance with earlier findings for spindle and piezo in stiffness loop between tool and workpiece. Figure 4.7(a) for spindle and 4.7(b) for piezo-actuator show graphs for the result of force and displacement in the Z direction.



(a) (b)

Figure 4.7: Stiffness experiment

The stiffness between the tool and workpiece is calculated using the equation

$$k = \frac{G}{x_d} \quad (4.3)$$

Where k is the stiffness on Z direction, G is the force acting on the structure and x_d is displacement.

For the spindle, $k = \frac{30}{4.1} = 7.31N / \mu m$

And the piezo device, $k = \frac{10}{7.1} = 1.4N / \mu m$

4.3.2 Static analysis

The fundamental finite element analysis is a static analysis or structural analysis. The principal advantage of static analysis is the fact that it can reveal errors that do not manifest themselves until a disaster occurs weeks, months or years after release. Furthermore, static analysis is only the first step in a comprehensive software quality-control regime. After static analysis has been done, dynamic analysis is often performed in an effort to uncover subtle defects or vulnerabilities. In computer terminology, static means fixed, while dynamic means capable of action and/or change.

The overall equilibrium equations for linear structural static analysis are:

$$[K]\{u\} = \{F\} \quad (4.4)$$

Or,

$$[K]\{u\} = \{F^a\} + \{F^r\} \quad (4.5)$$

Where, $[K]$ is total stiffness matrix $= \sum_{m=1}^N [K_m]$, $\{u\}$ is nodal displacement vector, N is number of elements, $[K_m]$ is element stiffness matrix, $\{F^r\}$ is reaction load vector and $\{F^a\}$ is a total applied load vector. All this is defined by:

$$\{F^a\} = \{F^{nd}\} + \{F^{ac}\} + \sum_{m=1}^N (\{F_m^{th}\} + \{F_m^{pr}\}) \quad (4.6)$$

Where, $\{F^{nd}\}$ is applied nodal load vector, $\{F^{ac}\} = -[M]\{a_c\}$ is acceleration load vector, $[M]$ is total mass matrix, F_m^{th} is element thermal load vector and F_m^{pr} is element pressure load vector.

The main function of static structural analysis is to investigate the gravitational force that acts on the endmill tool tip. The gravitational force that has been applied is 9.80665 m/s². The gravitational acceleration toward an object with mass is given by,

$$g = \frac{-mG}{l^2} \times l \quad (4.7)$$

Where l is distance from the centre of the object, l^2 is unit length vector from centre of the object and G is a gravitational constant. The reason for finding the value for static analysis is to evaluate the displacement error when the machine in a static condition affected by gravitational force.

The selected analysis modelled the desktop vibration assisted micro-machine, for example static analysis, hammer testing, frequency response function analysis and finally modal

updating and comparison with experimental results. Figure 4.8 shows the spring has been modelled for stiffness in air bearing spindle.

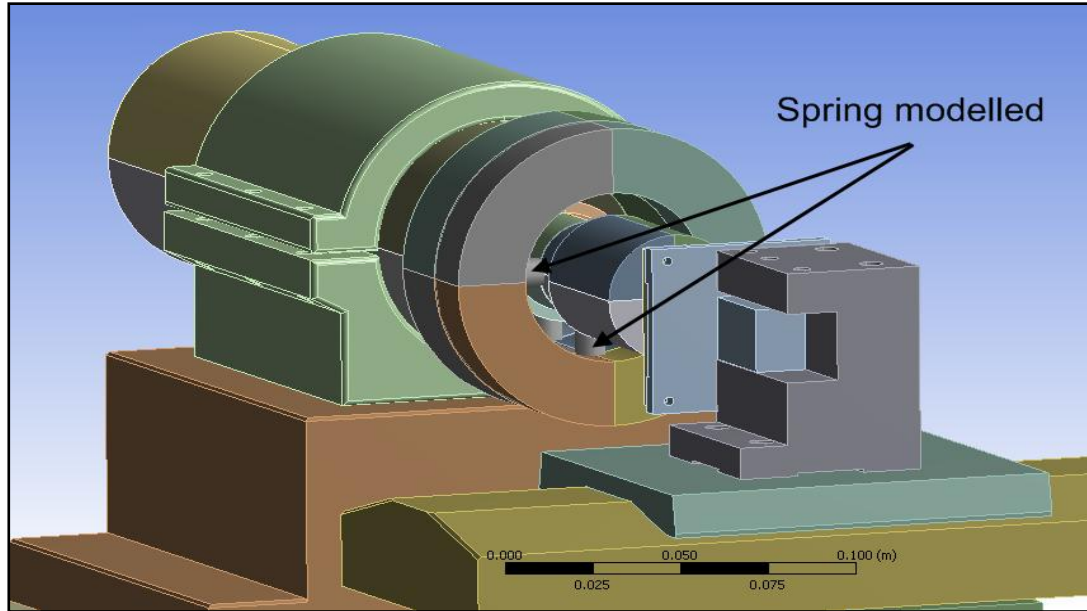


Figure 4.8: Spring modelled for air bearing stiffness

During the static structural analysis work in Ansys software, the influence of gravitational force on the spindle tool tip was found to be $0.0089 \mu\text{m}$. This value is very small and can be ignored as the other disturbance force is much bigger. The reason for finding the value for static analysis is to evaluate the displacement from gravitational force error when the machine is in static conditions. The second reason is to find the weakest point of the desktop machine which will have the greatest effect during machining in terms of further modification and model updating.

4.3.3 Modal analysis

The mechanical systems and components with an input and an output have to be identified. Adapted frequency-domain estimators designed to examine huge amounts of information/data in a reasonable amount of time are used. Hammer testing is required as a practical approach and finally the conclusions will be drawn.

Modes are used as a simple and efficient means of characterizing resonant vibration. The majority of structures can be made to resonate. Under the best experimental conditions, a structure can be made to vibrate with excessive, sustained, oscillatory motion. Resonant vibration is caused by an interaction between the inertial and elastic properties of the materials within a structure. Resonant vibration is often the cause of, or at least a contributing factor to, many of the vibration related problems that occur in structures and operating machinery. To better understand any structural vibration problem, the resonances of a structure need to be identified and quantified. A common way of doing this is to define the structure's modal parameters (Guillaume, 2006).

Vibration and modes

All vibration is a combination of both forced and resonant vibration. Forced vibration can be due to,

- ✚ Internally generated forces
- ✚ Imbalances
- ✚ External loads
- ✚ Ambient excitation

Resonant vibration occurs when one or more of the resonances or natural modes of vibration of a machine or structure is excited. Resonant vibration typically amplifies the vibration response far beyond the levels of deflection, stress, and strain caused by static loading (Brian, et. al 2009).

Modes and resonances are intrinsic properties of a structure and shape. Resonances are determined by the material properties (mass, stiffness, and damping properties) and boundary conditions of the structure. Each mode is defined by a natural (modal or resonant) frequency, modal damping, and a mode shape. If the material properties or the boundary condition of a structure change, its modes will definitely change. For example, if mass is added to a beam structural, it will vibrate in a different way because its modes have changed.

At or near the natural frequency of a mode, the overall vibration shape (operating deflection shape) of a machine or structure will tend to be dominated by the mode shape of the resonance.

Mode shape in multiple degrees of freedom system

Mode shape can be described as multiple-degree-of-freedom (MDOF) systems in mechanical structures such as bridge, machine, turbine blade, vehicle, etc. Figure 4.9 shows the design in a 2DOF system, although the general expression and solution will be described in the basic solution.

For an undamped MDOF system with N degrees of freedom, the governing equations of motion can be written in matrix form as,

$$M\ddot{x}(t) + K\dot{x}(t) + Cx(t) = f(t) \tag{4.8}$$

Where M , K and C are mass, stiffness and damping coefficient matrices respectively. This equation expresses the sum of all forces acting on the mass M should be equal to zero with $f(t)$. An external applied force $M\ddot{x}(t)$ is inertial force, $C\dot{x}(t)$ the damping force and $Kx(t)$ the restoring force. The variable $x(t)$ is present in the position of the M with respect to the position of the mass when $f(t) \equiv 0$.

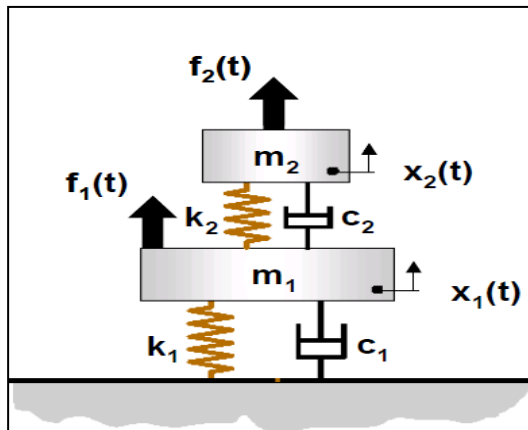


Figure 4.9: MDOF system

Therefore,

$$m_1 \ddot{x}_1(t) + (k_1 + k_2) \dot{x}_1(t) - k_2 \dot{x}_2(t) + (c_1 + c_2)x_1(t) - c_2 x_2(t) = f_1(t) \quad (4.9)$$

$$m_2 \ddot{x}_2(t) - k_2 \dot{x}_1(t) + k_2 \dot{x}_2(t) - c_2 x_1(t) + c_2 x_2(t) = f_2(t) \quad (4.10)$$

Or,

$$M = \begin{bmatrix} m_1 & 0 \\ 0 & m_2 \end{bmatrix} \quad f(t) = \begin{Bmatrix} f_1(t) \\ f_2(t) \end{Bmatrix}$$

$$K = \begin{bmatrix} k_1 + k_2 & -k_2 \\ -k_2 & k_2 \end{bmatrix} \quad x(t) = \begin{Bmatrix} x_1(t) \\ x_2(t) \end{Bmatrix}$$

$$C = \begin{bmatrix} c_1 + c_2 & -c_2 \\ -c_2 & c_2 \end{bmatrix}$$

In matrix form,

$$M \begin{bmatrix} \ddot{x}_1(t) \\ \ddot{x}_2(t) \end{bmatrix} + K \begin{bmatrix} \dot{x}_1(t) \\ \dot{x}_2(t) \end{bmatrix} + C \begin{bmatrix} x_1(t) \\ x_2(t) \end{bmatrix} = f(t) \quad (4.11)$$

Applying Laplace transform on Equation 4.11.

$$M \begin{bmatrix} s^2 X_1(s) \\ s^2 X_2(s) \end{bmatrix} + K \begin{bmatrix} sX_1(s) \\ sX_2(s) \end{bmatrix} + C \begin{bmatrix} X_1(s) \\ X_2(s) \end{bmatrix} = \begin{bmatrix} F_1(s) \\ F_2(s) \end{bmatrix} \quad (4.12)$$

$$Ms^2 \begin{bmatrix} X_1(s) \\ X_2(s) \end{bmatrix} + Ks \begin{bmatrix} X_1(s) \\ X_2(s) \end{bmatrix} + C \begin{bmatrix} X_1(s) \\ X_2(s) \end{bmatrix} = F(s) \quad (4.13)$$

$$(Ms^2 + Ks + C) \begin{bmatrix} X_1(s) \\ X_2(s) \end{bmatrix} = F(s) \quad (4.14)$$

The matrices are defined for a 2-DOF system with both DOF along the vertical x-axis. So, by transforming (4.8) to the Laplace domain (zero initial condition) yields,

$$Z(s)X(s) = F(s) \quad (4.15)$$

With $Z(s) = Ms^2 + Cs + k$

Deflection shape and operating deflection shapes

The modal shape or mode shape, also called the operating deflection shape (ODS), is defined as any forced motion of two or more points on a structure. This is because the specifying of the motion of two or more points defines a shape. Stated differently, a shape is the motion of one point relative to all others (Schwarz, et al. 1999).

While motion is a vector quantity that has both location and direction coupled with it. Motion at a point in a direction is also called a Degree of Freedom, or DOF. “All experimental modal parameters are obtained from measured ODS. That is, experimental modal parameters are obtained by artificially exciting a machine or structure, measuring its operating deflection shapes (motion at two or more DOFs), and post-processing the vibration data.

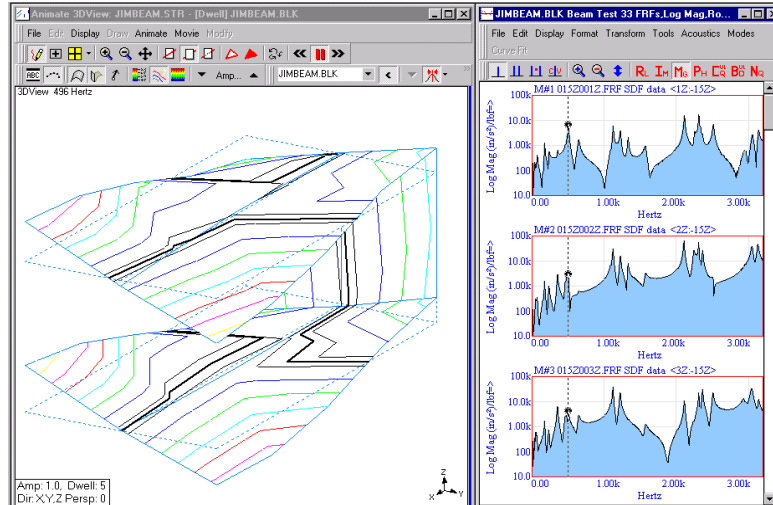


Figure 4.10: Frequency Domain ODS from a set of FRF (Schwarz & Richardson, 1999)

Figure 4.10 shows an operating deflection shape being displayed from a set of frequency response function (FRF) measurements, with the cursor located at a resonance peak by the simple beam structure.

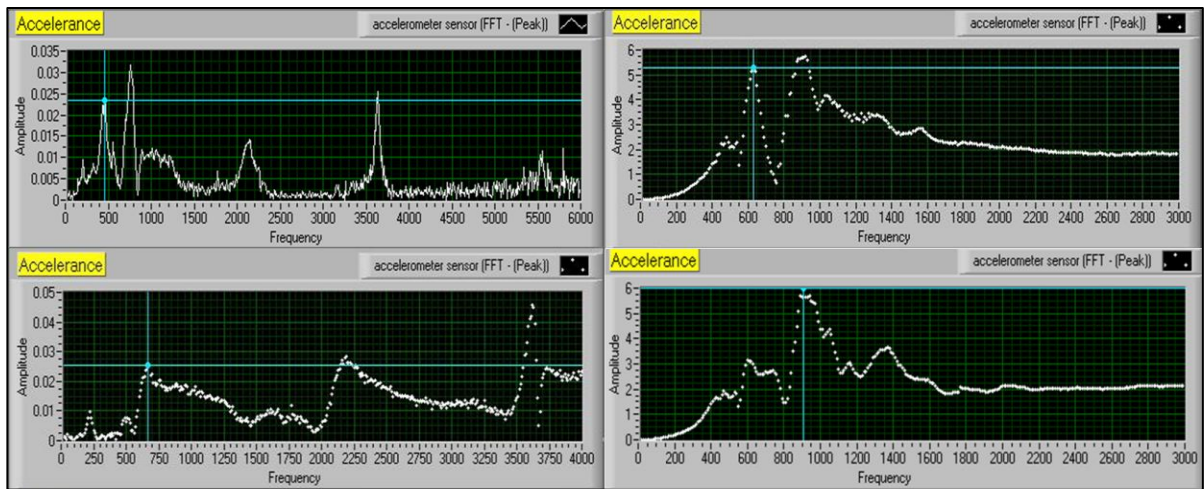


Figure 4.11: Graph in LabView 7.1 with 4 natural frequencies

The experimental modal analysis was based on impulse testing conducted to obtain the receptance-ratio of output displacement to input force for the structure of the horizontal milling machine. A number of experiments were conducted to investigate the modal analysis using an impact hammer. Figure 4.11 shows the DVAM in operating deflection shape from a

set of frequency response function (FRF) measurements by LabView 8.5 software using impact hammer testing. The acceleration signals were captured by an accelerometer attached to the air spindle. It was found from this hammer testing that 460 Hz (bending, up-down), 630 Hz (bending, left-right), 670 Hz (twisting) and 910 Hz (bending, up-down) were the frequencies to avoid. In this case, the operating deflection shape is being dominated by a mode and therefore is a close approximation to the mode shape.

Modes are further characterized as either rigid body or flexible body modes. All structures can have up to six rigid body modes or more depending on the equipment sensitivity, the structure shape and boundary condition. For the common cases, it up to 4 modes which are 2 translational modes and 2 rotational modes. If the structure merely bounces on some soft springs, its motion approximates a rigid body mode.

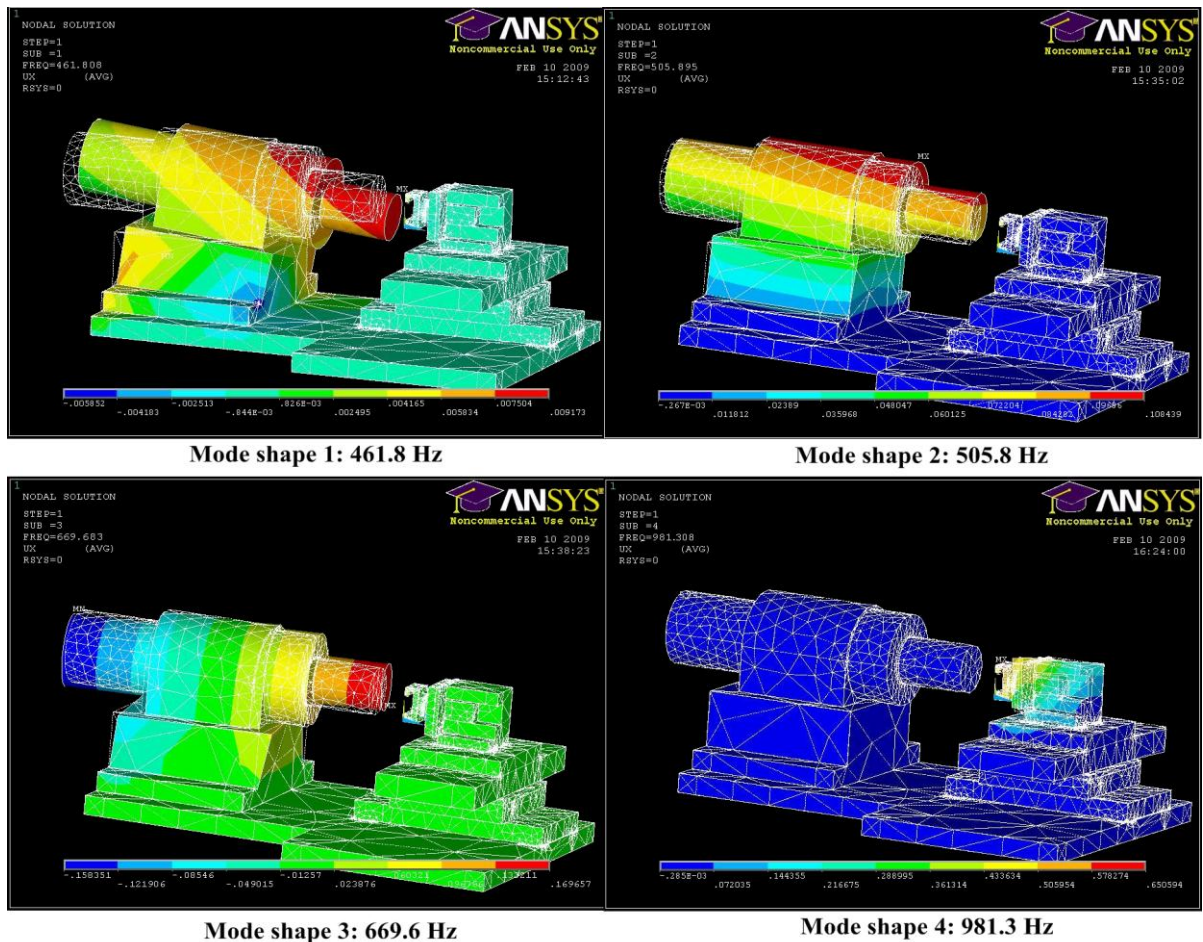


Figure 4.12: The first four natural frequencies and mode shapes

The air spindle was modelled by using a spring element from Ansys workbench 11.0. The values used for stiffness of the air bearing were $7.4 \text{ N}/\mu\text{m}$ for radial and $68 \text{ N}/\mu\text{m}$ for axial direction (Loadpoint, 2008). The modelled spring was selected to be sufficient to compensate the modal shape for the whole structure including spindle shaft, casing and spindle block that support the spindle part. This is a reasonable assumption since the spindle was supported by a block of aluminium which has low Young's modulus compared to the stainless steel on the casing itself.

For the first, second and natural frequency, the mode shape was bending towards up, down and left respectively and included the spindle itself. It is predicted that the spindle nose maximum displacement occurs where the tool is clamped during machining. This is very important for future analysis to predict the surface roughness, for instance by including the frequency response function. From the modal shape, it is possible to distinguish in which part the maximum value of error or deflection occurs and what range of natural frequency is.

For a fundamental basic idea, any vibration problems in the machine structure are caused, or at least amplified, by the excitation of one or more flexible body modes. Figure 4.12 shows some of the common fundamental (low frequency) modes of the test rig. The first four fundamental modes are given names: bending up and down, bending left and right, twisting and bending on the other side.

4.3.4 Hammer testing

The impulse input, like the impact hammer, is widely used in vibration testing to obtain the natural frequency, mode shape, and frequency response function (FRF) because of its convenience and simplicity for experiments (Roy et al, 1995).

In most cases, however, the signals acquired from impact hammer testing have been dealt with as periodic and stationary, although they are obviously neither periodic nor stationary. The equipment consists of an impact hammer, filter box, power supply, displacement sensor or acceleration sensor, usually with a set of different tips and heads which serve to extend the frequency and force level ranges for testing a variety of different structures (Figure 4.13).

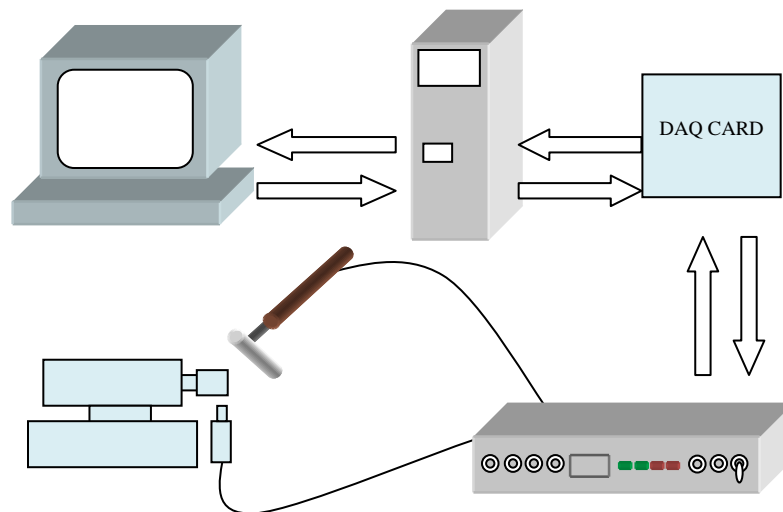


Figure 4.13: Hammer testing equipment setup

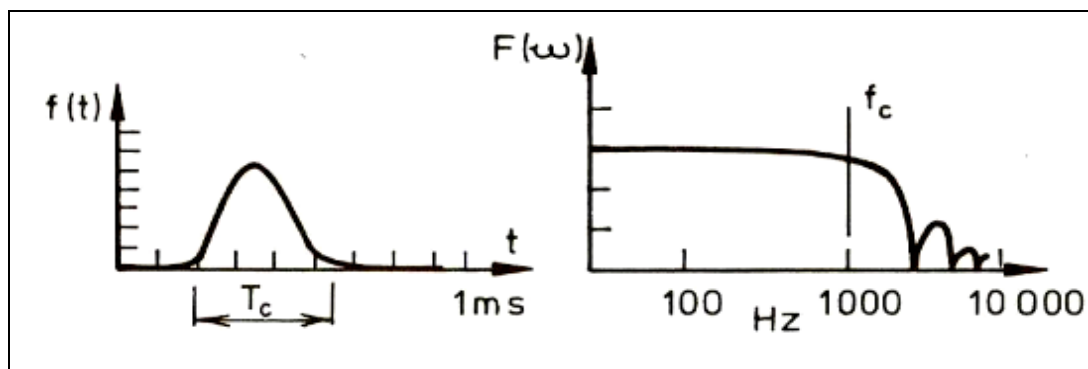
There are many important considerations when performing impact hammer testing. The two most important are:

- ✚ Choice of hammer head/point has important effect on the measurements acquired. This is because the input of excitation frequency range is controlled mainly by the hardness of the head selection. The harder the tip, the wider the frequency ranges that is excited by the excited force. The hardness of head of the hammer will be excited only at certain modes ranges. For instance, with a too soft tip the modes will not be excited adequately in high ranges of modes in order to obtain a good measurement. The input power spectrum does not excite all of the frequency range because of the roll-off of the power spectrum (Avitabile, 2001).
- ✚ The second important aspect in dealing with the impact testing relates to the use of an impact window for the response transducer. Generally, for a lightly damped structure, the response of the structure due to the impact excitation will not die down to zero by the end of the sample interval. If this occurs, the transform data will suffer significantly from a digital signal processing effect referred to as leakage.

Basically, the magnitude of the impact is determined by the mass of the hammer head and the velocity with which it is moving when it hits the structure. Often the operator will control the velocity rather than the force level itself and so an appropriate way of adjusting the order of the force level is by varying the mass of the hammer head.

The frequency range which is effectively excited by this type of device is controlled by the stiffness of the contacting surfaces and the mass of the impactor head: there is a system resonance at a frequency given by (contact stiffness/impactor mass) with which it is difficult to deliver energy into this structure. When the hammer tips impact the test structure, this will experience a force pulse which is substantially that of a half-sine shape, as shown in Figure 4.14(a).

The principle of hammer testing is the hammer tip impacts the test structure, this will excite a force pulse which is substantially that of a half-sine shape, as shown in Figure 4.14(a). A pulse of this type can be shown to have a frequency content of the form illustrated in Figure 4.14(b), which is essentially flat up to a certain frequency (f_c) and then of diminished and uncertain strength thereafter.



(a) Time history

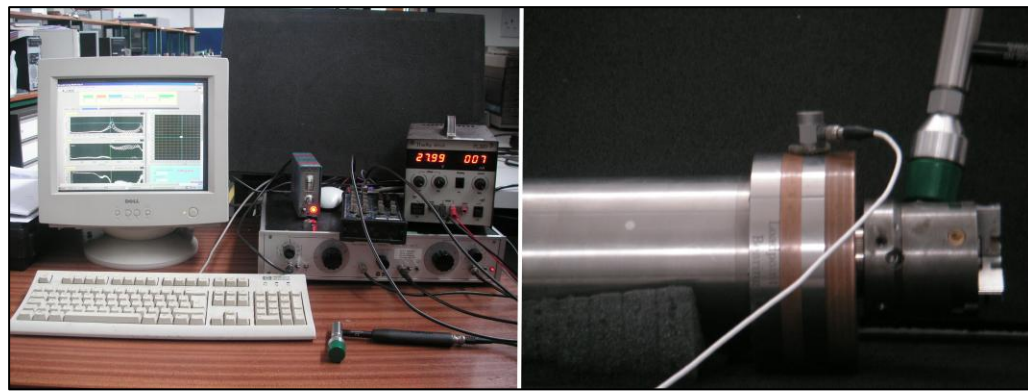
(b) Frequency spectrum

Figure 4.14: Typical impact force pulse and spectrum

It can be shown that there is a direct relationship between the first cut-off frequency (f_c) and the duration of the pulse, (T_c) and that in order to raise the frequency range it is

necessary to induce a shorter pulse length. This in turn can be seen to be related to the stiffness (not hardness) of the contacting surfaces and the mass of the impactor head. The stiffer the materials, the shorter will be the duration of the pulse and the higher will be the frequency range covered by the impact.

The difficulties to enable this system to work well in applying excitation using a hammer to ensure that each impact is essentially the same as the previous one, not so much in magnitude (as this is accommodated in the force and response measurement process). At the same time, multiple impacts or hammer bounce must be avoided as these create difficulties in the signal processing stage. A problem that needs to be considered when using the hammer type of excitation derives from the essentially transient nature of the vibrations under which the measurements are being made.



(a) Impact hammer experimental setup (b) Hammer and sensor position

Figure 4.15: Instrument for hammer testing

In modal analysis or transient force excitation, the impact forces were applied on the air bearing spindle nose by an impact hammer. By using the displacement sensor the corresponding signals were recorded in the LabView 8.5 program to produce frequency versus amplitude graphs. The displacement sensor was pointing vertically towards the chuck of the air bearing spindle.

During the modal analysis experiment, the impulse forces were applied in the surrounding area on the desktop-machine by an impact hammer to determine inaccuracies in the FEA results due to uncertainties in boundary conditions and structural damping. The hammer

testing setup is shown in Figure 4.15(a). The impact hammer was PCB piezotronic Model 653A01 with frequency range of up to 8,000 Hz, and displacement sensor having a 10 kHz frequency range, as shown in Figure 4.15(b). The result of the hammer testing is shown in Figure 4.16.

Standard impact hammer tests were conducted on the DVAM to determine its modal parameters (natural frequencies and modes shapes) and to validate the finite element model. As illustrated in Figure 4.13(b), the impact hammer was used to strike the air bearing spindle suspended by an air bearing system mounted on the solid steel table.

A load cell, located in the tip of the hammer, was used to measure the force input while a tri-axial accelerometer was employed to measure the acceleration along three perpendicular directions. Hammer testing is a procedure to predict and validate how many modes there are in the bandwidth of interest and then estimate a pole for each mode. A residue is estimated for each mode. Mode shapes are curve fitted and computed based on these estimates using commercially available software.

Even though the number of points at which measurements were made is small, the experimental mode shapes are practically identical to those predicted by the finite element analysis. Figure 4.16 compares the finite element predictions of the natural frequencies with the experimentally measured values.

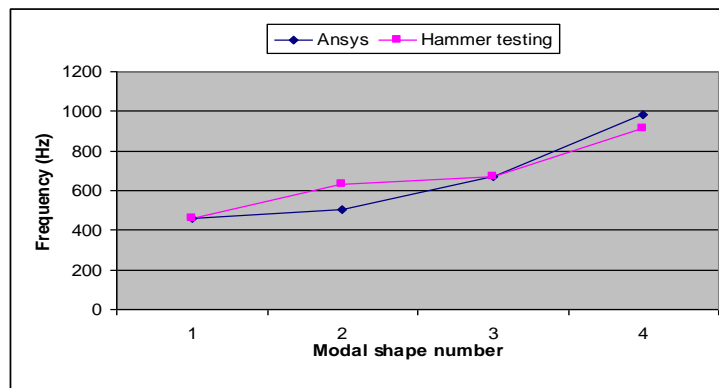


Figure 4.16: Comparison of natural frequency by Ansys and hammer testing

With the exception of the frequencies obtained for the first mode, the results agree quite well. The small discrepancies between the measured and calculated frequencies can be partially attributed to several factors in signal processing. For instance, noise background, accuracy of sensor and mass of the sensor.

Four modes have been investigated by this analysis. The natural frequencies from both the experimental modal analysis and the FE analysis are summarized in Table 4.1. The natural frequencies obtained from the FE analysis agree well with below 10% margin of total error, those from 4 modes the experimental modal analysis. The natural mode shapes from the experimental modal analysis also agree with those from the FE analysis which have been shown before.

Table 4.1: Comparison of finite element predictions with modal test results

Mode	Frequency (Hz) Ansys simulation	Frequency (Hz) experiment (Hammer testing)	Error Percentage
1	461	460	0.4%
2	505	630	19%
3	669	670	0.04%
4	981	910	7.8%
Average percentage of error			6.8%

Other reasons for these frequency differences may include inaccuracies in the constitutive equations; impact signals may be poorly suited for the frequency response function measurements; resolution bias errors may be present in the spectral estimates; and the system relating the output and input may not be linear.

4.3.5 Frequency response function

The input frequency is varied and the output characteristics are computed or represented as a function of the frequency. Frequency response analysis provides useful insights into the stability and performance characteristics of the structural system. Frequency response

functions were collected in different locations (both laterally and tangentially) and they were combined to produce the mode shapes. Rigorously, a frequency response function (FRF) is the direct linear relationship between the mechanical force input and the measured response output of a test specimen (Figure 4.17). It is described by the formula,

$$H(\omega) = \frac{y(t)}{F_0 e^{i\omega t}} \quad (4.16)$$

Where $y(t)$ is the output function, F_0 is the input force, and $e^{i\omega t}$ is the exponential harmonic frequency function. This procedure is firstly to estimate how many modes there are in the bandwidth of interest, and then estimate a pole for each mode. Mode shapes are curve fitted and computed based on these estimates using commercially available software.

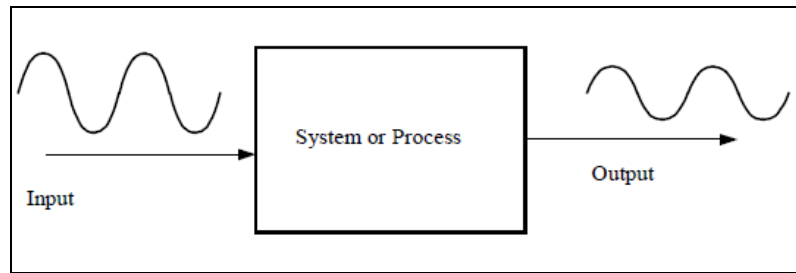


Figure 4.17: Frequency response functions defined

Taking a sine wave as a signal force from impact hammer, a simple system is subject to an input of the form,

$$x(t) = A \sin(\omega t) \quad t > 0 \quad (4.17)$$

After some initial transient period, the output settles down to a sine wave of the form,

$$y(t) = B \sin(\omega t + \phi) \quad (4.18)$$

The amplitude and phase are changed by the system, but the frequency remains the same. This is shown in Figure 4.18.

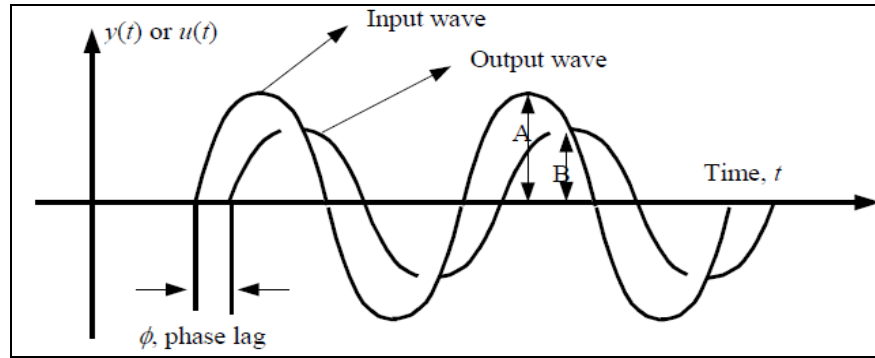


Figure 4.18: Frequency response

The output wave lags behind the input. ϕ is defined as a phase lag usually expressed in degree or radians. The output amplitude is different from the input, and we can define a ratio:

$$\text{AmplitudeRatio} = \frac{B_2}{A_1} \quad (4.19)$$

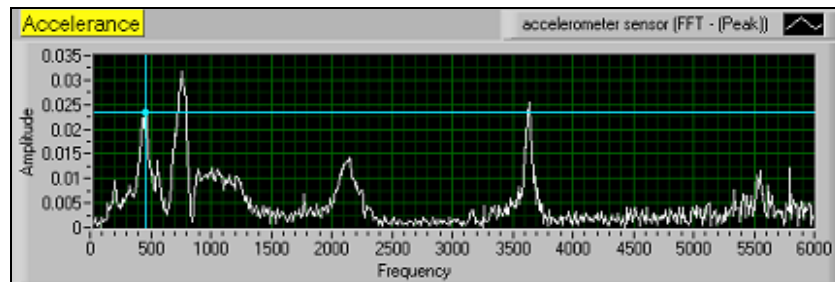


Figure 4.19: A sample of FRF plot taken from 2D VAM test bed

Figure 4.19 shows the frequency response of desktop vibration assisted micro-milling by LabVIEW. Experiments for natural frequency and their modes can be expanded via frequency response in order to get the response loads. The frequency response analysis is able to verify whether or not the designs will successfully overcome resonance and the harmful effects of forces vibrations.

4.4 Mechanism of the piezo-electric actuator and controller

The piezoelectric effect occurs only in non conductive materials. Piezoelectric materials can be divided into 2 main groups: crystals and ceramics. The most well-known piezoelectric material is quartz (SiO_2). Piezoelectric materials are crystalline solids whose asymmetric

structures create an electric dipole moment in the crystal lattice, which is sensitive to both elastic strain and applied electrical field.

PZT materials are ferroelectric materials subject to the Curie temperature: the poling process gives the material high electric fields at the Curie temperature. If the material is subjected to a temperature that is greater than its Curie temperature, it is no longer piezoelectric again in some conditions. As very high electric field corresponds to only tiny changes in the width of the crystal, this width can be changed with better than micrometer precision, making piezo crystals the most important tool for vibrating and positioning objects with extreme accuracy. For this reason they are used in actuators.

For some applications, multilayer ceramics will be used as a layer thinner than 100 microns, allowing for the reaching of high electric fields with voltage lower than 150 Volt. These ceramics are used within two kinds of actuators: direct piezo actuators and amplified piezo actuators. While a direct actuator's stroke is generally lower than 100 microns, amplified piezo actuators can reach millimetre strokes.

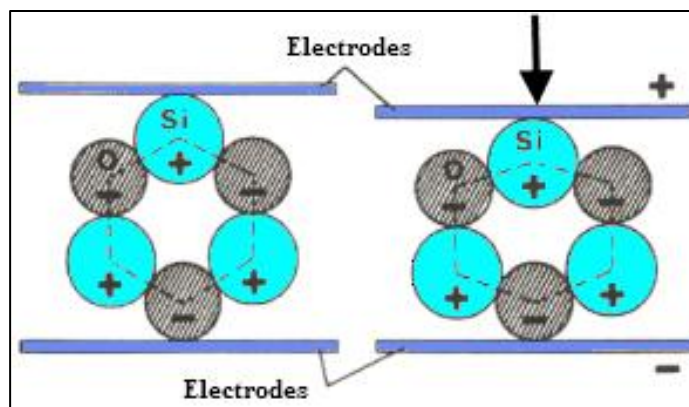


Figure 4.20: Piezo ceramic basic principal

The principal operation of a piezoelectric actuator is the dimensional change transformed into force energy, which is an act on two opposing faces of the PZT element. The advantage of piezo-electric is that it can be used in any design of actuator. The different modes for loading the piezoelectric element can be used for example in longitudinal, transversal and shear. Figure 4.20 shows the principle of piezo-actuator elongation and the changes in shape.

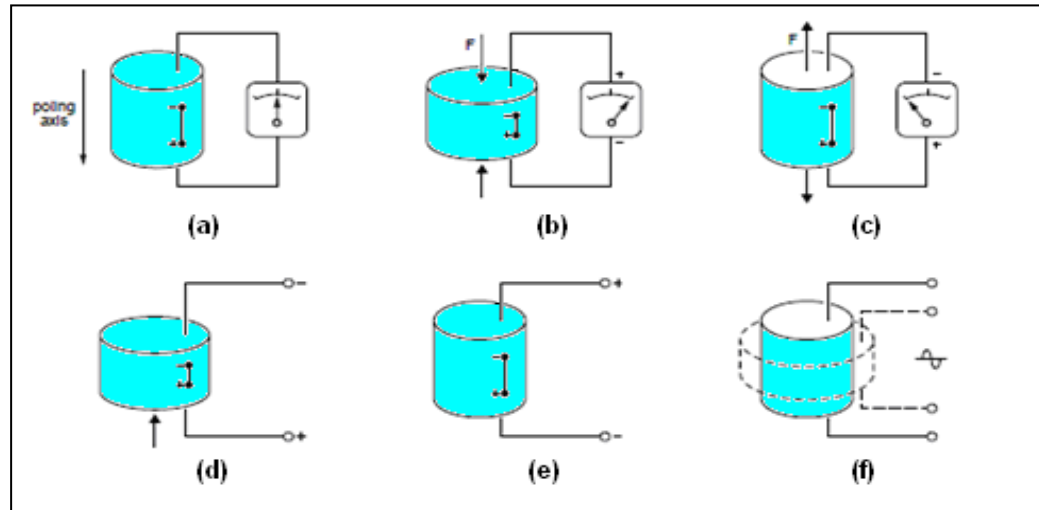


Figure 4.21: Piezoelectric effects on body shape

Figure 4.21(a) shows the cylinder under no-load conditions. If an external force produces compressive or tensile strain in the material, the resulting change in dipole moment causes a voltage to appear between the electrodes. If the cylinder is compressed, the voltage will have the same polarity as the poling voltage in Figure 4.21(b). If it is stretched, the voltage across the electrodes will have opposite polarity to the poling voltage, as in Figure 4.21(c).

For instance, a piezo-electric effect in generator action is the conversion of mechanical energy into electrical energy or vice versa. Other examples of piezoelectric-induced generator action can be found in cigarette and gas lighters, guitar pickup and microphones. If a voltage of opposite polarity to the poling voltage is applied to the electrodes, the cylinder will shorten as in Figure 4.21(3d). If the applied voltage has the same polarity as the poling voltages, the cylinder will lengthen as in Figure 4.21(e).

Finally, if an alternating voltage is applied to the electrodes, the cylinder will grow and shrink at the same frequency as that of the applied voltage, as in Figure 4.21(f). These are examples of motor or actuator action, conversion of electrical energy into mechanical energy.

Electrical fields in piezo-electric are affected by Young' modulus of the ceramic. This is because the stresses and strains are related to the properties of material that depend on the

Young' modulus and vice versa. In addition, the electrical displacement is related to the electrical field because the ceramic is a dielectric medium. These relationships can be expressed as:

$$\{S\} = [s^E]\{T\} + [d^t]\{E\} \quad (4.20)$$

$$\{D\} = [d_z]\{T\} + [\xi^T]\{E\} \quad (4.21)$$

Where S is strain, T is stress, D is induction, E is field, S^E is compliance at constant field, d is piezoelectric strain per unit of field and ε^T is permittivity at constant stress in matrices.

4.4.1 Permittivity

Piezo-electric ceramic is influenced by a permittivity towards displacement. The electric displacement field D represents how an electric field E influences the organization of electrical charges in a given medium, including charge migration and electric dipole reorientation to permittivity in the very simple case of linear.

$$D = \varepsilon E \quad (4.22)$$

where the permittivity ε is a scalar. The basic principle is that permittivity is not a constant as it can vary the position in the medium, and the frequency of the field applied, for instance humidity, temperature, etc. In SI units, permittivity is measured in farads per meter (F/m). The displacement field D is measured in units of coulombs per square meter (C/m^2). The electric field is measured in volts per meter (V/m).

The subscript of the direction of the dielectric displacement, the second indicates the electric field direction. For example,

e_{11}^T is the permittivity for the dielectric displacement and electric field in the 1- direction under conditions of constant stress. e_{11}^T is the permittivity for dielectric displacement and

electric field in the 3-direction under conditions of constant stress. The table of principal properties gives the relative permittivity,

$$\epsilon_r = \frac{\epsilon}{\epsilon_0} \quad (\epsilon_0 \text{ is the permittivity of vacuum} = 8.85 \times 10^{-12} \text{ F/m}).$$

4.5 Finite element analysis of the piezo actuator

4.5.1 Static behaviour of the piezoactive actuator

In most cases the displacement ΔU is in the primary interest. The changing of piezo-actuator depends on both the applied voltage V and the generated force.

$$\Delta U = (NV - F) / K \quad (4.23)$$

where N is the force factor of the actuator and K is the stiffness.

Furthermore, in dealing with a vibration actuator, the most common component in ultrasonic transducer and fast tool servo is typically using Lead Zirconate Titanate (PZT) ceramic, thus the design was improved by an amplification horn and a diamond tool. The kinematics of such systems, and the basis for all vibration assisted machining, involves moving the diamond tool into and out of contact with the workpiece (Cerniway, 2003).

4.5.2 Static structural analysis

Static structural analysis will be used to predict the displacement, stress, strain and forces in machine component/structure caused by a load that does not induce inertia and damping effects. The XY25XS component is shown in Figure 4.22. The piezo-actuator was designed to excite a workpiece to perform slot cutting in the horizontal axis. It is assembled with the interface and jig, and mounted on a workpiece holder on the slideway platform. This piezo electric device will vibrate the workpiece in 2 dimensional modes of chosen (1,000 Hz to 3,000 Hz) frequency range and amplitude to assist the machining process.

The piezo-actuator, mechanical structures and electrical circuit was covered by a protecting box made from plastic. There is sensitivity area on piezo-electric structure in the circuit where the -20 volt to +150 volt has been actuated in high frequency oscillation. To reduce the electricity shock risk and ease machine maintenance, the 2D vibration desktop test bed used an air blow pressures instead of fluid injection coolant.

There are four piezo-ceramic stacks fixed in the mechanical oval structure electrically compressed and expanded to transmit movement to the jig which holds the workpiece. The piezo stack actuation is in pairs, where each pair in a series will receive maximum and minimum voltage to work in 2D mode, corresponding to actuation in X and Y axis.

The control voltage was amplified by an intermediate amplifier to -20 V to +150 V which was then used to drive the piezo-actuator. Figure 4.23 shows the piezo device, jig, interface and workpiece holder mounted in the DMVAM. The piezo-electric mechanical hinges were made from spring steel and the platform made from aluminium. The maximum unloaded displacement was 20 μm . The overall dimension of the XY25XS is 50 \times 50 \times 15 mm including the jig as a workpiece holder.

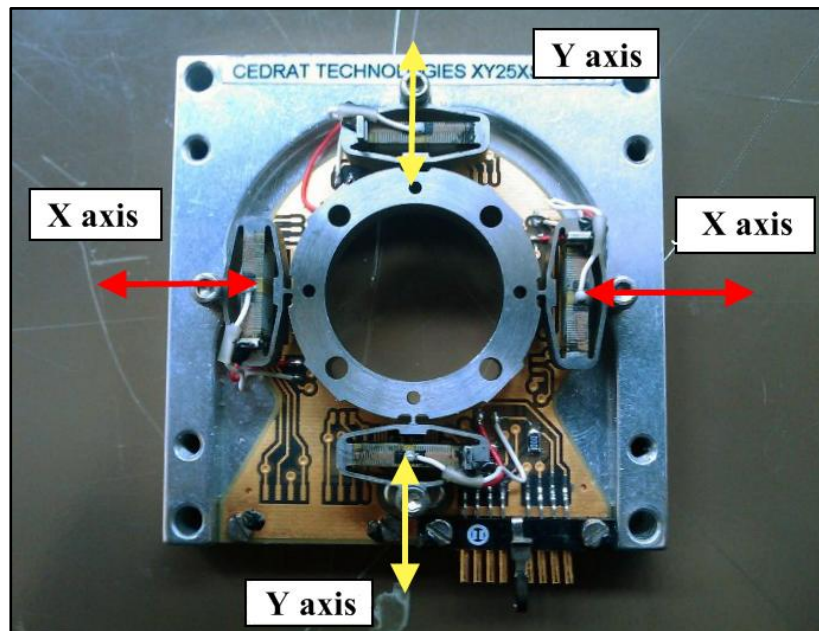


Figure 4.22: The XY25XS model piezo-actuator

Steady loading and response conditions are assumed; that is, the loads and the structure's response are assumed to vary slowly with respect to time. The types of loading that can be applied in a static analysis include:

- Externally applied forces and pressures
- Steady-state inertial forces (such as gravity or rotational velocity)
- Imposed (nonzero) displacements
- Temperatures (for thermal strain)

The analysis can be done in linear and non-linear. All types of nonlinearities are allowed - large deformations, plasticity, stress stiffening, contact (gap) elements, hyperelasticity and so on. This section focused on linear static structural analyses, with brief references to nonlinearities.

Further analysis on the piezo-actuator mechanical structure, static stiffness and modal analysis was performed to determine:

- (a) Stiffness in stroke direction.
- (b) Stroke displacement influenced by hinge on mechanical structure.

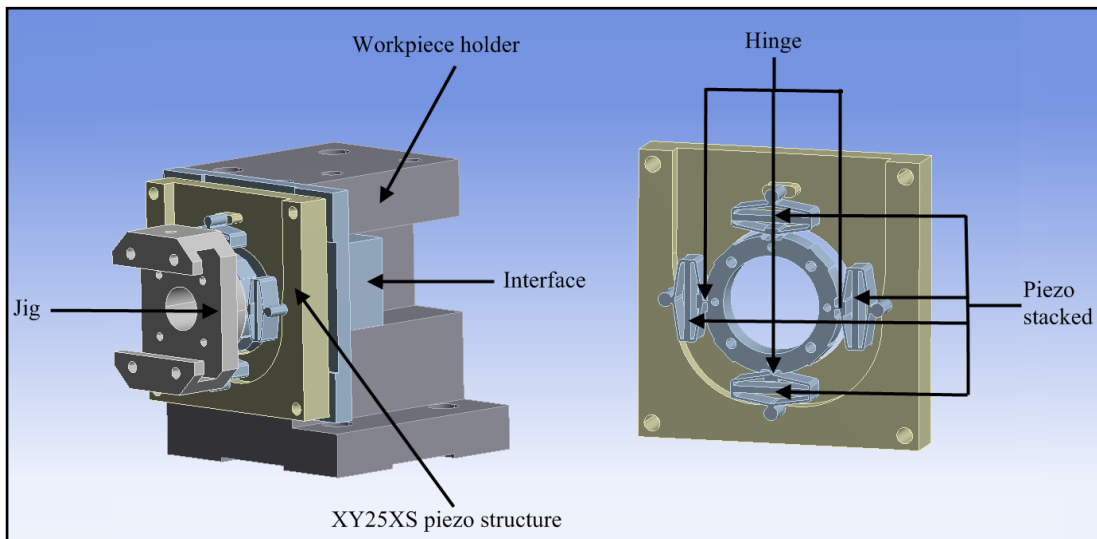


Figure 4.23: 3D drawing and piezo-actuator in detail

A force of 100 N was applied on the piezo-actuator in the X and Y direction to measure the stiffness of the structure, including the hinge. The result obtained for stiffness was 2.5 N/ μm .

By using the equation (Huo and Cheng, 2009) we can calculate the effective stroke of piezo structure was calculated, including the flexures hinge.

$$\Delta L_{eff} = \Delta L_{piezo} \frac{K_{piezo}}{K_{piezo} + K_{hinge}} \quad (4.24)$$

Where, ΔL_{eff} is the effective stroke, ΔL_{piezo} is the nominal stroke, ΔK_{piezo} is the nominal stiffness of the piezo actuator, and K_{hinge} is the stiffness of the flexure hinge in the actuation direction.

So,
$$\Delta L_{eff} = 20 \times \frac{20}{20 + 2.5} = 17.0 \mu\text{m} \quad (4.25)$$

And stroke reduction = $(20 - 17)/20 = 15\%$

Stroke reductions in 2 cases above are below the design requirement and it should be noted that stroke reduction will be higher if the piezo-actuator preloaded effect is taken into account.

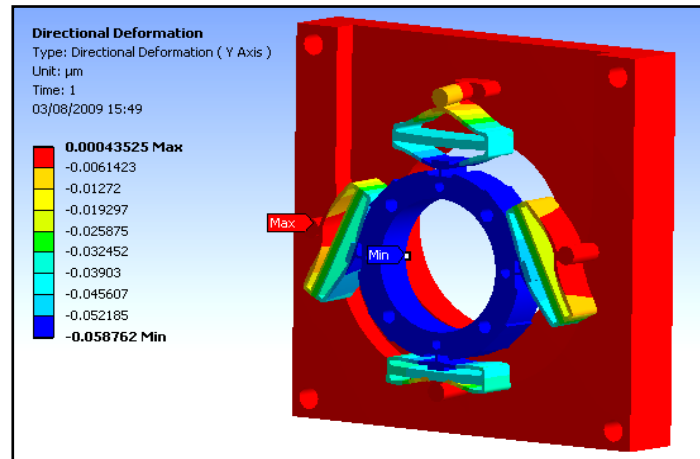


Figure 4.24: Static displacement on piezo and structure

The analysis investigates the reaction of the piezo and the mechanical structure response towards load applied. The load applied can be assuming the force excited by piezo-actuator

via the mechanical structure. The piezo-electric platform, coloured red, is considered a boundary condition as it was fixed by a screw into the workpiece holder by solid aluminium interface as shown in Figure 4.24.

Displacement in the Y axis has been considered for static structural analysis for this piezo and included in the mechanical structure. The standard earth gravity was applied at 9.8066 ms^{-2} in a single degree of freedom. The result of $5.8762\text{e-}002 \text{ }\mu\text{m}$ displacement along with Y axis has been found in this XY25XS model designed by Cedrat Technologies SA. The static structural analysis for piezo-electric can be ignored as the value was very small to put into account.

4.5.3 Modal analysis

This section explains briefly an investigation of XY25XS piezo-actuator in modal analysis. It will determine the vibration characteristics (natural frequencies and mode shapes) of a whole structure including mechanical structure, hinges, piezo-ceramic and base platform without taking into account the other components of the machine. It can also serve as a starting point in a more detailed dynamic analysis, such as a transient dynamic analysis, a harmonic response analysis, or a spectrum analysis.

The natural frequencies and mode shapes are important parameters in the design of a structure for dynamic loading conditions. In this section, the first four natural frequencies and their vibration mode shape were extracted for both configurations using block lanczos method. Table 4.2 lists the first ten natural frequencies and the description of the mode for the piezo-actuator including structure. Detailed pictorial descriptions of the first four vibration modes are shown in Figure 4.25.

The modal FEA results show that the lowest natural frequency was found on the twisting mode. It is predicted that it may be attributed to the weakest part, which is the four hinges that support the cutting components. The first natural frequency was 1756.8 Hz, 2048.7 Hz, and tenth 6669.2 Hz, which is higher than the vibration assisted machining frequency applied during machining.

Table 4.2: First ten natural frequencies of the piezo-actuator

Mode no.	Frequency	Description of mode
1	1756.8	X rotational
2	2048.7	X sliding
3	2063.5	Y sliding
4	2678	Z sliding
5	3872.9	X tilting
6	3885.4	Y tilting
7	6092.2	Complex vibration shapes
8	6308.0	Complex vibration shapes
9	6440.7	Complex vibration shapes
10	6669.2	Complex vibration shapes

The stiffness of the piezo-actuator platform dominated the different frequencies and vibration modes, while the machine component/frame vibration was not excited in the lower frequency range for both configurations. Increasing the stiffness and optimizing arrangement of a piezo-actuator platform and machine component frame are the most effective ways to enhance the machining dynamic performance.

It should be noted that in conventional precision machine design, the first natural frequency is expected to be higher than the machining operation frequency (Shore et al, 2005). However, it cannot be the case in vibration assisted machining, because the maximum spindle speed in DVAM can be up to 15,000 rpm. Modal analysis results provide a desktop vibration assisted machining machine operation frequency that is safe in both condition of natural frequency. Thus, this is the selection guide rather than a threshold for maximum spindle speed.

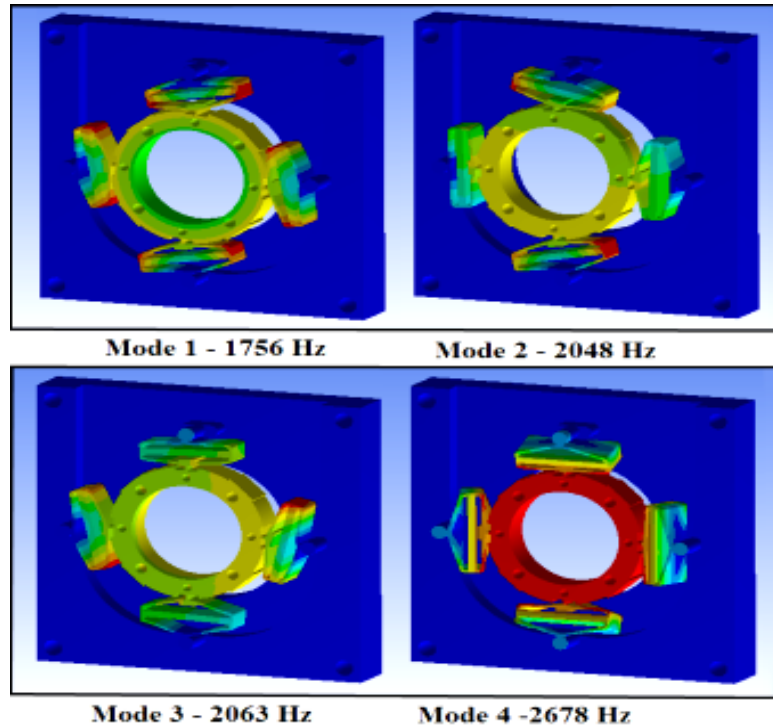


Figure 4.25: 4 Modal shapes of piezo-actuator

By using FE modal analysis, the first four natural mode shape modes of flexure structure were investigated. Figure 4.25 shows the results of natural frequencies of piezo-electric structure starting from 1756.7 Hz, 2048.7 Hz, 2063.5 Hz and 2678 Hz for 1st mode to 4th mode respectively, and the modal shape for the XY25XS piezo-electric including the vibration mechanism of the mechanical flexure.

4.6 Dynamic capacitance and electrical driver response

A model of XY25XY piezo-actuator is constructed by multilayer of piezo ceramic that laminated and very brittle. It cannot bear any tensile force, i.e bending, and any twisting movement must be avoided as far as possible. A piezoelectric actuator is a capacitive device whose capacitance is often very large, as much as 10 microfarads. Such a device is a difficult load for its driving electronics, since charge transfer rate is necessary to achieve a fast response. In addition the actuator will produce electrical energy when submitted to a mechanical load.

4.6.1 Electrical limits

This section gives some rules about the dynamic behaviour and capacitive nature of the piezo-actuator. The piezo-actuator has a limitation of voltage limit that is under the preload compression. The maximum applied voltage is limited to 150 V by the insulating layer. Since the thickness of the layer in the MLA is 100 μm , it corresponds to an electrical field of 1.5 kV/mm. The applied voltage cannot be decreased under -20 V (Shore 2005), otherwise the polarization would be reversed, as shown in Figure 4.26.

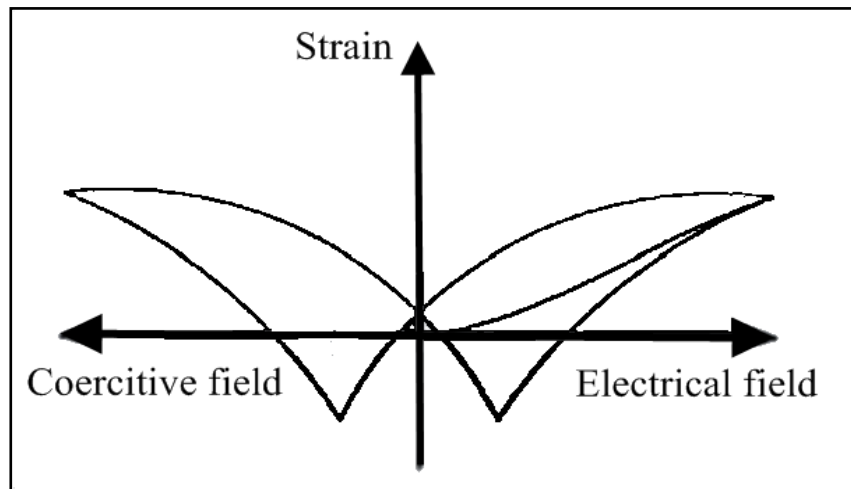


Figure 4.26: Electrical field-strain relation in a piezoelectric material

In dynamic strain non-resonant operation, electrical limits may be encountered. As investigation of the capacitive nature of the piezo-actuators shows, the higher the frequency is, the higher current should be applied.

4.6.2 Thermal limits

Due to dielectric and mechanical losses, the piezoelectric actuator warms up under continuous excitation. Losses are mainly non-linear and depend on the excitation frequency, the voltage amplitude and the humidity level. To avoid a de-polling effect of the ceramic, the temperature in the actuator should be monitored to ensure that it stays well below the ceramic's Curie temperature. The typical temperature range from -40° C to 80° C can be observed.

As a consequence, the duty cycle of a piezo-electric actuator in dynamic operation is limited by its thermal behaviour. For example, to maintain a constant temperature on the model APASM actuator, the duty cycle should be reduced as the driving frequency increases, as shown in Figure 4.27.

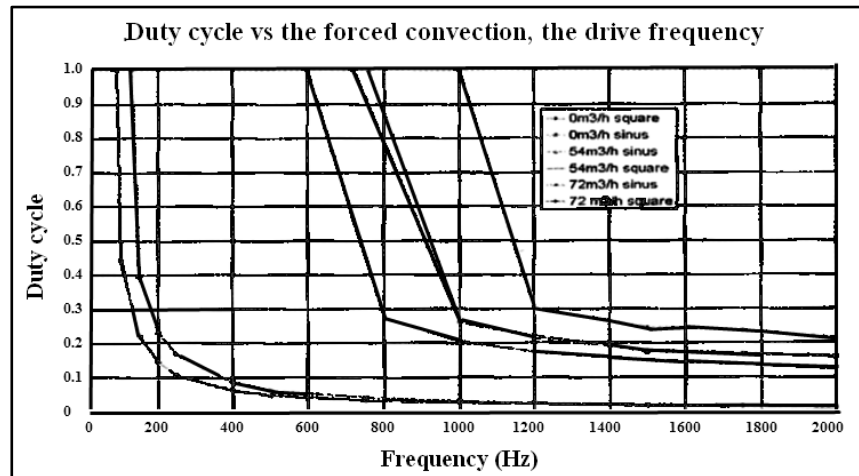


Figure 4.27: Limitation of the standard of piezo due to self heating

Thermo-mechanics may be an issue in the case of a fine positioning application over a large range of temperatures. It is because the piezo-electric actuator designs in the multilayer technique display various Coefficients of Thermal Expansion (CTE). A standard amplified piezoelectric actuator displays fairly large CTE due to some thermal mismatch between the piezo component and the shell material.

4.6.3 Driving and electrical response

To power the piezoelectric actuator, the linear amplifier has been selected to send a high signal to noise ratio. Switched power amplifiers are more efficient under reactive loading in dynamic applications, but are more difficult to control. The general synoptic of the driving system for a piezoelectric system is shown in Figure 4.28.

With a linear amplifier, the voltage applied to the actuator is directly proportional to the input signal. The gain in power from the original manufacture of the amplifier is set to 20. Therefore, to obtain the whole stroke of the actuator, one should input a signal varying from

-1 V to 7.5 V, which means the applied voltage on the piezo-electric actuator will then vary from -20 V to 150 V.

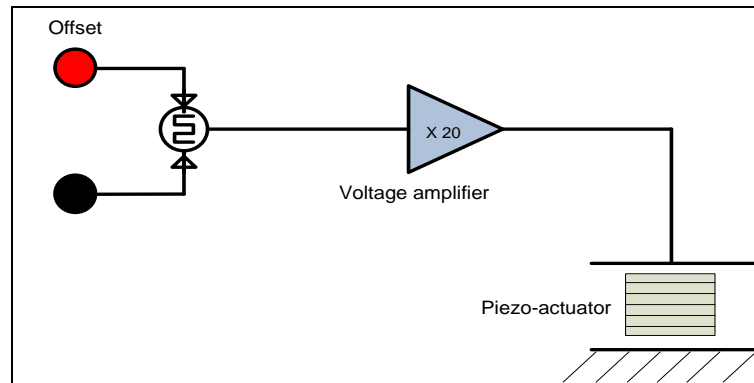


Figure 4.28: Synoptic of a driving system

The resolution of a piezoelectric actuator is limited by the electrical noise of the driving system. Typical values of the signal to noise ratio of the driving electronic is below the resonance frequency of the actuator range from 80 to 120 dB.

Each of the piezo-actuators has a hysteresis. Most of them are large when fixed with a mechanical structure such as a hinge, spring, damper, etc. which limits the positioning accuracy. Other effects for instance drift, also limit the actuator linearity. Therefore, displacement sensors are often used to ensure a linear response of the piezo-electric actuator through a closed-loop as shown in Figure 4.29.

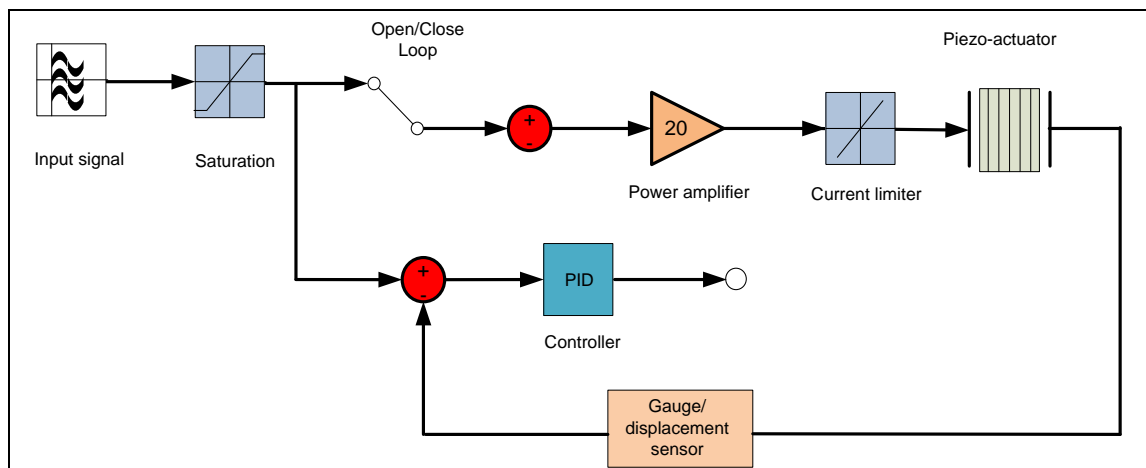


Figure 4.29: Synoptic of a closed loop system

Two types of driving electronics are available: the linear type offers a good signal to noise ratio, while the switching type is more efficient. If high accuracy is required, a closed loop including the actuator, a position sensor and controller are necessary to remove the hysteresis behaviour.

4.7 Summary

This chapter explains the utilisation of theoretical and practical work in the research. Initially, the related principles of machine dynamics, including an electrical component response, have been elaborated. This is to investigate the interaction and effect of parts/components assembled together on the machine dynamics and the influence of disturbance factors such as gravitational force, impact force and other noise factors, all of which can disturb the machine system.

Furthermore, the in-depth studies of static and modal analysis for machine structure and piezo-actuator mechanical structure are also included. With the theoretical and practical information of machine dynamics, the formulations of a real experimental environment using an impact hammer have been performed.

In order to characterize the influence parameters, results with the simulation images are presented. Besides the fundamental aspects of the electrical component, driving system research work is investigated. The perspective application of the response system is also studied. Furthermore, the formulation includes the theoretical picture of machining process, and the equation of motion and manipulation. To optimise the machine system design, both the electrical and control response as related to machine specification are also inspected.

Chapter 5 Process modelling and simulation

5.1 Introduction

This chapter presents the process modelling and simulation in investigating surface roughness, tool wear and material removal rate (Figure 5.1). The simulation and modelling was focused on the cutting process and cutting mechanism in vibration assisted micro-milling. The modelling of mechanical cutting force proposed from conventional machining has been explained, and is thus carried out for the vibration assisted machining. The effects of the cutting force, feed rate, vibration, vibration amplitude and frequency and spindle speed have been investigated in generation of a surface and on the cutting performance.

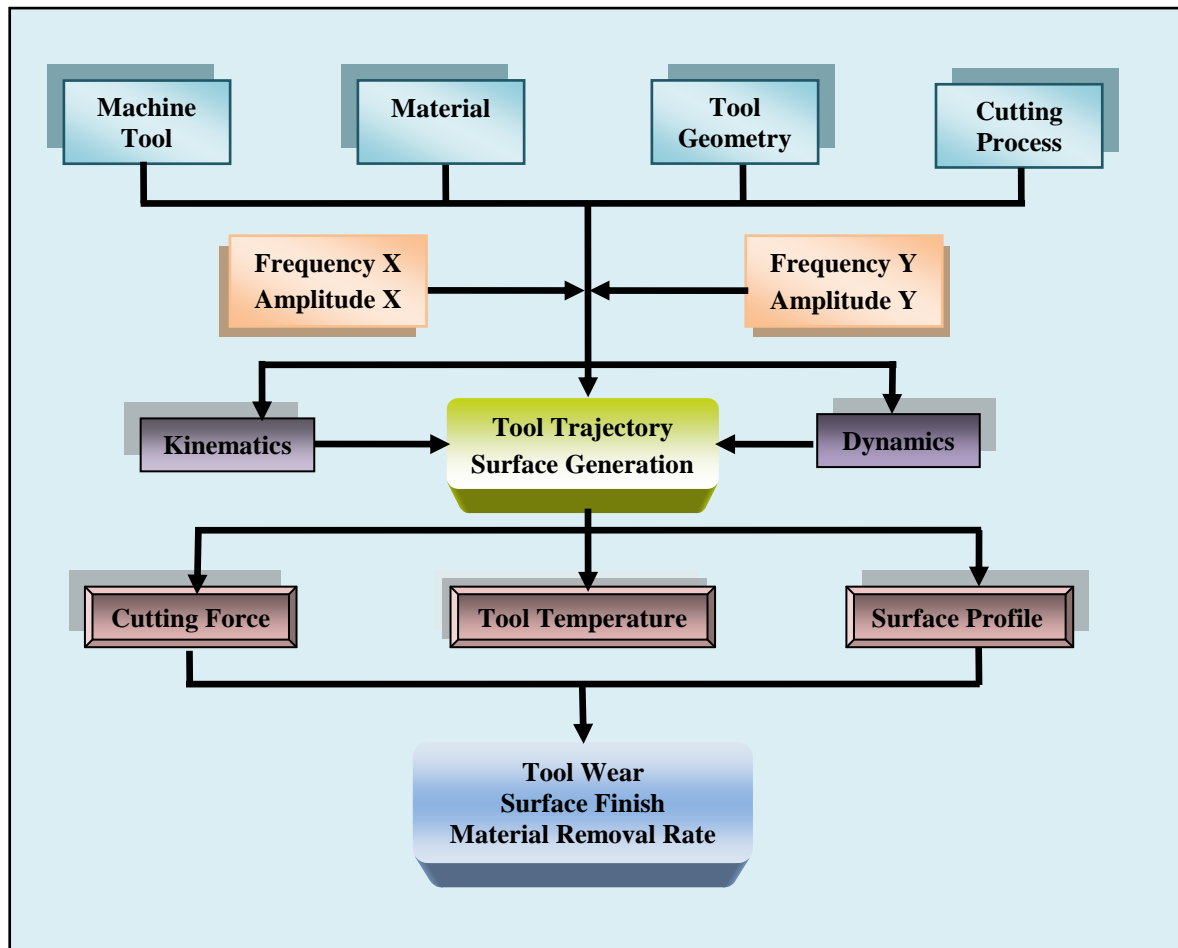


Figure 5.1: Process modelling and simulation

5.2 Process modelling approach

Macro cutting and micro cutting are obviously defined in different ways. In macro cutting, the depth of cut is larger than the tool edge radius and then the effect of the tool radius can surely be ignored (Figure 5.2). On the other hand, in micro cutting, the radius has an effect on the mechanism in cases where the elastic recovery occurs in the flank face of the workpiece. The tool radius is sliding due to contact between the tool and workpiece, and ploughing due to the tool edge is regarded as a major cutting mechanism (Arcona, 1998).

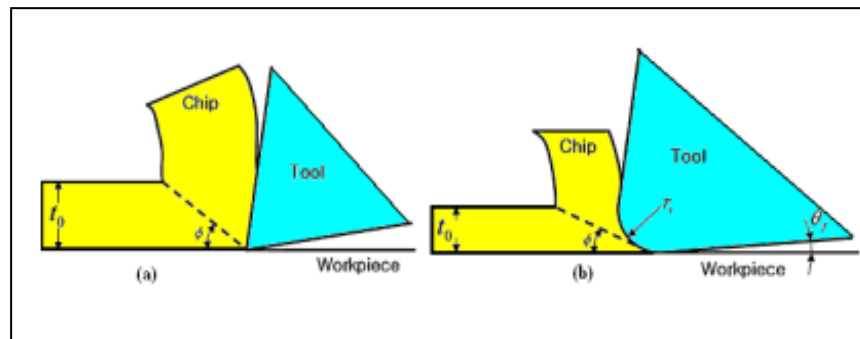


Figure 5.2: Micro and macro cutting mechanics

From the previous researchers, experimental results illustrate that elastic deformation of the machined workpiece surface plays an important role, even in diamond machining. In order to investigate the tool cutting force, the above must be taken into account even in machining with a very sharp tool (Arcona and Dow, 1992). The material spring back behaviour has already been discussed by Arcona and some others researchers. Ikawa and Shimada (1989) have predicted the relationship for spring back and plotted it as a linear function of the tool edge radius and the ratio of material hardness by elastic modulus, which has been referred to by many researchers.

The best correlation found between the measured and calculation for spring back with 0 degree rake and 8 degree of clearance angle is 43° , referred to in the Ikawa and Shimada work (Ikawa et al, 1997). To define the effect of the elastic recovery of material in the flank face of the workpiece, the relief angle and the springback of the material which was used for L_f can be obtained with the following expressions:

$$L_f = \frac{S}{\sin \theta_f} \quad (5.1)$$

Where S is a springback involving $k_1 r_t H / E$, k_1 is the constant, r_t is tool edge radius, H and E are Vicker's hardness and the material elastic modulus, and θ_f is the relief angle of a tool. It has been shown that the friction coefficient is very much dependent on the sliding velocity. A new friction model has been identified based on the average local sliding velocity (Rech et al, 2009).

The sliding of contact surface in contact frictional force from the tool-workpiece contact following the elasticity recovery in the flank face can be expressed from the material yield strength and the contact length. In order to define the direction of component, the tool workpiece contact frictional force in the flank face is F_{fc} and F_{ft} . The horizontal and the vertical components towards the cutting direction can be expressed as:

$$\begin{cases} F_{fc} = \frac{CY}{\sqrt{3}} L_f b \\ F_{ft} = CY L_f b \end{cases} \quad (5.2)$$

The model predicted by Tlustý and MacNeil to obtain cutting force is heavily dependent on the yield and flow stresses that can be got from the material property, where the C will be constant and determine the compensation for the properties of the material (Tlustý et al, 1975).

The Coulomb model with a constant coefficient, irrespective of temperature and pressure, is usually used to simulate the friction phenomena at these interfaces. However, in metal cutting, a wide range of cutting speed is issued. The temperature at interfaces is directly influenced by the friction velocity. Moreover the sliding velocities in the rubbing zone and in the secondary shear zone are very much different.

The shear plane and the contact friction of the flank face are considered in the cutting force of micro cutting. The shear plane that will be forced by the normal component can be obtained as:

$$\begin{cases} F_s = \frac{\bar{\sigma} bh}{\sqrt{3} \sin \phi} \\ N_s = \frac{\bar{\sigma} bh}{\sin \phi} \end{cases} \quad (5.3)$$

Consequently, in the micro cutting, the principal cutting force and thrust cutting force can be calculated as equation (5.4). They are expressed in the form in which the frictional force of contact on the flank face is added to the existing two-dimensional cutting.

$$\begin{cases} F_c = F_s \cos \phi + N_s \sin \phi + F_{fc} \\ F_t = -F_s \sin \phi + N_s \cos \phi + F_{ft} \end{cases} \quad (5.4)$$

The cutting force obtained from Equation (5.4) applies to the model of Tlustý that is widely used in the conventional end-milling process shows in Figure 5.3 (Tlustý et al, 1975).

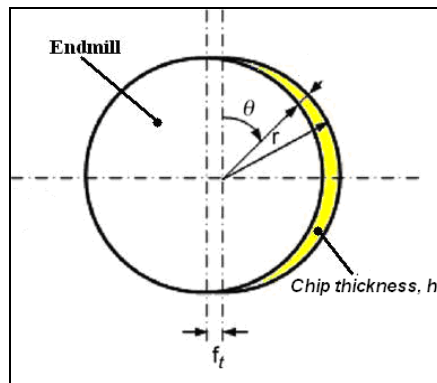


Figure 5.3: Conventional end milling

According to the conventional cutting force model by Tlustý and MacNeil, the cutting force in micro-end milling can be predicted by using the same principle of cutting force F_c and

thrust cutting force F_t and the tool edge radius needs to be considered. Tlusty and Mcneil proposed the cutting force model by developing three assumptions in their calculation, which were:

i) Assumption 1

The tangential cutting force F_t is directly proportional to the cutting area, which can be expressed:

$$F_t = K_m bh \quad (5.5)$$

ii) Assumption 2

The radial cutting force, F_r , is proportional to the tangential cutting force, which can be expressed:

$$F_r = pF_t \quad (5.6)$$

iii) Assumption 3

The tangential cutting force F_t , can be obtained by the modelling above for the end mill cutting process. Thus the chip thickness h in conventional end milling can be calculated as the function of tool rotation angle as in the expression below:

$$h = f_t \sin \theta \quad (5.7)$$

According to the model of Tlusty as shown in Figure 5.4, the chip thickness varies in end milling, thus the area of cutting force acting toward the workpiece differs at each position depending on tool rotation angle. Moreover, the cutting force element of principal cutting force and thrust force can be presented as Equation (5.8).

$$\begin{cases} dF_c = \left(\frac{\bar{\sigma} f_t r \cos \phi}{\sqrt{3} \sin \phi \tan \beta} \sin \theta + \frac{\bar{\sigma} f_t r}{\tan \beta} \sin \theta + \frac{Y L_f r}{\sqrt{3} \tan \beta} \right) d\theta \\ dF_t = \left(-\frac{\bar{\sigma} f_t r}{\sqrt{3} \tan \beta} \sin \theta + \frac{\bar{\sigma} f_t r \cos \phi}{\sin \phi \tan \beta} \sin \theta + \frac{Y L_f r}{\tan \beta} \right) d\theta \end{cases} \quad (5.8)$$

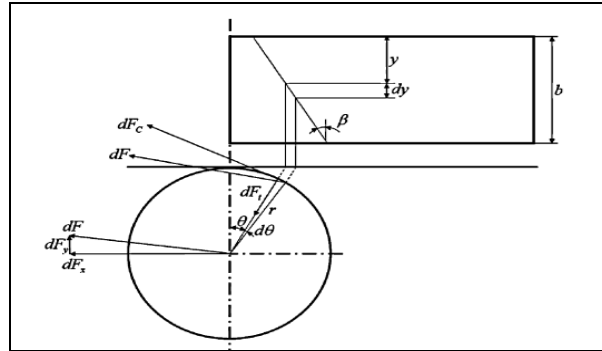


Figure 5.4: Contribution of element cutting edge

Where β , b , r and y is tool helix angle, width of cut, radius of tool and normal direction respectively.

5.2.1 The proposed model for 2D VAM

The modelling of 2D VAM is carried out based on the conventional machining modelling by investigating the mechanism during the cutting process. The general idea is by adding the 2 vibration axes which is acting on the X and Y axis simultaneously (X in horizontal for feedrate direction).

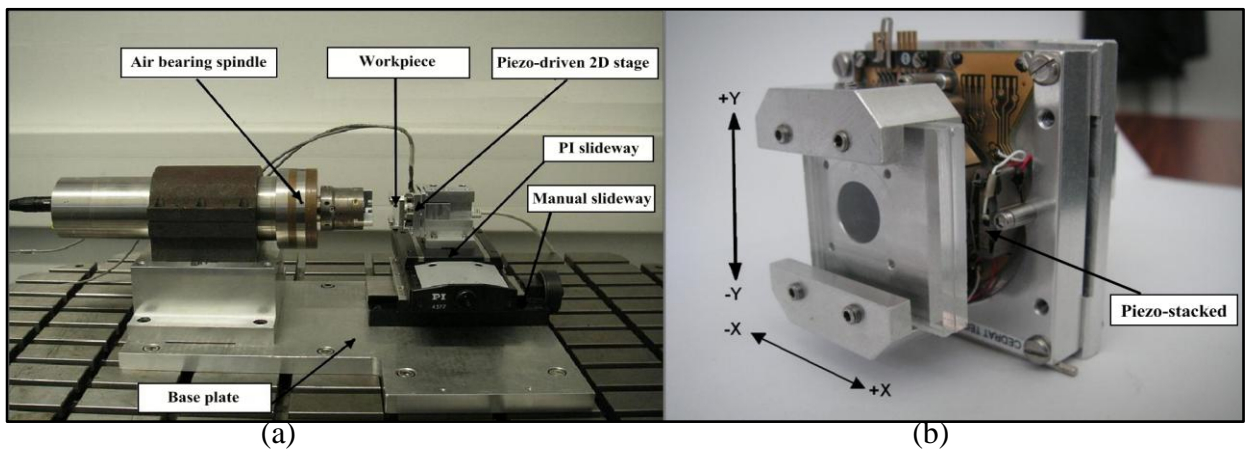


Figure 5.5: 2D VAM setup

Figure 5.5(a) shows the experimental setup of 2D vibration assisted micro-milling and Figure 5.5(b) is a close view of the vibrating platform assembled with piezo structure and workpiece jig to clamp the workpiece during the cutting process. X axis is feed direction and Y axis is normal direction.

In order to get a scientific understanding of the kinematics and mechanics in vibration assisted milling, it is important to investigate the process cutting mechanism. During tool cutting, the friction between the tool and the chip in metal cutting influences the cutting force chip formation, build up edge formation and tool temperature.

It is necessary, to understand tool chip friction, to develop an accurate model for cutting forces with the frictional stresses and heat generated, and to use this as a basic boundary condition. The tool-chip friction coefficient, μ_e is to be define as the ratio of the cutting force, P parallel to the tool rake face to the force normal to the rake face, N_f :

$$\mu_e = \frac{P}{N_f} \quad (5.9)$$

For a milling machining oblique model process, the resulting force components in orthogonal direction are shown in Figure 5.6. F_n and F_c are the force components to the normal cutting edge and parallel to the cutting velocity respectively.

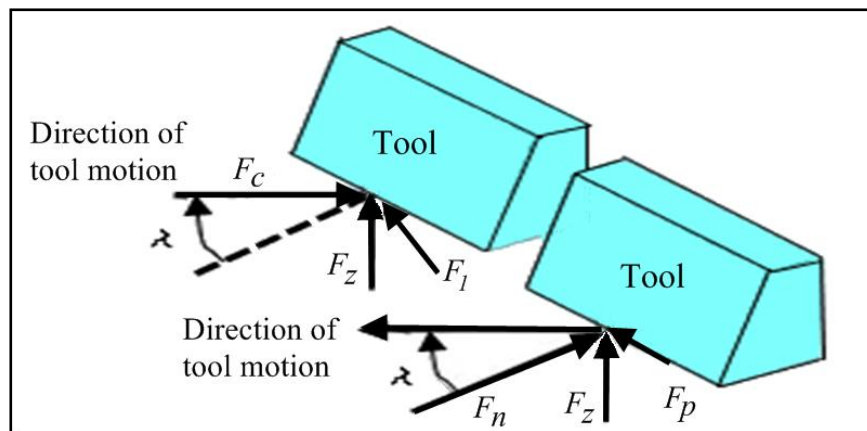


Figure 5.6: Oblique cutting force

Figure 5.6 shows the basic oblique cutting force. F_p is the force component parallel to the cutting edge, F_z is the normal component acting on the plane which can be expressed as F_n and F_p , where the F_1 is the force component normal to the plane by F_c and F_z . F_p , F_c , F_1 and F_n are distinguished by the inclination angle λ which can be expressed as:

$$\begin{aligned} F_n &= F_c \cos \lambda + F_1 \sin \lambda \\ F_p &= F_c \sin \lambda + F_1 \cos \lambda \end{aligned} \quad (5.10)$$

Vibration assisted micro-milling in 2 dimensions is different from the normal cutting model as it is imposed by two vibration axes in X and Y direction, as shown in Figure 5.7.

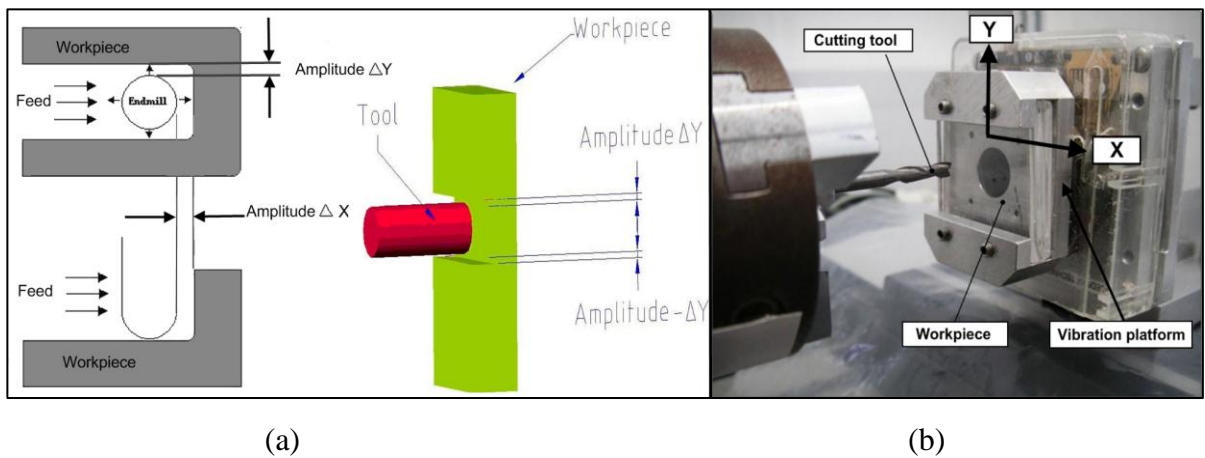


Figure 5.7: (a) physical model (b) real setup model

5.2.2 Motion shape in 2D VAM

The combination of sinusoidal signals acting in X and Y vibration in different axes creates an ellipse or round shape of tool motion. Cerniway had studied the VAM and used an eclipse shape in his model. However, Shamoto and Moriwaki used a circular tool motion to investigate the VAM cutting mechanism. For the wide horizontal elliptical tool motion modelled by Cerniway, vertical vibration (Y axis) velocity increased slowly related to the horizontal axis (X axis) in the circle tool path. Modelled by Shamoto and Moriwaki it is explained that the vibration amplitude in X and Y is the same displacement/amplitude, the

vertical vibration (Y axis) increased faster than the circular one. The mathematical equation of these two models can be described,

$$\frac{x^2}{a^2} + \frac{y^2}{b^2} = 1 \quad (5.11)$$

Defining the X and Y axis amplitude of the tool in Equation (5.11). Both axes can be expressed as,

$$\begin{aligned} x &= A \cos(2\pi ft) \\ y &= b \sin(2\pi ft) \end{aligned} \quad (5.12)$$

Figure 5.8 shows the a and b respectively related to the major and minor axis to the axial component of ellipse or circular motion of tool. The size and shape of the tool path motion depends on the value of a and b which is in micron.

A significant finding was explained when Negishi and Shamoto claimed that the chip formation in 2D VAM was influenced by the combination of the ratio of a and b through their experimental study. The indication of chip long thickness can be controlled through this method leading to reduced burr, surface roughness and improved accuracy (Brehl, 2008).

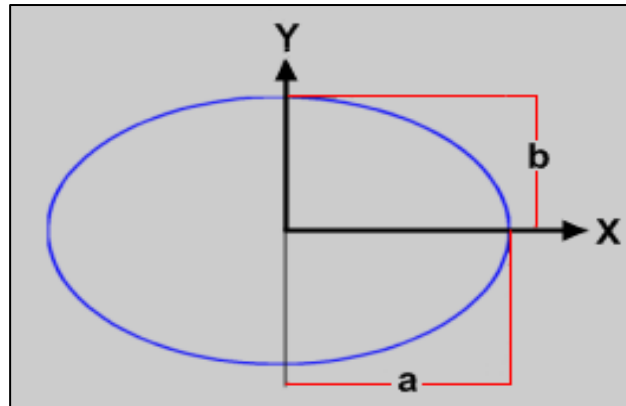


Figure 5.8: Effect value a and b in VAM

5.2.3 Tool path trajectory

In conventional milling, the trajectory of the tool path depends on the spindle speed and feedrate relative to the workpiece. The spindle speed is the important part as it carries the tool tip edge to the round shape, but it will be different and change shape when the feedrate starts to move. The centre of the endmill tool bar must be described in order to know the behaviour of the tool tip motion later. It is because the boundary of the tool bar is taken as a reference to drive the tool tip motion. It can be expressed as:

$$\begin{cases} x_2 = ft + A \sin(2\pi f_x t + \phi_x) \\ y_2 = B \sin(2\pi f_y t + \phi_y) \end{cases} \quad (5.13)$$

Bao and Tansel modelled the tool tip trajectory and tried to investigate the chip thickness and difference from the Tlustý and Macneil model using Equation (5.14).

$$\begin{cases} x = \frac{ft}{60} + r \sin\left(\omega t - \frac{2\pi z}{Z}\right) \\ y = r \cos\left(\omega t - \frac{2\pi z}{Z}\right) \end{cases} \quad (5.14)$$

Liu and Cheng modelled a tool path as simply traces by the spindle rotation angular velocity, tool cutter helix angle, regenerative cutter displacement and the cutting tool radius. However, in 2 dimensional VAM, the tool tip motion relative to the workpiece is complex and cannot be considered a helix shape as the vibration acts on the X and Y axes simultaneously.

So, the component of 2D VAM can be obtained when the described components in Equation 5.12, 5.13 and 5.14 are combined together, which can be expressed by.

$$\begin{cases} x1 = ft + r \sin[\omega t - \frac{2\pi(z_i - 1)}{Z}] + A \sin(2\pi f_x t + \phi_x) \\ y1 = r \cos[\omega t - \frac{2\pi(z_i - 1)}{Z}] + B \sin(2\pi f_y t + \phi_y) \end{cases} \quad (5.15)$$

The trajectory of the tool locus in 2D VAM is robust. Depending on the 4 important factors described in Figure 5.7, it contains:

- Vibration frequency X and Y axis
- Vibration amplitude X and Y axis
- Spindle speed
- Feedrate

The two dimensional vibrations assisted milling process is shown in Figure 5.7, where the X axis feed direction and amplitude is in the X axis, the Y axis is the normal direction and the Z axis is the depth of cut in order to determine the locus of the tool simulation relatively in to the workpiece.

To determine the tool cutting edge to get the boundary of the overlapping tool path related to the centre point of the tool, a new equation is formed by combining Equations (5.13) and (5.15) which can be expressed as:

$$(y2 - y1) \times x - (x2 - x1) \times y - x1 \times y2 + x2 \times y1 = 0 \quad (5.16)$$

Shamoto (1998) explained that the circular motion of tool in 2D VAM with the vertical velocity could drive the thrust force in the reverse direction. During the tool motion, direction exceeds the shear angle, the tool is moving faster than the chip and the friction direction is reversed. From this point onward, the friction is no longer restraining chip motion but is assisting it. The reduced or reversed friction leads to significant reduction in cutting force, energy and heat generation.

The tool locus of 2D VAM becomes complex when the feedrate and vibration in X is periodically merged in relation to workpiece edge. The substitution of feedrate factor into chip thickness calculation in 2D VAM cutting force can be expressed as:

$$\begin{cases} F_c = \frac{\bar{\sigma} hr \cos \phi}{\sqrt{3} \sin \phi \tan \beta} + \frac{\bar{\sigma} hr}{\tan \beta} + \frac{YL_f r}{\sqrt{3} \tan \beta} \\ F_t = -\frac{\bar{\sigma} hr}{\sqrt{3} \tan \beta} + \frac{\bar{\sigma} hr \cos \phi}{\sin \phi \tan \beta} + \frac{YL_f r}{\tan \beta} \end{cases} \quad (5.17)$$

Where F_c is the principal cutting force, F_t is thrust cutting force, h is the chip thickness. The accuracy of the cutting mechanics been proved with the aid of cutting force theories has been investigate by principal force and thrust force.

According to Zaman's cutting force model in micro-milling the axial component of the cutting force is the vertical component of the principal force.

$$F_a = F_c \cos\left(\frac{\pi}{2} - \beta\right) \quad (5.18)$$

Accordingly, the three dimensional cutting force model of 2D VAM can be expressed,

$$\begin{cases} F_c = \frac{\bar{\sigma} bh \cos \phi}{\sqrt{3} \sin \phi} + \bar{\sigma} bh + \frac{Y}{\sqrt{3}} L_f b \\ F_t = -\frac{\bar{\sigma} bh}{\sqrt{3}} + \frac{\bar{\sigma} bh \cos \phi}{\sin \phi} + YL_f b \\ F_a = F_c \cos\left(\frac{\pi}{2} - \beta\right) \end{cases} \quad (5.19)$$

From Equations 5.18 and 5.19, the three cutting force components can be developed, which are feed (x), normal force (y) and axial (z) in the direction of the axis. This can be presented as follows:

$$\begin{cases} F_x = \left(-\frac{\bar{\sigma}bh \cos \phi}{\sqrt{3} \sin \phi} - \bar{\sigma}bh - \frac{Y}{\sqrt{3}}L_f b \right) \cos \theta + \left(\frac{\bar{\sigma}bh}{\sqrt{3}} - \frac{\bar{\sigma}bh \cos \phi}{\sin \phi} - YL_f b \right) \sin \theta \\ F_y = \left(\frac{\bar{\sigma}bh \cos \phi}{\sqrt{3} \sin \phi} + \bar{\sigma}bh + \frac{Y}{\sqrt{3}}L_f b \right) \sin \theta + \left(\frac{\bar{\sigma}bh}{\sqrt{3}} - \frac{\bar{\sigma}bh \cos \phi}{\sin \phi} - YL_f b \right) \cos \theta \\ F_z = \left(-\frac{\bar{\sigma}bh \cos \phi}{\sqrt{3} \sin \phi} - \bar{\sigma}bh - \frac{Y}{\sqrt{3}}L_f b \right) \cos \theta \sin \beta + \left(\frac{\bar{\sigma}bh}{\sqrt{3}} - \frac{\bar{\sigma}bh \cos \phi}{\sin \phi} - YL_f b \right) \sin \theta \sin \beta \end{cases} \quad (5.20)$$

5.2.4 Vibration cutting ratio

To get a better understanding of 2D VAM, the ratio of the contact tool and non-contact tool to the workpiece must be studied in order to investigate the efficiency of the system, such as chip thickness, chip formation, etc. The frequency and amplitude are the most dominant factors for this ratio. However, the feedrate and spindle speed can make small changes which can provide the optimum chip removal efficiency.

Altintas (2000) explained that periodic loading causes cyclic mechanical and thermal stresses on the tool, causing the tool life to be shortened. Nevertheless, his model focused on the conventional cutting with the ratio of contact cycle in one. That means that for 100% of cutting time the rake face is in contact with the workpiece, which is hugely different from 2D VAM. Contact and non-contact tool ratios can be obtained by using this equation,

$$CuttingRatio = \frac{Time_{noncontact}}{Time_{totaltime}} \times 100\% \quad (5.21)$$

Where $Time_{noncontact}$ the sum of time that the rake faces, or the tool tip is not in contact with the workpiece. $Time_{totaltime}$ is the sum total of time the tool is in the cutting area. The higher the *cutting ratio* the more time the tool is separated from the workpiece, which can be of higher benefit for chip removal efficiency, cutting force reduction, cutting temperature,

extending tool life, etc (Stephenson, 2006). The impact and ploughing with which the tool tip penetrates the workpiece in 2D VAM can be predicted since it can be controlled by vibration and frequency to achieve a ductile region to improve surface roughness (Adachi et. al, 1997) Therefore the ratio of amplitude towards the feedrate motion must be identified to predict the cutting ductile region because the small forces of amplitude in controlled distance promote micro-crack and micro-fracture damage to the workpiece. Negeishi (2003) performed cutting with 2D VAM and maintained ductile cutting to 3.5 μm depth into the silicon carbide. By taking this benefit into account, the amplitude feed ratio has been introduced to investigate the relationship of amplitude effect on the feed per tooth, which can be mathematically defined as:

$$AmplitudeFeed = \frac{A_{\max chip}}{f_{tooth}} \quad (5.22)$$

Where the $A_{\max chip}$ is the maximum amplitude of chip thickness and F_{tooth} is feed per tooth. The trajectory of the tool point will reveal the regularity which is affecting the workpiece thus taken into account from the area of cutting. It has been discussed before that the amplitude and shape of circle depends on the value of a and b (Ding, 2010). However, the oscillations number is controlled by three factors, f_x , f_y and n , which can be expressed as:

$$\frac{60}{n} = \frac{M}{f_x} = \frac{N}{f_y} \quad (5.23)$$

Where M is vibration time in 1 cutting cycle in X axis, N is vibration time in 1 cutting cycle in Y axis and n is a spindle speed. Increasing the frequency f_x or f_y will give more chances for the tool to vibrate into certain areas of the workpiece. This ratio is important to determine the chip thickness and shape produced at a certain frequency.

5.3 Cutting mechanics in 2 dimensional VAM

Table 5.1 shows the advantages of vibration assisted machining compared to the conventional machining in a wide range of applications.

Table 5.1: Comparison between 2D VAM and conventional machining

	Conventional milling	Vibration assisted milling	Comments
Cutting force	<ul style="list-style-type: none"> • The rake angle and clearance angle are in permanent contact in one area toward workpiece. • The chip produced is constant with no overlapping tool path. • Long, thick and longer chip produced. 	<ul style="list-style-type: none"> • The movement of tool point in ellipse motion altering the effective rake angle toward the workpiece for reducing the cutting force (rake angle becomes progressively more negative). • The tool force reduction is due to making chips that are thinner and shorter than the overall feed per tooth in conventional cutting. These thin chips occur because of the consecutive overlapping elliptical tool paths. • Tool velocity exceeding the chip velocity, producing a reversal of the direction of the tool-chip friction force and reduction or reversal of the thrust force. 	<ul style="list-style-type: none"> • Rake angle and clearance angle of tool in both machining is differ during approach to the workpiece. • 2D VAM generate overlapping tool motion to divide the cutting force in smaller section cutting area.
Chip thickness	<ul style="list-style-type: none"> • Chip always thicker and dependent on feedrate and spindle speed only. 	<ul style="list-style-type: none"> • Chip thickness thinner and strongly dependent on the amplitude, spindle speed, smaller amplitude, and thinner chip produced. • The consecutive overlapping toolpaths result in chips that are thinner than the feed per tooth. 	<ul style="list-style-type: none"> • Conv. machining cutting a w/p in each single rotation in one cycle, but 2D VAM cutting a w/p much smaller cause the frequency and amplitude effect.
Chip formation	<ul style="list-style-type: none"> • Chip longer and dependent on feedrate and spindle speed only. 	<ul style="list-style-type: none"> • Discontinuous/shorter chip strongly dependent on the frequency, amplitude and spindle speed. Higher frequency, smaller chip produced. • Instantaneous uncut chip thickness at each point in the tool path is less than feed per tooth. 	<ul style="list-style-type: none"> • Conv. machining cuts a workpiece in each single rotation in one cycle, but 2D VAM cuts the workpiece much smaller causing the frequency and amplitude effect.
Cutting temperature	<ul style="list-style-type: none"> • No gap to dissipate heat energy. • Tool always making contact with workpiece. 	<ul style="list-style-type: none"> • Alternating cycles (gap) promotes heat to dissipate between cutting tool and workpiece, therefore 40% to 50% heat reduced. • Less time contact between tool and workpiece providing chances of tool and workpiece to release heat energy. 	<ul style="list-style-type: none"> • 100% of cutting time tool point is kept in contact on conv. machining with the workpiece, but in 2D VAM, clearance distance has been

		<ul style="list-style-type: none"> • Lubricated flowing results from periodic tool-work separation. • the work-tool contact area varies at several points on the elliptical path. 	<p>created when the tool point is retracted from the workpiece.</p>
Tool life	<ul style="list-style-type: none"> • Temperature rising accumulates to soften the tool. • Tool always in contact and always in stress condition. 	<ul style="list-style-type: none"> • Constant temperatures encourage tool cutter to maintenance the hardness and strength ability. • 40% to 50% time contact reduced between rake angle and clearance angle and workpiece. Chance for tool to release stress force. • Intermittent contact between tool and work material in VAM reduces the time available for graphitization and other wear reactions. 	<ul style="list-style-type: none"> • Tool life in conv. machining is reduced due to thermal softening, but in 2D VAM, the temperature is constant and reduced 30%-40%. • Tool failure ratio from stress and strain is low.
Material removal rate	<ul style="list-style-type: none"> • Constant rake angle and clearance angle toward the workpiece. • Higher cutting force, slower material to be cut. 	<ul style="list-style-type: none"> • Various/changeable rake angle reduces the cutting force. Therefore, faster cutting process promotes faster material removal rate. • Less cutting force promotes faster cutting process and more material to be cut. 	<ul style="list-style-type: none"> • 2D VAM has high material removal rate benefit from the reducing cutting force, extended tool life, ductile cutting etc compared with conv. machining.
Surface roughness	<ul style="list-style-type: none"> • Material cracking non-uniform. • Continuous chip promoted higher peak to peak. • No secondary motion to remove residual bur. 	<ul style="list-style-type: none"> • Uniform alternating cycles between tool point and the workpiece provide uniform cracking and delimitation of material. • Discontinuous chip creates lower peak to peak (Rt), roughness average (Ra). • Ellipse tool motion promotes the separation of the residual burr in the workpiece efficiently. • Help cutting material in ductile mode. 	<ul style="list-style-type: none"> • Cutting region in 2D VAM controlled by small amplitude and frequency, but in conv. machining the cutting region is unpredictable and uncontrollable. • In 2D VAM cutting method, the cutting scale is in micro scale in ductile cutting regime, but in conv. machining, they are always in macro/larger scale cutting condition.

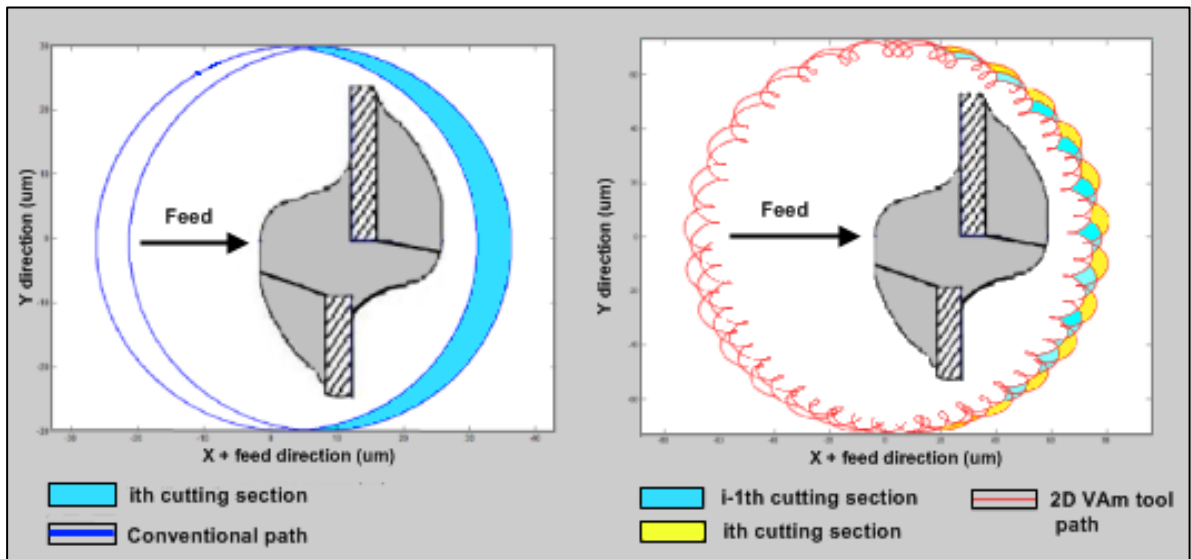
5.3.1 Cutting force and chip thickness

Many researchers have modelled the cutting force in a different way and shown their accuracy by developing a chip thickness theory. For instance, Thusty modelled based on the cutting trajectory. Merchant was taking a shear plane and slip-line field analysis to define the cutting force. Mohammad and Simon introduced ploughing coefficients, which are the ploughing forces per unit of ploughed volume by investigating the elastic recovery, and tool vibration including the effect of tool path trajectory.

The elastic recovery is identified using the instrumented scratch tests instead of the tool itself to void the tool breakage. However, in this section, the model of 2D VAM for cutting force is investigated by looking at a trajectory of the tool path and predicting the chip thickness. From the chip thickness the cutting force is calculated by merging the vibration effect into the original tool locus.

According to the Ding model of vibration assisted micro-milling, for calculating the cutting force in 2D vibration micro-milling, it is based on the chip thickness from the trajectory of the tool locus. The assumption is that the cutting force is proportional to the cutting area.

Figure 5.9, generated by MatLab programming, revealed the cutting mechanics in 2D, with effect of vibration frequency and amplitude, promoted that many cycles take place in a specified time interval. It is clear that the cutting force is reduced when the tool point of the tool is in high force to remove the material in one single cut. In 2D VAM, the vibration introduced non-contact within the tool and workpiece, helping to cut the material to smaller pieces while opposing the frequency and amplitude.



(a) Conventional machining

(b) 2D VAM

Figure 5.9: Difference of chip thickness affecting cutting force reduction

The tool forces have been reduced by the effect of the thinning eclipse motion to produce the chips. 2D VAM is shown to be the consequence of several mechanisms that modify chip

geometry as well as interactions between the tool rake face and the chip as it is extracted from the workpiece. A comprehensive model for predicting 2D VAM forces has not yet been published, but it appears that the dominant cause of tool force reduction depends on the geometry of the elliptical tool path.

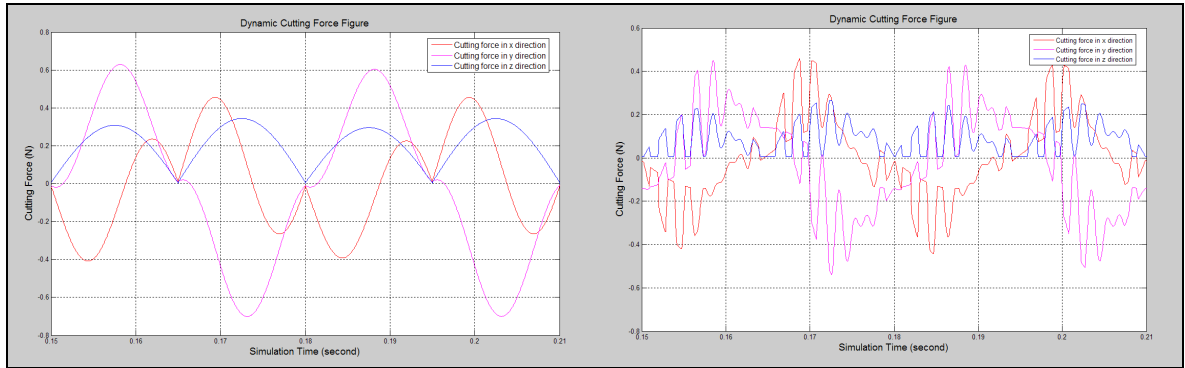
The first theory in reducing the tool force is that the effect of the repeated overlapping tool paths results in chips that are thinner than chip load in conventional machining. For the second, the effect of the tool path from the vibration intermittent loop, it reduced the tool forces because in the condition the tool velocity exceeding the chip velocity, producing a reversal of the direction of the tool-chip friction force and reduction or reversal of the thrust force.

Figure 5.9 is a simulation figure performed by Matlab. The simulation model was used for the same parameter conditions in spindle speed and feedrate. By composing a 2D VAM it is obviously shown that the chip thickness and formation are changed (the chip thickness is coloured in cyan).

Therefore, in 2D VAM much smaller and shorter chips are produced, instead of a large and continuous chip as in conventional cutting. In addition, the tool motion operates with lower average force for a much larger cumulative distance in repetitive passes, compared to conventional machining in the same amount of time. In the same volumetric material removal, the work performed by 2D VAM is therefore much more consistent than with conventional machining.

Cutting force reduction has been explained in the simulated Figure 5.10 where (a) is conventional cutting and (b) 2D VAM. The parameter was the same, the only differences was opposing the vibration aid. Without vibration the maximum cutting force in the X, Y and Z are approximately 0.62 N, 0.43 N and 0.26 N respectively, but it is reduced to 0.42 N, 0.41 N and 0.21 N respectively with vibration assisted.

The tool used was 2-flute end mill having diameter of 1.0 mm. The spindle rotation was 7,000 rpm. The vibration frequency and vibration amplitude applied on X and Y was 1,000 Hz and 1 μm respectively.



(a) (b)
 Figure 5.10: Comparison between VAM and conventional machining in cutting force

The theory of reducing the cutting force in VAM has been experimentally demonstrated by Shamoto and Moriwaki. Through their experimental study with a low frequency system operating at frequencies of 0 to 6 Hz found that the instantaneous force (peak) cutting and thrust force are the same value as with conventional cutting. But there is a zero time period when the tool has no cutting force at all. It is believed the zero cutting force condition came from the kinematic disengagement (tool separation) when there is non-contact between the tool edge and the workpiece. Shamoto and Moriwaki claimed a reduction of cutting force of approximately 30% to 40% from conventional machining.

Ahmed et al (2007) claimed that the increase in the vibration amplitude leads to a 52% decrease in the average cutting force in vibration assisted machining. This is because of an increased part of the cycle of ultrasonic vibration without contact between the tool and chip.

An increase in the vibration frequency from 10 to 30 kHz results in a 47% drop in the level of average cutting forces, which could be attributed to an increased velocity of the tool vibration. Hence, an increase in either vibration frequency or amplitude leads to a decrease in cutting force that is beneficial to increasing the accuracy and improving material removal rates.

5.3.2 Cutting temperature and tool life

Rubbing and friction during ploughing and shearing in the milling process create thermal energy in the exponential rate. As a consequence the energy will convert to heat and spread between the tool and the workpiece. The temperature on the rake face angle has a strong effect on tool life (Negeishi, 2003). When the tool tip temperature increases, soften the tool rapidly. The increasing of temperature will affect the tool life because of:

- Raising of cutting force/speed
- Constant stress between tool and workpiece
- Inappropriate cooling medium
- Tool becoming blunt

Intermittent cutting in VAM creates a gap between the tool and the workpiece. This can be expressed:

$$\begin{aligned}y &= a \sin \omega t \\x &= b \cos \omega t\end{aligned}\tag{5.24}$$

Where y , x and ω are the displacement, amplitude acting in X, Y axis and angular velocity of tool tip respectively.

In conventional machining, the tool is always kept in contact with the workpiece so the heat will increase as long as it is still in contact. Figure 5.11 shows the graph of temperature versus hardness of cutting tool and coatings material. In 2D VAM, this will not happen as the temperature remains constant so as to maintain the tool's hardness.

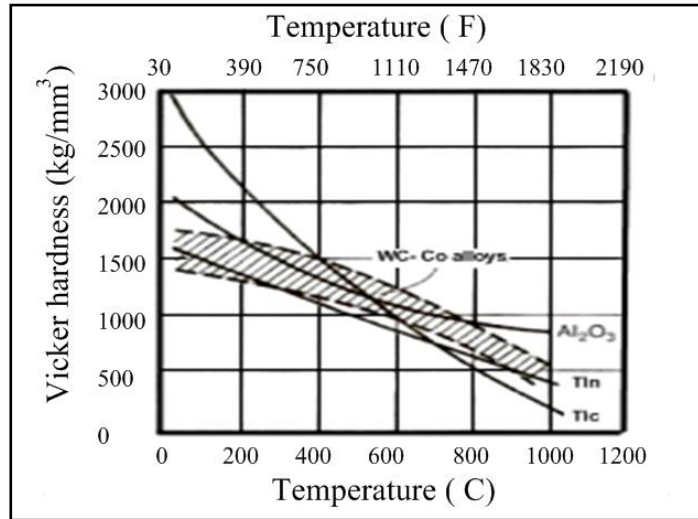


Figure 5.11: Variation of hardness with temperature for tool materials and coatings

Figure 5.12 shows the mechanism in orthogonal cutting of VAM towards workpiece. It also shows how the intermittent mechanism, by amplitude and frequency pulse impacts on tool separation from the chip, promotes aerodynamic lubrication increases. It also shows the tool path mechanism of conventional machining. In addition, the clearance angle and rake angle are free from cutting force and release the stress of pressure from the rubbing and ploughing process.

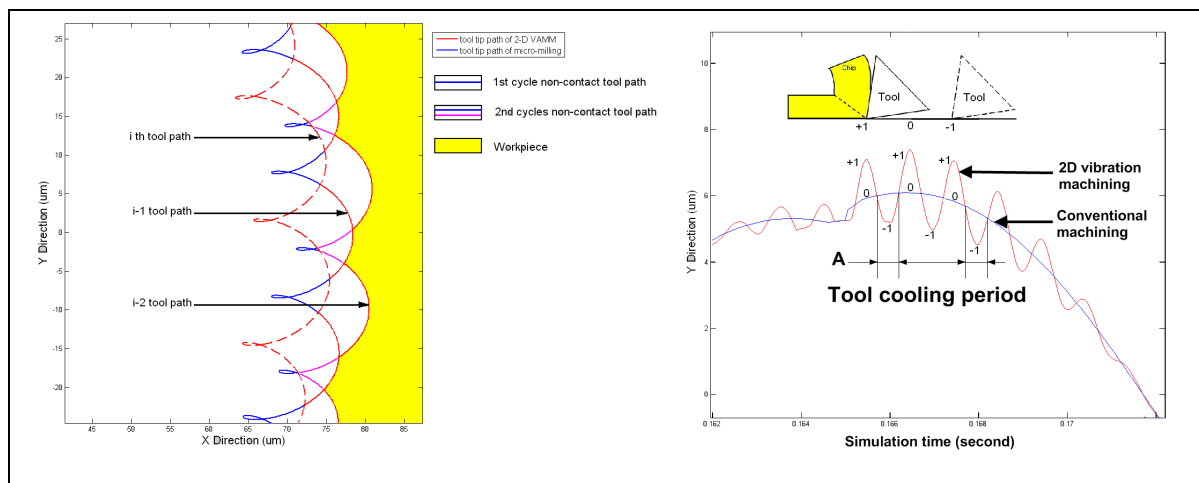


Figure 5.12: Cutting mechanism in VAM 2D VAM during the cooling period

The displacement tool vibration in the cutting direction at a frequency period of A . The digging/ploughing between point +1 and -1 to remove material causes chips to form. The retraction tool and workpiece between points +1 to -1 promoted dynamic force for the chip to leave the cutting area efficiently.

Figure 5.13 shows a simulation created from Matlab platform showing the cooling gap that has been created during the VAM cutting process. With the parameters a is $3\ \mu\text{m}$, b is $1\ \mu\text{m}$, frequency X and Y are 1,000 Hz, feedrate is $2\ \mu\text{m}$ per tooth and spindle speed is 2,000 rpm. The clearance or gap during alternating motion allows heat transfer to work efficiently toward air or coolant, cooling down the tool and surface of the workpiece, which prevents the cutting temperature on the tool and workpiece rising especially, in very hard and very soft materials. It also reduces the time available for tools to change their molecular structure or for other types of wear.

Tough material, like stainless steel, hardened steel and nickel, cause high tool forces acting on the tool itself, so creating high stress in the tool. VAM promotes the opportunity to reduce the stress in the tools, thus leading to improvements in the stability of the tool from chipping and fracture.

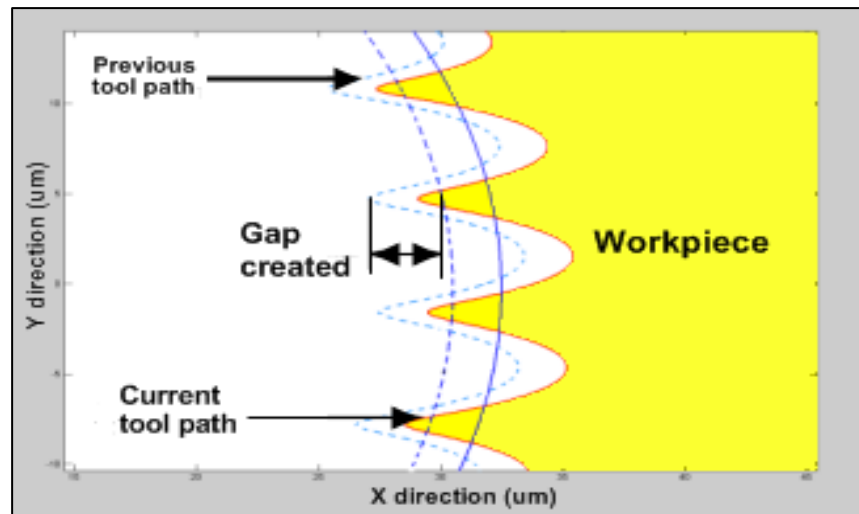


Figure 5.13: Gap in 2D VAM and its influence on tool temperature and tool life

It is found, during the intermittent cutting, that VAM creates a small energy instantaneous mechanics to lower down tool force affect the decreasing the local stress on the tool.

5.3.3 Surface roughness (R_a) and chip formation

The surface produced by conventional milling depends on the result of geometric and kinematic reproduction of the tool point shape factor (Wang and Chang, 2004). Through their experimental studies the concavity and axial relief angle in the end mill has a big effect on the surface produced, especially on the peak to valley measurement.

The measurement of surface finish between conventional machining and 2D VAM has been investigated by using the arithmetical mean deviation (R_a) which is can be expressed:

$$R_a = \frac{1}{L} \int_0^L |z(x)| dx \quad (5.25)$$

Where L is length of measurement and z is the ordinate of the profile curve. Figure 5.14 shows the illustration of the surface measurement using peak to valley average over the sampling length.

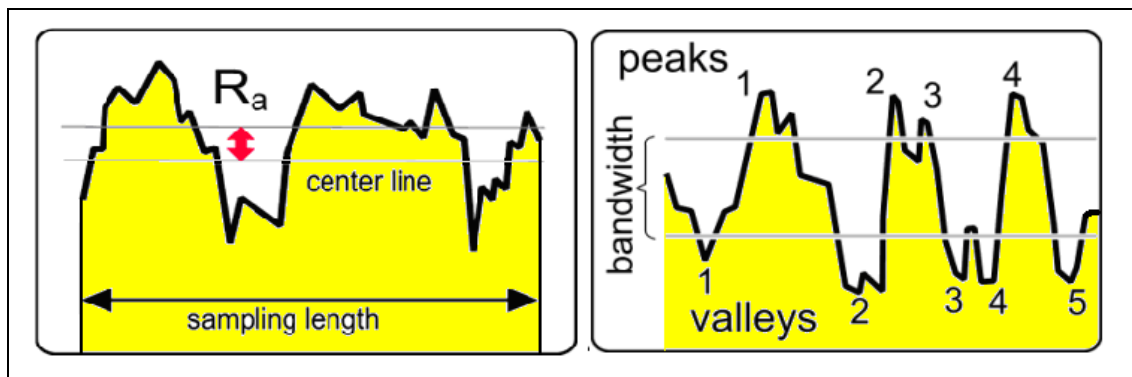


Figure 5.14: Illustration of R_a and peak to valley as determined

Figure 5.15 shows the simulation of cutting by conventional machining and 2D VAM. The circular motion nature of VAM allows the tool cutting point to traverse the cut area from the preceding cycle and remove the material peaks and valleys left over from the last time.

During the cutting circular motion of VAM, the smaller force will reduce the average force and promote surface accuracy and surface finish by compensating for the relative vibration between cutter and workpiece. In addition, from that point the reduced tool cutting force also reduced chatter on the surface produced.

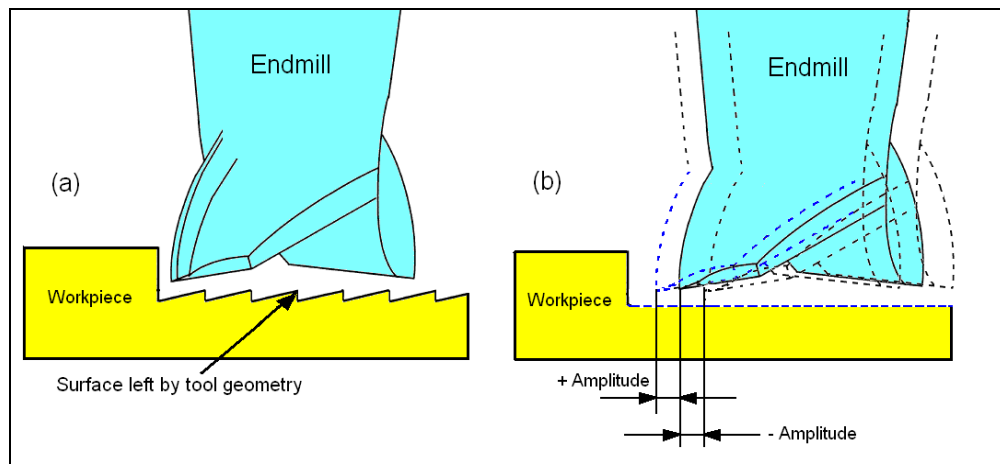


Figure 5.15: Effect of VAM in surface tool produced (a) Without VAM, (b) with VAM

So, by investigating the Figure 5.15, the peak to valley of the surface has been reduced by the cutter via an overlapped process. The higher frequency of cutting, the more chances there is of the tool cutter in one particular area reducing the peak and valley to obtain a good surface result. Kim and Choi (1998) found the crest from the surface of 2D VAM has been eliminated by the alternating cycles phenomena. From this, it is concluded that the good surface is made by cutting the crests and peak on the surface with the vibratory tool.

5.3.4 Ductile regime cutting in chip formation

2D VAM has encouraged a small ploughing depth of cut that is very useful when cutting a hard and brittle material that has rapid crack propagation with low energy release and without significant plastic deformation. The ductile regime cutting will produce a plastic flow with very minimal subsurface cracking. It will induce a tool to cut a very small chip

with fine formation in 1 μm depth or less. Ding and Rasidi (2010) have cut a hardened steel material HRC 58 and found the chip thickness is very fine grain, like flour, and that it is difficult to determine the thickness. These are important findings related to micro-crack and micro-fracture in brittle material.

5.4 Machining dynamics model of 2D VAM

The machining dynamics involve the dynamic behaviour of the machine itself. For the analysis and the design of a machining dynamics system, for instance, a desktop vibration assisted machine, the most fundamental system identification method is an experimental modal analysis which is a feasible and practical approach. It can be used to identify the machine structural dynamics characteristics, particularly focused on the stiffness and natural modes of the machine.

For feasible machining conditions, it is essential to keep the machine in a condition of high stability and to avoid disturbance forces from cutting the machining itself. The dynamics of the machine structures can be modelled and analysed. Even though the dynamics of a machine is a complex system, its modelling can be done by focussing on the structural dynamics only at the cutting zone (Ding and Cheng, 2010).

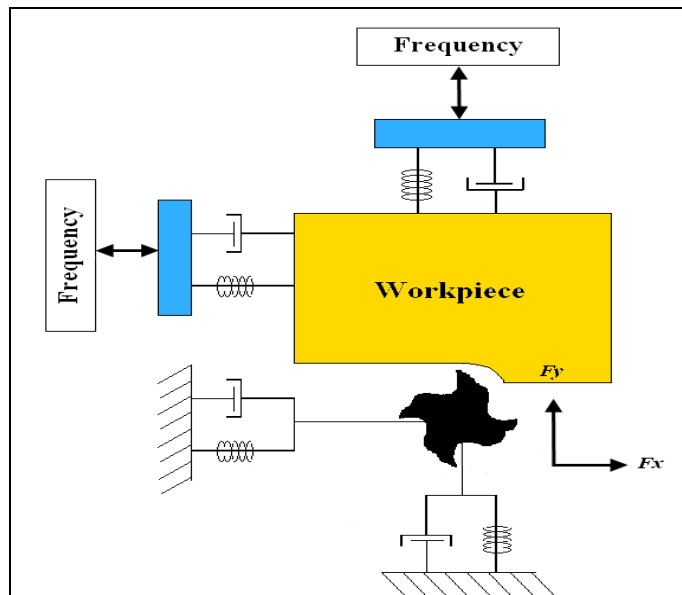


Figure 5.16: Spring damper vibratory model

Figure 5.16 shows the machining dynamics model. To simplify the dynamic workpiece and cutting tool, the second-order spring damper vibratory system have been introduced into this model acting in the X, Y and Z directions. Figure 5.16 also shows how the cutting force excites the dynamic displacement related to the cutting force and the workpiece in the three directions of X, Y and Z respectively. Therefore, the whole cutting system can be express as:

$$\begin{cases} m_{xt}\ddot{x}_t(t) + c_{xt}\dot{x}_t(t) + k_{xt}x_t(t) = F_x(t) \\ m_{yt}\ddot{y}_t(t) + c_{yt}\dot{y}_t(t) + k_{yt}y_t(t) = F_y(t) \\ m_{zt}\ddot{z}_t(t) + c_{zt}\dot{z}_t(t) + k_{zt}z_t(t) = F_z(t) \\ m_{xw}\ddot{x}_w(t) + c_{xw}\dot{x}_w(t) + k_{xw}x_w(t) = -F_x(t) \\ m_{yw}\ddot{y}_w(t) + c_{yw}\dot{y}_w(t) + k_{yw}y_w(t) = -F_y(t) \\ m_{zw}\ddot{z}_w(t) + c_{zw}\dot{z}_w(t) + k_{zw}z_w(t) = -F_z(t) \end{cases} \quad (5.26)$$

where,

- m_{at} - the mass equivalent of the tooling system in the X, Y and Z directions;
- c_{at} - damping coefficient of the tool system in the X, Y and Z directions;
- k_{at} - stiffness of the tooling system in the X, Y and Z directions;
- m_{aw} - the mass equivalent of the workpiece system in the X, Y and Z directions;
- c_{aw} - damping coefficient of the workpiece system in the X, Y and Z directions;
- k_{aw} - stiffness of the workpiece system in the X, Y and Z directions.

To simplify the dynamic cutting model in the Equation (5.26) it can be transformed into frequency domain by Laplace transform and can be described as:

$$\begin{cases} X_t(s) = (m_{xt}s^2 + c_{xt}s + k_{xt})^{-1} F_x(s) \\ Y_t(s) = (m_{yt}s^2 + c_{yt}s + k_{yt})^{-1} F_y(s) \\ Z_t(s) = (m_{zt}s^2 + c_{zt}s + k_{zt})^{-1} F_z(s) \\ X_w(s) = -(m_{xw}s^2 + c_{xw}s + k_{xw})^{-1} F_x(s) \\ Y_w(s) = -(m_{yw}s^2 + c_{yw}s + k_{yw})^{-1} F_y(s) \\ Z_w(s) = -(m_{zw}s^2 + c_{zw}s + k_{zw})^{-1} F_z(s) \end{cases} \quad (5.27)$$

Furthermore, from the Equations (5.26, 5.27) the relative dynamic displacement acting between the cutting tool and the workpiece can be expressed as:

$$\begin{cases} \Delta x = x_t - x_w \\ \Delta y = y_t - y_w \\ \Delta z = z_t - z_w \end{cases} \quad (5.28)$$

5.5 Summary

This chapter explains the approach of process modelling and simulation in order to study the mechanism and mechanics of 2 dimensional vibrations assisted micro-milling. The modelling approach is based on the conventional micro-milling and adding together vibrations in X and Y axes from the workpiece holder as investigated in depth. A three dimensional cutting force model for 2 dimensional vibrations micro-milling is proposed, which calculates the chip thickness by investigating the tool trajectory between tool edges relative to the workpiece as the tool rotates.

Furthermore, the workpiece travelling in feed direction and the vibration in X and Y axes simultaneously are taken into account. The model covers the dynamic displacement of the machine and cutting tool and enabling prediction of the dynamic cutting force, chip thickness and surface roughness.

Chapter 6 Validation of the modelling and simulation through machining trials

6.1 Introduction

Modelling and simulation results provide vital information for decisions and actions in many areas of experiment and investigation. Verification and validation are processes that help to ensure that models and simulations are correct and reliable. Although significant advances have occurred in the past 15 years, significant challenges remain that impede the full potential of modelling and simulation (Pace, 2004).

In the previous chapters, the theoretical studies were performed on modelling of dynamic cutting force, chip thickness and surface roughness generation in vibration assisted micro-machining. This chapter tends to focus on the experimental studies on the validation of the modelling and simulation through machining trials in the real machine environment setup. A total number of 81 machining trials were carried out for the purposes of:

- ✚ Evaluation and validation of the modelling approach by measuring the cutting force and machine surface.
- ✚ In-depth study on the effects of the parameter/variables setup, focused on vibration frequency, vibration amplitude, spindle speed and feedrate into the material removal rate, tool life and surface roughness.
- ✚ Further investigation into the machining dynamics and its effects on machine performance.

6.2 Facilities and workpiece materials for cutting experiments

6.2.1 Facilities for vibration assisted machining experiments

The facilities in the experimental study include the machining system, which is a desktop vibration assisted micro-milling machine and cutting tool, three Kistler displacement sensors for measuring the vibration frequency, vibration amplitude and spindle run-out. Surface

measurement will be carried out by the Zygo New View 5000 optical 3D surface profiler. The configuration of the cutting trials is shown in Figure 6.1. The movement of X is controlled by the PI linear motion programming system driven by leadscrews. For the Z axis, directions feed is by manual handling and driven by leadscrews. Its spindle speed can vary up to 1,500 rpm control by commons power amplifier. An endmill with diameter 1.0 mm coated carbide was used in the machining trials where some process variables can be easily changed as desire. The endmill tool cutting tools are purchased from RS Component LTD from Dormer. There are in one Kistler displacement sensor at the spindle chuck towards X axis and two sensors remaining on the piezo structure both in X and Y directions.

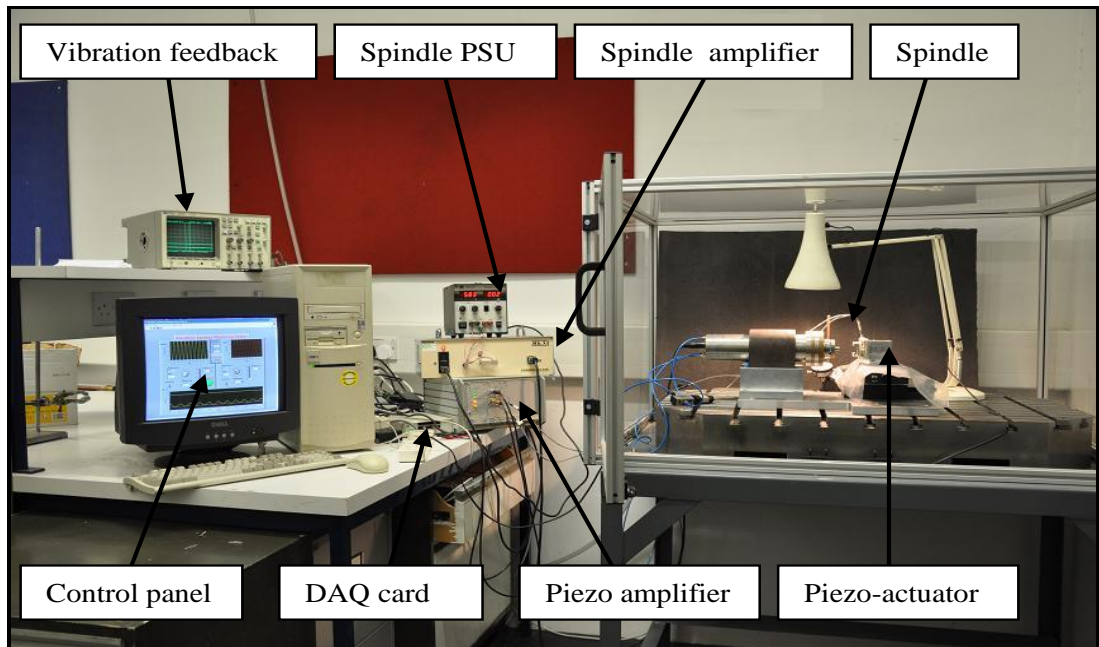


Figure 6.1: Experimental configuration of the cutting trials

The components structure and devices have been mounted on the solid metal table 100 mm thickness to ensure great rigidity and natural frequency. The workpiece is secured clamped inside the workpiece holder by an interface connected to the workpiece holder as shown in Figure 6.2.

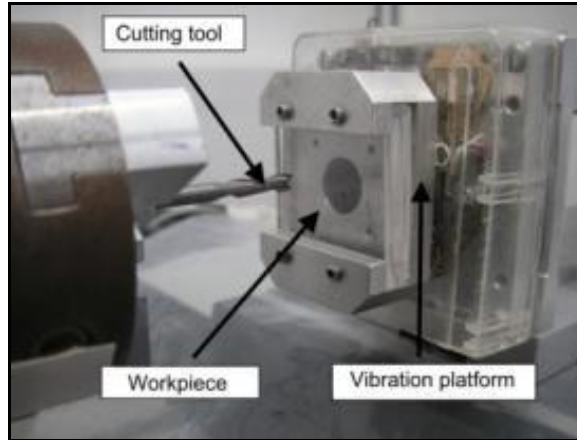


Figure 6.2: Cutting setup

During the machining process, the capacitive sensor pointing to the X and Y axis on workpiece holder will transfer the information into the CPU. The CPU will connect for close loop control to ensure the right frequency and amplitude.

The amplified frequency and amplitude signal is input into the computer through an A/D converter by an A/D data card (2 input & output channel). The software LabView 8.5 and PI Mercury 4.2 installed in the computer is used for controlling the hardware, acquisition, analysis, modelling and presentation of the machining objectives.

After the machining trials the machined surfaces of each workpiece was measured by the 3D surface profiler Zygo New View 5000 optical microscope, which is a general purpose three dimensional surface structure analyzer. For the tool wear validation, the TESA 200 optical microscope was used to observe the wear mark on the tool cutting edge. Both of these machines provide non contact, high resolution numerical measurement and analysis to accurately characterize the surface structure of the test parts.

The configuration of the Zygo New View system can be broken into two basic subsystems, the microscope and the computer, as shown in Figure 6.3.

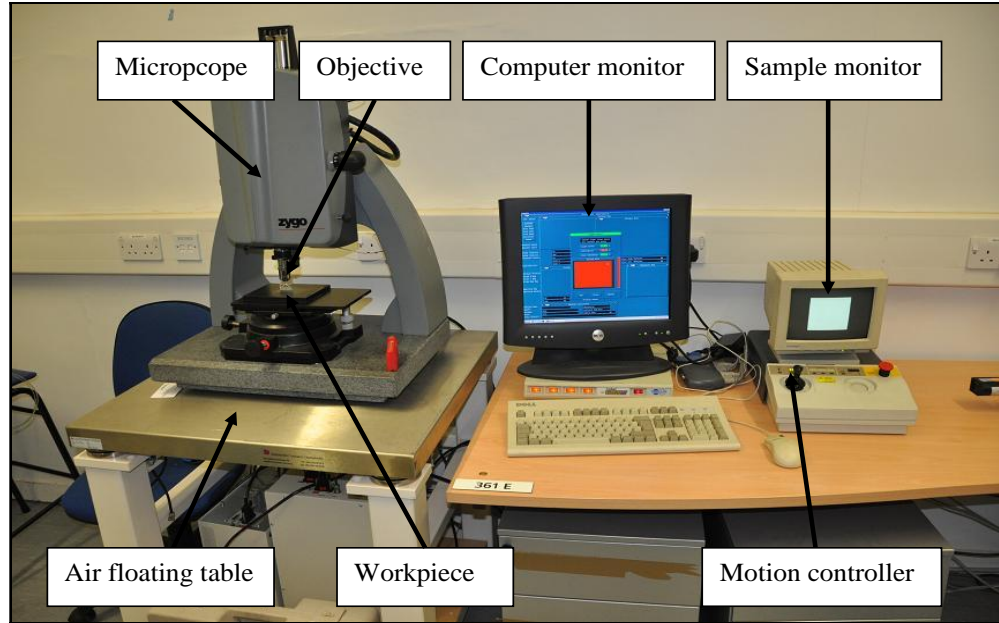


Figure 6.3: Zygo New View 5000 optical microscope

The microscope provides the raw data needed for analysis; it includes a granite base (on a pneumatic vibration free table provided by Integrated Dynamics Engineering), a stable gantry column, interferometric objective (gathering light from the test part and forming a real image of it), stages (holding the part under test and providing for position under objective), motorized focus control, video monitor (displaying a monochrome live image of the part under test) and electronic enclosure (housing system electronics and providing power to the microscope and interface to the computer).

The computer controls the surface measurement process, performs calculations, analysis and visualizes the measurement results on a colour monitor. The Zygo MetroPro™ software is installed in the computer system so as to implement those functions.

6.2.2 Workpiece materials for desktop vibration assisted machining

In this research, two types of workpiece materials were used. These were aluminium T6061 and low carbon steel. The dimensions of the workpiece were $30 \times 30 \times 3$ mm square. The material properties are listed below in Table 6.1. Aluminium T6061 has been chosen because the property of this material is suitable for investigating the new cutting method at the initial stage. Secondly, this material is widely used in the industry for fabricating lightweight

components, and for precision in manufacturing industries. Figure 6.4 shows a sample used in the cutting experiments and measurements.

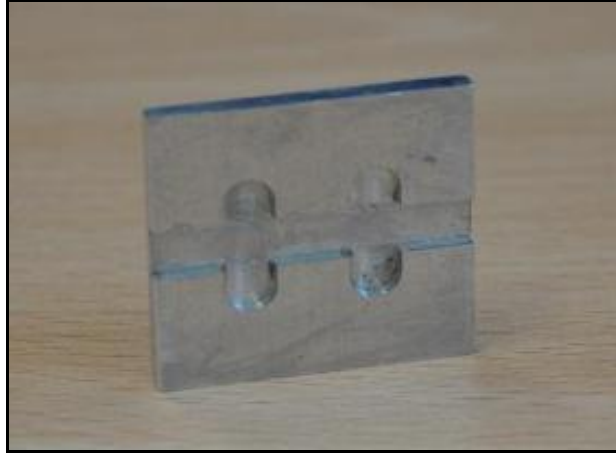


Figure 6.4: A sample in cutting trials

Table 6.1: Material properties of the workpiece in VAM

Workpiece material	Aluminium T 6061
Density (g/cm ³)	2.7
Tensile strength (Mpa)	310
Modulus of elasticity (GPa)	69
Poisson's Ratio	0.33
Shear Modulus (GPa)	26
Shear strength (MPa)	207
Yield stress (MPa)	270
Vickers Hardness (GPa)	1.0

6.2.3 Cutting tools

The endmill 1.0 mm with shank diameter 3.0 mm was used for the cutting trials. Coated carbide and uncoated carbide tool with same rake angle, clearance angle and tool nose radius were used. Their dimension and geometric are listed in Table 6.2.

Table 6.2: Dimension and geometry of the cutting tools in VAM

Material	Tool diameter (mm)	Tool edge radius (μm)	Flute
High speed steel (HSS)	1.0	5 - 6	2
High speed steel coated with titanium carbide	1.0	5 - 6	2

6.3 The experimental plans

6.3.1 Machine setup accuracy

i) Air bearing spindle

The condition of the machine should be analyzed before the cutting experiment can be done. The rotational run-out of the spindle is measured accurately by Kistler's displacement sensor as shown in Figure 6.5. About $0.1 \mu\text{m}$ is found when the spindle rotation up to 15,000 rpm. The straightness of both slideways is roughly measured using dial gauge.

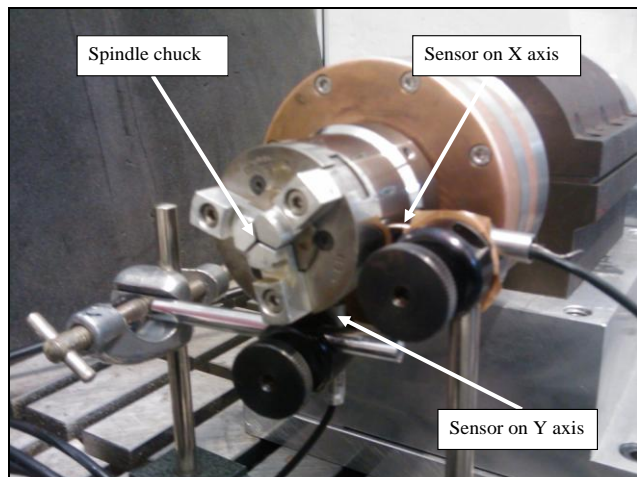


Figure 6.5: Measuring the run-out of spindle

ii) Piezo-actuator

The piezo-actuator response to the signal input has been analyzed by using a capacitive sensor. Figure 6.6 shows that the sensor has been attached firmly toward Y direction of vibration. The signal from output and input has been analysed and shows there are no significant lag and distortion of signal patterns during the cutting process.



Figure 6.6: Piezo-actuator and the signal response

6.3.2 Machining trials plan

The experiment particularly investigates the influences of vibration frequency, vibration amplitude, feedrate and spindle speed on the rate, tool life, surface roughness and material removal, as shown in Figure 6.7.

During the experiment, the cutting control will be varied at three levels which are low, medium and high in order to investigate the influence of each factor. The samples have been measured on average by 5 times in surface roughness for the accuracy and readability of result. A zero-cutting plane has been cut before the real experiment in order to make sure the condition of the initial cut is parallel and accurate to the machine plane.

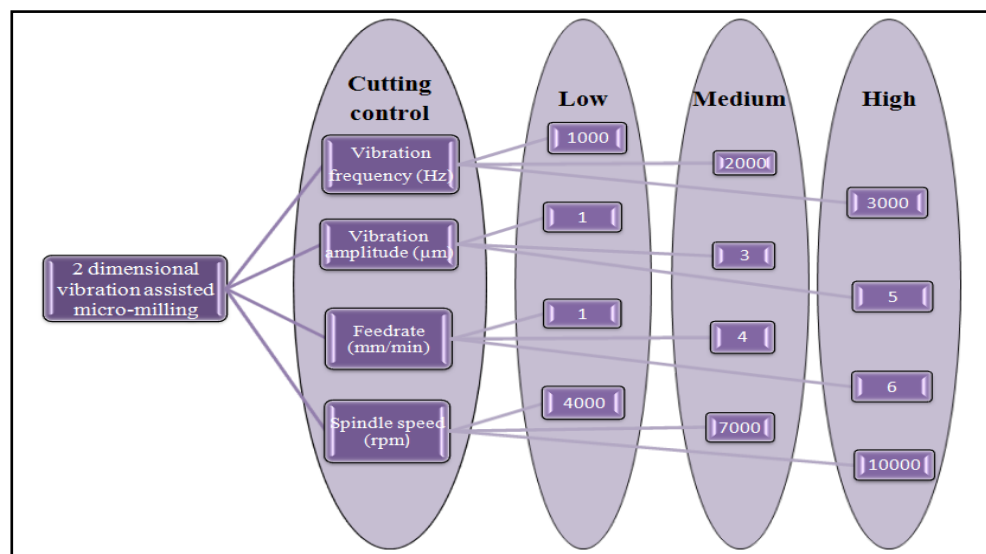









Figure 6.7: Experimental plan and flow chart

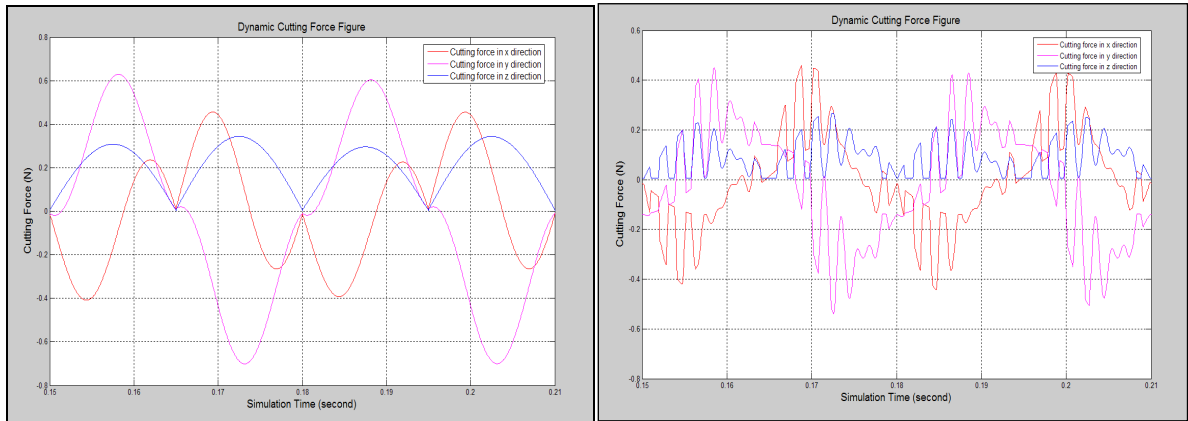
6.4 Result and discussions

The results of the cutting trial and samples have been listed in appendix III. The cutting force and characterisation parameter of the 2 dimensional vibration assisted machining have been evaluated according to the experimental plan. This will evaluate the modelling approach and study the effect of factors on the surface roughness, tool life and material removal rate.

6.4.1 Cutting force validation

Figure 6.8 shows the comparison of the cutting force between without 2D VAM and with 2 dimensional vibrations assisted machining. The machining parameters are:

	Vibration frequency in X	=	1,000 Hz
	Vibration frequency in Y	=	1,000 Hz
	Vibration amplitude in X	=	1 μm
	Vibration amplitude in Y	=	1 μm
	Feedrate	=	1 mm/min
	Spindle speed	=	2,000 rpm
	Depth of cut	=	0.5 mm



(a) Without 2D VAM

(b) With 2D VAM

Figure 6.8: Simulated cutting forces in X, Y and Z axis directions

Figure 6.8 shows the instantaneous force measurement obtained in MatLab programming. The condition of machining without 2D VAM is the same as the parameter condition except the composition of the vibration in X and Y axis. It can be seen clearly that the cutting

without 2D VAM is approximately 0.67 N, and 0.41 N with 2D VAM. The percentage of reduction in cutting force is estimated at about 50% to 60%. This agrees well with Shamoto and Moriwaki: the cutting force is significantly reduced in a vibration assisted machining especially in the average force.

The amount of peak/spike in Figure 6.8 can be increased by increasing the frequency and the height of the peak can be changed by changing the amplitude. Shamoto and Moriwaki (1999) measured instantaneous thrust force in the turning machine. They conclude that the average cutting force is significantly reduced by looking into the tool contact present in the peak period.

Improving lubrication resulting from non-contact of the tool in VAM has been studied by Ahn et al, 1999, Kim and Lee et al, 1994, Zhou et al, 2003 and Zhong et al, 2005. Further more Mitroanov et al. (2005) found in 1D VAM the peak of cutting force were reduced by 10%-20% for the proper lubrication system. However, the lubrication in VAM seems to appear as of secondary importance because there is no quantitative and qualitative investigation to explain this phenomenon.

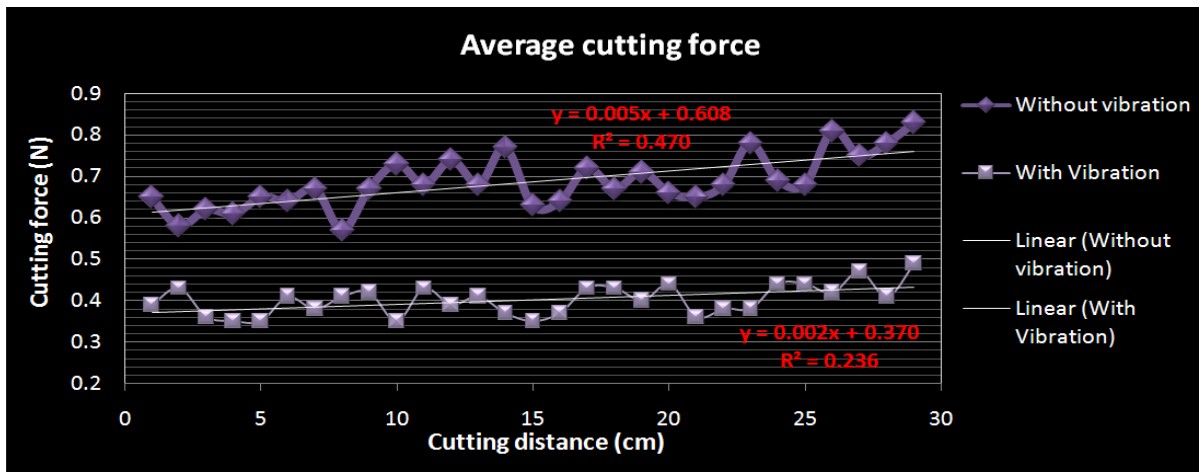


Figure 6.9: Average cutting force without and with 2D VAM

Typical data showing 2 dimensional tool forces have been plotted in Figure 6.9 which shows the average cutting force as a function of cutting distance. 30 chosen samples have been recorded in Figure 6.9. It can be observed that the average of cutting forces without 2D

VAM in Y linear function is 0.470 N which is approximately double that with 2D VAM at 0.236 N. It is predicted that cutting without 2D VAM will increase in linear scale because of the following reasons:

- ✚ Increasing of cutting edge radius
- ✚ Temperature in cutting area keeps increasing
- ✚ Non-efficient chip removal

6.4.2 Surface roughness validation

Figure 6.10 shows the machining surface measured by Zygo 3D surface profiler and Figure 6.11 shows the simulated surface by modelling approach. The topography and the direction of cutting have been shown clearly on the surface generated. The measured machine surface and simulated model surface with vibration show clearly that the pattern of topography agrees well. The differences between machined surface and simulated surface have been found in the profiles of peak and valley. The peak and valley from machined surfaces are sharp at the top but from the simulated surface are quite dull and soft.

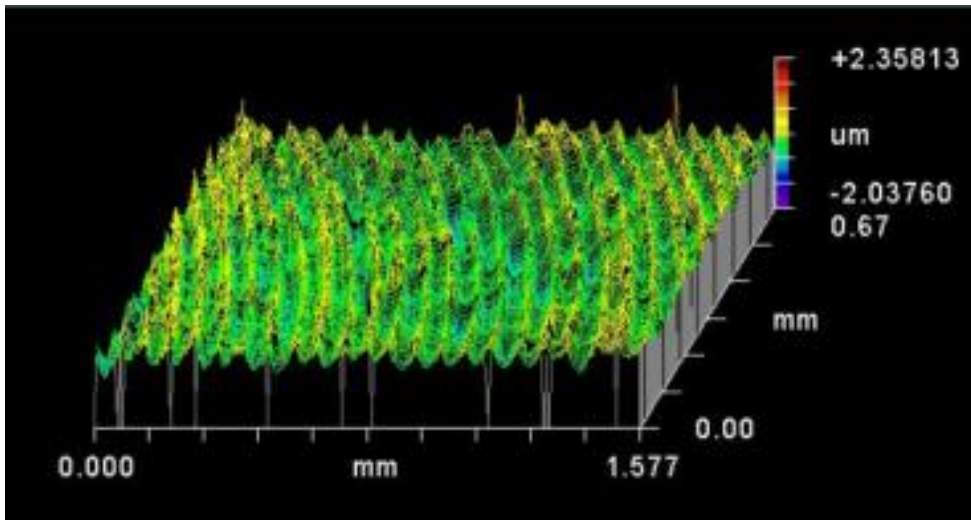


Figure 6.10: Machined surface

The differences between the experimental result and the simulated result may be caused by the tool bending, tool geometry and some other factors that are very difficult to model. However, many similar profiles can be observed, such as the tool rotation direction, peak and valley deviation and feed direction.

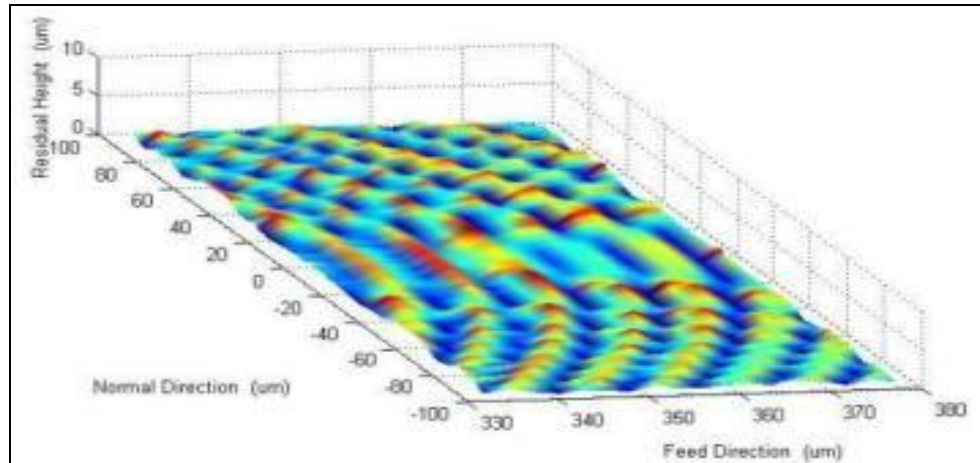


Figure 6.11: Simulated surface

Figure 6.12(a) shows cutting without vibration assistance, and Figure 6.12(b) cutting with vibration assistance with the parameters above. The surface profile without vibration was uneven and random with Ra value of $3.1 \mu\text{m}$, but with vibration assistance the surface profile was more uniform and followed the vibration curve as predicted. The value for Ra is $0.6 \mu\text{m}$ with vibration.

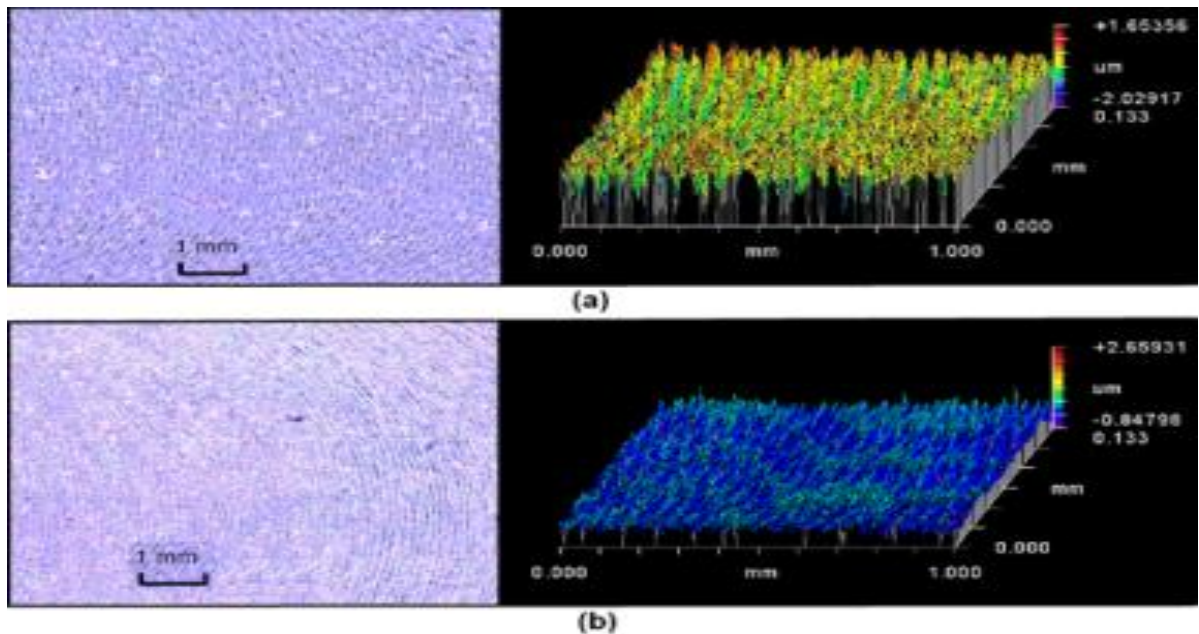


Figure 6.12: Cutting trials result

Influence of vibration frequency and vibration

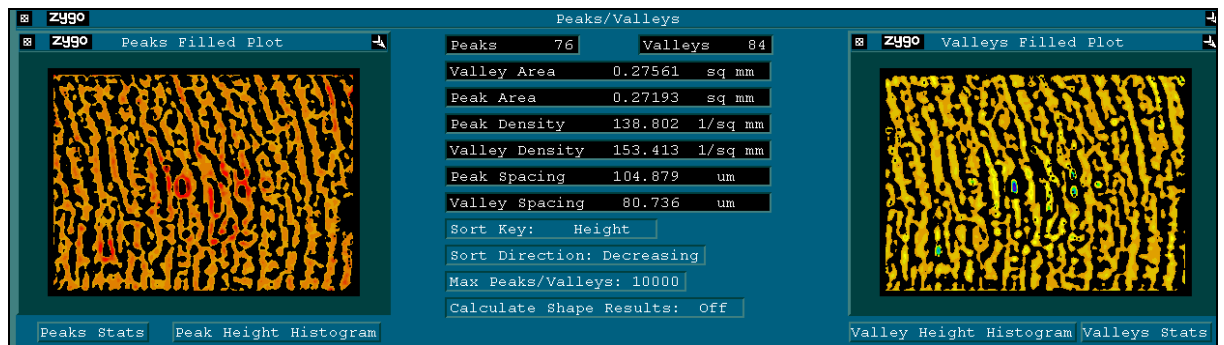
In measuring a sample for surface roughness topography, the important value to investigate the surface integrity is the peak and valley. In this experimental research, the surface roughness in R_a standard will be used to investigate the effect of vibration frequency, vibration amplitude and feedrate. Figure 6.13 shows the variation of peak and valley surface map with 2D VAM and without 2D VAM.



(a) Peak height map

With vibration

(b) valley height map



(c) Peak height map

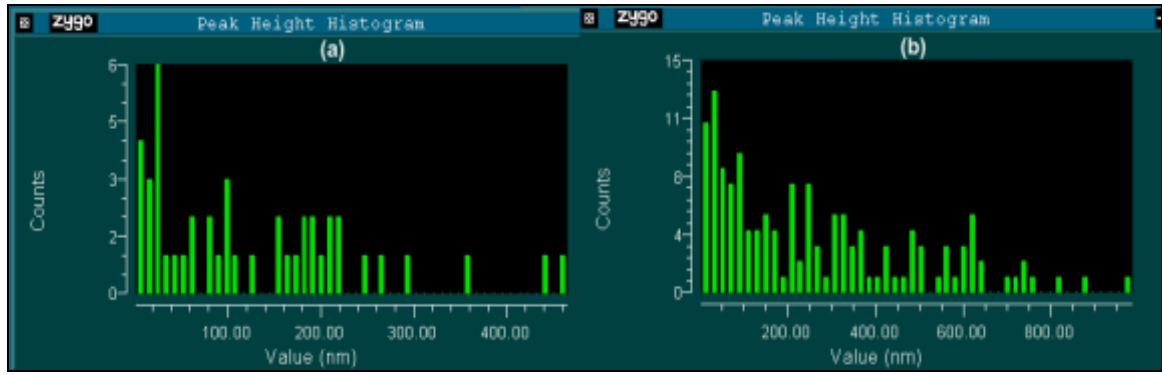
Without vibration

(b) valley height map

Figure 6.13: Peak and valley surface maps with 2D VAM and without 2 DVAM

The value of the peak from the 2D VAM surface is 35 points and the valley is 62 points. But, the value of the peak from without 2D VAM surface is 76 points and the valley 84 points. There are huge differences of peak density between the peak density from 2D VAM and without 2D VAM where the results are 80.968 1/sq mm and 138.802 1/sq mm respectively. The results of peak spacing and valley spacing from 2D VAM cutting surface is 94.679 μm and 111.555 μm respectively, and without 2D VAM is 104.846 μm and 80.736 μm respectively.

From these result data, it is clear that the vibration frequency and vibration amplitude promotes the effect of reducing the peak and valley level on the surface topography in order to improve surface roughness.



(a) cutting with 2D VAM

(b) cutting without 2D VAM

Figure 6.14: Peak height histogram

Vibration frequency and vibration amplitude offer a significant effect to the surface roughness when the tool path overlaps which can reduce the distance between peak and valley gap. Figure 6.14 shows the comparison of peak heights result in a histogram chart. It can be seen clearly that the peak height in 2D VAM surface cutting is less and shorter compared with the surface cutting without 2D VAM.

6.4.3 Tool wear validation

Optical microscopy is one of the widely used methods to study tool wear. In this method, wear on the tool reflects more light than un-worn surfaces and therefore show as lighter. Figure 6.15 shows the different in surface light reflection and therefore the tool wear is clearly visible. The amount of tool wear is determined by measurement of the length of wear mark.

These experimental trials were conducted using an uncoated RS Cutter model HC209 solid carbide endmill diameter 1.0 mm. The cutting parameters and the conditions used were the same as the surface roughness experiment described. In order to observe the tool wear, a 600 mm total distance cutting slot was cut using the same cutting tool. In this experiment, a TESA Optical 200 was used to observe the tool face in the vertical axis.

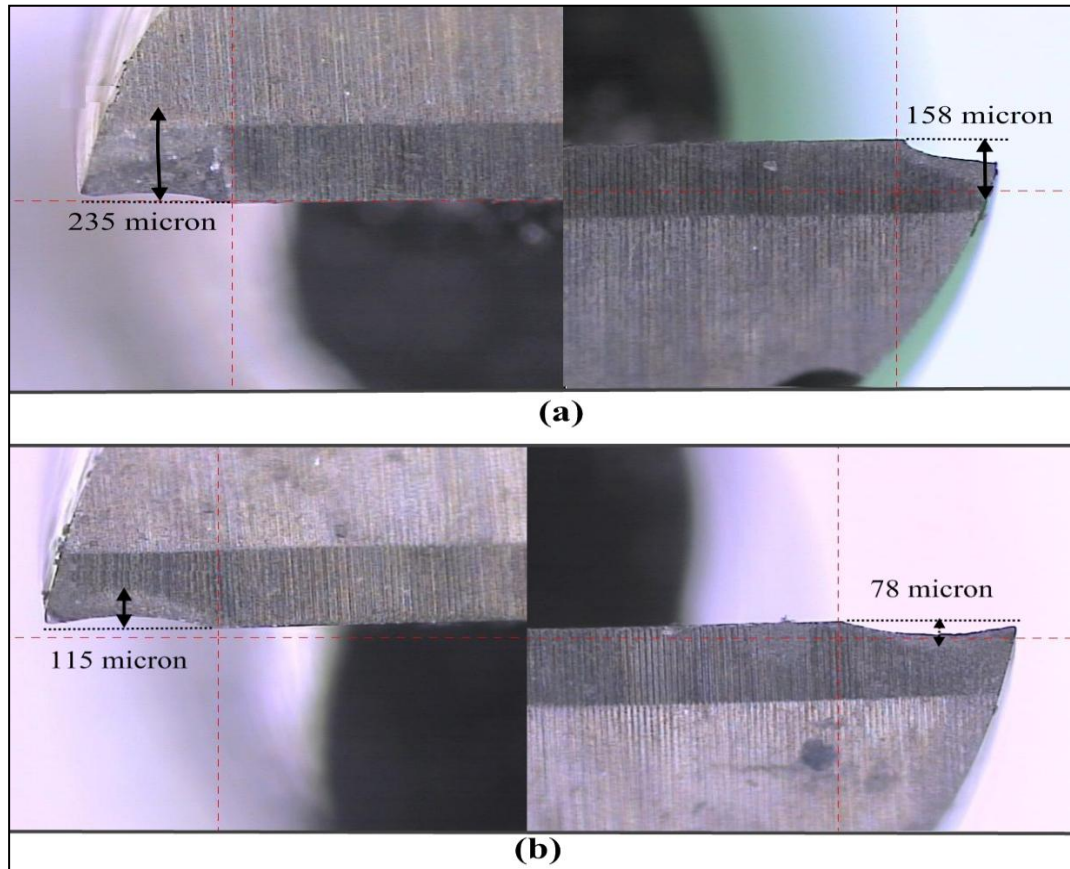


Figure 6.15: (a) Endmill without vibration (b) Endmill cutter with vibration assisted

Figure 6.15(a) shows cutting with vibration assistance and 6.15(b) shows cutting without vibration assistance that the tool surface cutting edge without vibration has more rubbing and friction marks and is broken at the tool point. The observation is measured based on the wear mark and friction at the clearance angle plane. The measurements were taken from the tool point up to the end of the friction mark. Figure 6.15(a) shows cutting without vibration and the tool surface shows more friction and wear marks with the length of wear is 235 μm and 158 μm . Figure 6.15(b) shows cutting with vibration assisted and the tool have less friction and wear marks with the length of wear is 115 μm and 78 μm both side. Comparison between Figures 6.15(a) and 6.15(b) shows the tool wear improved significantly using vibration assisted machining.

6.4.4 Material removal rate validation

Material removal rate in the vibration assisted machining has been validated using the Abbott-Firestone Curve or bearing ratio function in Zygo surface profiler machine. The bearing ratio wear function is used to simulate and measure the effect of wear/material removal on a bearing surface. It is calculated based on a division of the depth scale into three regions, peak region, middle and bottom, or valley region.

Figure 6.16 shows the material removal rate calculated based on the material that has been removed during the cutting process. The selection between the 'volume above' and volume below determine the area which will be calculated in $\text{mm}^3/\mu\text{m}$.

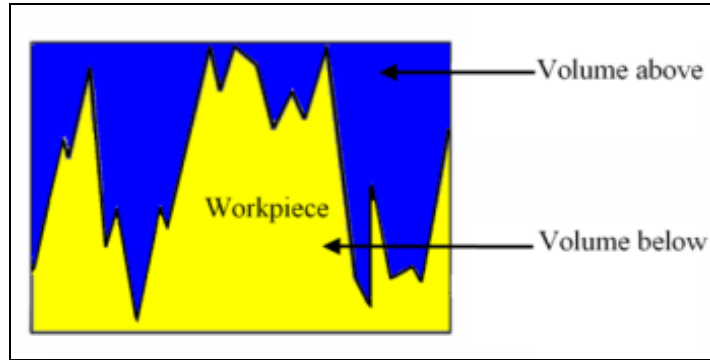


Figure 6.16: The specified volume calculated

25 chosen samples from the cutting trial have been measured and the volume in mm^3 per second (mm^3/s) recorded. The data have been taken from the Zygo Abbott-Firestone Curve which is a direct measurement taken from the surface profile calculated in the Zygo system. Figure 6.17 shows the material removal rate for cutting with the help of vibration assistance (blue) and without the help of vibration assistance (red).

It is clear in Figure 6.17 that the volume with help of 2D VAM is greater than that without 2D VAM where the linear function of y in 2D VAM is $0.139 \text{ mm}^3/\text{s}$ and without vibration is $0.084 \text{ mm}^3/\text{s}$ respectively. From the y linear function, we can observe that the increment of material removal rate volume in VAM is much more efficient, with differences incline of $y = 0.055$ related to the surface roughness average.

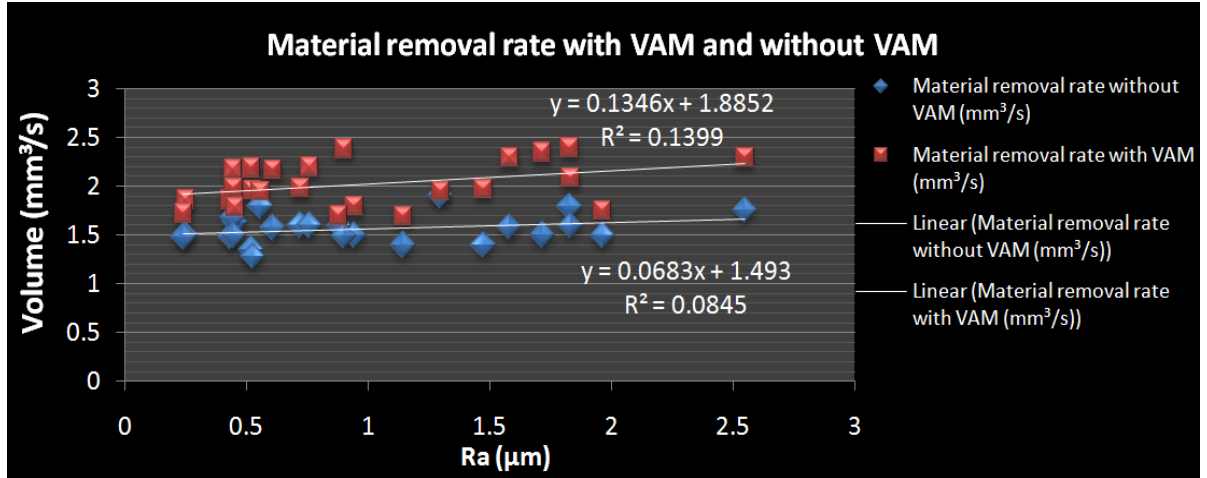


Figure 6.17: Material removal rate with and without 2D VAM

6.5 Summary

This chapter explains the validation of the modelling approach and experimental results particularly between with and without 2D VAM cutting. The machine used is the desktop vibration assisted micro-milling developed by the author. From the scientific observation of comparison between two cutting phenomena, the following conclusion in this chapter can be summarized.

- ✚ That the results between modelling simulations and cutting trials agree quite well. The proposed modelling approach can be used to predict the cutting force and surface roughness even though some of the other variables are very difficult to take into account, such as tool bending, piezo damping, etc. However, it can be useful for future modelling in investigating the dimensional vibration assisted micro-milling.

- ✚ Both the vibration amplitude and vibration frequency have a significant effect on the surface roughness where it can eliminate the peak and level the valley. It has been investigated in the previous chapter that the overlapping tool path will suppress the peak and valley to promote level surfaces.

- ✚ The intermittent tool cutting edge contact with the workpiece has been proved to reduce the tool wear, thus extending the tool life. Where the experiment has been conducted we can observe that the wear and friction marks are less in the VAM tool.

✚ In vibration assisted micro-milling the material removal rate has increased significantly this is investigated by measuring the volume that has been removed on the surfaces with using Abbott-Firestone Curve function.

Chapter 7 Process optimisation and control

7.1 Introduction

The optimization of cutting parameters is the key component in the planning of machining processes. However, deep analysis of cutting involves certain costs, particularly in the case of small series. In the case of individual machining it is particularly necessary to shorten as much as possible the procedure for determination of the optimum cutting parameters, otherwise the cost of analysis might exceed the economic efficiency which could be reached if working with optimum conditions.

Optimum selection of cutting conditions importantly contributes to the increase of productivity and the reduction of costs, therefore utmost attention is paid to this problem in this contribution (Franci and Zuper).

This chapter investigates the prediction of machineability of the process model and determine the optimal values of process parameters. The tools used are ANOVA, Taguchi method and Response surface methodology. This subject area is highly interesting for researchers and manufacturing engineers to control the production in a scientific manner.

In order to do that, the machineability database system is essential for the selection of the process planning stage. The aim is to produce high quality and reliable machined components throughout the machining process.

7.2 Optimization control

The optimization control in this research is defined by the following three categories.

- a) The surface roughness of the machined
- b) The wear mark of the tool face
- c) The volume of material that has been removed

By controlling the machine parameters and vibration actuator it is predicted to achieve the required surface roughness, tool life and faster material removal rate in the machining process. It can help to increase the machining effectiveness, reduce the machining costs and improve productivity.

7.3 Optimization parameters

The importance of making a selection of machine parameter has higher impact on the production in terms of product quality, production costs and production times. The quality and costs are much related to surface roughness, tool life and material removal rate which are functions of the process parameters such as vibration frequency, vibration amplitude, feedrate and spindle speed. This model is based on optimization, although it is also carried out through back-propagation in a non-continuous mode.

The Taguchi method, ANOVA and response surface method (RSM) are used for the optimization purpose. The machining trials have been carried out by the total of 81 cutting experiments which means in three coded levels. The 81 experiments data have been used to generate, compare and measure the proposed model against the requirement surface roughness, tool life and material removal rate.

7.4 Optimization modelling

7.4.1 Surface roughness, tool wear and material removal rate

Surface roughness, tool wear and material removal rate are often the most important factors that need to be considered in the machining technology environment.

By selecting the optimum condition, the machining condition will be expanded to optimize the minimum production costs, maximum production rate and maximum profit rate per item. These important criteria have been considered in both the constrained and unconstrained problems of machining economics.

Many researchers investigate the general effect of the process parameter such as feed rate, spindle speed, depth of cut, to determine the best prediction of tool life, cutting force, material removal rate and surface roughness. Many of them model and simulate based on regression analysis (RA). The most important objective is to provide a qualitative understanding from the basic physics of tool wear so to the gradual wear of a tool can be described quantitatively.

In modern industries, there is a significant factor which will be taken into account when looking for higher profits. Tool wear, surface roughness and material removal rate have been one of them in relation to cost, time, design feature and product quality in the production line. The modelling and modes are critical constraints for process parameter selection in process planning systems. This model can only be evaluated and validated with experimental work on specific material under specific conditions.

In this research there are 81 sets of experimental data in Box-Bohnken 3 responses. The responses include surface roughness, tool wear and material removal rate. The desktop vibration assisted micro-milling was used to predict the machineability model using response surface method (RSM), Taguchi method and ANOVA. The machineability models were compared against each other using the relative error analysis, descriptive and hypothesis testing.

7.5 Design of experiment

Design of experiment (DOE) is a structured, organized method that is used to determine the relationship between the different factors/parameter/variables (Xs) affecting a process and the output of that process (Y) (Arnab, 2009). This method was first developed in the 1920s and 1930s by Ronald A. Fisher.

It is necessary to have a clear idea in advance of exactly what is going to be studied, the data collected, and a qualitative understanding of how this data is to be analyzed. DOE requires designing a set of multiple experiments where all the relevant factors (X's) are varied systematically. Through this process, it will be possible to analyze and identify optimal conditions, the factors that most influence the results, and those that do not, as well as details, for example the existence of interaction and synergies between factors. DoE methods require well-structured data matrices. When applied to a well-structured matrix, analysis of variance delivers accurate results, even when the matrix that is analyzed is quite small.

The objectives of the experiment are focused on:

- 1) To identify the most influential variable towards surface roughness (SR), tool wear (TW) and material removal rate (MRR).
- 2) To determine optimal process parameters and their effects on SR, TW and MRR through the Taguchi and response surface methodology.
- 3) To identify the best set of parameters group to minimize the noise and better SR, TW and MRR.

In this work, the experimental design has been chosen in process development or process troubleshooting to improve process performance or to obtain a process that is robust or insensitive to external sources of variability. It also can be good as a guideline in establishing statistical control of a process and be used to identify all these process influence variables. This is a critically important engineering tool to improve a manufacturing process. It also has extensive application in the development of these techniques early in process development, which can result in:

- a) Improved yield
- b) Reduced variability and closer conformance
- c) Reduced development time
- d) Reduced overall cost

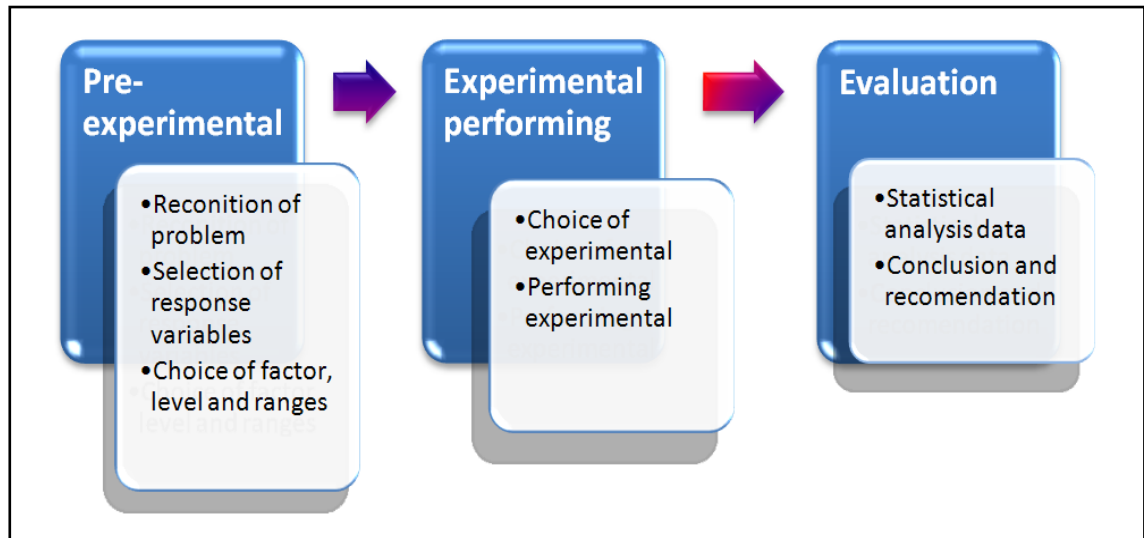


Figure 7.1: Design of experiment flow chart

Figure 7.1 shows the guideline and the recommended procedures for designing an experiment by Montgomery (2004).

1) Problem recognition

In order to start the design of an experiment, it is important to know the objectives and experimental requirements to develop an understanding of problem recognition. A better understanding of the problem often contributes to the new phenomenon being studied.

2) Factor and level

It is significant to consider the factors involved that may influence the performance of a process system. It is usually discovered that these factors can be classified as either potential design factors or nuisance factors.

In this research work, a total of 81 machining trials were carried out to evaluate and validate the modelling approach and study the influences of linear and non linear factors under different operational conditions. There are four machining parameters that have been considered, which are vibration amplitude (μm), vibration frequency (Hz), feedrate (mm/min) and spindle speed (rpm). The outputs are surface finish (R_a , μm), tool wear (mm) and material removal rate (min/mm) as shown in Table 7.1. There are four factors for the experiment and three levels for factors. These are divided into 3 levels which are level 1 (L1), level 2 (L2) and level 3 (L3). In the surface finish experiment, HSS coated titanium carbide is used. The spindles are chosen of 4,000 rpm, 7,000 rpm and 10,000 rpm.

Table 7.1: Machining parameters and their coded labels

Process variable	Levels		
	L1 (L)	L2 (M)	L3 (H)
Vibration amplitude, (μm)	1	3	5
Vibration frequency, (Hz)	1,000	2,000	3,000
Feed, (mm/min)	1	4	6
Spindle speed, (rpm)	4,000	7,000	10,000
Feed per tooth, (μm)	0.1	0.2	0.3

3) Response factors and variables

Selection of the response variable must be identified and will provide useful information about the process to study. It is of critical importance to identify issues related to defining the response of interest and how these are to be measured before conducting the experimental studies. Where there are inaccuracies in experimental data capability, then only relatively large factors will be detected by the experiment or additional replication will be required.

However, the designed experiments employed are strongly recommended to study and improve the performance of the measurement system. The experiments are conducted based on machining trial plan, as attached in appendix III.

4) Performing the experiment

It is essential to monitor the experiment process to certify the experimental plan is running smoothly without any errors. The critical point is to get rid of errors that can make the data collection invalid, thus wiping out the experimental validity. However, it is easy to underestimate the logistical and planning aspects of running a designed experiment in a complex manufacturing or research and development environment.

According to Montgomery and Coleman (1993), it is very helpful if a few trials are run or a pilot test before conducting the experiment, to collect information about the consistency of experimental material. The measurement system should also give some basic idea of machine capability.

5) Statistical data analysis

Statistical data analysis should be used to analyze and observe the results, so that the conclusion and objective can be drawn up instead of using a judgment in nature. However, if the experiment has been designed correctly and performance exactly follows the experimental design, the statistical methods required are not elaborate.

In this modern technological age, hundreds of statistical software packages have been designed to assist in data calculation and analysis. The software packages often interpret the results in a simple graphical method that plays an important role in data analysis because they are much easier to observe and understand. The software packages are also very helpful in presenting the results in terms of an empirical model which is an equation derived from data expressing the relationship between the response and the significant design factors.

However, statistical methods cannot prove that factors have a particular effect. It only offers guidelines to the reliability and validity of the results. It has been accepted by the engineer that statistical techniques combined with good engineering or process knowledge will usually lead to the best conclusion.

6) Conclusions and recommendations

Data have been collected and analyzed and the experiment finds a practical conclusion according to the results and recommend further action to be taken. One of the most popular methods is using graphical techniques in order to present the results to other researchers. It is recommended by Montgomery to do a follow-up run and confirmation testing to validate the conclusions from the experiments that have been done.

7.5.1 Minitab 15

Minitab 15 is a statistical software package for analyzing data in a statistical environment that allows the user to get fast, accurate and reliable results. Minitab also combines statistical methods in one software package, including ANOVA, regression analysis, Factorial, Taguchi, Response surface methodology, quality tools, reliability/survival, control multivariate design, etc. in one single package of software. The user can calculate, examine, investigate and verify the results using different methods in this package.

7.5.2 ANOVA

ANOVA is a method of calculation to identify the differences between two or more independent groups of data collected. Source of variation are explained in their degree of freedom (DF), total sum of square (SS), and the mean square (MS). The analysis will calculate also the F-statistic and p-values which are to determine whether the predictor of factors is significant/dominant related to the response.

7.5.3 Response surface method (RSM)

Response Surface Methodology is one of the useful tools in statistical analysis used to investigate the relationship between one or more response variables and a set of quantitative experimental variables. It is common in industries when the data may not be manageable and un-structure leads to an impact in waste of energy and accuracy of components. RSM is a method of identifying the controllable and uncontrollable to find the optimum performance to optimise the response. In this experimental work RSM is chosen because there is a suspected curvature in the response surface. In order to observe the relationship between the surface machine, tool wear and material removal rate towards process parameters, RSM has

been chosen to carry out this task. Optimisation and parameter control will be analyzed from the relationship of response which has been taken for further analysis.

7.5.4 Taguchi method

Taguchi is a statistical experimental design to calculate a single or multiple groups of data (variable) to find the optimum and consistency in the operating environment (response). It also can recognize the controllable and un-controllable factors in order to minimize the effect of noise factors.

Taguchi design is used in an orthogonal array which can estimate the effect of each factor relative to the means and variation. The orthogonal array design is for investigating the effect of each factor independently from the other in an economic way which reduces time and cost efficiently. The main objective is to identify the factors that affect the mean response and control them into the optimum level.

7.6 Optimisation analysis of surface roughness, tool wear and material removal rate

The next section investigates the optimisation process from the experimental trials. It is significant to examine the efficiency of data results before proceeding to the next analysis and for the optimisation process. First, to check the experimental data are in conformance with probability; second, to check whether the vibration frequency and amplitude giving a most impact to the response.

7.6.1 Regression analysis and ANOVA

Regression analysis is important to determine the relationship between the variables. It is commonly used in industries to get an understanding of how the typical value is affected by the others variable that have been predicted. It must be clarified that the regression model must fit into the set of data investigated. In this section, the three responses are surface roughness, tool wear and material removal rate as examined.

Linear regression analysis, which can be expressed as:

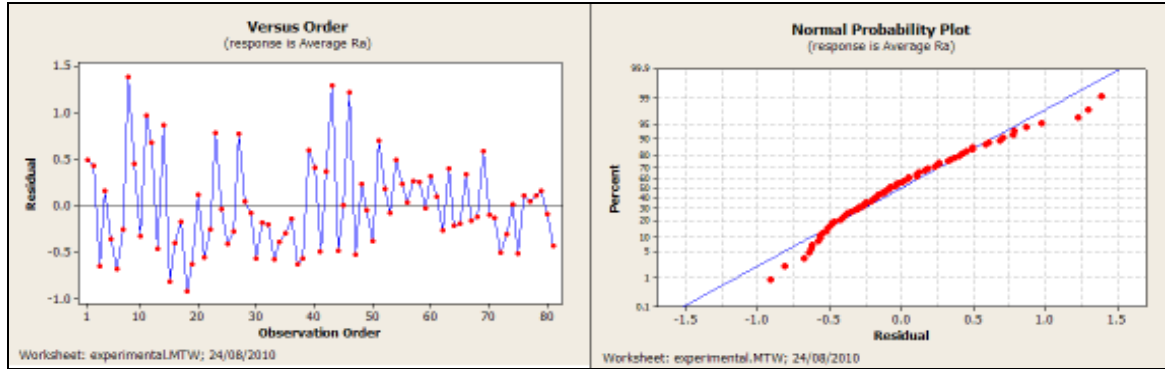
$$y = \beta_0 + \beta_1 x_1 + \beta_2 x_2 + \beta_3 x_3 \dots \beta_k x_k \quad (7.1)$$

where the y is response, β_0 is a response variable when predictor is zero, x is a value predictor variable and β_1, β_2 is estimated change in mean response for each unit change in predictor.

By using Equation 7-1, the regression analysis is calculated on the surface roughness, tool wear and material removal rate. It has been observed that the surface roughness, tool wear and material removal rates can be predicted using the Taguchi and surface response method and explained in the next chapter. The regression analysis is for finding:

- i) The normal probability response of surface roughness, tool wear and material removal rate;
- ii) Fitted value and the residual response to output;
- iii) The rank of influence factors to identify each optimum setup in factors

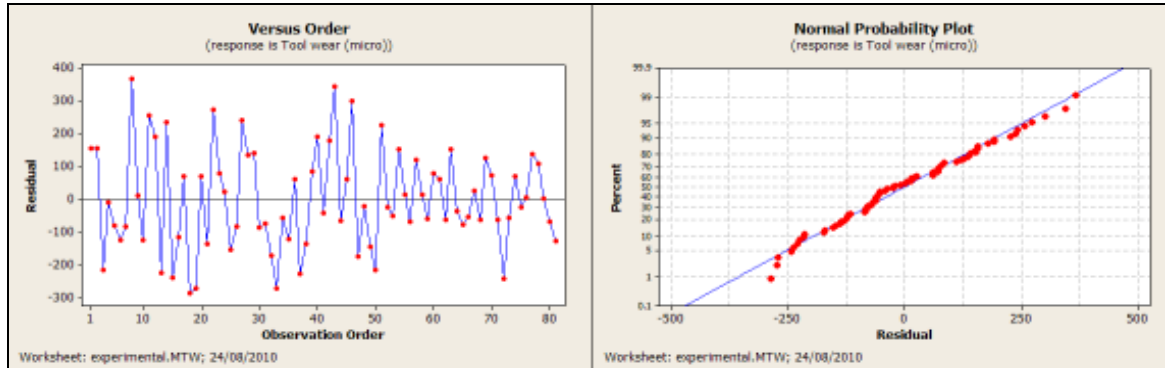
In regression analysis, vibration amplitude, vibration frequency, feedrate and spindle speed are identified as the main factors considered. The cross effect of the two factors is obtained to investigate the relationship between the main factors.



(a)

(b)

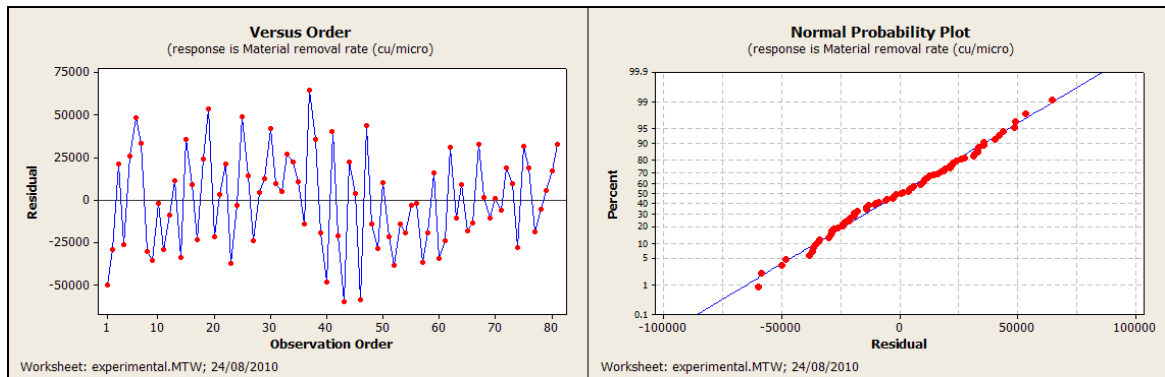
Figure 7.2: Average Ra versus fr (mm/min), Amp. (micron) ...



(a)

(b)

Figure 7.3: Tool wear versus fr (mm/min), Amp. (micron) ...



(a)

(b)

Figure 7.4: Material removal rate versus fr (mm/min), Amp. (micron, ...

Figures 7.2 - 7.4 show the regression analysis plots in surface roughness, tool wear and material removal rate plot. Figures 7.2(a) – 7.4(a) show the values that have below the

reference values and indicate the predicted value are greater than the observed values. However, for the surface roughness linear F-ratio value is greater than the regression P-values, which are 4.5 and 0.003 respectively. The others plots for tool wear and material removal rate the F-ratio value is 4.85 and 7.23; and P-values are 2.58 and 2.18 respectively. The greater F-ratio than the P-value value means that the value in the plot is significant.

Figures 7.2(b) – 7.4(b) show the residual value versus a percentage of each response. Value can be seen clearly in the experimental data and the residual percentage agrees with the probability plot which follows the linear blue line. Based on the diagnostic on the normal probability plot of residual, there are small amounts of point out of the linear model. About 10% to 15% of point is away from the ideal curve. The data in this experiment is accurate for the next analysis.

Moreover, in order to develop a model in exponential form that will comply with the empirical data a linear regression is generated that can be expressed.

The regression equation is,

$$\begin{aligned} \text{Average Ra} = & - 0.257 + 0.105 \text{ fr (mm/min)} + 0.386 \text{ Amp. (micron)} \\ & + 0.000007 \text{ Freq (Hz)} + 0.000071 \text{ Spindle Rpm} - 0.0199 \text{ fr*fr} \\ & - 0.0405 \text{ amp*amp} + 0.000000 \text{ freq*freq*} + 0.000000 \text{ RPM*RPM} \\ & + 0.0045 \text{ fr*amp} - 0.000018 \text{ fr_*freq} + 0.000003 \text{ fr*RPM} \\ & - 0.000058 \text{ amp*freq} + 0.000000 \text{ freq*RPM} \end{aligned}$$

$$\begin{aligned} \text{Tool wear (micro)} = & 48 - 29.4 \text{ fr (mm/min)} + 121 \text{ Amp. (micron)} + 0.113 \text{ Freq (Hz)} \\ & + 0.0061 \text{ Spindle Rpm} - 0.07 \text{ fr*fr} - 12.5 \text{ amp*amp} \\ & + 0.000004 \text{ freq*freq*} + 0.000002 \text{ RPM*RPM} + 0.81 \text{ fr*amp} \\ & - 0.0099 \text{ fr_*freq} + 0.00621 \text{ fr*RPM} - 0.0141 \text{ amp*freq} \\ & - 0.000010 \text{ freq*RPM} \end{aligned}$$

$$\begin{aligned} \text{Material removal rate (cu/micro)} = & 169005 + 17474 \text{ fr (mm/min)} \\ & - 16147 \text{ Amp. (micron)} + 21.7 \text{ Freq (Hz)} \\ & - 7.78 \text{ Spindle Rpm} - 1202 \text{ fr*fr} + 2269 \text{ amp*am} \\ & - 0.00431 \text{ freq*freq*} + 0.000207 \text{ RPM*RPM} \\ & - 964 \text{ fr*amp} - 1.55 \text{ fr_*freq} - 0.533 \text{ fr*RPM} \\ & - 0.02 \text{ amp*freq} + 0.00001 \text{ freq*RPM} \end{aligned}$$

Using the Minitab 16, ANOVA one-way analysis investigation has been made into this data to find the optimum parameter to get the good surface finish, reduce tool wear and high

material removal rate in each single factor and output. With the Quality Check (QC) for both the surface finish and the tool wear, the smaller the better. However, with the material removal rate the larger the better.

7.6.2 Taguchi analysis

The analysis continued to examine the effect of the SN ratio three levels of factors. In a linear model analysis which can observe the coefficients value for each factor at the low level, identify the p-values and an analysis of variance table. The calculation of the result is used to determine whether the factors are significantly related to the response data and each factor's relative importance in the model. In the Taguchi analysis, the coefficient by absolute indicates the relative importance of each single factor. The Taguchi analyses have been shown that the amplitude is the most significant factors by observing the Delta values which is higher the better. By performing an analysis for each individual response related to the variables as shown below. The ANOVA and Taguchi shows the same rank of dominant factor thus it some for verification process.

From Taguchi, the rank of the significant factor can be determined, which is summarized below. The optimum condition cutting process also has been shown in the Taguchi investigation.

For surface roughness,

Taguchi Analysis: Ra versus Feedrate, Vibration am, Vibration fr, Spindle speed

Response Table for Signal to Noise Ratios
Smaller is better

Level	Feedrate	Vibration amplitude	Vibration frequency	Spindle speed
1	-3.8781	4.1820	-0.1042	-0.8610
2	0.8165	-5.4478	1.0829	2.0323
3	2.4159	0.6202	-1.6243	-1.8170
Delta	6.2940	9.6297	2.7071	3.8494
Rank	2	1	4	3

For tool wear,

Taguchi Analysis: Tool wear versus Feedrate, Vibration am, Vibration fr

Response Table for Signal to Noise Ratios
Smaller is better

Level	Feedrate	Vibration amplitude	Vibration frequency	Spindle speed
1	-55.24	-48.42	-52.41	-53.04
2	-50.38	-56.25	-50.37	-50.88
3	-50.80	-51.75	-53.64	-52.50
Delta	4.86	7.83	3.27	2.16
Rank	2	1	3	4

For material removal rate,

Taguchi Analysis: MRR versus Feedrate, Vibration am, Vibration fr

Response Table for Signal to Noise Ratios
Larger is better

Level	Feedrate	Vibration amplitude	Vibration frequency	Spindle speed
1	99.83	103.24	101.47	101.29
2	102.73	99.32	102.76	103.15
3	102.77	102.77	101.10	100.89
Delta	2.94	3.92	1.66	2.26
Rank	2	1	4	3

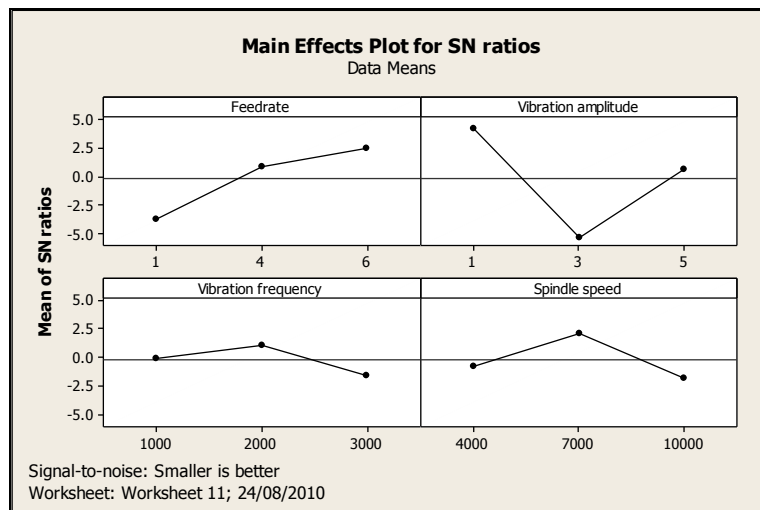


Figure 7.5: Optimum setup SN ratio in surface roughness

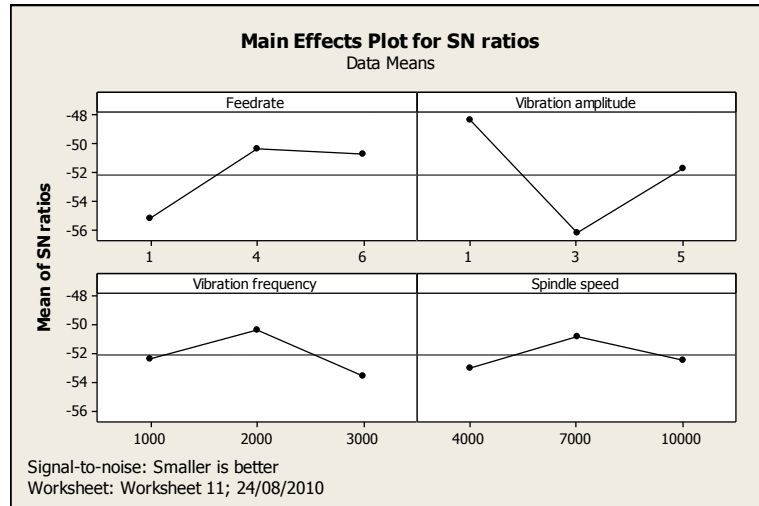


Figure 7.6: Optimum setup SN ratio in tool wear

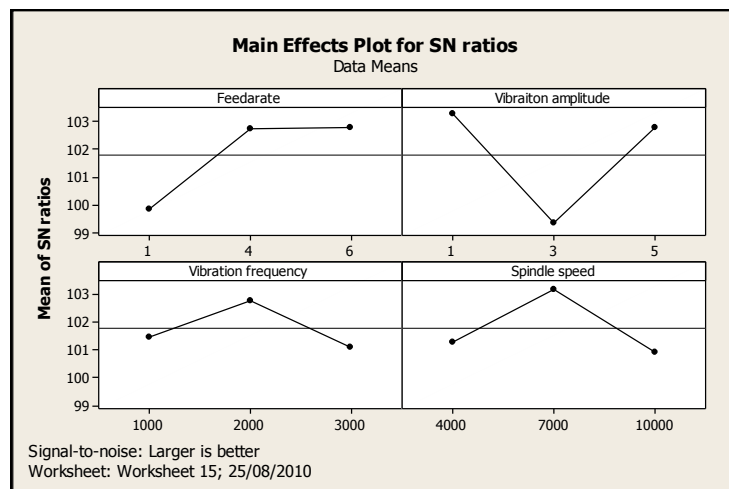


Figure 7.7: Optimum setup SN ratio in material removal rate

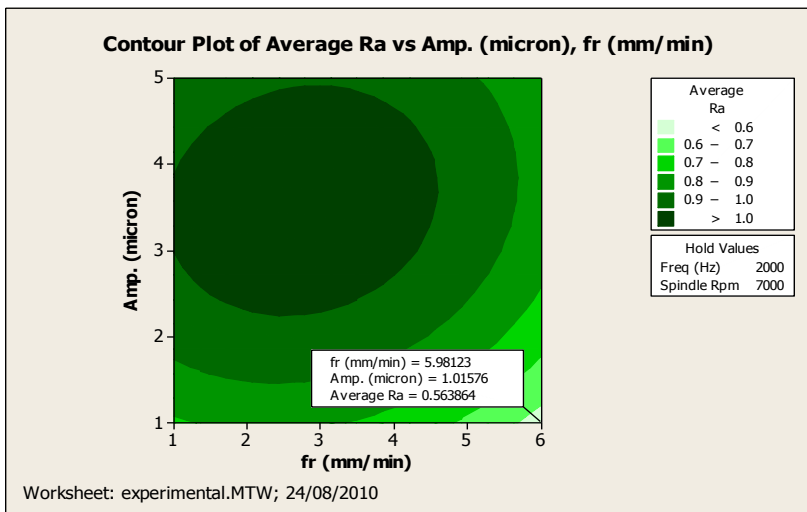
The response table shows the average of the SN ratio for each level of factor. The rank of the factor is determined by the delta statistic in relation to the magnitude of the effect. Figures 7.5 to 7.7 show the main effect plot for SN ratio in surface roughness, tool wear and material removal rate. A summary of the optimum setup machining condition can be found in Table 7.2.

Table 7.2: Optimum of each factor at the response

Level	Feedrate mm/min	Vibration amplitude (μm)	Vibration frequency (Hz)	Spindle Speed (rpm)
Surface roughness	6	1	2000	7000
Tool wear	4	1	2000	7000
Material removal rate	6	1	2000	7000

7.6.3 Contour plot in response to surface methodology

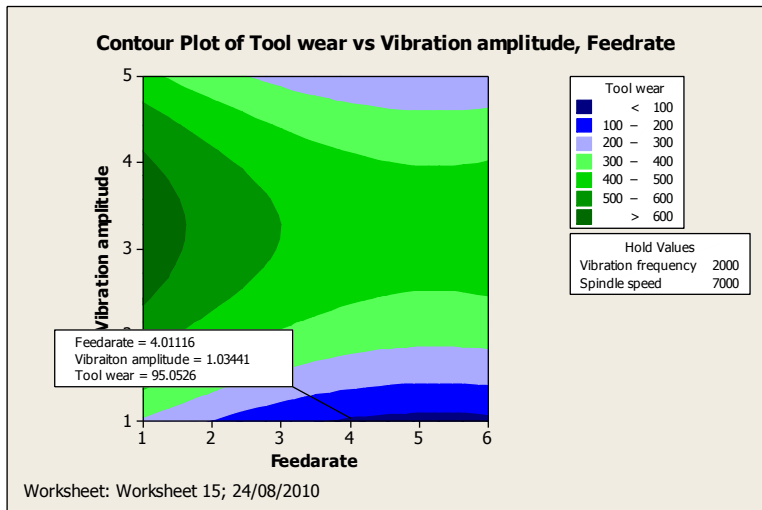
The next step for optimisation in this research work is a prediction of optimum value surface plot by using a response surface methodology function. The value of optimum setting is followed by the Taguchi result, which is in Table 7.2.



Predicted value
S/N Ratio Mean
3.84150 0.601586

Figure 7.8: Contour plot in Ra

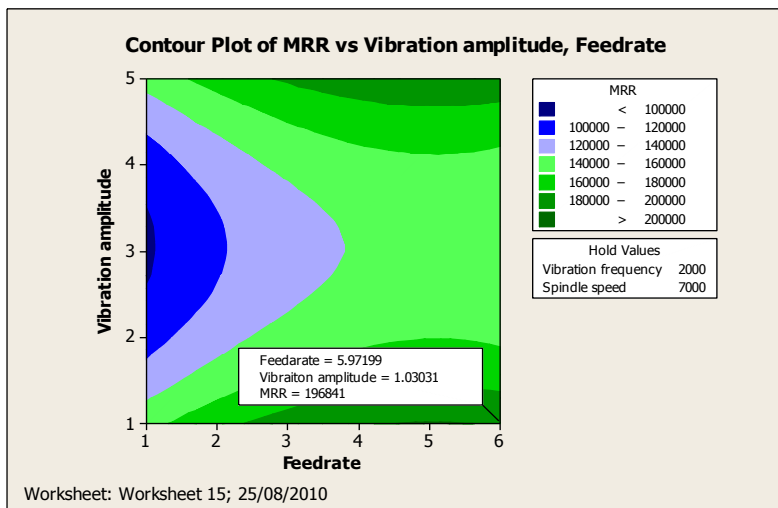
The optimum setup for surface roughness has been proved in Figure 7.8. The prediction given by RSM design for S/N ratio is 3.84150 and the mean is 0.6015 μm . The hold value predicted by RSM for vibration frequency is 2,000 Hz, spindle speed 7,000 rpm. The feedrate is 6 mm/min, vibration amplitude 1 μm . It is clearly shown that a contour plot of the area in the 6 and 1 is about 0.5638 μm as verified by the RSM analysis design. On the other hand, the value of Ra significantly changes when the feedrate is decreased and becomes worst with the amplitude range of 2.8 μm to 4.9 μm



Predicted value
S/N Ratio Mean
43.6299 91

Figure 7.9: Contour plot in tool wear

Next, the tool wear in the contour plot shows the prediction of RSM design is given by S/N ratio 43.6299 and mean value is 91 μm . The observed value from the contour plot is approximately 95.052 μm . The hold values for this setup are the same as the Ra setting. The predicted value and the contour plot agree with a 5% difference. However, the range of 200 μm – 300 μm tool wear is observed as the vibration amplitude starts at 4.5 μm to 5 μm with the feedrate from 2 mm to 6 mm.



Predicted value
S/N Ratio Mean
106.593 198342

Figure 7.10: Contour plot in MRR

By observing and analyzing Figure 7.10 the surface contour shows the similarity between the predicted values and contour value. The hold value is the same as the previous setting. The QC setting for MRR is the larger the better the goal is for plenty of material being removed in the 2D VAM. It is 198,342 cu/μm and 196,421 cu/μm from the prediction and contour surface respectively when the vibration amplitude is 1 μm and 6 μm for feedrate.

However, similar MRR can be observed at feedrate 4.8 μm to 5.5 μm in the range. On the other hand, less of MRR can be found when the 1 mm of feedrate and 2.6 μm to 3.6 μm vibrations can found which result of less than 10,000 cu/μm.

7.6.4 Interaction between factors

Figures 7.11 to 7.13 show the interaction factors relative to each of the responses. An interactions plot is a plot of means for each level of a factor with the level of a second factor held constant. The usefulness of the interaction plot is in concluding and judging between each factor of interaction (Minitab). This interaction plot is in balanced design where uses of the two types of factor are identical.

Interaction is present when the response at a factor level depends upon the level(s) of other factors. Parallel lines in an interactions plot indicate no interaction. The greater the departure of the lines from the parallel state, the higher the degree of interaction.

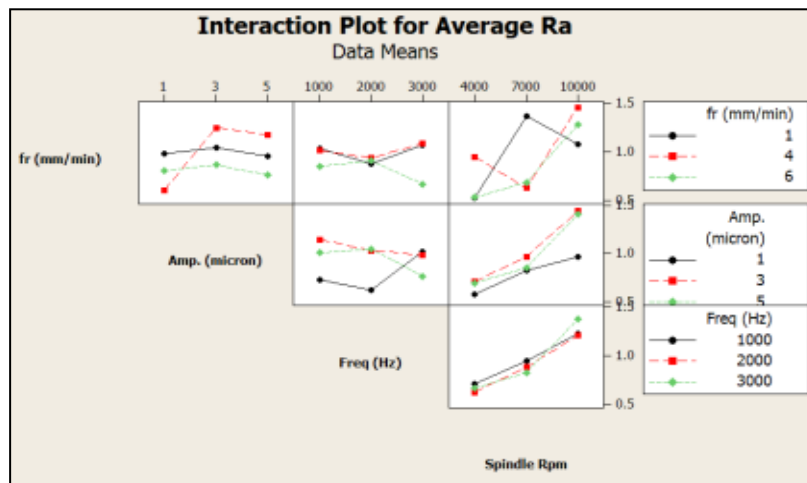


Figure 7.11: Interaction between factors for surface finish

Figure 7.11 shows the interaction plot between the feedrate, vibration amplitude, vibration frequency and spindle speed relative to the surface roughness. When this data is examined by experimental analysis, the vibration amplitude is the most significant factor followed by feedrate, spindle speed and vibration frequency. Firstly, with the surface finish at mean $0.596 \mu\text{m}$, the amplitude needs to be $1 \mu\text{m}$ and the feedrate is 4 mm/min . Secondly, the mean of $R_a 0.625 \mu\text{m}$ can be achieved from the $1 \mu\text{m}$ of vibration amplitude and $2,000 \text{ Hz}$ of vibration frequency. The result of interaction agrees well with the Taguchi analysis in section 7.6.2 above.

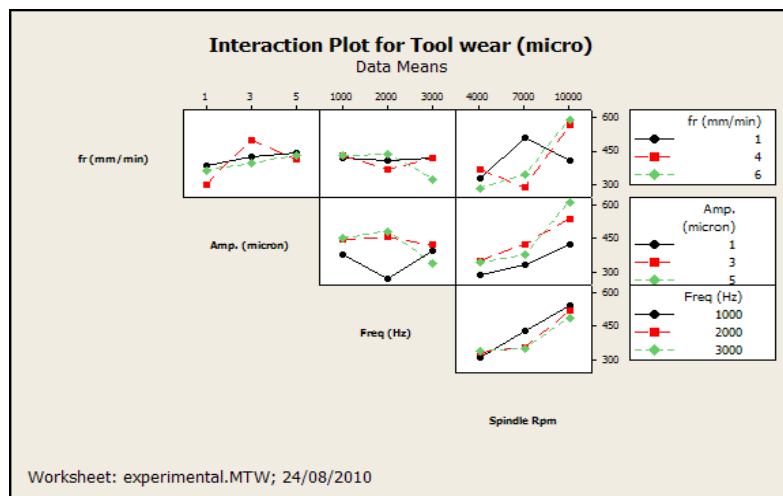


Figure 7.12: Interaction between factors for tool wear

Figure 7.12 shows the interaction plot between the feedrate, vibration amplitude, vibration frequency and spindle speed relative to the tool wear. When this data is examined by the experimental analysis, the vibration amplitude is the most significant factor, followed by feedrate, vibration frequency and spindle speed. The first interaction result plot has been observed at the value of $296.667 \mu\text{m}$ where the amplitude is $1 \mu\text{m}$ and the feedrate is 4 mm/min .

Secondly, the mean of $257.396 \mu\text{m}$ can be achieved from the $1 \mu\text{m}$ of vibration amplitude $2,000 \text{ Hz}$ of vibration frequency. And the third is feedrate is $4 \mu\text{m}$ and the spindle speed is $7,000 \text{ rpm}$ giving the means of $263.44 \mu\text{m}$. The result of interaction factors agrees well with the Taguchi analysis in section 7.6.2 above. The important factor in tool wear is vibration

amplitude which is shown clearly from the interaction effect plot when the vibration amplitude leads to impact of tool wear rate on an interaction group.

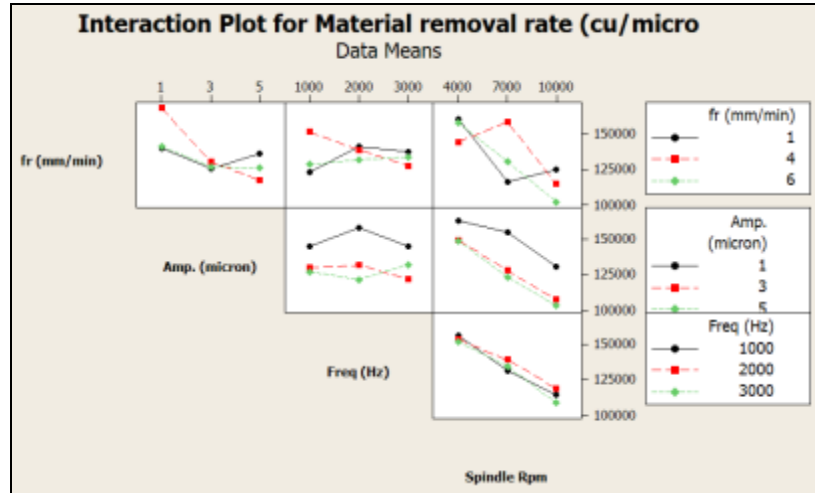


Figure 7.13: Interaction between factors for MRR

Figure 7.13 shows the interaction plot between the feedrate, vibration amplitude, vibration frequency and spindle speed relative to the tool wear. The QC in material removal rate is “the larger the better”. When this data is examined by the experimental analysis, the vibration amplitude is the most significant factor, followed by feedrate, spindle speed and vibration frequency.

The first interaction result plot has been observed at the value of 168,087 $\text{cu}/\mu\text{m}$ where the amplitude is 1 μm and the feedrate is 4 mm/min. For the second group it is 158,244 $\text{cu}/\mu\text{m}$, the amplitude needed is 1 μm and the vibration frequency is 2,000 Hz. And the third is vibration amplitude is 1 μm and the spindle speed is 4,000 rpm giving the mean of 165,272 $\text{cu}/\mu\text{m}$. The result of interaction agrees well with the Taguchi analysis in section 7.6.2 which is a significant factor with high impact on the response.

7.7 Summary

This chapter presents the optimisation of surface roughness, tool wear and material removal rate using several tools, which are regression analysis, ANOVA, Taguchi and response surface methodology. The regression analysis is used to investigate and model the

relationship between the response variable and the input parameters. It can also be concluded that the result value of the experiment is highly probable to be taken into the analysis. ANOVA is not only used to verify the dominant factors for the three responses, but also includes the F-statistic and p-value that determine whether the factors are significantly related to the response. Taguchi analysis is responsible for examining the rank and the level of factors that have a significant effect on the responses. Lastly, the interaction plot between factors explains when changes in response from the low level to the high level of one factor are not the same as the changes in response at the same two levels of a second factor. The effect of one factor is dependent upon a second factor. The interactions plots can also be used to compare the relative strength of the effects across factors.

The optimisation and the relationships between factors from the trial experiments and predictions agree well using the regression, ANOVA, Taguchi and Response surface methodology. The dominant factors and the rank of variables are examined and there is quite marked agreement between the observations. The best optimum cutting setup is shown in Table 7.2. The surface roughness and material removal rate share the same level but not with tool wear. The feedrate is 4 instead of 6. With the information gathered and presented, there are possible ways to choose the machine quality and quantity of products by following the guidelines presented in this chapter.

Chapter 8 Conclusions and recommendations for future work

8.1 Conclusions

All the data presented in this chapter are based on trials and experiments which have been carried out and confined to the aims and objective of the research. The experimental and trial data are validated by measurement and inspection on Zygo NewView 5000 3D Profiler, Microscopic TESA and additionally the modelling and simulations. All the data obtained are presented through graphs to show the trends and to check the consistency of results. With the extension of the data obtained, they are compared, analysed and discussed. The prototype of a vibration micro-milling machine has been designed with a cost effective method of fabrication and taking account of accuracy and easy to operate.

Firstly, a detailed investigation into machine dynamics has been carried out by using the FEA tool and experimental apparatus. The use of Ansys Classical and Ansys workbench helps examine “hidden” information about the machine design.

This research provides a modelling approach for investigating the 2 dimensional vibrations assisted machining in micro-milling. The development modelling approach has shown the relationship between the machined surfaces and the cutting parameter which is focused on the vibration amplitude and vibration frequency.

In depth investigation into micro-milling is continued with the optimisation and is examined qualitatively and quantitatively, followed by an analytical scientific approach. Statistical software tools such as ANOVA, Taguchi and RSM have been applied to verify the optimum setup for the cutting process.

This research project has led to the following contribution to knowledge:

- (1) Development of the prototype horizontal desktop vibration assisted micro-milling machine.
- (2) Development of theoretical models that can predict the surface finish, tool wear and material removal rate quantitatively.
- (3) Establishing in depth for use of vibration assisted machining principles.
- (4) Optimisation of cutting process parameters and conditions through the simulations and machining trials for the through investigation of vibration assisted machining.

8.2 Recommendations for future work

The recommendations for future work are summarised as follows:

- 1) Further research on dynamic machine behaviour for micro-milling machines should focus on the cutting tool and condition monitoring.
- 2) Re-assessment of the framework of design concept. The assembly and machine component error should especially be taken into account.
- 3) More understanding of vibration assisted machining mechanism phenomena in precision engineering to develop a robust knowledge and to implement new machine technology.
- 4) Investigation into the lubrication and coolant potential in vibration assisted micro-milling.

References

Abrao, M., and Aspinwall, K. "The surface integrity of turned and ground hardened bearing steel". *Wear*, Vol. 196, 1996, pp. 179-284.

Adachi, K., Arai, N., Harada, S., Okita, K., and Wakisaka, S. "A study on burr in low frequency vibratory drilling of aluminum". *Surface metrology, Measurement Science and Technology*, Vol. 8, 1997, pp. 955-972.

Ahn, J., Lim, H., and Son, S. "Improvement of micromachining accuracy by 2 Dimensional vibration cutting". *Proceedings of ASPE*, Vol. 20, 1999, pp. 150-153.

Akasawa, T., Fukuda, I., Nakamura, K., and T. Tanaka. "Effect of microstructure and hardness on the machinability of medium-carbon chrome-molybdenum steel". *Journal of Materials Processing Technology*, Vol. 153-154, 2004, pp. 48-53.

Altintas, Y., "Manufacturing Automation: Metal Cutting Mechanics, Machine Tool Vibrations and CNC Design". Cambridge University Press, Cambridge, UK, 2000.

Arcona, C., and Dow, A. "An empirical tool force model for precision machining of ductile of materials". *Proceedings of the 1992 NSF Des. and Manufacturing System Conference*, Atlanta Georgia, 1992, pp. 123-129.

Arnab, R., Sushanta, P, Shamsuzzaman, M., and Ishfaqur, R. "Design of an optimum antenna system for maximum power transfer using statistical design of experiment approach". *PIERS Proceedings*, Beijing, China, 2009, pp. 23-27.

Asheghi, M. [online]. "About Ansys". Available at: www.me.cmu.edu/academics/academics/courses/NSF_EDU_Proj/hF1Engr_ANSYS/. (Accessed on 13th Nov 2009).

Astash, K., and Babitsky, I. "Ultrasonic cutting as a nonlinear (vibro-impact) process". *Ultrasonics*, Vol. 36, 1998, pp. 89-96.

Avitabile, P. "Experimental Modal Analysis", A simple Non-Mathematical Presentation, *Sound and Vibration, Modal Analysis and Control Laboratory*, Lowell USA, 2001.

Axinte, A., and Dewes, C. "Surface integrity of hot work tool steel after high speed milling- experimental data and empirical models". *Journal of Materials Processing Technology*, Vol. 127, 2002, pp. 325-335.

Axinte, A., Gindy, N., Fox, K., and Unanue, I. "Process monitoring to assist the workpiece surface quality in machining". *International Journal of Machine Tools & Manufacture*, Vol. 44, 2004, pp. 1091-1108.

Babitsky, I., Mitrofanov, V., and Silberschmidt, V. "Ultrasonically-assisted turning of aviation materials: simulations and experimental study". *Ultrasonics*, Vol. 6, 2004, pp. 42-81.

Babitsky, V., and Kalanishikov, N. "Ultrasonically turning in aviation material". *Journal of Materials Processing Technology*, Vol. 132, 2003, pp. 157-167.

Benning, O. "Non-destructive determination of load and residual stresses by the x-ray stress method". *The Rigaku Journal*, Vol. 6, 1989, pp. 15-21.

Billings, A. "Optics, Optoelectronics and Photonics". *Engineering Principles and Applications*, Prentice Hall of Australia Pty Ltd., Impact Printing, Brunswick, NSW, 1993.

Bonifacio, M. and Diniz, E., "Correlating tool wear, tool life, surface roughness and tool vibration in finish turning with coated carbide tools". *Wear*, Vol. 173, 1994, pp. 137-144.

Bottcher, J. [online]. Available at: <http://en.wikipedia.org/wiki/Permittivity> (Accessed on 23rd May 2009).

Bradley, C., and Wong, S. "Surface texture indicators of tool wear – a machine vision approach". *International Journal of Advanced Manufacturing Technology*, Vol. 17, 2001, pp. 435-443.

Brehl, D. "Review of vibration assisted machining". *Precision Engineering*, Vol. 32, 2008, pp. 153-173.

Brehl, E., Dow, A., Garrad, K., and Sohn, A. "Microstructure fabrication using elliptical vibration-assisted machining". *Proceedings of ASPE*, Vol. 39, 2006, pp. 511-514.

Brehl, E., and Dow, A. (Editors). "Vibration assisted machining technology". *Proceedings ASPE*, Vol. 40, 2007, pp. 150-156.

Brinksmeier, E., Minke, E., and Nowag, L. "Residual stresses in precision components". *The 5th International Conference on Industrial Tooling*, Vol. 10-11, 2003, pp. 1-21.

Bruckner, D. "Remarks on the wearing process in grinding". *Industrie Anzeiger*, Vol. 8, 1960, pp. 23-28.

Casto, L., Lombardo, A., Valvo L., and Ruisi, F. "Computer vision profilometer: equipment and evaluation of measurements". *Wear*, Vol. 146, 1991, pp. 53-61.

Cedrat Technologies SA. "Compact, Dynamic and Precise, Piezo Product Catalogue". Version 3.3.0, 2010-2011.

Cerniway, M. "Elliptical Diamond Milling: Kinematics, Force and Tool". MSc Dissertation Graduate Faculty, North Carolina State University, 2005.

Cheng, K. (Edior) "Machining Dynamics: Fundamental, Applications and Practices". Springer Series in Advanced Manufacturing, Springer Verlag London, 2008.

Chern, L., and Chang, C. "Using two-dimensional cutting for micro-milling". International Journal of Machine Tools & Manufacture, Vol. 46, 2006, pp. 659-666.

Cho, W., and Eman, F. "In-process identification of milling operation". International Journal Machine Tools and Manufacture, Vol. 30, 1990, pp. 325-337.

Corbani, F., Delvó, P., Fiorina, L., Mariottini, C., and Rizzi, L. "Speckle interferometry, fibre optic sensors and laser induced ultrasounds as solutions to industrial demands". Optics and Lasers in Engineering, Vol. 37, 2002, pp. 369-383.

Deutsche N. "Determination of Surface Roughness Values Ra, Rz, Rmax, with Electric Stylus Instruments-Basic Data". Berlin Beuth Verlag, GmbH, 1974.

Dong, P., Sullivan, J., and Stout, J. "Comprehensive study of parameters for characterizing three dimensional surface topography I: Some inherent properties of parameter variation". Wear, Vol.159, 1992, pp. 161-171.

Dongming Li, Rasidi Ibrahim, Ying Jia, and Xiaoyu Wang: "Study and development of a kind of electric-pneumatic transfer device with piezoelectric structure". International Conference on Computer, Mechatronics, Control and Electronic Engineering (CMCE 2010), Changchun, China, August 24-26, 2010.

Endo, T., Tsujimoto, T., and Mitsui, K. "Study of vibration-assisted micro-EDM: the effect of vibration on machining time and stability of discharge". Precision Engineering, Vol. 32, 2008, pp. 269-277.

Fang, F., and Zhang, X. "An experimental study of optical glass machining". International Journal of Advanced Manufacturing Technology. Vol. 23, 2004, pp. 155-160.

Franci, C., and Zuper, U. "Approach to optimization of cutting condition by using artificial neural network". *Journal of Materials Processing Technology*, Vol. 3, 2006, pp. 281-290.

Groover, P. "Fundamental of Modern Manufacturing: Materials Processes and Systems". Third edition, John Wiley & Sons, Inc. 2007.

Grum, J. "A review of the influence of grinding conditions on resulting residual stresses after induction surface hardening and grinding". *Journal of Materials Processing Technology*, Vol. 114, 2001, pp. 212-226.

Guillaume, P. "Modal analysis". Department of Mechanical Engineering, University of Brussel, Belgium, 2006, pp. 1-14.

Handbook of analytical methods for materials, Practical solutions to materials problems through technology and innovation. Materials Evaluation and Engineering, Inc. 13805 1st Avenue North, Suite 400 Plymouth, MN 55441-5447.

Higham, J. "MATLAB Guide Second edition, Society for Industrial and Applied Mathematics (SIAM)". ISBN 0-89871-578-4, 2005.

Hirakuri, K., and Yoshii, M. "The effect of ultrasonic vibration on CVD diamond nucleation". *Diamond and Related Materials*, Vol. 6, 1997, pp. 1031-1035.

Hopkins, J. "APL Technical Digest". Vol. 25, 2004, No. 2, pp. 87-95.

Hussin, Z., Cheng, K., Crispin, A., and Ward, R., "On-line measurement of workpiece surface topography and texture by using laser scattering". Proceedings of the 7th International Conference and Exhibition on Laser Metrology, Machine Tool, CMM & Robotic Performance-Laser Metrology and Machine Performance VII, 2005, pp. 574-583.

Hwan, J., Seok, H., Seong L., and Min, S. "Improvement of Micro-machining Accuracy by 2-Dimensional Vibration Cutting". American Society of Precision Engineers Conference Proceedings, Vol. 20, 1999, pp. 150-155.

Ibrahim, R., and Cheng, K. "Vibration assisted micro-milling: theoretical models and instrumental implementation". Proceedings of the 5th International Conference on Manufacturing Research, 2007, Vol. 5, pp. 17-20.

Ibrahim, R., Cheng, K., Bateman, R., Wang, C., and Au, J. "Design and analysis of a desktop micro-machine for vibration-assisted micromachining". Proceedings of the IMechE, Part B: Journal of Engineering Manufacture, 2010 (In press).

Ibrahim, R., Hao Wang and Kai Cheng: Surface roughness optimisation in vibration assisted micro-milling of aluminium T6061 using response surface method: Proceedings of the 21st International Computer-Aided Production Engineering Conference (CAPE 2010), The University of Edinburgh, 13-14 April 2010.

ITI GMBH, Webergesen, "Modelling and simulation of a new hydraulic piezo valve". Simulation Software Engineering, 2006, pp. 1-5.

Jain, K. "Modelling of material removal in mechanical type advanced machining processes: a state-of-art review". International Journal of Machine Tools & Manufacture, Vol. 41, 2001, pp. 1573-1635.

Jang, Y., Choi, G., Kim, G., and Hsiao, A. "Study of the correlation between surface roughness and cutting vibrations to develop an on-line roughness measuring technique in hard turning". International Journal of Machine Tools and Manufacture, Vol. 36, 1996, pp. 453-464.

Jin, C., and Bao, K. "Surface detection and 3D profilometry for micro-structure using optical metrology". Optics and Lasers in Engineering, Vol. 36, 2001, pp. 1-9.

Jordan, W., and Smith, P. "Mathematical Techniques: An Introduction for the Engineering, Physical, and Mathematical Sciences". Oxford University Press Inc., New York, 2002.

Jungles, J. "High speed measurement of engineering surfaces". International Journal of Machine Tools and Manufacture. Vol. 32, 1992, pp. 27-32.

Kim, G., and Loh, B. "An ultrasonic elliptical vibration cutting device for micro V-groove machining: Kinematical analysis and micro V-groove machining characteristics". Journal of Materials Processing Technology, Vol. 190, 2007, pp. 181-188.

Kim, H., Jeon, C., and Kwon, D. "Determining Brinell hardness from analysis of indentation load-depth curve without optical measurement". Transactions of the ASME, Journal of Engineering Material Technology, Vol. 127, 2005, pp. 154-158.

Kim, J., and Choi, H. "Characteristics of chip generation by ultrasonic vibration cutting with extremely low cutting velocity". International Journal of Advanced Manufacturing Technology, 1998, Vol. 14, pp. 2-6.

Kim, J., and Lee, E. "Study of ultrasonic vibration cutting of carbon fibre reinforced plastics". International Journal of Advanced Manufacturing Technology. Vol. 12, 1996, pp. 78-86.

Kim, Y, Shen, F., and Ahn, H. "Development of surface roughness measurement system using reflected laser beam". Journal of Materials Processing Technology, Vol. 130-131, 2002, pp. 662-667.

Kölemen, U. "Analysis of ISE in micro-hardness measurements of bulk MgB₂ superconductors using different models". Journal of Alloys and Compounds, Vol. 425, 2006, pp. 429-435.

Lai, W. "Modelling of Cutting Forces in End Milling Operations". *Journal of Science and Engineering*, Vol. 3, 2000, Vol. 1, pp. 15-22.

Lee, W., Mayor, R., and Ni, J. "Dynamic analysis of mesoscale machine tools". *Transactions of the ASME: Journal of Manufacture Science and Engineering*, Vol. 128, 2006, pp. 194-203.

Lee, Y., Juan, H., and Yu, F. "A study of computer vision for measuring surface roughness in the turning process". *International Journal of Advanced Manufacturing Technology*, Vol. 19, 2002, pp. 295-301.

Lee Y., and Kang, M. "Simulation of surface roughness and profile in high speed end milling", *Journal of Materials Processing Technology*, Vol. 11, 2001, pp. 410-415.

Li, X., and Zhang, D. "Ultrasonic elliptical vibration transducer driven by single actuator and its application in precision cutting". *Journal of Materials Processing Technology*, Vol. 180, 2006, pp. 91-95.

Li, X., Wang, L., and Cai, N. "Machine-vision-based surface finish inspection for cutting tool replacement in production". *International Journal of Production Research*, Vol. 42, 2004, pp. 2279-2287.

Liu, G., Toncich, J., Harvey, C., and Yuan, F. "Diagnostic technique for laser micromachining of multi-layer thin films". *International Journal of Machine Tools & Manufacture*, Vol. 45, 2005, pp. 583-589.

Liu, K., and Rahman, M. "Study of ductile mode cutting in grooving of tungsten carbide with and without ultrasonic vibration assistance". *International Journal of Advanced Manufacturing Technology*, Vol. 24, 2004, pp. 389-394.

- Liu, N., and Loftus, M. "Surface finish visualization in high speed ball nose milling applications". *International Journal of Machine Tools & Manufacture*, Vol. 45, 2005, pp. 1152-1161.
- Liu, W. Cheng, K., Webb, D. and Luo, X., "Improved Dynamic Cutting Force Model in Peripheral Milling Part I: Theoretical Model and Simulation". *International Journal of Advanced Manufacturing Technology*, Vol. 20, 2002, pp. 631-638.
- Liu, W., Cheng, K., Webb, D. and Luo, X., "Improved Dynamic Cutting Force Model in Peripheral Milling Part II: experimental verification and prediction". *International Journal of Advanced Manufacturing Technology*, Vol. 24, 2004, pp. 794-805.
- Liu, X. and Cheng, K., "Modelling the machining dynamics of peripheral milling". *International Journal of Machine Tools and Manufacture*, Vol. 45, 2005, pp. 1301-1320.
- Lucca, A., Seo, W., and Rhorer, L. "Energies in the ultra-precision machining of ductile materials". *Proceedings of the 1992 NSF, Design and Manufacturing System Conference*, pp. 123-129.
- Luo, X. "High Precision Surfaces Generation: Modelling, Simulation and Machining Verification". PhD Thesis, Leeds Metropolitan University, April 2004.
- Stephenson, A., and Agapiu, S. "Metal Cutting Theory and Practice". 2nd Edition. CRC, Taylor and Francis Group Publication, 2006.
- Kovacic, M. "Evolutionary approach for cutting forces prediction in milling". *Journal of Materials Processing Technology*. Vol. 155, 2004, pp. 1647-1652.
- Ma, C., Shamoto, E., and Moriwaki, T. "Suppression of burrs in turning with ultrasonic elliptical vibration cutting". *International Journal of Machine Tools & Manufacture*, Vol. 45, 2005, pp. 1295-1300.

Mackerle, J. "Finite element analysis of machine elements, A bibliography". Engineering Computation, 1999, Vol. 16, pp. 677-748.

Malkin, S., and Cook, N.H. "The wear of grinding wheels. Part 2: fracture wear". Journal of Engineering for Industry, Vol. 4, 1971, pp. 1129-1133.

Mannan, M. "Detection and location of structural cracks using FRF measurements". IMAC VIII, January 1990.

Masako, J., and Murukawa, M. "Development of practical ultrasonic vibration cutting tool system". Journal of Materials Processing Technology, Vol. 113, 2001, pp. 342-347.

Matsumura, T. "Glass machining with micro-endmill". Japan Society of Mechanical Engineers (JSME), Vol. 16, 2005, pp. 139-158.

McConnell, G. "Vibration Testing: Theory and Practice", Wiley, New York, 1987, Randall, R.B Frequency Analysis, B & K Ltd., Denmark,

Metropro™ Surface Texture Parameters, by Zygo Corporation, 2002, [Online] Available at: http://www.lamdapacific.com/mlx_manage/upload/200611211405734.pdf, (Accessed on 3rd January 2006).

Milos, G., and Milutinovic, D. "Desktop 3- parallel kinematic milling machine". International Journal of Advanced Manufacturing Technology, 2009, Vol. 46, pp. 51-60.

Mitsui, K. "In-process sensors for surface roughness and their applications". Precision Engineering, Vol. 8, 1986, pp. 212-220.

Montgomery, C. "Design and Analysis of Experiments". 6th Edition, John Wiley & Sons, Inc. 2005.

Moriwaki, T., and Shamamoto, E. "Ultra-precision diamond cutting of hardened steel by elliptical vibration cutting", *Annals of the CIRP*, Vol. 48, 1999, pp. 441-444.

Moriwaki, T., and Shamoto, E. "Ultraprecision diamond turning of stainless steel by applying ultrasonic vibration". *Annals of the CIRP*, Vol. 40, 1991, pp. 559-562.

Nobuhiko, N., and Thomas, A. "Elliptical vibration assisted diamond turning". *Precision Engineering*, Vol. 20, 1996, pp. 4-19.

Ohlsson, R., Wihlborg, A., and Westberg, H. "The accuracy of fast 3D topography measurements". *International Journal of Machine Tools & Manufacture*, Vol. 41, 2001, pp. 1899-1907.

Okazaki, Y., Mishima, N., and Ashida, K. "Microfactory and micro machine tools". *Proceedings of the 1st Korea-Japan Conference on Positioning Technology*, Daejon, Korea, 2002, pp. 79-88.

Ozel, T., Hsu, K., and Zeren, E. "Effects of cutting edge geometry, workpiece hardness, feed rate and cutting speed on surface roughness and forces in finish turning of hardened AISI H13 steel". *International Journal of Advanced Manufacturing Technology*, Vol. 25, 2005, pp. 262-269.

Palanisamy, P., Rajendran, I., and Shanmugasundaram, S. "Optimisation of machining parameters using genetic algorithm and experimental validation for end-milling operations". *International Journal of Advanced Manufacturing Technology*, Vol. 32, 2007, pp. 644-655.

Persson, U. "A fibre-optic surface-roughness sensor". *Journal of Materials Processing Technology*, Vol. 95, 1999, pp. 107-111.

Persson, U. "Real time measurement of surface roughness on ground surfaces using speckle-contrast technique". *Optics and Lasers in Engineering*, Vol. 17, 1992, pp. 61-67.

Prieto, F., Redarce, T., Lepage, R., and Boulanger, P. "An automated inspection system". *International Journal of Advanced Manufacturing Technology*, Vol. 19, 2002, pp. 917-925.

Qu, W., and Wang, K. "Using vibration-assisted grinding to reduce subsurface damage". *International Journal of Machine Tools & Manufacture*, Vol. 44, 2004, pp. 1567-1576.

Raja, J., Muralikrishnan, B., and Fu, S. "Recent advances in separation of roughness, waviness and form". *Journal of the International Societies for Precision Engineering and Nanotechnology*, Vol. 26, 2002, pp. 222-235.

Qu, W., and Wang, K. "Using vibration-assisted grinding to reduce subsurface damage". *International Journal of Machine Tools & Manufacture*, Vol. 44, 2004, pp. 1567-1576.

Rech, J., Claudin, C., and DREAMO, E. "Identification of a friction model - Application to the context of dry cutting of an AISI 104 annealed steel with a TiN-coated carbide tool". *Tribology International*, Vol. 42, 2009, pp. 738-744.

Sargent, M., and Page, F. "Factors affecting the measurement of hardness and hardness anisotropy". *Journal of Materials Science*, Vol. 20, 1985, pp. 2388-2398.

Schwarz, J., and Richardson, H. "Experimental Modal Analysis". Vibrant Technology, Inc. Jamestown, California, 1997.

Shamoto, E., and Moriwaki, T. "Ultra-precision diamond cutting of hardened steel by applying elliptical vibration cutting". *Annals of the CIRP*, Vol. 48, 1999, pp. 441-444.

Shamoto, E., and Suzuki, N. "Development of Ultrasonic Elliptical Vibration Controller for Elliptical Vibration Cutting". Production Engineering Research Laboratory, Hitachi, Ltd., Yokohama, Japan, 1984.

Shamoto, E., Hirokazu, M., and Moriwaki, T. "Ultraprecision 6- Axis table driven by means of walking drive". Department of Mechanical Engineering, Kobe University, Vol. 49, 2006, pp. 299-302.

Shore, P., Morants, P., Luo, X., Tonnelier, R., Collin, R., Roberts, A., Miller R., Read, R. "Big oprix ultraprecision grinding/measuring system". Proceedings of SPIE The International Society for Optical Engineering, 2005, pp. 134-145

Sigh, R., and Khamba, J. "Macromodel for ultrasonic machining of titanium and its alloys: design experiment". Proceeding of the IMechE, Part B: Journal of Engineering Manufacture, Vol. 221, 2007, pp. 221-229.

Skelton, C. "Turning with an oscillating tool". International of Journal Machine Tools Des. & Res., 1968, Vol. 8, pp. 239-259.

Stephenson, D., and Agapiou, S. "Metal Cutting Theory and Practice". Manufacturing Engineering and Materials Processing 2nd Edition, CRC Taylor and Francis.

Slocum, A. "Precision Machine Design". Prentice Hall Publication Inc., 1992.

Sommargren, E. "An optical measurement of surface profile". Precision Engineering, Vol.3, Issue 3, 1981, pp. 131-136.

Suzuki, N., and Nakamura, A. "Ultraprecision micromachining of hardened steel by applying ultrasonic elliptical vibration cutting". Proceedings of the 2003 International Symposium. Vol. 3, 2003, pp. 221-226.

Stout, J. "Development of Methods for the Characterisation of Roughness in Three Dimensions". Penton Press, Kogan Page Ltd, London N1 9JN, 2000.

Sweeney, F., and Spedding, A. "A simulation technique to investigate rough surface scatter". *Wear*, Vol. 109, 1986, pp. 43-56.

Svanrtal, H. [online]. Available at: www.camo.com/rt/Resource/design_of_experiment.html/design_of_experiment.html. (Accessed on 10th January, 2007).

Schwarz, J., and Richardson, H. "Experimental Modal Analysis", California Vibrant Technology, 1999, pp. 1-12.

The American Society of Mechanical Engineers, Surface Texture (Surface roughness, waviness, and lay). ASME B46.1-1995, New York, NY 10017, 1996.

Thomas, M., Beauchamp, Y., Youssef, Y., and Masounave, J. "Effect of tool vibrations on surface roughness during lathe dry turning process". *Computer and Industrial Engineering*, Vol. 31, 1994, pp. 637-644.

Travis, J. "LabVIEW for Everyone". Prentice Hall PTR, Upper saddle river, NJ 07458, USA. October 2002, pp. 21.

Toh, K. "Vibration analysis in high speed rough and finish milling hardened steel". *Journal of Sound and Vibration*, Vol. 278, 2004, pp. 101-115.

Vorburger, V. [Online]. "Methods for characterizing surface topography (Tutorials in Optics)". Optical Society of America, 2010 Massachusetts Avenue, NW, Washington, DC 2003. (Accessed on 15th Sept 2007).

Wang, X., Zhou M., Gan K., and Ngoi, B. "Theoretical and experimental studies of ultraprecision machining of brittle materials with ultrasonic vibration". *International Journal of Advanced Manufacturing Technology*. Vol. 20, 2002, pp. 99-102.

Wang, W., Kweon, H., and Yang, H. "A study of the micro-milled surface produces a miniaturized machine tool". *Journal of Materials Processing Technology*, Vol. 162, 2005, pp. 702-708.

Wardany, E., Kishawy, A., and Elbestawi, A. "Surface integrity of die material in high speed hard machining, Part 1: Micrographical analysis". *Journal of Manufacturing Science and Engineering*, Vol. 122, 2000, pp. 620-632.

Weber, H., Herberger, J., and Pilz, R. "Turning of machineable glass ceramics with an ultrasonically vibrated tool". *Annals of the CIRP*, Vol. 33, 1984, 85-87.

Williams, C. "Optical Methods in Engineering Metrology". Chapman & Hall, London, Chapter 1, 1993.

Wu, Y., and Fan, Y. "Develop an ultrasonic elliptical vibration shoe centerless technique". *Journal of Materials Processing Technology*, 2003, pp. 155-156.

Viotti, R., Sutério, R., Albertazzi, A., and Kaufmanna, H. "Residual stress measurement using a radial in-plane speckle interferometer and laser annealing: preliminary results". *Optics and Lasers in Engineering*. Vol. 42, 2004, pp. 71-84.

Xiao, M., and Sato, K. "The effect of tool nose radius in ultrasonic vibration cutting of hard metal". *International Journal of Machine Tools & Manufacture*, Vol. 43, 2003, pp. 1375-1382.

Ye, D., Tong, X., Yao, L., and Yin, X. "Fatigue hardening/softening behaviour investigated through Vickers micro-hardness measurement during high-cycle fatigue". *Materials Chemistry and Physics*, Vol. 56, 1998, pp. 199-204.

Young, T. "Optics for Beginners". Department of Astronomy & Mount Laguna Observatory, San Diego State University, 5500 Campanile Drive, San Diego.

Zaman, T., Kumar, A., Rahman M., Sreeram, S. "A three dimensional analytical cutting force model for micro end milling operation". International Journal of Machine Tools & Manufacture, Vol. 46, 2006, pp. 247-255.

Zhou, L., and Cheng, K. "Dynamic cutting process modelling and its impact on the generation of surface topography and texture in nano/micro cutting". Proceedings of the IMechE, Part B: Journal of Engineering Manufacture, Vol. 223, 2009, pp. 247-265.

Zhou, M., Wang, J., Ngoi, B., and Gan, J. "Brittle-ductile transition in the diamond cutting of glasses with the aid of ultrasonic vibration". Journal of Materials Process Technology, Vol.121, 2002, pp. 243-251.

Zhou, M., Gan, J., and X. Wang. "Ultraprecision diamond turning of glass with ultrasonic vibration". International Journal of Advanced Manufacturing Technology. Vol. 21, 2003, pp. 952-955.

Zhou, M., Eow, Y., Ngoi, B., Lim, E. "Vibration-assisted precision machining of steel with PCD tools". Material Manufacturing Process, Vol. 18, 2003, pp. 825-834.

Zhong Z., and Lin, G. "Diamond turning of a metal matrix composite with ultrasonic vibrations". Material Manufacturing Process, Vol. 20, 2005, 727-735.

Appendices

Appendix 1

List of Publications Arising from this Research

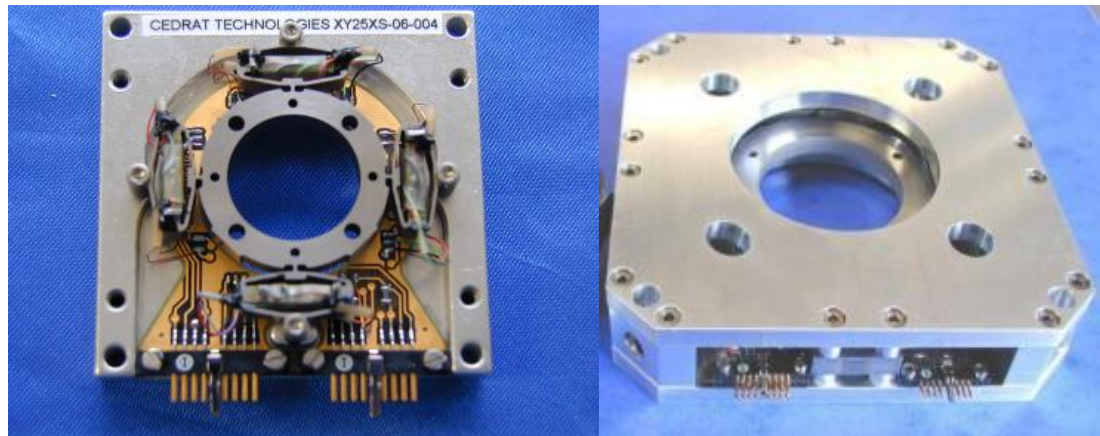
List of publications arising from this research

1. R. Ibrahim, K. Cheng, R. Bateman, C. Wang and Joe Au: Design and analysis of a desktop micro-machine for vibration-assisted micromachining. Proceedings of the IMechE, Part B: Journal of Engineering Manufacture (In press).
2. Hui Ding, Rasidi Ibrahim and Kai Cheng: Experimental study on machine-ability improvement of hardened tool steel using two-dimensional vibration-assisted micro-end-milling. International Journal of Machine Tools and Manufacture, Vol. 50, 2010, pp. 1115-1118.
3. Hui Ding, Shin-Jin Chen, Rasidi Ibrahim and Kai Cheng: Investigation of Size Effect on Burr Formation in Two Dimensional Vibration-assisted Micro End Milling. Proceedings of the IMechE, Part B: Journal of Engineering Manufacture (In press).
4. Dongming Li, Rasidi Ibrahim, Ying Jia, and Xiaoyu Wang: Study and development of a Kind of Electric-pneumatic Transfer Device with Piezoelectric Structure. International Conference on Computer, Mechatronics, Control and Electronic Engineering (CMCE 2010) Changchun, China, August 24-26 2010.
- 5 Rasidi Ibrahim, Hao Wang and Kai Cheng: Surface roughness optimisation in vibration assisted micro-milling of aluminium T6061 using response surface method: Proceeding of the 21st International Computer-Aided Production Engineering Conference (CAPE 2010), The University of Edinburgh, 13-14 April 2010, pp. 145-153.
6. R. Ibrahim and K. Cheng; Vibration assisted micro-milling: Theoretical models and instrumental implementation; Proceeding of the 5th International Conference on Manufacturing Research, Leicester, United Kingdom, 11-13 September 2007, pp. 175-176.

Appendix II

Desktop Vibration Assisted Micro-milling Drawing Details

XY PIEZOELECTRIC STAGE - PRODUCT AND WARRANTY INFORMATION



Version : 3.1.1

Date 06/02/06

Mechanical mounting

XY stages are composed of 2 sub systems, which are :

- the frame, generally attached,
- the moving frame, including the piezoelectric actuators and moving the payload.

To get good results and a safe mechanisms, it is important to use the foreseen mechanical interfaces both on the frame and on the moving frame (see annex 2).

In any case, please take care during the mounting procedure, to avoid excessive moments in the moving frame, when tightening the screws

The correct order for the operations is the following :

1. Tighten the payload onto the moving frame

2. Tighten the frame onto the attachment basis : use standard screws and a progressive tightened procedure (each screws is first pre tightened and in a second step tightened at the correct standard torque

Electrical connections

Electrical connector are used for the stage driving, and in option position sensors.

During the mounting operation, electrical charges can be produced by the stage, through any applied force and the direct piezoelectric effect.

Before the electrical connection, please refer to the electrical connection scheme to avoid exchanging the driving and the sensing connectors.

The piezoelectric stage can be delivered with a full bridge of strain gauges (SG option) per axis. For these actuators, purchased without the sensing electronic, the connection between the strain gauges and the electronic must be realized with the customer : the electrical interface is described below :

The Strain Gauges used by CEDRAT TECHNOLOGIES display an Ohmic resistance of 350Ω for all the actuators and mechanisms.

For the strain gauges 350Ω the driving voltage ($V_{cc}-GND$) should not be higher than 10V

The reduction of the driving voltage reduces the dissipated power and the related thermal effect, but also reduces the sensitivity of the bridge.

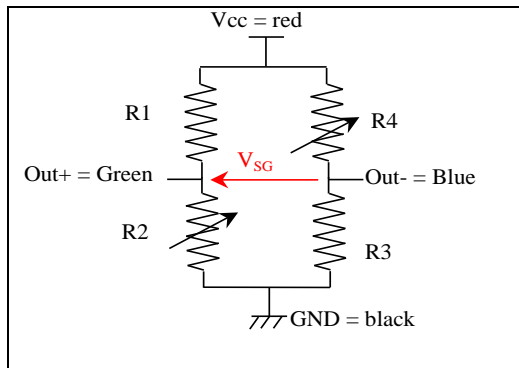
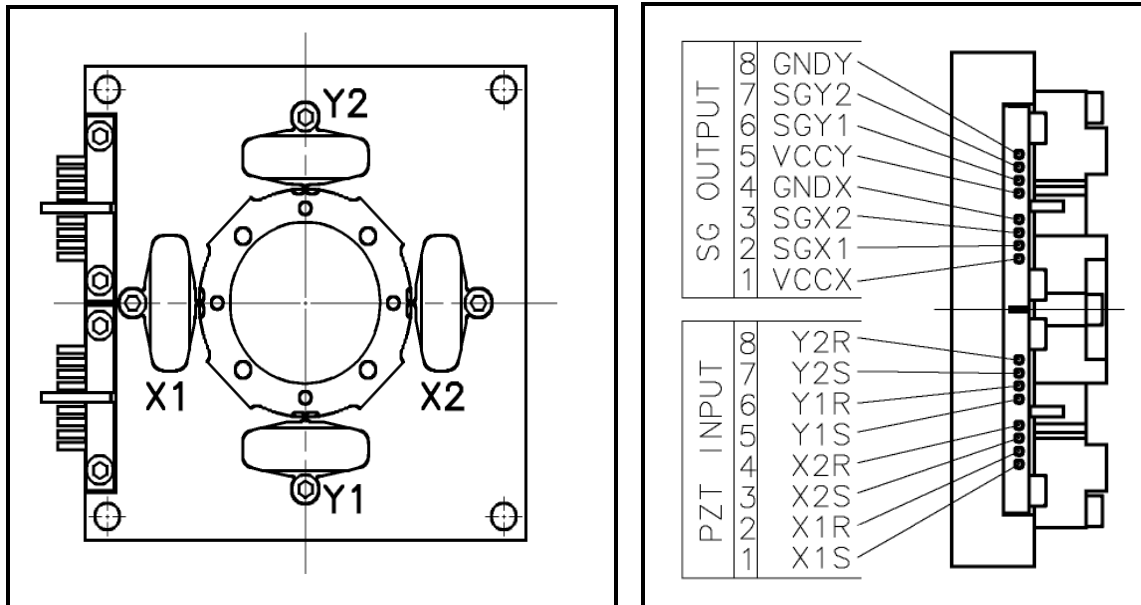
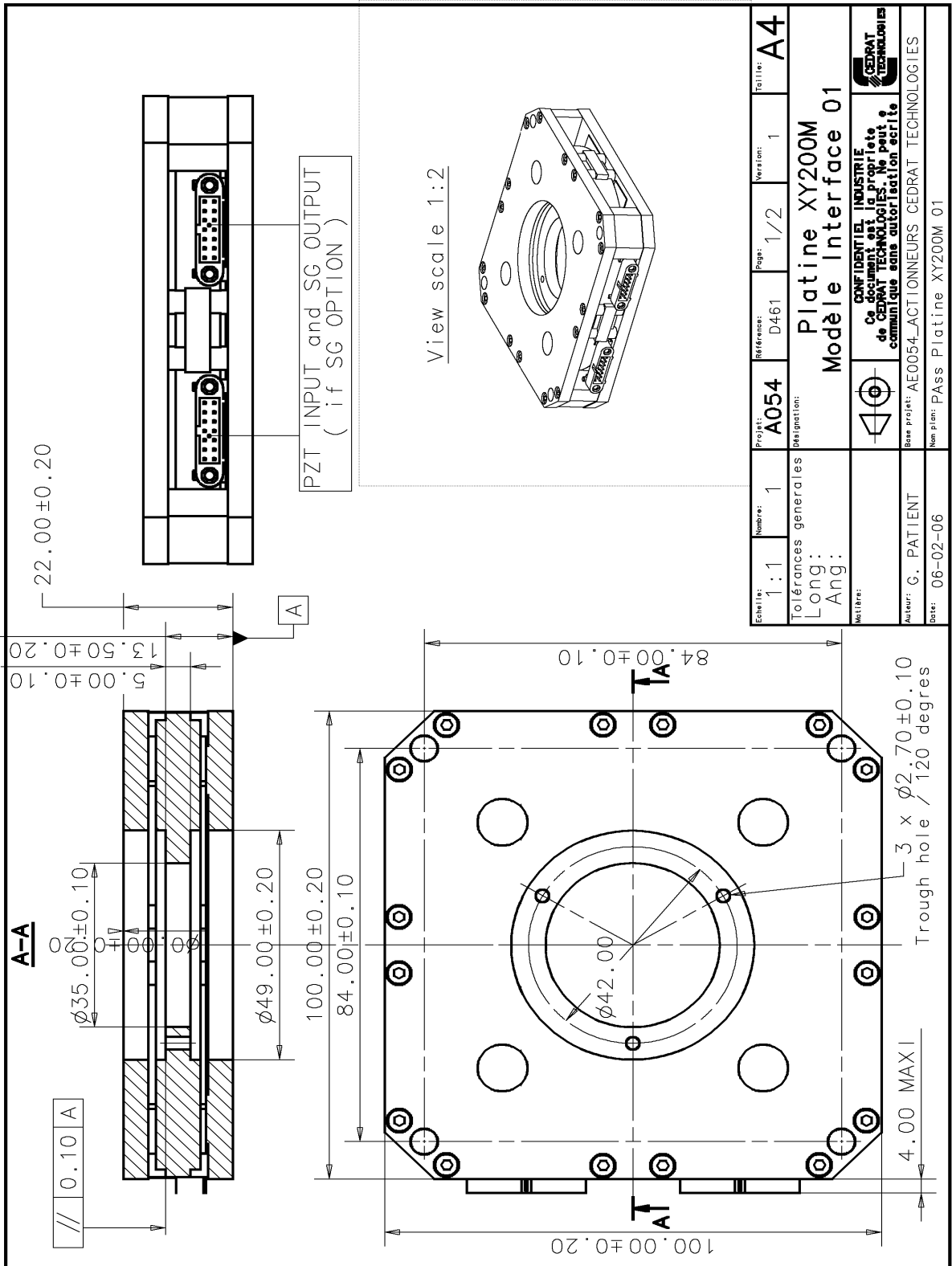


Figure 8.1 : Schematic of the Strain

Connection scheme XY25XS



XY25XS STAGE			
	N° PIN	Name	FUNCTION
SG sensor	8	GNDY	Electrical ground Y axis
	7	SGY2	Sensor Signal Y2
	6	SGY1	Sensor Signal Y1
	5	VCCY	Sensor drive Y axis
	4	GNDX	Electrical ground X axis
	3	SGX2	Sensor Signal X2
	2	SGX1	Sensor Signal X1
	1	VCCX	Sensor drive X axis
Stage drive	8	Y2R	Piezo Y2 return
	7	Y2S	Piezo Y2 signal
	6	Y1R	Piezo Y1 return
	5	Y1S	Piezo Y1 signal
	4	X2R	Piezo X2 return
	3	X2S	Piezo X2 signal
	2	X1R	Piezo X1 return
	1	X1S	Piezo X1 Signal





6.3 XY piezoelectric stages

The piezoelectric stage XY200M has a stroke of 200 μm along the X and Y axis and is able to bear a high load up to 3 kg. Applications include Atomic Force or Scanning Tunneling Microscopes, mask positioning. This stage is based on APA200M Actuators and owns a high stiffness. The stage can be equipped with Strain Gauges or Eddy Current Sensors (ECS option), to get a very fine accuracy up to 10nm. Parasitic rotations (along X, Y and Z rotation) are very limited. The moving frame can be custom design (attachment points, holes...). The compact XY25XS stage is well suited to integrated devices for fiber positioning, micro scanning, ...

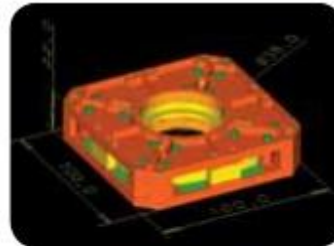


Figure 6.2.a: Dimensions of the XY200M stage

References	Unit	XY25XS	XY200M
Notes		-	-
Sensors option		SG	SG, ECS
Active axis		TX, TY	TX, TY
Max. No-load displacement [Tx, Ty]	μm	20	180
Max. out of plane Z displacement	μm	0,50	1,00
Max. parasitic Z rotation	μrad	50	240
Max. parasitic X Y rotations	μrad	10	50
Voltage range	V	-20 ... 150	-20 ... 150
Stiffness	N/ μm	2,50	0,66
Height (Z axis)	mm	18,0	22,0
Dimensions (X & Y axis)	mm	50*50	100*100
Resolution	nm	0,2	1,8
Mass	g	80	180
Unloaded resonance frequency (in the actuator's direction)	Hz	2200	500
Response time	ms	0,23	0,91
Capacitance (per electrical port)	μF	0,50	6,30
Mechanical interfaces (payload)		1 \varnothing 17 mm hole + 4 \varnothing 1,8mm on \varnothing 20 mm	3 \varnothing 2,7 mm holes on \square 38
Mechanical interfaces (frame)		4 \varnothing 2,8 mm holes on \square 45	4 \varnothing 4,5 mm holes on \square 84
Electrical interfaces		2 RG178BU coaxial cables	2 RG178BU coaxial cables

Table 6.2: Characteristics of the XY stages

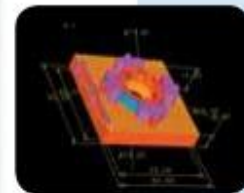


Figure 6.2.b: Dimensions of the XY25XS stage

Other stages based on APA from the XS,S, SM, ML and L serie can be defined

The technical informations of this leaflet are not contractual and can be changed without prior notice.

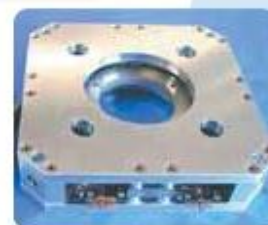
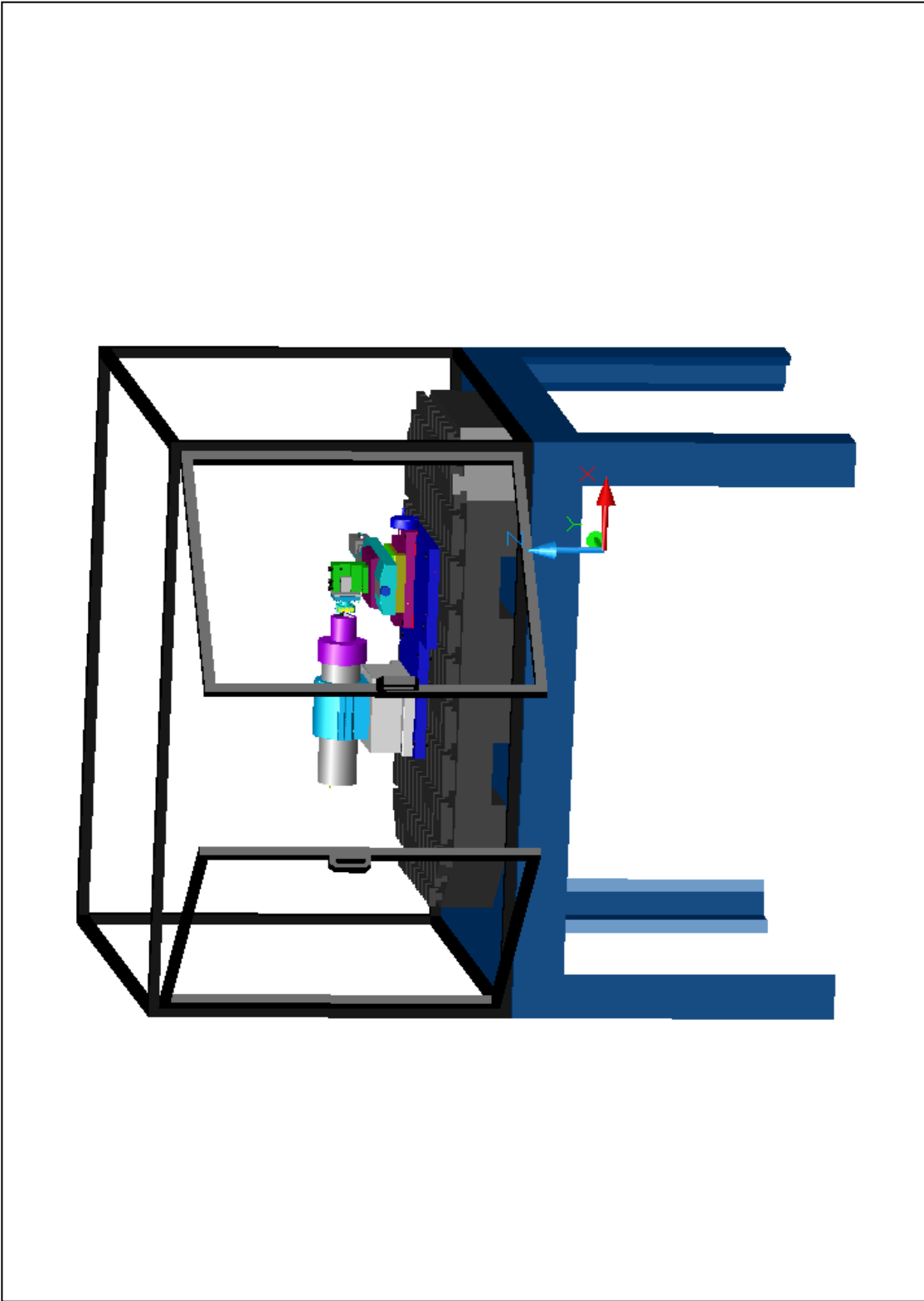
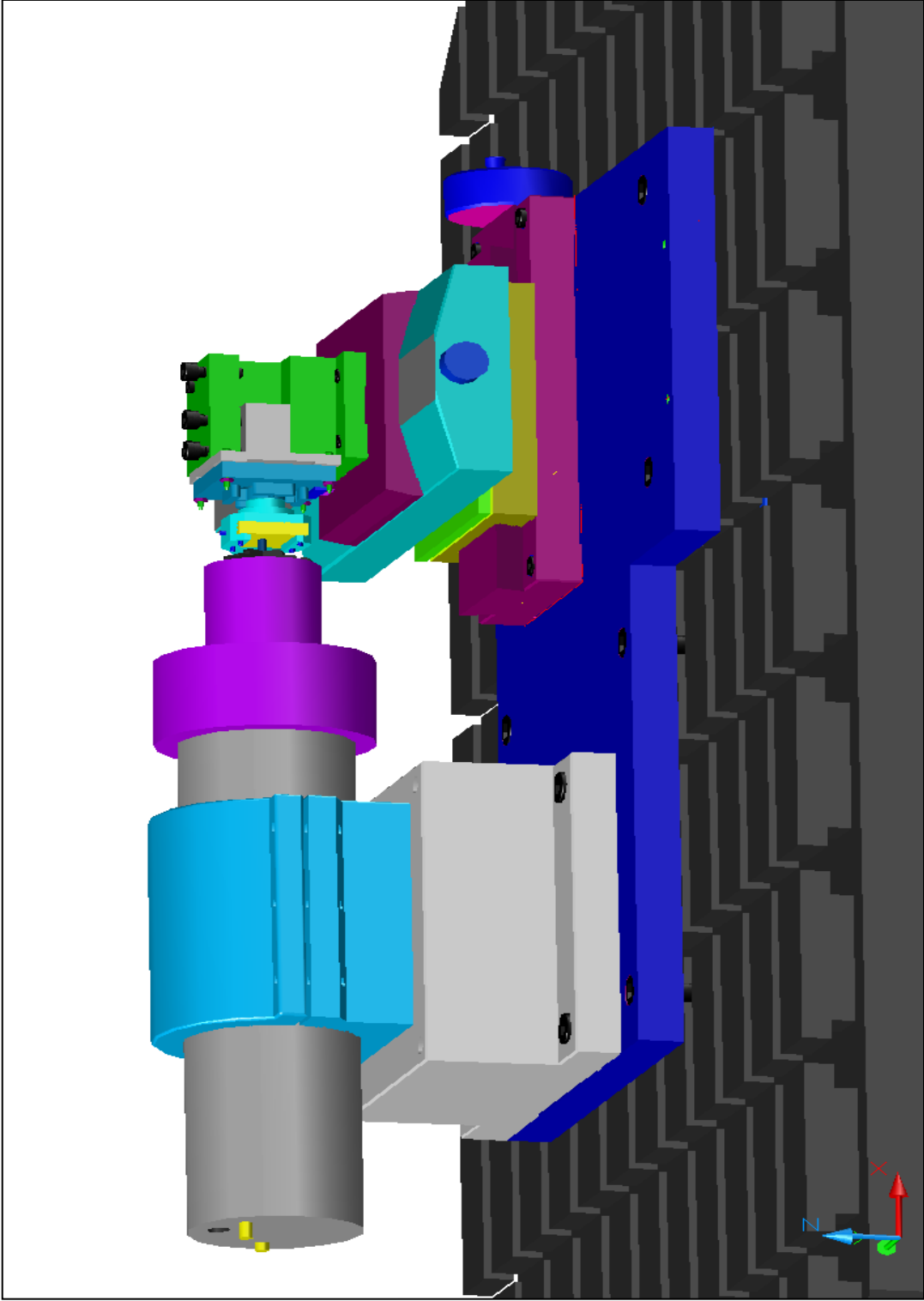


Figure 6.3: View of the XY200M stage

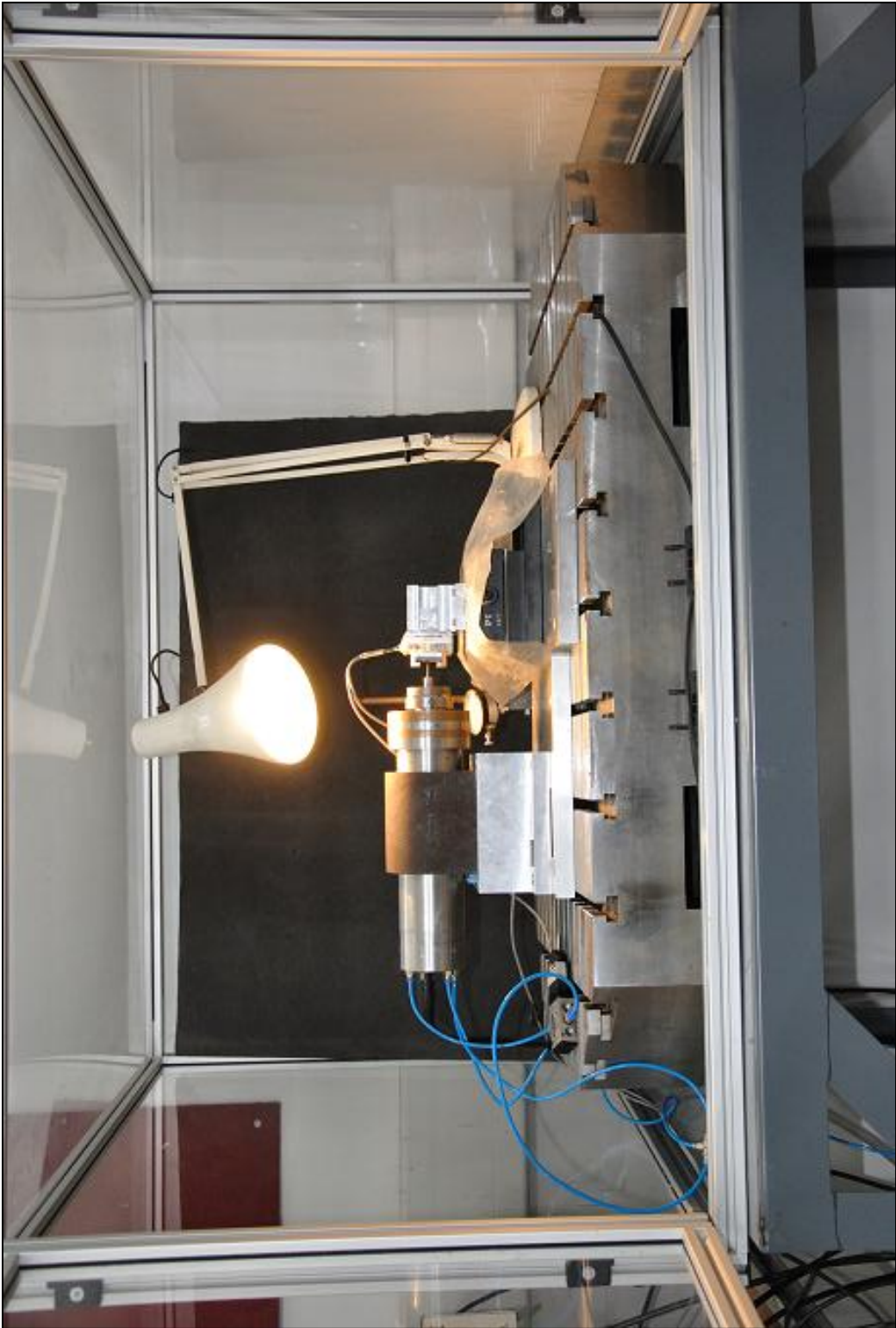




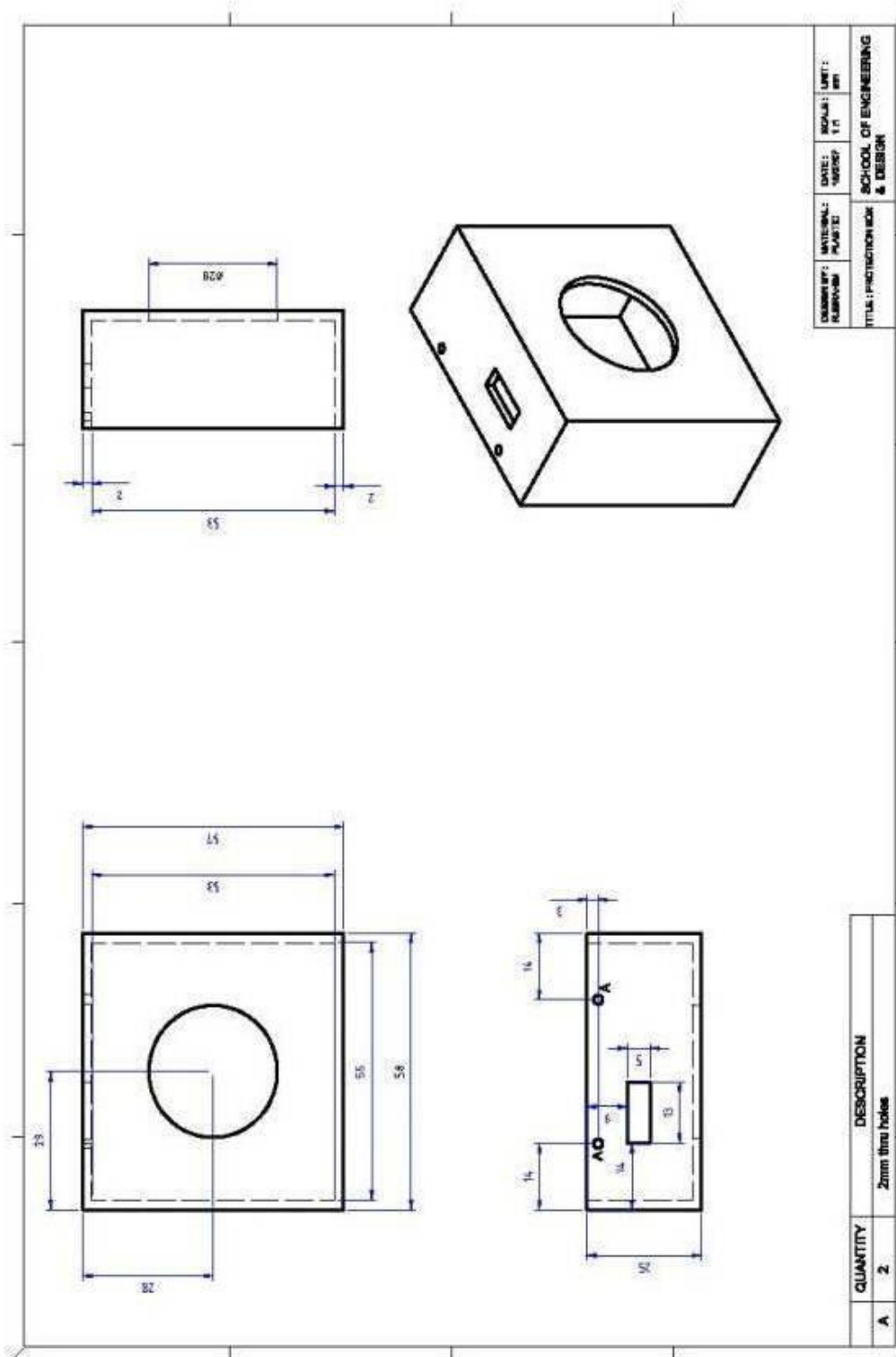
DVAMM in CAD design



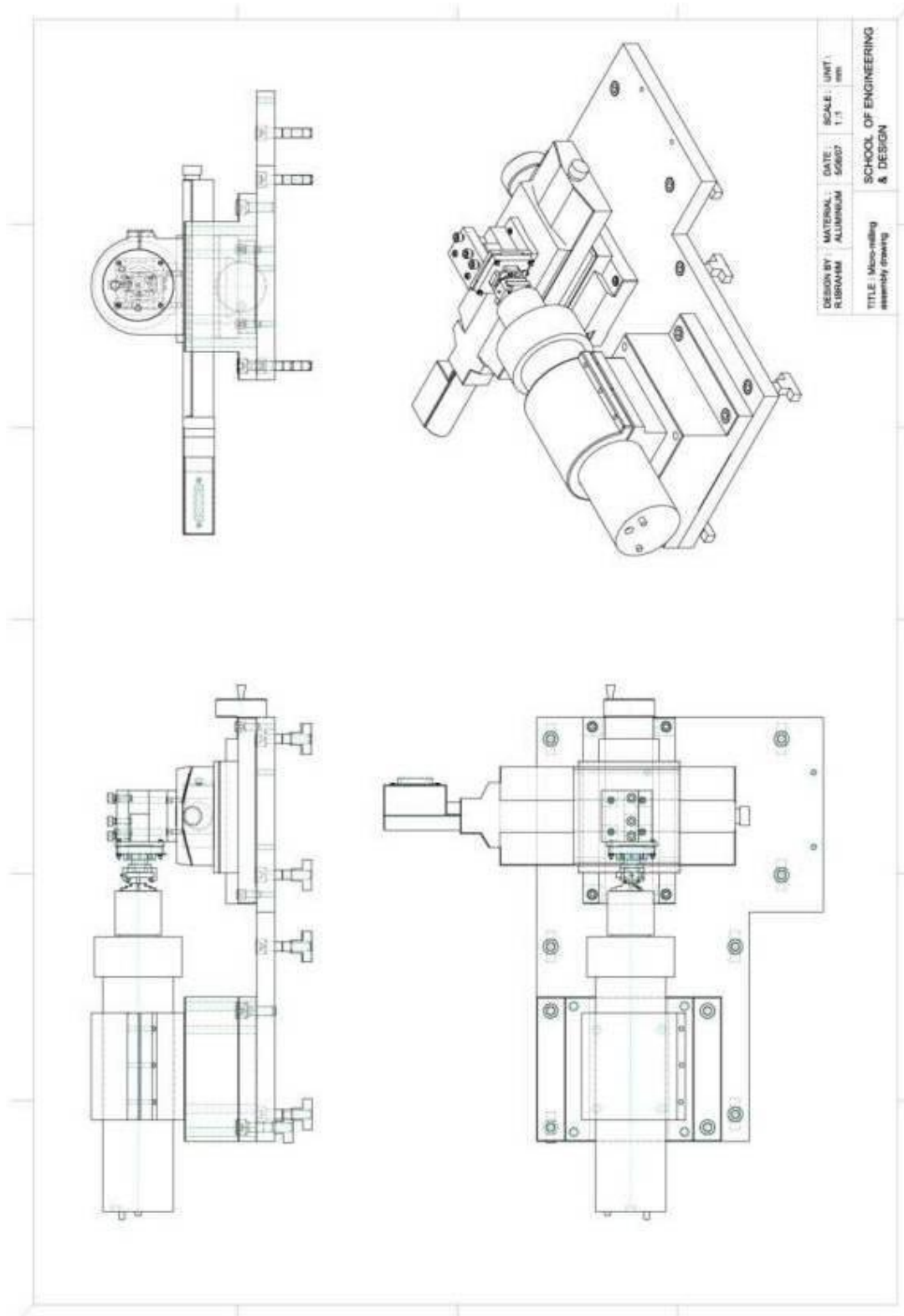
DVAMM equipped with piezo-actuator



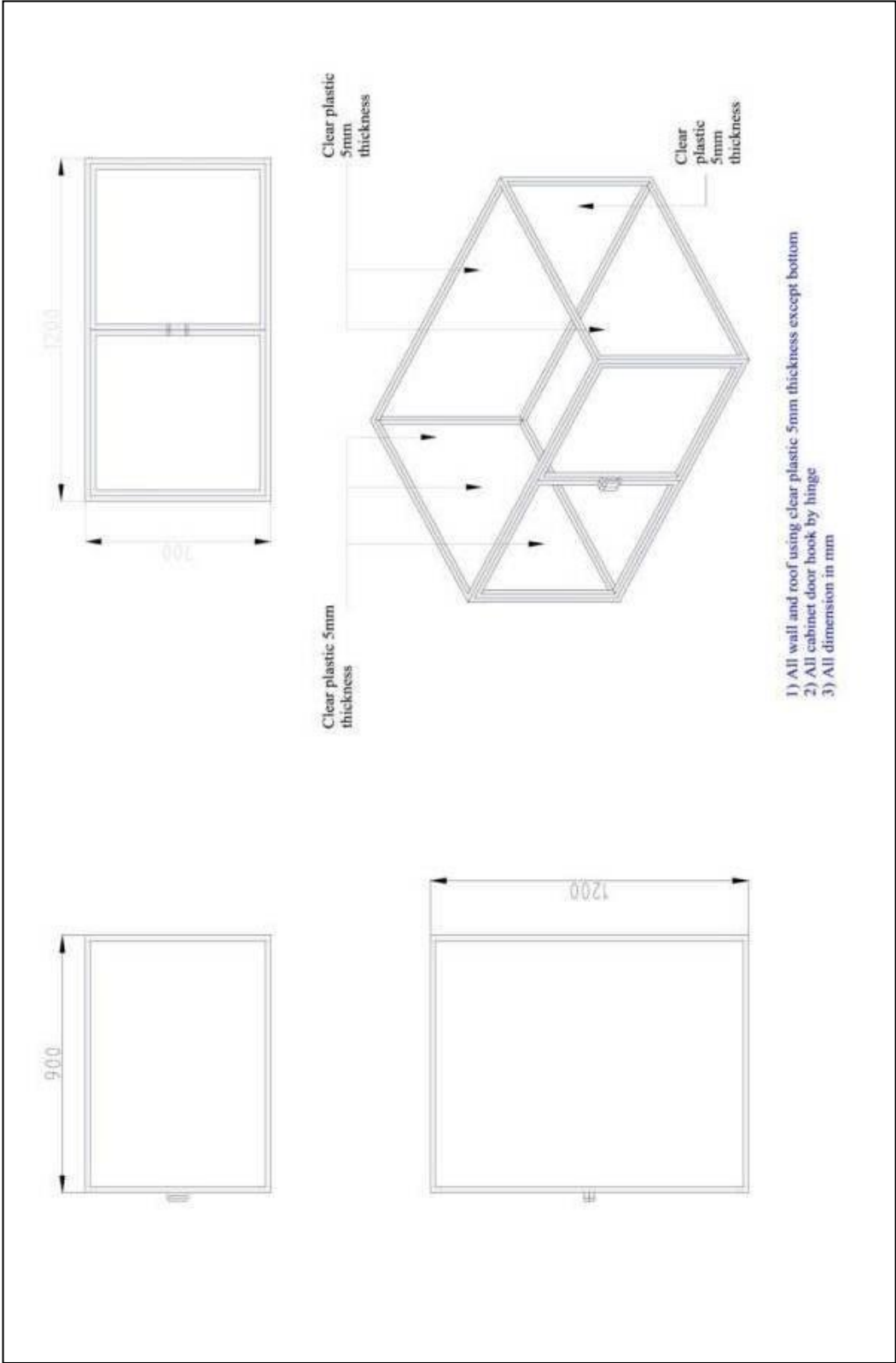
DVAMM in real experimental setup



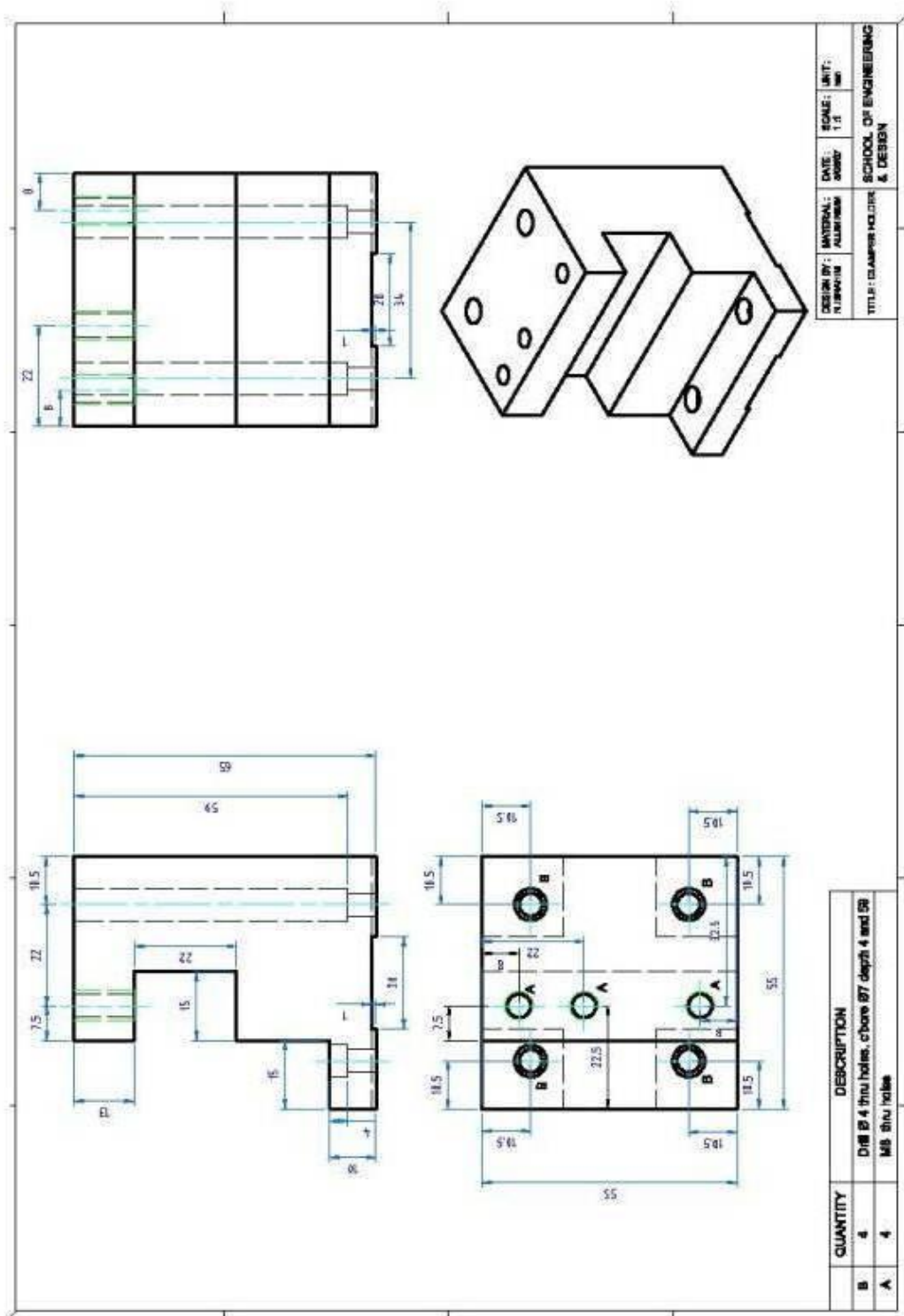
Protector box detail drawing



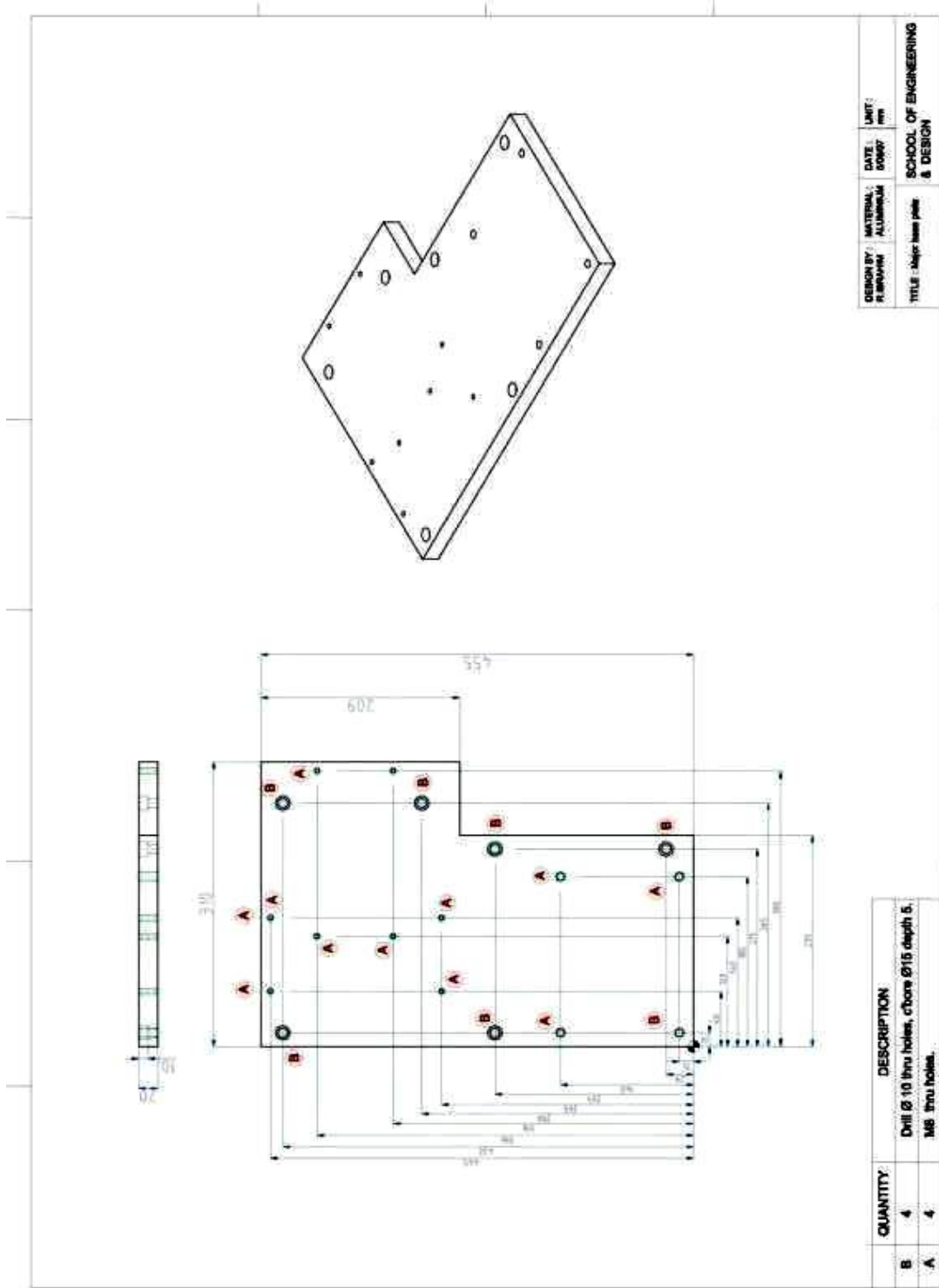
DVAMM detail drawing



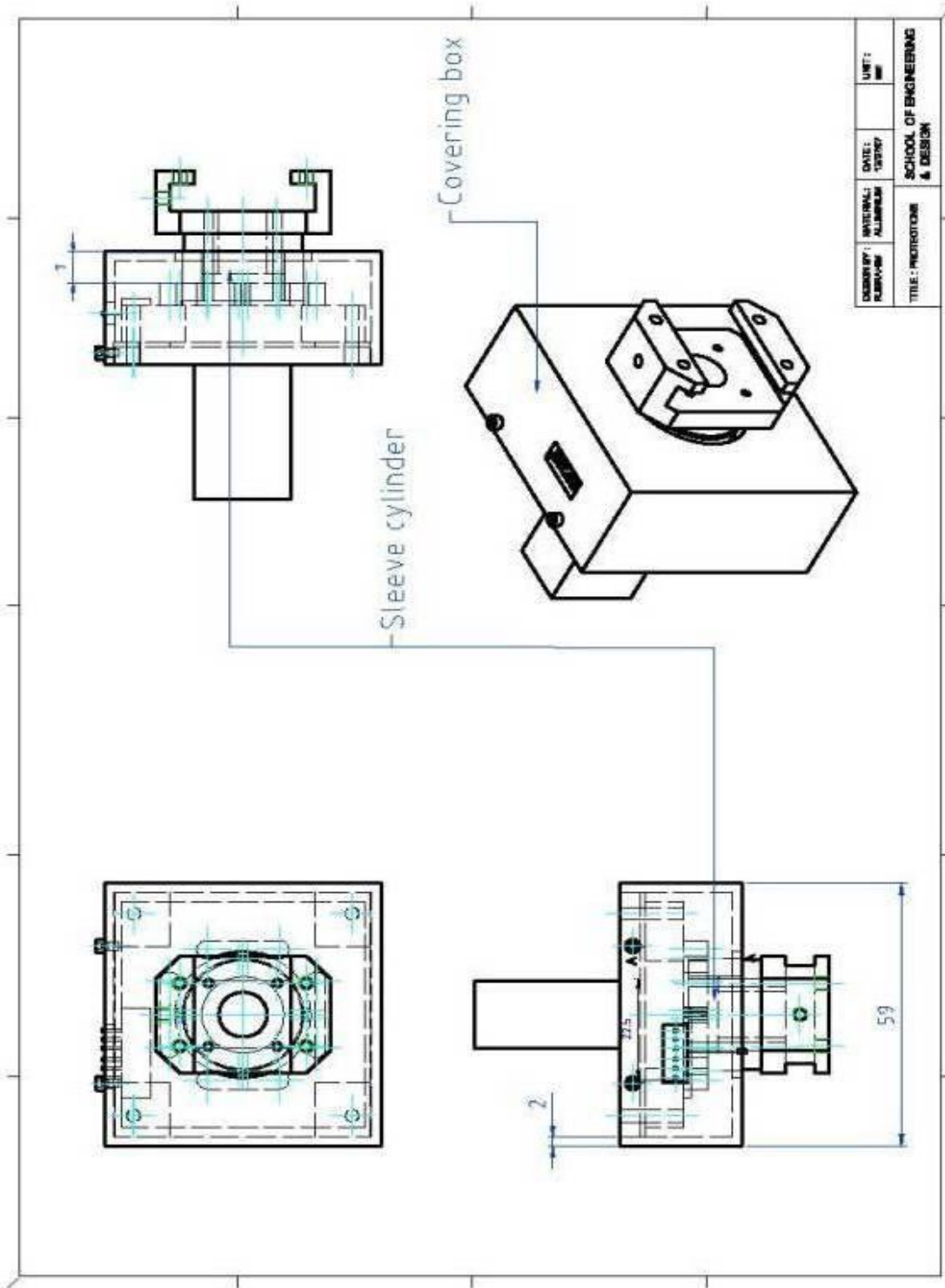
Safety cage drawing



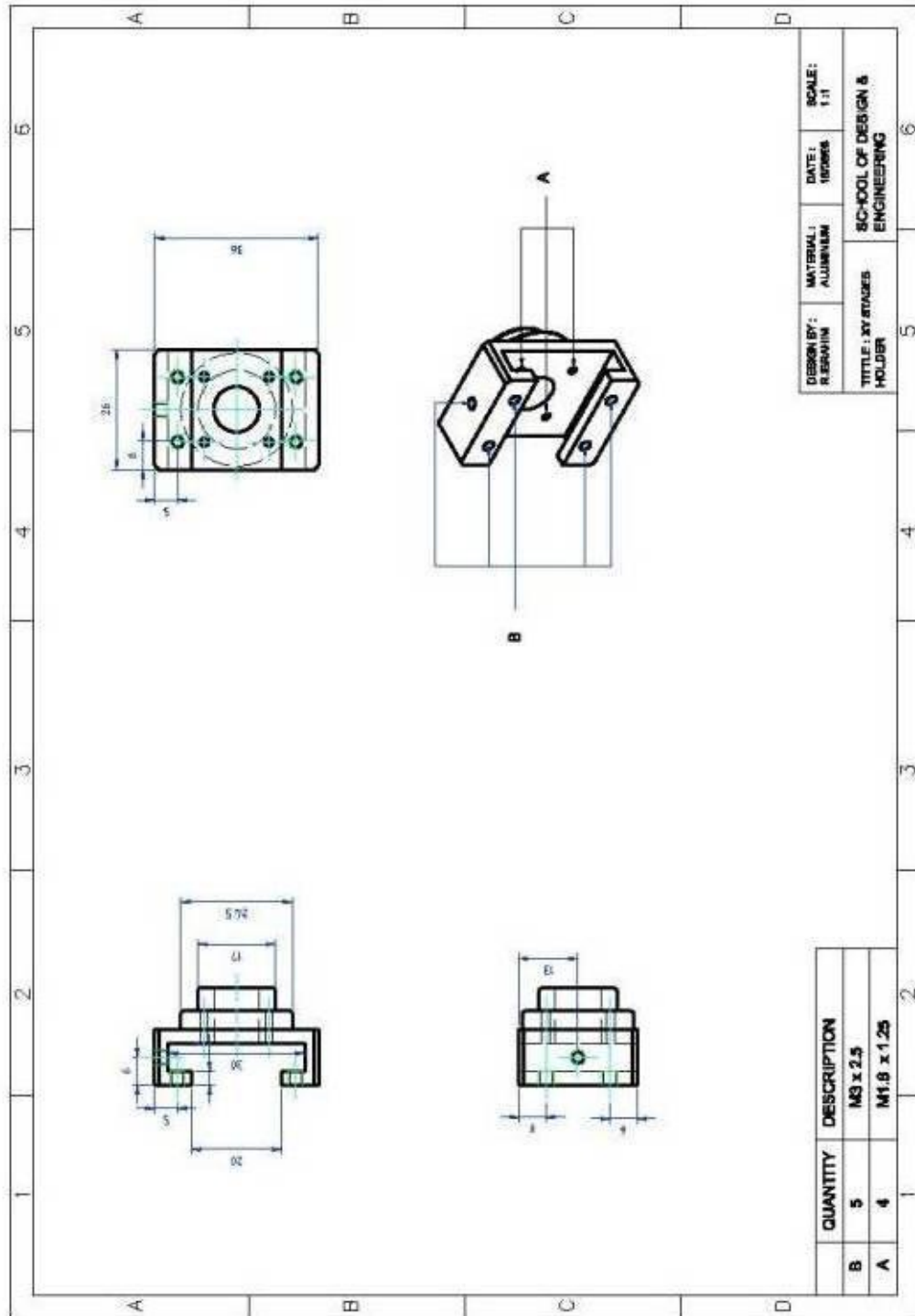
Tool holder detail drawing



Base plate detail drawing



Assembly drawing of piezo actuator



Jig detail drawing

TECHNICAL DATA SHEET

XY25XS

v3.1.2

TABLE OF STANDARD PROPERTIES OF USE AND MEASUREMENT

The properties defined in the table below, are set up according to the technical conditions of use and measurement. These properties are warranted within their variation range and in compliance with the standard technical conditions of use.

Properties XY25XS	Standard technical conditions	Unit	Nominal values	Min. values	Max. values
Notes		-	-	-	-
Sensor options	SG	-	-	-	-
Mastered motions	TX, TY	-	-	-	-
Max. no load displacement	Quasistatic excitation, blocked-free	µm	20	18	20
Out of plane Z displacement		µm	0,50	0,30	0,70
Max. parasitic Z rotation		µrad	50,00	42,50	57,50
Max. parasitic XY rotation		µrad	10,00	8,50	11,50
Blocked force	Quasistatic excitation, blocked-free	N	40	32	48
Stiffness	Quasistatic excitation, blocked-free	N/µm	2,50	2,00	2,75
Unloaded resonance frequency (in the actuator's direction)	Harmonic excitation, blocked-free, on the admittance curve	Hz	3600	2700	3600
Unloaded response time	Quasistatic excitation, blocked-free	ms	0,17	0,15	0,19
Capacitance (per electrical port)	Quasistatic excitation, blocked-free, on the admittance curve	µF	0,50	0,45	0,65
Resolution		nm	0,20	-	-
Height		mm	18,00	17,90	18,10
Diameter		mm	45,00	44,90	45,10
Mass		g	80,0	-	-
Standard mechanical interface (payload)	1 Ø 17 mm hole + 4 Ø1,8mm on Ø 20mm	-	-	-	-
Standard mechanical interface (base)	4 Ø 2,6 mm holes on [7,45]	-	-	-	-
Standard electrical interface	2 RG178B/U coaxial cables	-	-	-	-

PROPERTIES STANDARD TECHNICAL CONDITIONS OF USE AND MEASUREMENT

- Free-free** : The actuator is not fixed
- Blocked-free** : The actuator is fixed to a mechanical support assumed infinitely stiff
- Quasistatic excitation** : AC voltage between -20 and 150 V at 1 Hz
- Harmonic excitation** : Voltage of 0.5 V_{rms}, sinusoidal mode from 0 to 100 kHz
- Max. harmonic excitation** : Voltage defined by the measurement of max. displacement, sinus at resonance frequency
- Displacement measurement** : Laser interferometer, capacitive displacement sensor
- Admittance measurement** : HP 4194 A electrical impedance analyser
- Environment** : Ambient temperature (15-25°C) and dry air (Humidity < 50 % rH)

Any technical conditions of use, different from those defined above, can lead to temporary or definitive alterations of properties. Thank you to contact CEDRAT TECHNOLOGIES before using actuators under non standard technical conditions,

FACTORY TESTS CARRIED OUT

- Test 1 : Electrical admittance vs. Frequency, free-free
- Test 2 : Displacement vs. input voltage

EXTRA FACTORY TESTS

- Test 3 : Gain and linearity of the sensor
- Test 4 : Step response in closed loop
- Test 5 : Stability in closed loop

Appendix III
Machining Trial Plan

Machining Trial Plan

Variables	Levels							
	Symbol	Unit	L1	L2	L3			
Feedrate	f	mm/min	1	4	6			
Vibr. amplitude	A	um	1	3	5			
Vibr. frequency	F	Hz	1000	2000	3000			
Spindle Speed	s	rpm	4000	7000	10000			
No.	fr, mm/min	Amp, mic	Freq, Hz	Rpm	Ra, um	TW, um	MRR, mm ³ /s	
1	1	1	1000	4000	1.0008	431	1.05938	
2	1	1	1000	7000	1.1134	457	1.12658	
3	1	1	1000	10000	0.337	189	1.46398	
4	1	1	2000	4000	0.766	324	1.35987	
5	1	1	2000	7000	0.4474	250	1.73618	
6	1	1	2000	10000	0.4474	287	1.79651	
7	1	1	3000	4000	0.5276	314	1.93658	
8	1	1	3000	7000	2.3856	738	1.15684	
9	1	1	3000	10000	1.797	437	9.3548	
10	1	3	1000	4000	0.537	265	1.36958	
11	1	3	1000	7000	2.0076	672	9.5362	
12	1	3	1000	10000	2.0174	711	9.8561	
13	1	3	2000	4000	0.368	195	1.56847	
14	1	3	2000	7000	1.8978	655	9.6885	
15	1	3	2000	10000	0.5386	259	1.49852	
16	1	3	3000	4000	0.4918	339	1.53247	
17	1	3	3000	7000	0.9402	501	1.06587	
18	1	3	3000	10000	0.54	197	1.36952	

Machining trial plan

19	1	5	1000	4000	0.2534	135	1.93685
20	1	5	1000	7000	1.1786	503	1.04364
21	1	5	1000	10000	0.8082	401	1.12638
22	1	5	2000	4000	0.484	680	1.68915
23	1	5	2000	7000	1.716	487	9.6125
24	1	5	2000	10000	1.296	508	1.13567
25	1	5	3000	4000	0.2566	262	1.95815
26	1	5	3000	7000	0.6196	307	1.46847
27	1	5	3000	10000	0.4658	685	9.1798
28	4	1	1000	4000	0.5716	365	1.79568
29	4	1	1000	7000	0.6588	457	1.68548
30	4	1	1000	10000	0.4984	395	1.76843
31	4	1	2000	4000	0.3858	184	1.86953
32	4	1	2000	7000	0.594	121	1.63254
33	4	1	2000	10000	0.5682	183	1.63854
34	4	1	3000	4000	0.2878	236	1.69854
35	4	1	3000	7000	0.6384	205	1.63259
36	4	1	3000	10000	1.1662	500	1.16849
37	4	3	1000	4000	0.2786	145	2.16958
38	4	3	1000	7000	0.5448	298	1.68951
39	4	3	1000	10000	2.0436	685	9.2568
40	4	3	2000	4000	1.2262	541	1.06896
41	4	3	2000	7000	0.556	367	1.76268
42	4	3	2000	10000	1.7648	726	9.3654
43	4	3	3000	4000	2.1064	699	9.0268
44	4	3	3000	7000	0.5842	322	1.53695
45	4	3	3000	10000	1.4402	563	1.13597
46	4	5	1000	4000	2.169	671	9.0326
47	4	5	1000	7000	0.6302	282	1.73651
48	4	5	1000	10000	1.716	600	9.4365

Machining trial plan

49	4	5	2000	4000	0.6902	195	1.23589
50	4	5	2000	7000	0.5916	185	1.43658
51	4	5	2000	10000	2.0224	765	9.0362
52	4	5	3000	4000	0.7938	295	1.09875
53	4	5	3000	7000	0.7856	301	1.14869
54	4	3	3000	10000	1.9288	654	9.0365
55	6	1	1000	4000	0.5702	213	1.73658
56	6	1	1000	7000	0.607	257	1.52369
57	6	1	1000	10000	1.1762	650	9.3265
58	6	1	2000	4000	0.5864	221	1.56397
59	6	1	2000	7000	0.5578	246	1.93658
60	6	1	2000	10000	1.2772	563	9.4632
61	6	1	3000	4000	0.511	281	1.43628
62	6	1	3000	7000	0.414	232	1.76528
63	6	1	3000	10000	1.478	600	1.10364
64	6	3	1000	4000	0.5124	285	1.59563
65	6	3	1000	7000	0.7606	368	1.10359
66	6	3	1000	10000	1.642	598	9.0364
67	6	3	2000	4000	0.4326	325	1.83657
68	6	3	2000	7000	0.727	338	1.29847
69	6	3	2000	10000	1.8066	705	9.3254
70	6	3	3000	4000	0.4534	360	1.43659
71	6	3	3000	7000	0.7162	298	1.14658
72	6	3	3000	10000	0.4774	271	1.15367
73	6	5	1000	4000	1.0254	290	1.53265
74	6	5	1000	7000	0.8432	541	9.3784
75	6	5	1000	10000	0.8432	652	1.28479
76	6	5	2000	4000	0.638	300	1.63297
77	6	5	2000	7000	0.835	534	1.03567
78	6	5	2000	10000	1.2682	684	9.2154

Machining trial plan

79	6	5	3000	4000	0.5276	256	1.43265
80	6	5	3000	7000	0.5574	258	1.32658
81	6	5	3000	10000	0.607	352	1.23657

Appendix IV
Part of Matlab Programming

MatLab Programming

```

clear
format long

%this program can simulate the dynamic chip thickness, cutting force,
%dynamic response of cutting system, and the tool tip path.

%%%%%%%%%%%%%%%%%%%%%%%%%%%%%%%%%%%%%%%%%%%%%%%%%%%%%%%%%%%%%%%%%%%%%%%%
%%%%%
%%%% tool parameters
r=1500;           % In micron toolbar radius
z=2;             % tooth number
rn=100e-9;       % cutting edge radius
thitaf=5*pi/180; % clearance angle
luoxuanjiao=pi/6; % helix angle
wear=0;          % wear length
%%%%%ÏËý cutting parameters
n=2000;          % (r/min) spindle speed
fz=6;            % um/©feed rate per tooth
fcross=2.0*r;    % (um) cutting width
zdepth=100e-6;   % cutting depth (

%%%%%ÖñŒ²ÏËý vibration parameters
A=6;             % (um) amplitude in x direction value)
fx=1000;         % (Hz) frequency in x direction
qx=0.0*pi;      % (rad) phase in x direction
B=6;             % (um) amplitude in y direction(value)
fy=1000;        % (Hz) frequency in y direction
qy=0.0*pi;      % (rad) phase in y direction
%%%%%²ÄÄÏ²ÏËý material properties
k=43;            % 43 constant 43
H=9.1e9;         % Pa hardness
E=520e9;        % Young's modulus
uf=15;           % °friction factor
gama=65*pi/180; % rad£© shear angle

```

```

%%simulation initial parameters
dx=0;          % X·
dy=0;          % Y·
dz=0;          % Z·

%%·Ã·ÿ³ÿ²ÿËÿ
starttime=0.0*60/n;          % start time the value)
if z==1          % initialize the tool tip path
    inicircle=10;          %)
elseif z==2
    inicircle=5;
end
realcircle=1.0;          % total simulation cycle (you
can change the value from 1 to 100)
buchang=0.00005;          % (s) increment
totaltime=(inicircle+realcircle)*60/n;          % (s) (w=2*pi*n/60;
% rad/s·@ angular velocity (you can not change the value)
fup=z*n*fz/60;          % (um/s) feed
validjiao=acos((r-fcross)/r);          %
%%simulation initial parameters
Baris10=0;
Baris 9=0;
Baris 8=0;
Baris 7=0;
Baris 6=0;
Baris 5=0;
Baris 4=0;
Baris 3=0;
Baris 2=0;
Baris 1=0;
jx=0;
Baris i1=0;
Baris i2=0;
nn=0;
totalreal=0;

```

```

%%%%%%%%%%%%%%%%%%%%%%%%%%%%%%%%%%%%%%%%%%%%%%%%%%%%%%%%%%%%%%%%%%%%%%%%
%%%%%%%%%%%%%%%%%%%%%%%%%%%%%%%%%%%%%%%%%%%%%%%%%%%%%%%%%%%%%%%%%%%%%%%%
%%%%%%%%%%%%%%%%%%%%%%%%%%%%%%%%%%%%%%%%%%%%%%%%%%%%%%%%%%%%%%%%%%%%%%%%

Bulatseparuh (jx,1); % 计算 t 时刻的位移

Bulatseparuh (jx,2);

(jx,1)=fup*(t-buchang)+A*sin(2*pi*fx*(t-buchang)+qx)+dx;
% 计算 t 时刻的位移

(jx,2)=B*sin(2*pi*fy*(t-buchang)+qy)+dy;

tooltip (tipx,tipy,xinlunkuo); % 计算 t 时刻的位移

neiwaixin==0

cd=0;

Bulatseparuh (jx,1)=
% 计算 t 时刻的位移

end

end

end

function
[Fc,Fr,Fa,forcex,forcey,forcez]=cuttingforcehanshu(rn,thitaf,luoxuanjiao,w
ear,n,zdepth,k,H,E,uf,gama,cd,t)

%%%%%%%%%%%%%%%%%%%%%%%%%%%%%%%%%%%%%%%%%%%%%%%%%%%%%%%%%%%%%%%%%%%%%%%%
%%%%%%%%%%%%%%%%%%%%%%%%%%%%%%%%%%%%%%%%%%%%%%%%%%%%%%%%%%%%%%%%%%%%%%%%

w=2*pi*n/60;

```

```
km=(cot(gama)/sqrt(3)+1)*H/3;
miu=(cos(gama)-sin(gama)/sqrt(3))/(cos(gama)/sqrt(3)+sin(gama));
p=miu;

Sb=k*rn*H/E;
Lf=rn+wear+Sb/sin(thitaf);

Ac=cd*zdepth;
Af=Lf*zdepth;

dertaf=0.62*H*sqrt(43*H/E);
Ffc=uf*Lf*zdepth*dertaf;
Ffr=Lf*zdepth*dertaf; %

Fc=km*Ac+Ffc;
Fr=p*km*Ac+Ffr;
Fa=Fc*sin(luoxuanjiao);

%if cd==0
%   Fc=0;
%   Fr=0;
%   Fa=0;

Bulatanpenuh =w*t;
forcex=-Fc*cos(jiajiao)-Fr*sin(jiajiao);
forcey=Fc*sin(jiajiao)-Fr*cos(jiajiao);
```

Appendix V

Part of Minitab Programming

Minitab

Surface roughness

Welcome to Minitab, press F1 for help.
Retrieving project from file: 'D:\Minitab\Ilias advice\Minitab full project.MPJ'

Results for: experimental.MTW

Regression Analysis: Average Ra versus fr (mm/min), Amp. (micron), ...

The regression equation is

$$\begin{aligned} \text{Average Ra} = & -0.257 + 0.105 \text{ fr (mm/min)} + 0.386 \text{ Amp. (micron)} \\ & + 0.000007 \text{ Freq (Hz)} + 0.000071 \text{ Spindle Rpm} - 0.0199 \text{ fr*fr} \\ & - 0.0405 \text{ amp*amp} + 0.000000 \text{ freq*freq*} + 0.000000 \text{ RPM*RPM} \\ & + 0.0045 \text{ fr*amp} - 0.000018 \text{ fr *frq} + 0.000003 \text{ fr*RPM} \\ & - 0.000058 \text{ amp*freq} + 0.000000 \text{ freq*RPM} \end{aligned}$$

Predictor	Coef	SE Coef	T	P
Constant	-0.2566	0.8240	-0.31	0.756
fr (mm/min)	0.1053	0.1913	0.55	0.584
Amp. (micron)	0.3864	0.2242	1.72	0.089
Freq (Hz)	0.0000072	0.0005838	0.01	0.990
Spindle Rpm	0.0000705	0.0001359	0.52	0.606
fr*fr	-0.01988	0.02125	-0.94	0.353
amp*amp	-0.04046	0.03143	-1.29	0.202
freq*freq*	0.00000005	0.00000013	0.36	0.722
RPM*RPM	0.00000000	0.00000001	0.05	0.961
fr*amp	0.00453	0.01787	0.25	0.801
fr_*frq	-0.00001771	0.00003572	-0.50	0.622
fr*RPM	0.00000290	0.00001158	0.25	0.803
amp*freq	-0.00005790	0.00004574	-1.27	0.210
freq*RPM	0.00000001	0.00000003	0.19	0.852

S = 0.535642 R-Sq = 26.8% R-Sq(adj) = 12.6%
Analysis of Variance

Source	DF	SS	MS	F	P
Regression	13	7.0538	0.5426	4.5	0.003
Residual Error	67	19.2231	0.2869		
Total	80	26.2769			

Source	DF	Seq SS
fr (mm/min)	1	0.3852
Amp. (micron)	1	0.3448
Freq (Hz)	1	0.0075
Spindle Rpm	1	4.9452
fr*fr	1	0.2889
amp*amp	1	0.4613
freq*freq*	1	0.0434
RPM*RPM	1	0.0000
fr*amp	1	0.0237
fr_*frq	1	0.0630
fr*RPM	1	0.0189

```
amp*freq      1  0.4618
freq*RPM      1  0.0101
```

Obs	fr (mm/min)	Average Ra	Fit	SE Fit	Residual	St Resid
1	1.00	1.0018	0.4793	0.2587	0.5225	1.11
2	1.00	1.1134	0.7322	0.2399	0.3812	0.80
3	1.00	0.3370	0.9942	0.2735	-0.6572	-1.43
4	1.00	0.7666	0.5681	0.2173	0.1985	0.41
5	1.00	0.4474	0.8372	0.1939	-0.3898	-0.78
6	1.00	0.4474	1.1154	0.2230	-0.6680	-1.37
7	1.00	0.5276	0.7475	0.2750	-0.2199	-0.48

R denotes an observation with a large standardized residual.
 X denotes an observation whose X value gives it large leverage.

Normplot of Residuals for Average Ra

Regression Analysis: Tool wear (m versus fr (mm/min), Amp. (micron, ...

The regression equation is
 Tool wear (micro) = 48 - 29.4 fr (mm/min) + 121 Amp. (micron) + 0.113 Freq (Hz)
 + 0.0061 Spindle Rpm - 0.07 fr*fr - 12.5 amp*amp
 + 0.000004 freq*freq* + 0.000002 RPM*RPM + 0.81 fr*amp
 - 0.0099 fr_*frq + 0.00621 fr*RPM - 0.0141 amp*freq
 - 0.000010 freq*RPM

Predictor	Coef	SE Coef	T	P
Constant	48.2	256.0	0.19	0.851
fr (mm/min)	-29.35	59.43	-0.49	0.623
Amp. (micron)	120.74	69.67	1.73	0.088
Freq (Hz)	0.1133	0.1814	0.62	0.534
Spindle Rpm	0.00606	0.04223	0.14	0.886
fr*fr	-0.066	6.602	-0.01	0.992
amp*amp	-12.460	9.764	-1.28	0.206
freq*freq*	0.00000432	0.00003932	0.11	0.913
RPM*RPM	0.00000165	0.00000320	0.52	0.607
fr*amp	0.809	5.551	0.15	0.885
fr_*frq	-0.00988	0.01110	-0.89	0.377
fr*RPM	0.006214	0.003598	1.73	0.089
amp*freq	-0.01409	0.01421	-0.99	0.325
freq*RPM	-0.00001020	0.00000891	-1.15	0.256

Normplot of Residuals for Tool wear (micro)

Regression Analysis: Material rem versus fr (mm/min), Amp. (micron, ...

The regression equation is
 Material removal rate (cu/micro) = 169005 + 17474 fr (mm/min)
 - 16147 Amp. (micron) + 21.7 Freq (Hz)
 - 7.78 Spindle Rpm - 1202 fr*fr + 2269 amp*amp

- 0.00431 freq*freq* + 0.000207 RPM*RPM
 - 964 fr*amp - 1.55 fr_*frq - 0.533 fr*RPM
 - 0.02 amp*freq + 0.00001 freq*RPM

Predictor	Coef	SE Coef	T	P
Constant	169005	46383	3.64	0.001
fr (mm/min)	17474	10768	1.62	0.109
Amp. (micron)	-16147	12623	-1.28	0.205
Freq (Hz)	21.66	32.86	0.66	0.512
Spindle Rpm	-7.783	7.652	-1.02	0.313
fr*fr	-1202	1196	-1.00	0.319

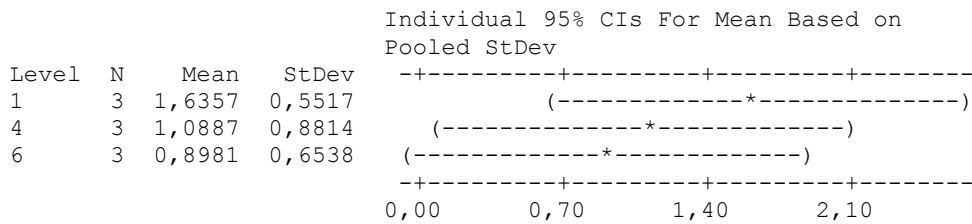
S = 30152.4 R-Sq = 35.6% R-Sq(adj) = 23.1%

Analysis of Variance

Source	DF	SS	MS	F	P
Regression	13	33650333542	2588487196	4.85	2.58
Residual Error	67	60914235523	909167694		
Total	80	94564569065			

Source	DF	Seq SS
fr (mm/min)	1	33605215
Amp. (micron)	1	6962809443
Freq (Hz)	1	47344845
Spindle Rpm	1	21907835024
fr*fr	1	829623743
amp*amp	1	1566394907
freq*freq*	1	322168680
RPM*RPM	1	727161
fr*amp	1	823286376
fr_*frq	1	547868214
fr*RPM	1	608554446
amp*freq	1	54418
freq*RPM	1	61070

Normplot of Residuals for Material removal rate (cu/micro ANOVA)
One-way ANOVA: Average RA versus Feedrate

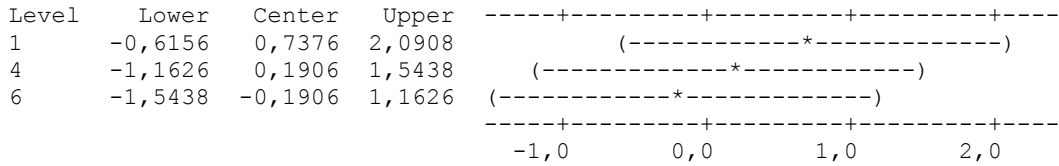


Pooled StDev = 0,7092

Hsu's MCB (Multiple Comparisons with the Best)

Family error rate = 0,05
 Critical value = 2,34

Intervals for level mean minus smallest of other level means



Grouping Information Using Tukey Method

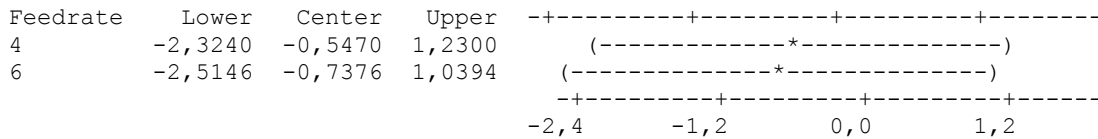
Feedrate	N	Mean	Grouping
1	3	1,6357	A
4	3	1,0887	A
6	3	0,8981	A

Means that do not share a letter are significantly different.

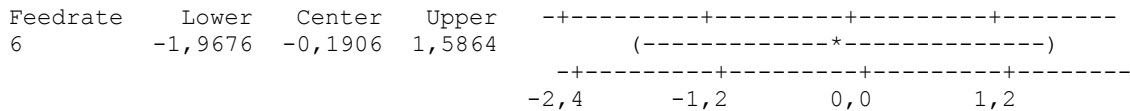
Tukey 95% Simultaneous Confidence Intervals
 All Pairwise Comparisons among Levels of Feedrate

Individual confidence level = 97,80%

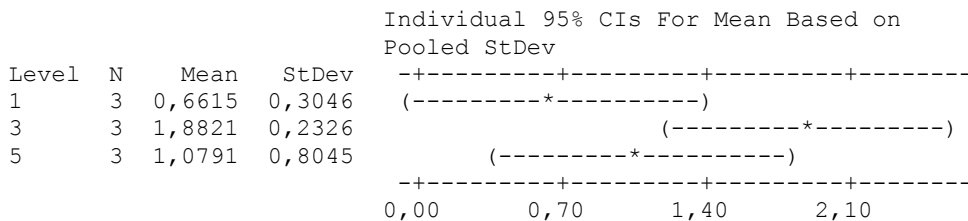
Feedrate = 1 subtracted from:



Feedrate = 4 subtracted from:



One-way ANOVA: Average RA versus Vib. Amp



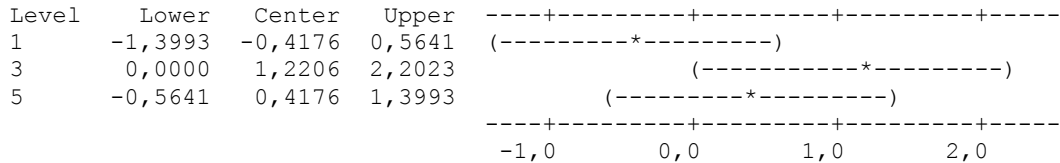
Pooled StDev = 0,5145

Hsu's MCB (Multiple Comparisons with the Best)

Family error rate = 0,05

Critical value = 2,34

Intervals for level mean minus smallest of other level means



Grouping Information Using Tukey Method

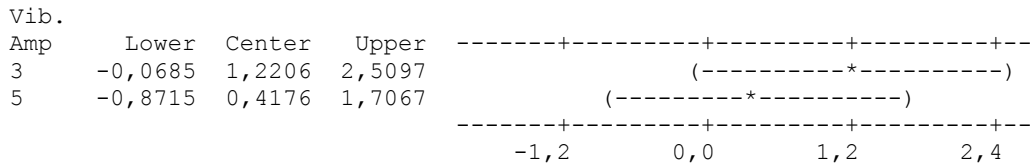
Vib.	Amp	N	Mean	Grouping
	3	3	1,8821	A
	5	3	1,0791	A
	1	3	0,6615	A

Means that do not share a letter are significantly different.

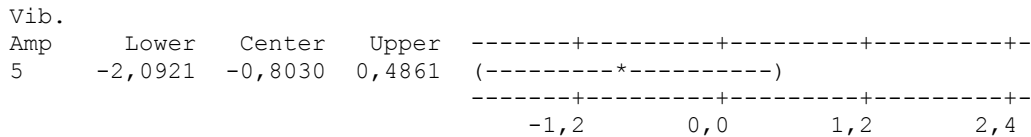
Tukey 95% Simultaneous Confidence Intervals
All Pairwise Comparisons among Levels of Vib. Amp

Individual confidence level = 97,80%

Vib. Amp = 1 subtracted from:



Vib. Amp = 3 subtracted from:



One-way ANOVA: Average RA versus Vibr. Freq

Individual 95% CIs For Mean Based on Pooled StDev

Level	N	Mean	StDev
1000	3	1,0785	0,5294
2000	3	1,0347	0,7483
3000	3	1,5095	0,9496

Pooled StDev = 0,7620

Taguchi

Taguchi Design

Taguchi Orthogonal Array Design

L9(3**4)

Factors: 4
Runs: 9

Columns of L9(3**4) Array

1 2 3 4

Results for: Worksheet 11

Taguchi Analysis: Ra versus Feedrate, Vibration am, Vibration fr, Spindle spee

The following terms cannot be estimated, and were removed.

Feedrate*Vibration amplitude
Feedrate*Vibration frequency
Feedrate*Spindle speed
Vibration amplitude*Vibration frequency
Vibration amplitude*Spindle speed
Vibration frequency*Spindle speed

Response Table for Signal to Noise Ratios
Smaller is better

Level	Feedrate	Vibration amplitude	Vibration frequency	Spindle speed
1	-3.8781	4.1820	-0.1042	-0.8610
2	0.8165	-5.4478	1.0829	2.0323
3	2.4159	0.6202	-1.6243	-1.8170
Delta	6.2940	9.6297	2.7071	3.8494
Rank	2	1	4	3

Response Table for Means

Level	Feedrate	Vibration amplitude	Vibration frequency	Spindle speed
-------	----------	---------------------	---------------------	---------------

1	1.6357	0.6615	1.0913	1.2487
2	1.1016	1.8821	1.0347	0.9808
3	0.8981	1.0919	1.5095	1.4059
Delta	0.7376	1.2206	0.4748	0.4251
Rank	2	1	3	4

Main Effects Plot for Means

Main Effects Plot for SN ratios

Taguchi Analysis: Tool wear versus Feedrate, Vibration am, Vibration fr, ...

The following terms cannot be estimated, and were removed.

Feedrate*Vibration amplitude
 Feedrate*Vibration frequency
 Feedrate*Spindle speed
 Vibration amplitude*Vibration frequency
 Vibration amplitude*Spindle speed
 Vibration frequency*Spindle speed

Response Table for Signal to Noise Ratios
 Smaller is better

Level	Feedrate	Vibration amplitude	Vibration frequency	Spindle speed
1	-55.24	-48.42	-52.41	-53.04
2	-50.38	-56.25	-50.37	-50.88
3	-50.80	-51.75	-53.64	-52.50
Delta	4.86	7.83	3.27	2.16
Rank	2	1	3	4

Response Table for Means

Level	Feedrate	Vibration amplitude	Vibration frequency	Spindle speed
1	590.3	282.0	437.0	476.7
2	388.0	650.7	379.3	389.7
3	376.7	422.3	538.7	488.7
Delta	213.7	368.7	159.3	99.0
Rank	2	1	3	4

Main Effects Plot for Means

Taguchi Analysis: MRR versus Feedrate, Vibration am, Vibration fr, Spindle spee

The following terms cannot be estimated, and were removed.

Feedrate*Vibration amplitude
 Feedrate*Vibration frequency

Feedrate*Spindle speed
Vibration amplitude*Vibration frequency
Vibration amplitude*Spindle speed
Vibration frequency*Spindle speed

Response Table for Signal to Noise Ratios
Larger is better

Level	Feedrate	Vibration amplitude	Vibration frequency	Spindle speed
1	99.83	103.24	101.47	101.29
2	102.73	99.32	102.76	103.15
3	102.77	102.77	101.10	100.89
Delta	2.94	3.92	1.66	2.26

Appendix VI
Part of LabView Programming

